'Development of silsesquioxane-polyurethane nanocomposites for use in microvascular networks.'

To be submitted for the degree of

Doctor of Philosophy (Ph.D.)

at the

University College London

by

Ruben Yap Kannan MBBS MRCSEd

ProQuest LLC
789 East Eisenhower Parkway
P.O. Box 1346
Ann Arbor, MI 48106-1346

Dedication

This thesis is dedicated to

the memory of

Dr. Muthu Venkataraman,

the man who taught me the meaning of courage.

CONTENTS

ACKNOWLEDGEMENTS 1

ABSTRACT 2

HYPOTHESIS 3

LIST OF FIGURES 4

LIST OF TABLES 9

1. THE ROLES OF TISSUE ENGINEERING AND VASCULARISATION IN THE DEVELOPMENT OF MICROVASCULAR NETWORKS: A REVIEW 10

1.1. INTRODUCTION 11
1.1.1. RECONSTRUCTIVE SURGERY 11
1.1.2. TISSUE ENGINEERING AND ITS LIMITED SUCCESS 12
1.1.3. MICROVESSEL DEVELOPMENT 13
1.1.4. TISSUE PERFUSION 15
1.2. SEARCH METHODS 18
1.3. TISSUE ENGINEERED MICROVESSEL BEDS 18
1.3.1. MICROVASCULAR TISSUE ENGINEERING 18
1.3.1.1. Types of prostheses 21
1.3.1.1.1. Macrovascular grafts 23
1.3.1.1.2. Microvascular grafts (Microvessels) 24
1.3.1.2. Configuration of vessels 27
1.3.2. EXTRACELLULAR MATRIX SCAFFOLDS 29
1.3.2.1. Biomaterial substitutes 30
1.3.2.1.1. Natural 33
1.3.2.1.2. Synthetic 34
1.3.2.1.3. Sol-gel systems 39
1.3.2.2. Superstructure 41
1.3.2.3. Cells seeded onto matrices 42
1.3.3. VASCULARISATION 43
1.3.3.1. Inosculation 43
1.3.3.2. Angioinduction 47
1.4. CONCLUSION 50

2. SYNTHESES AND PHYSICAL CHARACTERISATION OF POLYHEDRAL OLIGOMETRIC SILSESQUIOXANE INTEGRATED POLY (CARBONATE-UREA) URETHANE NANOCOMPOSITES WITH SINGLE AND TWIN HYDROXYL-FUNCTIONALISED DIOL GROUPS. 51

2.1. INTRODUCTION 52
2.2. METHOD & MATERIALS 55
2.2.1. SYNTHESIS 55
2.2.2. POLYMER CHARACTERISATION 56
2.2.2.1. Nuclear Magnetic Resonance Spectroscopy (NMR) 56
2.2.2.2. Fourier-Transform Infra-Red Spectrometry 57
2.2.2.3. Differential Scanning Calorimetry (DSC) 58
2.2.2.4. Mechanical Testing 58
2.3. RESULTS 59
2.3.1. SOLUTION-STATE NMR 59
2.3.1.1. $^{13}C(^{1}H)$ pure PCU/DMSO 298K (Control) 59
2.3.1.2. ^{1}H pure PCU/DMSO 298K (Control) 61
2.3.1.3. ^{13}C (^{1}H) Single hydroxyl functionalised POSS-PCU/DMSO 298K 62
2.3.1.4. (^{1}H) Single hydroxyl-functionalised POSS-PCU/DMSO 298K 64
2.3.2. SOLID-STATE NMR 65
2.3.2.1. ^{13}C CPMAS Single hydroxyl-functionalised POSS-PCU 65
2.3.2.2. ^{13}C MAS/Decoupling Ride - Single diol 2% POSS-PCU 65
2.3.2.3. ^{13}CPMAS NQS – Single hydroxyl-functionalised POSS-PCU 66
2.3.2.4. ^{13}C CPMAS NQS – Twin-diol POSS-PCU 67
2.3.2.5. ^{13}C MAS/Decoupling Ride – Twin hydroxyl-functionalised POSS-PCU 68
2.3.2.6. ^{13}C CPMAS TOSS – Single hydroxyl-functionalised POSS-PCU 68
2.3.2.7. ^{13}C CPMAS TOSS – Twin hydroxyl-functionalisedl POSS-PCU 70
2.3.2.8. ^{29}Si CPMAS – Single hydroxyl-functionalised POSS-PCU 70
2.3.2.9. ^{29}Si CPMAS – Twin hydroxyl-functionalised POSS-PCU 72
2.3.2.10. ^{15}N CPMAS – Single hydroxyl-functionalised POSS-PCU 72
2.3.2.11. ^{15}N CPMAS – Twin hydroxyl-functionalised POSS-PCU 73
2.3.3. FOURIER-TRANSFORM INFRA-RED SPECTROMETRY 74
2.3.4. DIFFERENTIAL SCANNING CALORIMETRY (DSC) 78
2.3.5. MECHANICAL TESTING 79
2.4. DISCUSSION 83

3. THE DEGRADATIVE RESISTANCE OF POLYHEDRAL OLIGOMERIC SILSESQUIOXANE (POSS) NANOCORE- INTEGRATED POLYURETHANES. 87

3.1. INTRODUCTION **88**
3.2. METHODS AND MATERIALS **90**
3.2.1. POLYMER SYNTHESIS 90
3.2.2. GRAFT FABRICATION 90
3.2.3. DEGRADATION PROTOCOL 91
3.2.3.1. Hydrolysis 91
3.2.3.2. Oxidation and peroxidation 91
3.2.3.3. Plasma protein fractions 92
3.2.3.4. Control 93
3.2.4. FOURIER TRANSFORM INFRA-RED SPECTROSCOPY 93
3.2.5. SCANNING ELECTRON MICROSCOPY 94
3.2.6. RADIAL STRESS-STRAIN ANALYSES 94
3.2.7. DIFFERENTIAL SCANNING CALORIMETRY 96
3.3. RESULT **96**
3.3.1. SURFACE DEGRADATION 96
3.3.2. SURFACE TOPOGRAPHY 104
3.3.3. RADIAL STRESS-STRAIN CURVES 108
3.3.4. THERMAL CHARACTERISTICS 111
3.4. DISCUSSION **116**

4. THE IN VIVO BIOCOMPATIBILITY AND BIOSTABILITY OF SILSESQUIOXANE NANOCOMPOSITES **119**

4.1. INTRODUCTION **120**
4.2. METHODS AND MATERIALS **122**
4.2.1. POLYMER SYNTHESIS 122
4.2.2. IMPLANTATION IN SHEEP 122
4.2.3. HISTOPATHOLOGY 123
4.2.4. FOURIER TRANSFORM INFRA-RED SPECTROSCOPY 125
4.2.5. SCANNING ELECTRON MICROSCOPY (SEM) 126
4.2.6. MEASUREMENT OF EQUILIBRIUM CONTACT ANGLE 126
4.2.7. FIBRINOGEN DIRECT ELISA 127
4.3. RESULTS **127**
4.3.1. GROSS MORPHOLOGY 127
4.3.2. HISTOPATHOLOGY 129
4.3.3. SURFACE DEGRADATION 131
4.3.4. YOUNG'S EQUILIBRIUM CONTACT ANGLE 136
4.3.5. FIBRINOGEN ADSORPTION 138
4.4. DISCUSSION **140**

5. ENDOTHELIALISATION OF POLYHEDRAL OLIGOMERIC SILSESQUIOXANE NANOCOMPOSITES FOR MICROVASCULAR TISSUE ENGINEERING: AN IN VITRO STUDY 145

5.1. INTRODUCTION 146
5.2. MATERIALS AND METHODS 149
5.2.1. POLYMER SYNTHESIS 149
5.2.2. PRIMARY ENDOTHELIAL CELL CULTURE 149
5.2.3. CELL VIABILITY ANALYSIS 150
5.2.3.1. Direct contact method 150
5.2.3.2. Diluent extraction method 150
5.2.3.3. High permeation liquid chromatography (HPLC) 152
5.2.4. CELL ADHESION ASSAY 152
5.2.5. CELL PROLIFERATION ASSAY 154
5.2.6. CELL CONFLUENCE MORPHOLOGY 155
5.2.6.1. Light microscopy 155
5.2.6.2. Electron microscopy 155
5.3. RESULTS 156
5.3.1. CELL VIABILITY 156
5.3.1.1. Direct effect of POSS-PCU 156
5.3.1.2. Indirect effect of POSS-PCU 157
5.3.1.3. HPLC 159
5.3.2. CELL ADHESION 159
5.3.3. CELL PROLIFERATION 161
5.3.4. CELL MORPHOLOGY 163
5.4. DISCUSSION 167

6. THE ANTI-THROMBOGENIC POTENTIAL OF A POLYHEDRAL OLIGOMERIC SILSESQUIOXANE (POSS) NANOCOMPOSITE. 170

6.1. INTRODUCTION 171
6.2. METHODS AND MATERIALS 174
6.2.1. POLYMER SYNTHESIS 174
6.2.2. SURFACE CHARACTERISATION 174
6.2.3. THROMBOELASTOGRAPHY 176
6.2.4. FIBRINOGEN ADSORPTION 177
6.2.5. ANTI-FACTOR XA ACTIVITY 178
6.2.6. PLATELET ADHESION 180
6.3. RESULTS 181

6.3.1. POSS NANOCAGE DISTRIBUTION 181
6.3.2. WATER CONTACT ANGLE MEASUREMENT 183
6.3.3. SURFACE TOPOGRAPHY 184
6.3.4. SURFACE COMPOSITION 190
6.3.5. THROMBOELASTOGRAPHY (TEG) 192
6.3.6. FIBRINOGEN ADSORPTION TESTS 194
6.3.7. ANTI-FACTOR XA ACTIVITY 195
6.3.8. PLATELET ADSORPTION TEST 197
6.4. DISCUSSION **202**

7. SMART BIOMIMETIC NANOCOMPOSITE MICROVESSELS: BUILDING BLOCKS OF AN ARTIFICIAL CAPILLARY BED. **210**

7.1. INTRODUCTION **211**
7.2. METHODS AND MATERIALS **212**
7.2.1. POLYMER SYNTHESIS 212
7.2.2. FABRICATION 212
7.2.2.1. Dip coating 214
7.2.2.2. Coagulation 216
7.2.2.3. Quality control 216
7.2.3. VESSEL WALL ANALYSIS 217
7.2.3.1. Hydraulic conductivity (K) 217
7.2.3.2. Radial compliance 217
7.2.3.3. Burst strength 219
7.3. RESULTS **220**
7.3.1. MICROVESSEL FABRICATION 220
7.3.1.1. Polymer dispersion 221
7.3.1.2. Polymer viscosity 221
7.3.1.3. Dipping technique 223
7.3.1.4. Mandrel preparation 223
7.3.1.5. Coagulating solution 224
7.3.2. MICROVESSEL WALL 229
7.3.2.1. Hydraulic conductivity 229
7.3.2.2. Radial compliance 230
7.3.3.3. Burst strength 233
7.4. DISCUSSION **234**

8. SUMMARY & FUTURE PROSPECTS **240**

BIBLIOGRAPHY 246

PUBLICATIONS 333

PRESENTATIONS 336

ACKNOWLEDGEMENTS

I am forever grateful to Professor Alex Seifalian for believing in my abilities and inspiring me to achieve my full potential as well as Dr. Henryk Salacinski and Dr. Kevin Sales; tissue engineers at the University College London in the same vein. My special thanks to Mrs. Karen Cheetham, Mr. Geoffrey Punshon and the staff at the Academic Department of Surgery at the Royal Free Hospital, London for their unceasing support of this project.

I wish to express my deepest gratitude to Mr. Peter Butler and Professor Marc Winslet for presenting me with the opportunity to be part of their team and being role models in themselves.

And lastly but most importantly my lovely wife, Thavamalar, my beautiful baby, Trinettra and my parents for standing by my side through thick and thin.

ABSTRACT

We have recently developed a nanocomposite based on polyhedral oligomeric silsesquixoane for medical device application for particular use in a microvascular network. Using spectroscopic analyses, we characterised the polymer before subjecting it to both in vitro and in vivo degradation. In the same setting, the foreign-body reaction of this polymer was determined. An in vitro feasibility study as to the efficacy of neo-endothelialisation was then performed. Next, the anti-thrombogenic nature of the nanocomposite was elicited. Based on the favourable outcomes of these experiments, nanocomposite microvessels were designed and fabricated to form the components of a microvascular network. Our results indicate that silsesquioxane is an optimal building material for microvascular grafts. This therefore constitutes the foundation on which we intend to construct an in vitro artificial capillary bed model.

HYPOTHESIS

'Silsesquioxane-polyurethane nanocomposites possess the optimal characteristics for the construction of microvascular networks such as artificial capillary beds as they are biocompatible, biostable, strong, tensile and have thromboresistant properties.'

LIST OF FIGURES

FIGURE 1.1. THE SERIES OF EVENTS ILLUSTRATING THE DUAL NATURE OF VESSEL DEVELOPMENT: ANGIOGENESIS AND ARTERIOGENESIS. 15

FIGURE 1.3. FLOW- AND DIFFUSION-LIMITED EXCHANGE. 17

FIGURE 1.3. FLOW- AND DIFFUSION-LIMITED EXCHANGE. 17

FIGURE 1.4. THE INTER-RELATIONSHIP BETWEEN VARIOUS MODELS OF VESSEL DEVELOPMENT. 19

FIGURE 1.5. THE TRIAD OF TISSUE VASCULARISATION. 20

FIGURE 1.6. A VIABLE MICROVESSEL PERFUSION SYSTEM. 26

FIGURE 1.7. THE EFFECT OF VESSEL CONFIGURATION ON TISSUE VASCULARISATION. GROUP I – CONTROL (ACELLULAR DERMIS), GROUP II – ARTERIO-VENOUS LOOP EMBEDDED IN THE MATRIX, GROUP III – ARTERIO-VENOUS BUNDLE LIGATED WITHIN THE MATRIX, GROUP IV – FLOW-THROUGH GRAFT 29

FIGURE 1.8. THE EFFECT OF CELL TRACTION ON TISSUE PATTERNS. 31

FIGURE 1.9. THE SYNTHESIS OF BIOMIMETIC GELS. 40

FIGURE 2.1. MOLECULAR STRUCTURE OF TWIN-HYDROXYL FUNCTIONALISED CYCLOHEXANE-DIOL SIDE-CHAIN SUBSTITUTED POSS 56

FIGURE 2.2. ^{13}C-(^{1}H) NMR OF CONTROL PCU. 61

FIGURE 2.3. ^{1}H-NMR SPECTRA OF CONTROL PCU. 62

FIGURE 2.4. ^{13}C-(^{1}H) NMR SPECTRA OF SINGLE-HYDROXYL FUNCTIONALISED POSS-PCU. 63

FIGURE 2.5. ^{1}H-NMR SPECTRA OF SINGLE-DIOL FUNCTIONALISED POSS-PCU. 64

FIGURE 2.6. ^{29}SI-CPMAS NMR OF SINGLE HYDROXYL-FUNCTIONALISED POSS-PCU 71

FIGURE 2.7. ^{15}N CPMAS NMR OF SINGLE HYDROXYL-FUNCTIONALISED POSS-PCU. 73

FIGURE 2.8A. ATR-FTIR ANALYSES OF THE EFFECT OF INCREASING POSS FEED RATIOS INTO PCU. 76

FIGURE 2.8B. FTIR ANALYSIS SHOWING THE BOND PATTERNS WITH INCREMENTAL CONCENTRATIONS OF POSS WITHIN PCU. 77

FIGURE 2.9. DSC TRACE COMPARING PCU AND THE INCREMENTAL DOSES OF POSS TO THE RESULTING NANOCOMPOSITE. 79

FIGURE 2.10A. COMPARISON OF TENSILE STRESS BETWEEN PLAIN PCU AND POSS-PCU NANOCOMPOSITES STRETCHED AT 100% AND 300 % NORMAL SHOWING THE INCREASED ELASTOMERIC PROPERTY OF POSS-PCU DUE TO POSS INTEGRATION. 81

FIGURE 2.10B. THE VARIATION IN TEAR STRENGTH BETWEEN PCU AND POSS-PCU INDICATING THE IMPROVED STRUCTURAL HOMOGENEITY OF POSS-PCU TAKEN AT RANDOM POINTS ACROSS ITS CROSS-SECTION; A CHARACTERISTIC DUE TO THE NANOSCALE INTEGRATION OF POSS INTO THE PCU MATRIX WHICH DECREASES PHASE SEPARATION AND PREVENTS THE FORMATION OF FOCAL STRESS POINTS IN PCU. 82

FIGURE 3.1. SUB-SURFACE BOND PATTERNS IN POSS-PCU NANOCOMPOSITES FOLLOWING EXPOSURE TO PLASMA PROTEIN FRACTIONS (PF I TO IV) SHOWING NO DIFFERENCE IN THE INTENSITIES OF 'SI-O', 'C-O-C', 'NH-CO'(UREA) AND '(NHCO)O'(URETHANE) BONDS ALTHOUGH ON CLOSER INSPECTION OF PF III-DEGRADED SAMPLES (MARKED IN RED), THERE IS A SLIGHT LEFT-SHIFT IN THE C-O=C BOND INDICATING A REDUCTION IN HYDROGEN BONDING. 98

FIGURE 3.2A. FTIR ANALYSES SHOWING THE SUB-SURFACE BOND PATTERNS IN POSS-PCU NANOCOMPOSITES AFTER BEING DEGRADED BY HYDROLYTIC SOLUTIONS WITH SIGNIFICANT DECREASES IN THE 'SI-O' BONDS OF THE POSS NANOCORES IN THE PLA-DEGRADED SAMPLES (MARKED IN RED).....99

FIGURE 3.2B. ONE-WAY ANOVA ANALYSES (N = 12) SHOWED A SIGNIFICANT DECREASE IN THE 'SI-O' BONDS OF THE PLA- DEGRADED SAMPLES COMPARED TO THE CONTROL, CE-DEGRADED AND CUMENE-DEGRADED SAMPLES ($P < 0.0001$). THE REMAINING BONDS DID NOT SHOW ANY SIGNIFICANT DIFFERENCE POST-DEGRADATION.....100

FIGURE 3.3B. ONE-WAY ANOVA ANALYSES OF THE MAIN BONDS WITHIN THE POSS-PCU NANOCOMPOSITE SHOWING A SIGNIFICANT DECREASE IN 'SI-O' BONDS FOLLOWING T-BUTYL/$CoCl_2$ AND GLUT/ T-BUTYL/$CoCl_2$ DEGRADATION WITH AN EFFECT ON THE' C-O=C' BONDS AS WELL IN THE LATTER.....103

FIGURE 3.4. COMPARISONS OF PLA-, GLUT/T-BUTYL-PEROXIDE, T-BUTYL-PEROXIDE DEGRADED AND CONTROL POLYMERS.....104

FIGURE 3.5A. SURFACE TOPOGRAPHY OF UNDEGRADED POSS-PCU (CONTROL).....106

FIGURE 3.5B. SURFACE TOPOGRAPHY OF PLA DEGRADED POSS-PCU NANOCOMPOSITE SHOWING INCREASED PITTING AND FISSURING.....107

FIGURE 3.5C. SURFACE TOPOGRAPHY OF T-BUTYL PEROXIDE DEGRADED POSS-PCU NANOCOMPOSITE REVEALING AN INCREASINGLY GLABROUS SURFACE.....108

FIGURE 3.6. RADIAL STRESS-STRAIN CURVES OF THE REPRESENTATIVE DEGRADATION GROUPS SHOWING THEIR SIMILARITY IN ELASTICITY.....110

FIGURE 3.7. COMPARISON OF DSC THERMAL ANALYSES OF T-BUTYL-DEGRADED, PLA-DEGRADED AND UNDEGRADED POLYMERS SHOWING THE STABILISING EFFECT OF POSS NANOCORES TO PCU DEGRADATION.113

FIGURE 4.1. SCHEMATIC REPRESENTATION OF THE INTERPLAY BETWEEN THE BIOLOGICAL HOST AND THE IMPLANT. 120

FIGURE 4.2. SUBCUTANEOUS INSERTION OF POSS-PCU CASTED SHEETS INTO THE BACK OF SHEEP (N = 6). 123

FIGURE 4.3A. POSS-PCU NANOCOMPOSITES IMPLANTED SUBCUTANEOUSLY FOR 36 MONTHS EXHIBITED NO SIGNIFICANT CAPSULE FORMATION.....128

FIGURE 4.3B. THE CONTROL SILOXANE IMPLANT AND ITS SURROUNDING CAPSULE INDICATING A SEVERE FOREIGN BODY REACTION.....129

FIGURE 4.4. 10X MAGNIFICATION OF THE H&E-STAINED INFLAMMATORY CAPSULE SURROUNDING THE SILOXANE CONTROL SHOWING THE INNERMOST FIBRIN LAYER FOLLOWED BY INFLAMMATORY MACROPHAGES, FIBROBLASTS AND VASCULARISATION.....130

FIGURE 4.5A. ATR-FTIR ANALYSIS OF IMPLANTED 2% POSS-PCU NANOCOMPOSITES BEFORE AND AFTER IMPLANTATION SHOWING NO DIFFERENCE IN AMPLITUDE AT THE SI-O GROUP WAVELENGTH OF 1109 CM^{-1}. ..132

FIGURE 4.5B. ATR-FTIR ANALYSIS OF THE DEGRADED CONTROL SILOXANE FOLLOWING IMPLANTATION SHOWING A SIGNIFICANT DECREASE IN 'SI-O' WAVELENGTH AMPLITUDE.....133

FIGURE 4.6A. SURFACE MORPHOLOGY OF DEGRADED 2% POSS-PCU NANOCOMPOSITES SHOWING MINIMAL EVIDENCE OF SURFACE DEGRADATION AND THE ABSENCE OF FIBROBLAST ATTACHMENT COMPARED TO THE CONTROL (SHOWN IN FIGURE 4.6B).....135

FIGURE 4.6B. SURFACE MORPHOLOGY OF SILOXANE SHOWING SIGNIFICANT SURFACE DEGRADATION WITH EVIDENCE

OF FISSURES, CRACKS A HEAVY DEPOSITION OF STELLATE-SHAPED FIBROBLASTS. 136

FIGURE 4.7. DERIVATION OF YOUNG'S EQUILIBRIUM CONTACT ANGLE USING DYNAMIC CONTACT ANGLE ANALYSES SHOWED THE AMPHILIC (COMBINED HYDROPHOBIC AND HYDROPHILIC) NATURE OF THE POSS-PCU NANOCOMPOSITE. 137

FIGURE 4.8. FIBRINOGEN DIRECT ELISA SHOWING SIGNIFICANTLY INCREASED FIBRINOGEN 139

_____ADSORPTION TO SILOXANE AS COMPARED TO POSS-PCU (ONE-WAY ANOVA, $P < 0.01$). .....

FIGURE 5.1. SCHEMATIC REPRESENTATION OF THE STAGES OF CELL SEEDING ON BIOMATERIALS. 148

FIGURE 5.2. DIRECT CONTACT ANALYSIS USING ALAMAR BLUE™ SPECTRAL ABSORPTION (ABSA) WHICH SHOWED NO SIGNIFICANT DIFFERENCE IN CELL VIABILITY BETWEEN STANDARD CELL CULTURES AND THOSE ON POSS-PCU (TWO-WAY ANOVA, P = NS). 157

FIGURE 5.3. DILUENT EXTRACTION ANALYSIS USING ALAMAR BLUE™ SPECTRAL ABSORPTION (ABSA) SHOWING NO SIGNIFICANT DIFFERENCES BETWEEN VARYING DOSES OF CELL MEDIA INCUBATED WITH THE NANOCOMPOSITE AT 0, 6, 12 AND 24 HOURS (TWO-WAY ANOVA, P = NS). MEAN AND STANDARD DEVIATION VALUES ARE TABULATED BELOW. 158

FIGURE 5.4A. ALAMAR BLUE™ ASSAY SHOWING SIGNIFICANT ENDOTHELIAL CELL ADHESION TO POSS-PCU WITHIN 30 MINUTES OF CONTACT (STUDENT'S T-TEST, $P < 0.05$) AND REACHING SATURATION AFTER 2 HOURS OF INCUBATION. THESE VALUES WERE SIGNIFICANTLY GREATER THAN ENDOTHELIAL CELL ADHESION TO MEDICAL-GRADE SILOXANE (TWO-WAY ANOVA, $P < 0.0001$). THERE WAS NO STATISTICAL DIFFERENCE IN EC ADHESION BETWEEN POSS-PCU AND STANDARD CELL CULTURE PLATES. 160

FIGURE 5.4B. WATER ABSORPTION INDEX (WAI) ASSAYS WHICH SHOW SIGNIFICANTLY HIGHER WATER ABSORPTION INDICES AND HENCE HYDROPHILICITY OF POSS-PCU AS COMPARED TO EPTFE AND PCU (ONE-WAY ANOVA, $P < 0.0001$). 161

FIGURE 5.5. PICOGREEN ASSAY SHOWING SIGNIFICANT INCREASES IN CELL PROLIFERATION ON POSS-PCU OVER 21 DAYS (ONE-WAY ANOVA, $P < 0.0001$) 162

FIGURE 5.6A. LIGHT MICROSCOPIC ANALYSIS (20X MAGNIFICATION) OF TOLUIDINE BLUE-STAINED ENDOTHELIAL CELLS SHOWING THEIR CONFLUENCE MORPHOLOGY ON POSS-PCU AT 48 HOURS 165

FIGURE 5.6B. TOLUIDINE BLUE-STAINED HUVECS ON POSS-PCU SHOWING IMPROVED CELLULAR CONFLUENCE BY 6 DAYS, COMPARED TO 48 HOURS (20 X MAGNIFICATION). 165

FIGURE 5.7. SCANNING ELECTRON MICROSCOPE PICTURES OF ENDOTHELIAL CELL ADSORPTION MORPHOLOGY ON POSS-PCU SHOWING THE PRESENCE OF A FLAT, SPINDLE-SHAPED CELLS WITH NUMEROUS FILOPODIA AND THE ABSENCE OF CELL RETRACTION. THIS INDICATES THE PRESENCE OF VIABLE, PROLIFERATING CELLS ON POSS-PCU AT 48 HOURS (320X MAGNIFICATION). 166

FIGURE 6.1A. EDXA MAP OF 2% POSS-PCU SHOWING THE DISTRIBUTION OF POSS (YELLOW) WITHIN THE HARD SEGMENT OF THE POLYMER (LIGHT PURPLE) WHILE SOFTER SEGMENTS CORRELATE TO PURPLE AREAS OF CARBON. THE RED LINE REPRESENTS THE COPPER GRID. ON CLOSER INSPECTION, SPECKLED YELLOW DOTS MAY ALSO BE SEEN WITHIN THE SOFT (PURPLE) SEGMENTS OF THE POLYMER INDICATING THAT POSS MOLECULES ALSO INTERACT WITH THE AMORPHOUS CARBONATE SEGMENT. 182

FIGURE 6.1B. TEM ANALYSIS OF A CROSS-SECTION OF 2% POSS-PCU CASTED SHEETS SHOWING THE DISTRIBUTION OF SILICON-RICH POSS SEGMENTS WITHIN THE DARKER, HARD SEGMENTS OF THE NANOCOMPOSITE WHILST

GRADUALLY ENCROACHING THE SOFT SEGMENTS, TYPICAL OF AN EXFOLIATED NANOCOMPOSITE. 183
FIGURE 6.2. THE LARGE CONTACT ANGLE HYSTERESIS LOOP OF 2 % POSS-PCU NANOCOMPOSITES. 184
FIGURE 6.3A. SEM IMAGE OF THE MICROVESSEL LUMEN SHOWING ITS SURFACE ULTRASTRUCTURE WITH THE CRYSTALLINE HARD SEGMENTS PROJECTING OUT OF ITS SURFACE. 186
FIGURE 6.3B. AFM IMAGE OF 2% POSS-PCU AT 25 X 25 μM RESOLUTION SHOWING LARGE PEAKS OF UP TO 8000 NM HIGH WITHIN THE CRYSTALLINE SEGMENT SHOWING INCREASED GEOMETRICAL DEFINITION. THE DOMES (300 TO 500 NM HIGH) AND TROUGHS ARE SUGGESTIVE OF POSS NANOCAGE INTERACTION WITH THE AMORPHOUS, SOFT SEGMENT 187
FIGURE 6.3C. MICROPHASE IMAGES OF 2% POSS-PCU AT THE NANOSCALE REVEALING ITS EXTENDED SURFACE ('MUSHROOM' CONFIGURATION) WITH 100 NM HIGH ELEVATIONS AND CORRESPONDING DEPRESSIONS. 188
FIGURE 6.3D. AFM ON THE 2% POSS-PCU NANOCOMPOSITE SURFACE SHOWING THE NANOSCALE INTERACTION BETWEEN THE POSS-RICH DARK SEGMENTS AND THE BRIGHTER AREAS WITH RELATIVELY LESS POSS CONTENT SPECIFICALLY IN THE INTERMEDIATE 'ZONE OF INTERCALATION'. 189
FIGURE 6.3E. SURFACE TOPOGRAPHY OF CONTROL PCU SHOWING THE ABSENCE OF CRYSTALLINE NANOPYRAMIDS AND A TWO-PHASE PEBBLE-STONE PHASE. 190
FIGURE 6.4. XPS SURFACE ANALYSIS AT 30° ANGLE OF INCIDENCE SHOWING AN ELEMENTAL SILICON SURFACE COMPOSITION OF THE LUMINAL SURFACE OF POSS-PCU MICROVESSELS OF 16 %. AS THE SILICON (SI 2P) BONDS OF POSS PREDOMINANTLY RESIDE ON THE SURFACE OF POSS-PCU, THIS INDICATES THAT THE LUMINAL SURFACES OF THE MICROVESSELS ARE POSS - ENRICHED. 191
FIGURE 6.5. TESTS SHOWING LOWER MAXIMUM AMPLITUDE VALUES AND INCREASED CLOT LYSIS AT 60 MINUTES OF 2% POSS-PCU COMPARED TO PCU AND THE POLYSTYRENE CONTROL (N = 6). 193
FIGURE 6.6. FIBRINOGEN ADSORPTION DIRECT ELISA TESTS ON 2% POSS-PCU, PCU AND PTFE (N = 4) 195
FIGURE 6.7. INCREMENTAL CONCENTRATIONS OF POSS WITHIN PCU CONFERRING GREATER ANTI-FXA ACTIVITY (N = 6). 196
FIGURE 6.8. PLATELET RETENTION INDICES ON 2% POSS-PCU, PCU AND PTFE AT 30, 60 AND 120 MINUTES (N = 6) SHOWING SIGNIFICANT DECREASE IN PLATELET ADSORPTION TO 2% POSS-PCU COMPARED TO PCU AND PTFE. 198
FIGURES 6.9A. SEM IMAGES OF PLATELET ADSORPTION ON PTFE AT 1250X MAGNIFICATION REVEAL UNIFORM PLATELET ADSORPTION ON PTFE (STAGE IV) AFTER INCUBATION FOR 120 MINUTES. 199
FIGURES 6.9B. SEM IMAGES OF PLATELET ADSORPTION ON 2% POSS-PCU AT 640X MAGNIFICATION SHOWING MINIMAL PLATELET ADSORPTION AT 120 MINUTES (STAGE I) ON 2 % POSS-PCU. 200
FIGURES 6.9C. SEM IMAGES OF THE CONTROL POSS-PCU 'WITHOUT' ANY PLATELETS, ... 200
SHOWING THE BASIC UNDULATING MORPHOLOGY OF THE NANOCOMPOSITE. 200
FIGURE 7.1A. THE PRINCIPLE OF SOLVENT AND NON-SOLVENT/WEAK SOLVENT EXCHANGE DURING THE COAGULATION OF POSS- PCU NANOCOMPOSITE IN DIMETHYLFORMAMIDE (DMF) TO FORM POROUS, VISCOELASTIC MICROVESSELS. 213
FIGURE 7.1B. THE MECHANISED DEVICE USED TO DIP-COAT POSS-PCU MICROVESSELS AT THE RATE OF 10 MM/S (B). 214
FIGURE 7.2. EFFECT OF DIP-COATING POSS-PCU CONCENTRATION (% W/V) ON VESSEL WALL THICKNESS SHOWING

THAT WHEN THE CAPILLARY NUMBER (N_{CA}) (DERIVED FROM LANDAU'S LAW) IS BETWEEN 0.0136 TO 0.0146, A MEAN MICROVESSEL WALL THICKNESS OF 32 TO 34 μM WITH THE LEAST STANDARD DEVIATION CAN BE CONSISTENTLY OBTAINED (N = 16). 222

FIGURE 7.3. THE EFFECT OF COAGULATING SOLVENT (DMF) SOLUBILITY ON THE WALL THICKNESS AND RADIAL UNIFORMITY OF POSS-PCU MICROVESSELS. BARTLETT'S TEST FOR EQUAL VARIANCES INDICATED A SIGNIFICANT VARIATION ($P < 0.001$) IN MICROVESSEL WALL THICKNESS WITH DECREASING COAGULANT SOLUBILITY WHILE MICROVESSEL WALL THICKNESS WAS SIGNIFICANTLY LOWER (ONE-WAY ANOVA, $P < 0.0001$) WHEN COAGULATED WITH WEAKER SOLVENTS. 225

FIGURE 7.4A. SEM IMAGES OF THE LUMINAL ARCHITECTURE OF 14 % (W/V) SOLUTION OF POSS-PCU COAGULATED IN 10 % DMF 227

FIGURE 7.4B. SEM IMAGES OF THE LUMINAL ARCHITECTURE OF 14 % (W/V) SOLUTION OF POSS-PCU COAGULATED IN DW 228

FIGURE 7.4C. SEM IMAGES OF THE LUMINAL ARCHITECTURE OF 14 % (W/V) SOLUTION OF POSS-PCU COAGULATED IN 5% $NaHCO_3$ SOLUTION. 229

FIGURE 7.5A A TYPICAL PULSE WAVEFORMS DISTENSION OF POSS-PCU MICROVESSELS AT LOW-PRESSURE, LOW-FLOW STATES (30 MMHG) 231

FIGURE 7.5B MIMICKING THE MICRO ARTERIAL PRESSURE-RESPONSIVE COMPLIANCE CURVE USING SYNTHETIC POSS-PCU MICROVESSELS. 232

LIST OF TABLES

TABLE 1.1. CURRENT STATUS OF MACRO- AND MICROVASCULAR GRAFTS. 22

TABLE 1.2. NON-CELLULAR COMPONENTS OF ECM AND THEIR FUNCTION {BADYLAK, 2002}. 30

TABLE 1.3. NATURAL MATERIALS USED IN ECM CONSTRUCTS 32

TABLE 1.4. SYNTHETIC MATERIALS USED FOR ECM CONSTRUCTION IN VARIOUS TISSUES. 37

TABLE 1.5. *IN VITRO* DEVELOPMENTAL MODELS OF ANGIOGENESIS AND VASCULOGENESIS. 45

TABLE 1.6. ROLE OF ANGIOGENIC GROWTH FACTORS DURING VASCULAR DEVELOPMENT {VAN DEN, 2003} 48

TABLE 3.1. SEM ANALYSES OF THE DEGRADED SAMPLES. 105

TABLE 3.2. SUMMARY OF DSC RESULTS ON UNDEGRADED, T-BUTYL-PEROXIDE DEGRADED AND PLA-DEGRADED POSS-PCU NANOCOMPOSITES. 115

TABLE 4.2. SUMMARY OF THE EXPERIMENTAL STUDY. 144

TABLE 6.1. COOPER'S CLASSIFICATION SCHEME FOR PLATELET ADSORPTION {KO, 1993} 201

TABLE 7.1. THE EFFECT OF COAGULATING SOLUTIONS ON THE PORE MORPHOLOGY OF POSS-PCU MICROVESSELS WAS STUDIED USING NEUTRAL (DW), BASIC (5% $NaHCO_3$) AND ACIDIC (DMF) SOLUTIONS RESPECTIVELY. OUR DATA SHOWS THAT COAGULATING IN BASIC 5% $NaHCO_3$ SOLUTIONS DURING FABRICATION ALLOWS FOR ARTERIOLAR-LIKE HYDRAULIC PERMEABILITY WITHIN THE POSS-PCU MICROVESSELS WITH THE MOST UNIFORMLY DISTRIBUTED PORES. 236

Chapter 1

1. The roles of tissue engineering and vascularisation in the development of microvascular networks: a review

1.1. INTRODUCTION

1.1.1. RECONSTRUCTIVE SURGERY

In current practice, reconstructive surgery is essential in order to achieve wound closure following major cancer resections and trauma. Traditionally, reconstructive surgeons have employed the reconstructive ladder concept; a hierarchical system by which the simplest option, usually skin grafting or primary closure, is chosen first. If this fails, then a slightly more complex procedure is selected. With the increasing demand for quality wound closure; maximal aesthetics with minimum morbidity, the concept of the 'reconstructive elevator' {Dunn, 2001} is applicable. As opposed to the reconstructive ladder the best option, which in most cases is a flap, is chosen initially.

A flap may be defined as a segment of tissue with an independent blood supply. These may be classified into local, regional and free flaps. Free flaps are based on the concept of angiosome {Taylor, 1987}; an area of tissue with an inherent vascular network supplied by a single vascular pedicle. Buncke and McLean performed the first microvascular tissue transplant in 1969 {McDowell, 1978}. Since then, free flaps have revolutionised reconstructive surgery as they are more versatile and reliable than other flaps. Flaps are now being pre-fabricated prior to surgery to become more case-specific {Song, 2001}. More recently, the introduction of perforator flaps has improved the utility of flaps as a reconstructive option {Kroll, 1988}. Nevertheless, free tissue transfer confers morbidity to the patient as one function is sacrificed for another {McGregor IA, 1995}. Therefore alternative sources of tissue for reconstruction are needed.

1.1.2. TISSUE ENGINEERING AND ITS LIMITED SUCCESS

More than 21 million patients per year in the US alone rely on biomedical implants {Vacanti, 1999}. These include bypass grafts, dental implants and artificial dermal substitutes like Integra®. Current technology limits the survival of these implants as they depend initially upon diffusion and in the later stages, on neovascularisation. Overdependence on the former limit the thickness of these implants while depending on neovascularisation can cause excessive fibrovascular ingrowth and hence scarring. There are no tissue-engineered constructs presently available which have an inherent vasculature such as a capillary bed ready to be connected to the host vascular system. This represents a major limitation as the driving force of living tissue is vascularity. Although attempts to develop small-diameter vascular grafts have been successful *in vitro* {Seifalian, 2002;Tiwari, 2002}, it remains to be seen through clinical studies whether they are reliable enough to sustain flow *in vivo* {Kidd, 2003;Mitchell, 2003;Fields, 2002}. Even so, they are limited by the absence of a viable capillary network for nutrient exchange. This missing link represents the bridge between the host and the tissue-engineered implant.

Most clinical studies in artificial tissue so far have utilised dermal substitutes like Integra™ in the treatment of burns. After application, it undergoes imbibition, fibroblast (Fb) migration, neovascularisation and finally vessel maturation. This process takes weeks, after which skin grafts or cultured keratinocytes may be applied. One centre used it in 30 patients with good results {Moiemen, 2001} while others have successfully seeded cultured Fb and keratinocytes onto it prior to clinical application. They found superior results when it was done with concurrent skin grafting {Wisser, 2003}. Sheridan and co-workers developed a composite skin replacement (CSR) composed of acellular allogeneic dermis which was seeded with cultured keratinocytes. The CSR was used in 12 paediatric burn wounds and by 14 days, 45.7 ± 14.2 % had vascularised as compared to 98 ± 1 % in split skin grafts {Sheridan, 2001}. However, no

clinical studies on scaffolds with an inherent vascular network or incorporated angiogenic factors have been done.

1.1.3. MICROVESSEL DEVELOPMENT

Human microvasculature begins with arteries dividing consecutively into smaller branches like meta-arterioles (80 – 100 μm) until finally forming capillaries (10 – 15 μm). These vessels serve to redistribute blood and its nutrients whilst lowering the pressure head. This allows blood to perfuse tissue allowing more efficient exchange of metabolites. Eventually, the capillaries unite into post-capillary venules (PCVs), venules and finally veins for the return of waste products. The venular component of vasculature also serve as capacitance vessels {Levick, 2000}.

The vascular tree is formed during the early gestation. Angiogenic cells form clusters which coalesce to form solid tubes which eventually canalise to form blood vessels {Buschmann, 2000}. The outer ring consists of angioblasts which form the vessel walls. The subsequent differentiation of these precursor angioblasts into endothelial cells (EC) and the *de novo* formation of a vascular network are termed 'vasculogenesis'. These vessels are capillary-like to begin with and eventually differentiate into either arteries or veins {Murohara, 2001}. The creation of this framework depends on guidance molecules within the matrix such as ephrins at the arterio-venous interface {Adams, 2000} and reversion-inducing cysteine-rich (RECK) protein for paracellular proteolysis {Welm, 2002}.

The adult vascular network remodels itself by arteriogenesis with the opening up and then the subsequent enlargement of existing collaterals (so called collateral enlargement) as well as the formation of completely new vessels from the already existing vessels (so called arterialisation) {Peirce, 2003}. Micro-vascular remodelling is a mechanistic process delineated to specific tissue type and specific stimuli. Therefore with the exceptions of skeletal muscle responding to exercise and the female menstrual cycle itself, micro-vascular remodelling is limited solely to pathological situations in particular inflammation, wound healing, ischemia, and that of hypoxia together with a few other rare circumstances.

Remodelling is mediated by monocytes and endothelial progenitor cells (EPCs) as shown in figure 1.1 and is a mechanism that is dependent on changes in shear stress. Studies have shown that turbulent flow at low flow rates of 1.5 dynes/cm^2 itself activates ECs while normal laminar shear stress of 8 to 15 dynes/cm^2 does not {Davies, 1986}. In a rabbit femoral artery occlusion model, collateral recruitment occurred within a week with removal of unwanted vessels by three weeks {Hoefer, 2001}. Angiogenesis is the coordinated migration and proliferation of EC and pericytes from the existing vascular bed {Lindner, 2001} and their subsequent maturation and stabilisation by enveloping smooth muscle cells (SMC) {Felmeden, 2003}. Stimulated by hypoxia, these vessels proliferate by either capillary sprouting {Peirce, 2003} or intussusceptions {Burri, 2002} particularly into venules. Vasculogenesis occurs from migrating dedifferentiated EPCs which form tubules {Tepper, 2003}.

Figure 1.1. The series of events illustrating the dual nature of vessel development: angiogenesis and arteriogenesis.

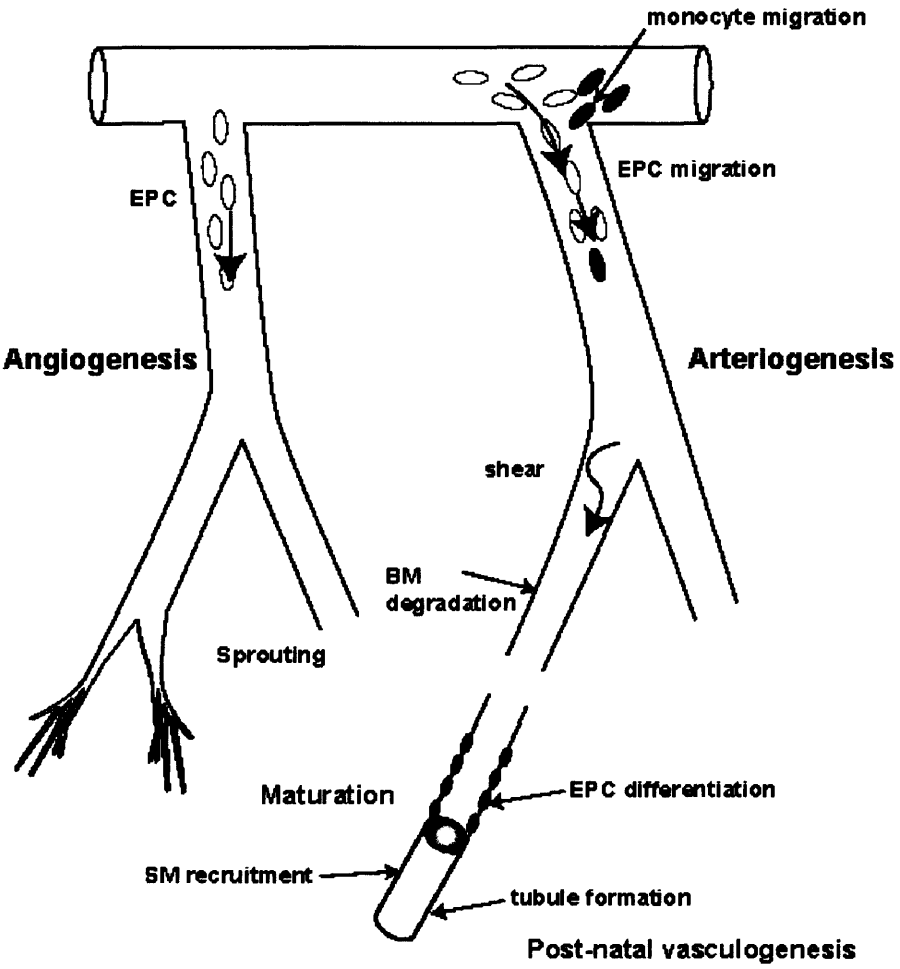

1.1.4. TISSUE PERFUSION

Microvessels divide into numerous smaller branches over a given volume of tissue thus maximising the available area for nutrient exchange. In this microenvironment, stasis of flow is prevented by the Fahraeus-Lindqvuist effect, repulsive charges between blood cells and vessel wall as well as the thin glycocalyx film on the endothelial layer (figure. 1.2) {Levick, 2000}.

Figure 1.2. Factors preventing thrombogenicity at low-flow states.

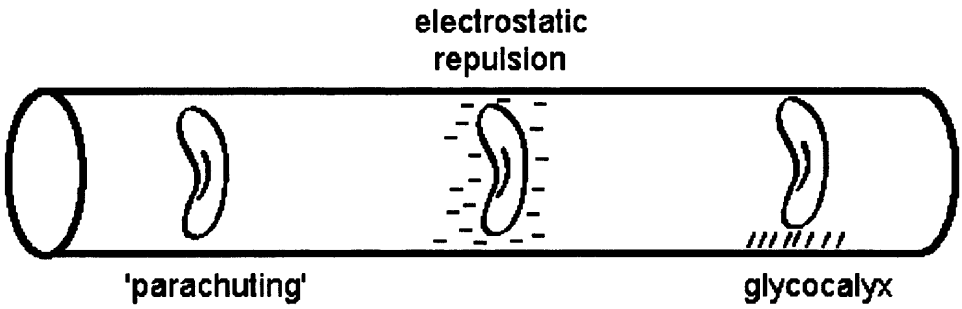

As blood slows down in the meta-arterioles, intra-vascular transit time increases. As this happens, nutrient exchange shifts from flow-limited to diffusion-limited exchange within the capillaries (figure 1.3). Diffusion (D) is dependent on the concentration gradient (C), permeability of the membrane (P) and surface area (S) as represented below,

$$D = -P.S.C$$

P in turn, depends on effective pore area (A) and pore length (L). Capillary exchange is a mixture of diffusion- and flow-limited exchange with the latter being important for the transfer of water-soluble molecules and the former for gas transport.

Figure 1.3. Flow- and diffusion-limited exchange.

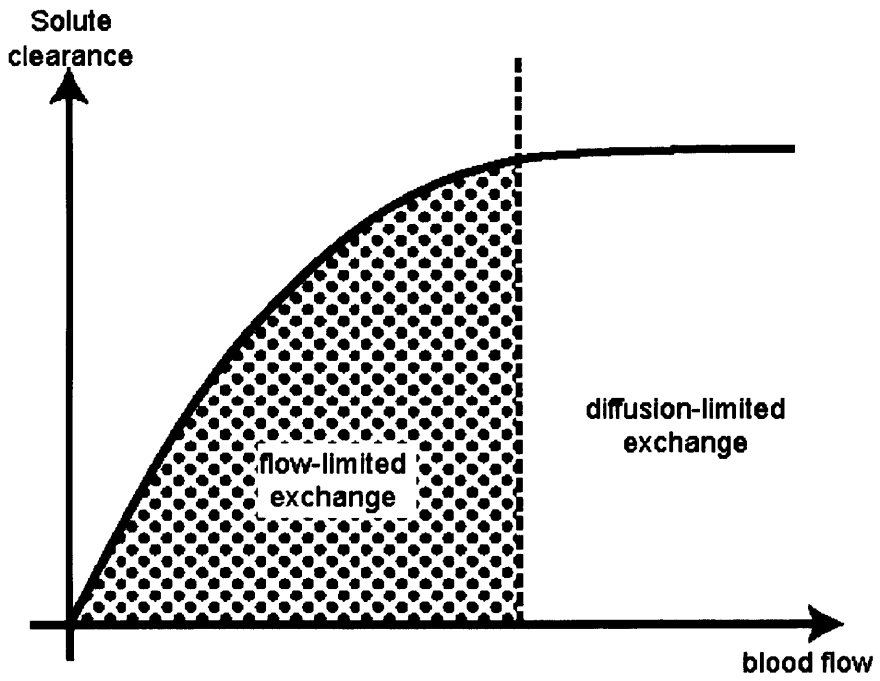

Plasma is a two-phase fluid consisting of solvent and solute phases. While solvents pass unimpeded into the extracellular matrix (ECM), solutes are transported by means of convection (bulk transport) and diffusion {Hughes D, 2000}, represented by the formula,

$$F = Q + D$$

Where F is solute flow and Q is convective flow. Solute efflux is dependent on the rate of solvent transfer within the medium. Solutes like glucose are transported via convection with water (solvent) whilst gaseous exchange is based on Krogh's diffusion model.

This is augmented by the 5 mmHg negative pressure as a result of ECM hydraulic conductivity; the ability of tissue to conduct water across it. Hydraulic conductivity (H) of ECM is proportional to the hydraulic radius of the gel (the ratio of its porosity, P to net surface area of the glycosaminoglycans (GAGs).

$$H\alpha\ \rho/S$$

The interstitial conductivity of ECM is proportional to its hydration and is usually in the range of 10^{-10} to10^{-13} cm^3/s per dyne. This force is balanced by the intrinsic hydraulic resistivity of the ECs lining the microvessels. Studies have shown this to be in the vicinity of 10^{-8} cm^3/s per dyne {Secomb, 1998}. Nutrient exchange depends on the balance between hydrostatic, osmotic and interstitial pressures {Levick, 2000}.

1.2. SEARCH METHODS

All the studies were identified by the following databases; Pubmed, Ovid Online, Infotrieve, Proquest, Science Direct, ISI Web of Science, BioMed Central, Ingenita select, Elsevier texts and Blackwell-synergy searches between years 1966-2003 with the following key words: tissue-engineered blood vessels; vascularisation of acellular tissue; vascularisation of tissue; angiogenesis; vascular tissue engineering; microvasculature; tissue engineered flaps; pre-fabricated flaps; soft tissue engineering; polymers in vascular tissue engineering; capillary beds; microvasculature; polymers in tissue engineering; collage; Dacron; PTFE, alginate.

1.3. TISSUE ENGINEERED MICROVESSEL BEDS

1.3.1. MICROVASCULAR TISSUE ENGINEERING

Microvessel beds provide the vascular infrastructure for living tissue {McGregor, 1995}. The development of independently vascularised artificial tissue requires a source of vascularisation (intrinsic existing blood vessels) and a matrix through which exuding nutrients can perfuse cells {Cassell, 2002}. The matrix functions as a reservoir of growth factors to

induce incoming blood vessel (angioinduction) as well as a scaffold to seed cells like EPCs which participate in the formation of newer blood vessels by the process of arteriogenesis (figure. 1.4). Microvessel networks, artificial matrices and neovascularisation constitute the triad of tissue vascularisation (figure 1.5).

Figure 1.4. The inter-relationship between various models of vessel development.

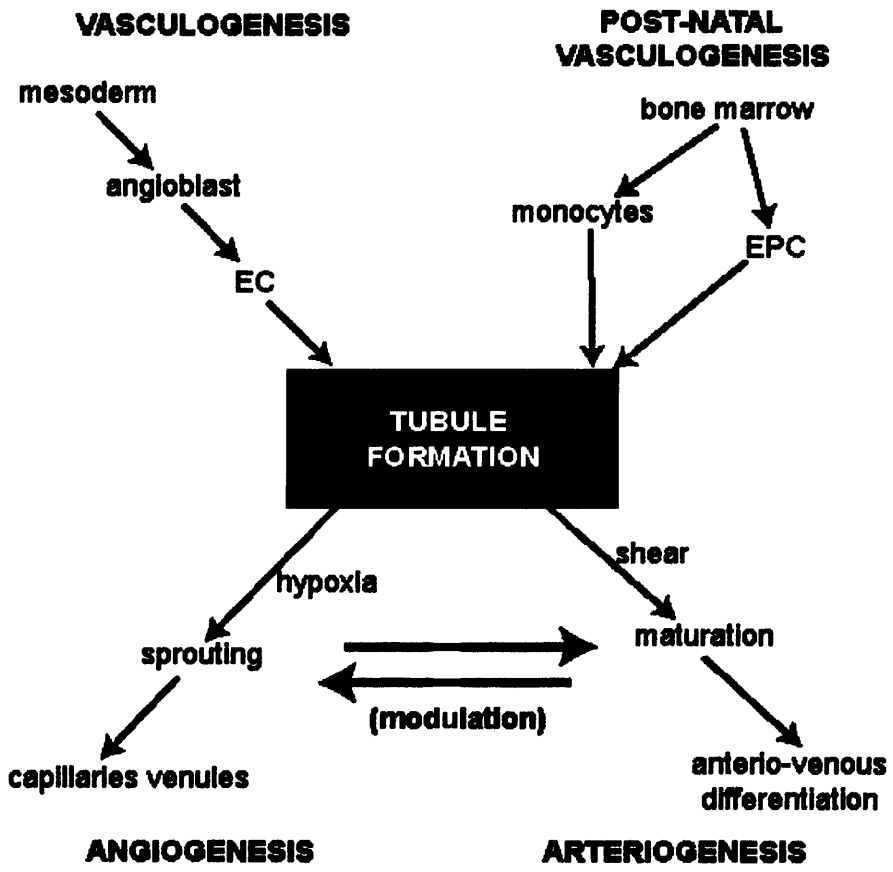

Figure 1.5. The triad of tissue vascularisation.

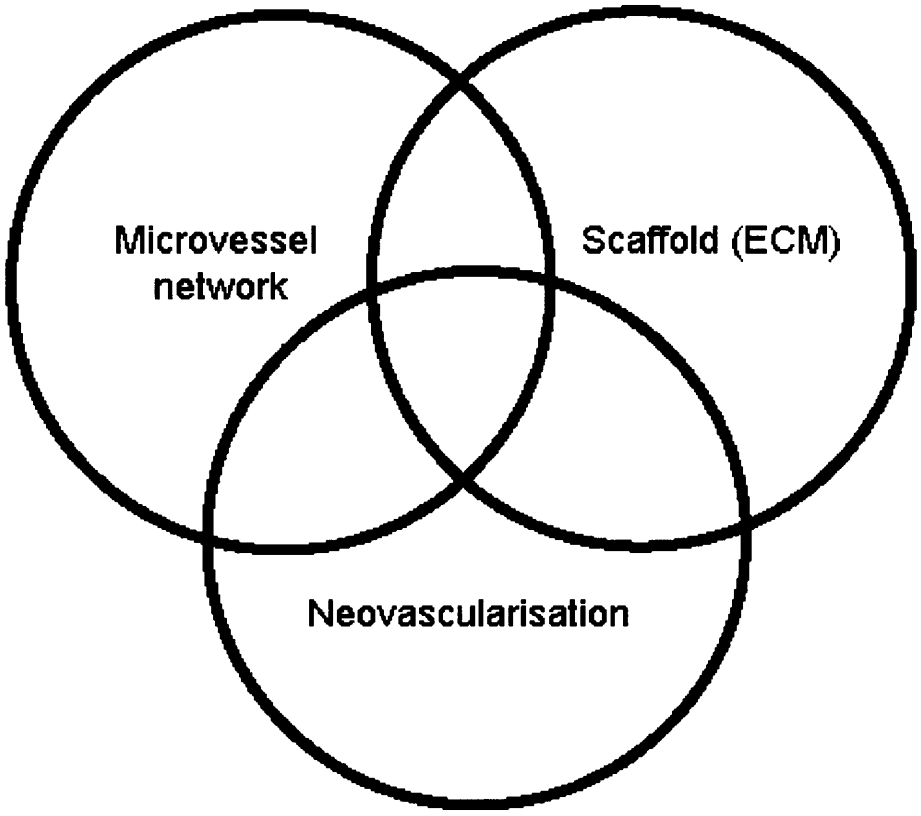

A successful microvascular system depends on the graft material and how it is arranged. The material would have to be non-thrombogenic, have similar compliance to native vessels to avoid intimal hyperplasia {Salacinski, 2001c} at its arterial end and be sufficiently porous to allow nutrient exchange at the capillary level. An artificial capillary network would include small arteries (1 to 2 mm) conducting blood into an arteriolar network (100 to 1000 μm) which would eventually end in capillary-like vessels of 10 to 15 μm. These end-capillaries would need to be within 150 to 200 μm of every target cell {Cassell, 2002} before converging into a venous collecting system. Therefore, both arteriolar and venular components of the scaffold would have to be in close proximity.

1.3.1.1. Types of prostheses

The following section has been subdivided into macro- and microvascular grafts. The reason being that micro-vessels are being developed from previous technology as used in the development of larger macro-vessels and only rarely, are completely new material based approaches used to date. This discussion is necessary to deal with the issues of potential overlaps and discrepancies during the transition between the high flow arterial system and the lower flow capillary system and how in light of these, tissue engineering of micro-vessels differs. The various graft options are summarised in table 1.1.

Table 1.1. Current status of macro- and microvascular grafts.

Authors	Graft Type	Subjects	ID (mm)	Vessels	Patency rates	Comments
{Harris, 2002}	PTFE	Rats	<1	Superficial epigastric	20% at 4 weeks	Vein grafts had 100 % patency
{Demiri, 1999}	PTFE	Rats	1	Femoral	25% at 4 weeks	Vein grafts had 100 % patency
{Seifalian, 2003}	CPU	Dogs	5	Aorto-iliac	100% at 3.5 yrs	Human trials under way
{Shinoka, 1998}	Polyglactin-PGA	Sheep	15	Pulmonary	100% at 7 weeks	Good tissue ingrowth but increase in vessel ID
{Shum-Tim, 1999}	PHA-PGA	Sheep	7	Aorta	100% at 21 weeks	Outer PHA ring prevented increase in vessel ID
{Meinhart, 2001}	EC-seeded ePTFE	Humans	6 to 7	Infra-popliteal	74% at 7 yrs	Comparable to vein grafts
{Lambert, 1999}	Heparin-coated Dacron	Humans	6 to 7	Infra-popliteal	58% at 2.5 yrs	Better results than plain Dacron
{Devine, 2001}	Heparin-bonded Dacron	Humans	7 to 9	Femoro-popliteal	55% at 3.5 yrs	This trial shows better results than PTFE
{Weinberg, 1986}	Collagen-Fb-SMC	*In vitro*	Unknown	_	_	92% EC coverage but weak bursting strength.
{L'Heureux, 1998}	Collagen-EC-SMC-Fb	*In vitro*	4.6	_	_	Comparable bursting strengths to human vessels
{Wilson, 1995}	AAM	Dogs	3 to 4	Coronary	44% at 6 months	All failures due to acute graft rejection
{Teebken, 2001}	AAM	Pigs	5	Carotid	38% at 4 months	Disappointing results due to graft rejection

Keys: AAM, Allogeneic acellularised matrix; ePTFE, expanded polytetrafluoroethylene; Dacron, Polyethylene tetraphthlate; CPU, compliant polyurethane graft; ID, internal diameter; PHA, Polyhydroxyalkanoate; PGA, Polyglycolic acid.

1.3.1.1.1. Macrovascular grafts

While results with PTFE and Dacron™ are satisfactory in peripheral bypass grafts {Meinhart, 2001}, patency is far lower in grafts 6 mm or smaller {Budd, 1991;Schmedlen, 2003;Teebken, 2001}. The primary problem at lower flow rates is thrombogenicity and the increased susceptibility of these vessels to intimal hyperplasia. Dacron™ and PTFE have been found to be increasingly thrombogenic at lower flow states and need surface modification. Luminal modification of vessels using irradiation, presealing and antiplatelet / anticoagulant / growth factor incorporation {Salacinski, 2002a;Salacinski, 2003;Cassell, 2002} to reduce thrombogenicity has been employed {Salacinski, 2001c} but endothelialisation is better {Salacinski, 2000;Salacinski, 2001a}. Endothelialisation of vascular prostheses is dependent on the biomaterial used and pore morphology. Matsuda and colleagues reported that pores between 18 and 50 μm in diameter are optimal for endothelialisation {Matsuda, 1996}. Smaller pores would elicit an inflammatory reaction {Ko, 2001} while increasing pore sizes and porosities improves the radial compliance of vessels {Kowligi, 1988} and hence reduces the likelihood of intimal hyperplasia.

More compliant biomaterials such as poly(carbonate-urea)urethane (PCU) are now being introduced. PCU, currently undergoing Phase I clinical trials in lower limb peripheral grafts, has been found to have similar compliance to native vessels and thus exhibit intimal hyperplasia to a lesser extent {Salacinski, 2002a;Tiwari, 2002}. Therefore it has the potential to be used as the biomaterial of choice to construct the arterial conducting component of artificial capillary beds. Synthetic protein polymers cross-linked by γ-irradiation represents a new generation of biopolymers. Preliminary reports suggest that it has similar elasticity to arteries with a controllable rate of degradation {Urry, 1997}. This recent trend illustrates the limitations of PTFE and Dacron™ at lower flow rates and stresses the need for alternative biomaterials.

1.3.1.1.2. Microvascular grafts (Microvessels)

Microvascular grafts are those with internal diameters of 1mm or less and may be classified into conducting arterial and distributing capillary vessels. The construction of arterial conduits is based on small calibre vascular graft technology. These vessels may be constructed using 1) newer polymers, 2) coating its lumen with heparin or endothelial cells and 3) constructing biological or bio-hybrid grafts *in vitro* prior to re-implantation {Bos, 1998}. As these vessels divide further, they need to branch into a distributing capillary network with larger pore sizes and thinner vessel walls for enhanced nutrient exchange. Although autologous vein grafts, the current gold standard for microvascular repairs, are compliant and non-thrombogenic, they are limited by the need for additional vein harvesting procedures. Furthermore, the construction of artificial vascularised tissue requires an inherent vascular network. Vein grafts are not suitable for this purpose as it is technically impossible to dissect out a capillary bed in its entirety.

As such, efforts have been under way to develop microvascular grafts using common biomaterials. An i*n vivo* study in a rabbit femoral artery model showed a 20 to 25 % patency rate at one month with PTFE microvessels (< 1 mm) while all vein grafts in similar settings remained patent {Demiri, 1999;Harris, 2002}. In order to improve patency rates, luminal endothelialisation has been attempted. In a study, 1 mm interpositional ePTFE vascular grafts in rat aortas, coated with ECM and incorporated with non-tumourigenic human keratinocyte cell line (HaCaT) or Epstein-Barr Virus (EBV) - transformed human B-cell lymphocyte (TOU II-4) cell lines, showed ablumenal vascularisation with the formation of an EC lining five weeks post-implantation {Kidd, 2003}. While this suggests that endothelialisation of these microvessels at lower flow rates is optimal, it is important to note that vascular grafts within young animal

models have been shown to endothelialise over time and as such, these results cannot be extrapolated to human subjects who tend to be older as well {Rashid, 2004;Tiwari, 2002}.

An *in vitro* biological microvascular model has been developed by Neumann and co-workers wherein 80 μm diameter nylon strands were used as templates onto which SMCs in a culture medium could attach to. After a week, this strand was physically removed and the grafts were perfused in a pulsatile flow chamber mimicking the arterial system (figure 1.6). After 28 days in culture, these vessels were shown to have 30 to 40 layers of SMCs evenly distributed throughout the lumen and strong enough to withstand its own weight. Non-absorbable nylon was preferred to absorbable cellulose since constructs based on cellulose had irregular, uneven luminal surfaces {Ko, 2001}. This model has the potential to form arterioles and capillaries *in vitro* which could then be transplanted into living tissue. Further results using ECs in a similar model are being undertaken {Neumann, 2003}.

Figure 1.6. A viable microvessel perfusion system.

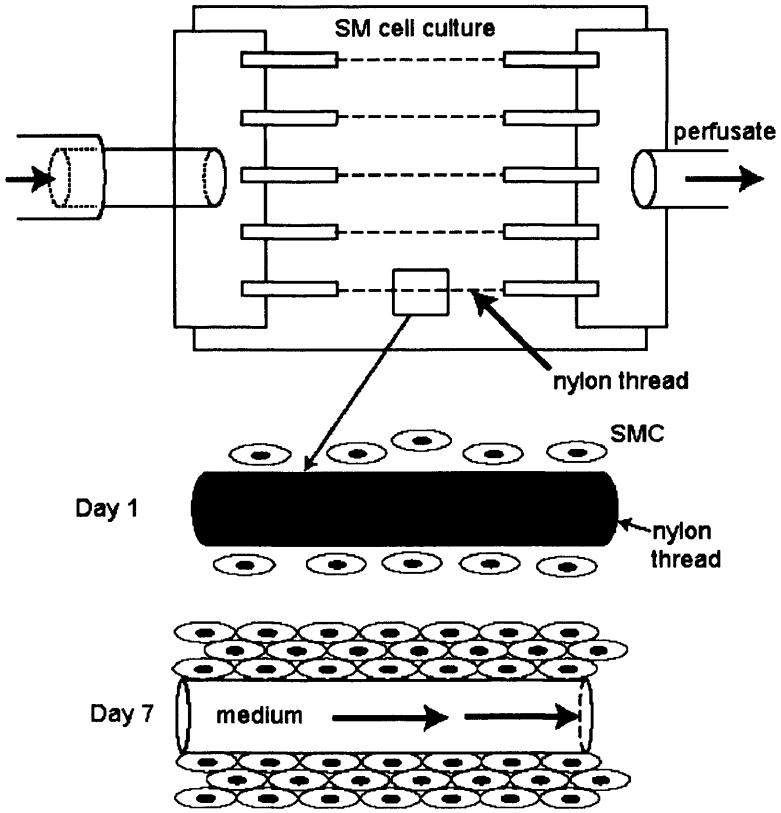

Bio-hybrid microvessels have also been developed *in vitro* using co-cultures of EC and SMC. These cells were passed through polypropylene capillaries at 3 dynes/cm^2 laminar shear stress. ECs lined the lumen of these tubes while SMCs managed to migrate outside these 150μm diameter microvessels through pores (0.5 μm) to form a two separate monolayers as in normal vessels {Redmond, 1995}. EC and SMC adhesion in such constructs can be improved with the use of cell adhesion peptide sequences such as the 'arginine-glycine-aspartate' (RGD) sequences and fibronectin-like engineered protein polymer (FEPP) {Massia, 2001;Merzkirch, 2001}. Although there are no reports of artificial capillary vessels so far, the advent of nanofabrication may soon see functional capillary-sized microvessels (15 to 50 μm) being developed.

1.3.1.2. Configuration of vessels

The limiting factor in metabolite exchange is the extra-vascular distance needed to be traversed. The physiological response to this is to pair up both the arteriolar and venular components together. Between them, numerous small capillaries run across tissue at a cross-sectional density of 1300 per mm^2 with an inter-capillary distance of 34 μm to form a rich perfusing network. This is well within the maximum diffusing distance of oxygen, glucose, carbon dioxide and other waste metabolites {Levick, 2000}. In studies on rat mesentery, it was found that arterioles and venules travelling together formed a 'counter-current' system responsible for auto-regulation and improved nutrient exchange {Harris, 2003}. Therefore, arteries and veins should be paired for greater efficacy.

A study of the temporal relationship of pre-fabricated flaps was performed by inserting a flap of tissue under rat abdominal skin. The femoral arterio-venous pedicles induced flap neovascularisation as early as two weeks post-surgery but it took up to eight weeks for the vascular pedicle to sustain the flap alone {Kostakoglu, 1997}. However in a similar study, the flap was found to survive after its pedicle was divided after three to four weeks {Ouyang, 1996}. Studies on hybrid flaps have also shown that the pedicle can be divided by four weeks, provided a highly porous biomaterial like polyethylene is used along with living tissue as a flap {Karatas, 2000;Can, 1998}.

Tanaka and associates used the rat femoral vessel system to determine whether loop, ligated bundles or flow-through pedicles were most effective in initiating and sustaining tissue perfusion and neovascularisation. Using a collagen I dermal implant in the rat groin, they formed four groups. In the first group, the implant was placed on a recipient bed with no vascular pedicle. In the second group, a vascular loop formed of either an arterial or venous

graft was employed. In the third group, an arteriovenous (AV) bundle ligated at one end was embedded within the matrix and in the fourth group, an AV flow-through graft was placed across the matrix (figure. 1.7). Four weeks later, the matrices were sectioned and stained. Matrices from group two showed the greatest increase in volume with flow rates of up to twenty times normal. However compared to the third group, it had less tissue organisation. AV ligation (group three) showed the densest vascularity and maximal tissue regeneration with predominant sprouting from the venous end. They concluded that while an AV loop quantitatively increased capillary and new tissue formation, ligating the loop ensured better tissue organisation {Tanaka, 2003}.

Figure 1.7. The effect of vessel configuration on tissue vascularisation. Group I – control (acellular dermis), Group II – Arterio-venous loop embedded in the matrix, Group III – Arterio-venous bundle ligated within the matrix, Group IV – flow-through graft.

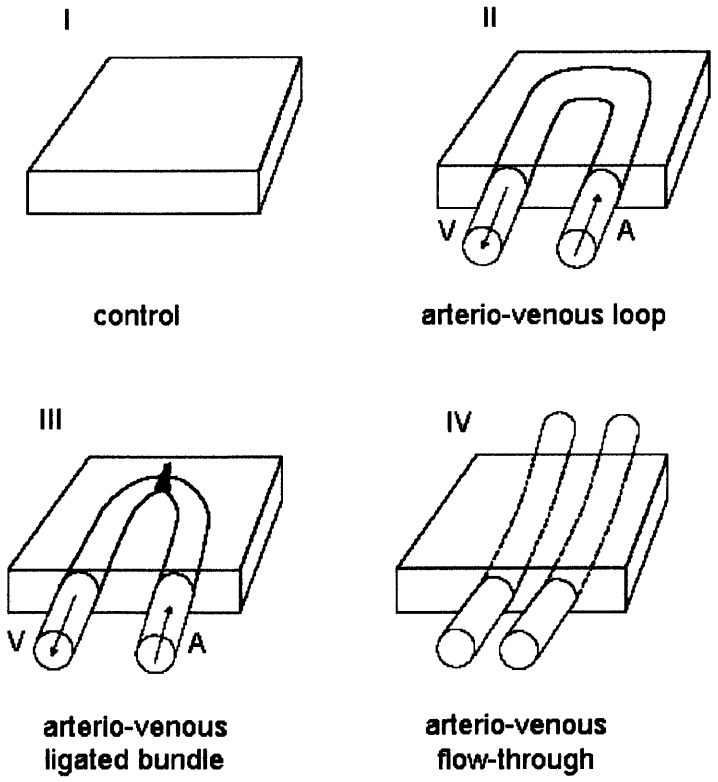

1.3.2. EXTRACELLULAR MATRIX SCAFFOLDS

Once a microvascular network is constructed, how and where do we place it ? How would nutrients from blood migrate across the blood-cell barrier into the surrounding areas and perfuse cells. This parameter is regulated by the extra-cellular matrix (ECM). In this section, we refer to the ECM scaffold into which a vascular network would be placed.

In the biological setting, ECM is composed of collagen, fibronectin, laminin, GAGs and water {Badylak, 2002}. Fibroblasts synthesise non-cellular components of the matrix as shown

in table 1.2. Using acellular dermal grafts in Sprague-Dawley rat groins, matrices were pre-fabricated by vascularising them with the superficial epigastric vessels. Histological analysis showed infiltration by mononuclear cells within the first 72 hours with neo-vascularisation occurring between days 3 and 14. Simultaneously, SMC and EC were laid along the lines of stress. Devascularised matrices (control group) had a 90 % hernia rate while those with an intact vascular pedicle within had no evidence of a hernia ($p<0.01$). Therefore, it was concluded that vascularised scaffolds were structurally and functionally superior to non-vascularised ones {Chung, 2003}.

Table 1.2. Non-cellular components of ECM and their function {Badylak, 2002}.

Component	**Function**
Collagen type I	Structural framework
Collagen type IV	Basement membrane for EC attachment
Collagen type VII	Keratinocyte attachment
Fibronectin	Cell adhesion
Laminin	Protein adhesion
GAGs	Cytokine and growth factor binding

1.3.2.1. Biomaterial substitutes

The ideal matrix to sustain a vascular network should be biocompatible, porous, supportive to its inherent vascular network, readily available, permeable to incoming vessels or chemicals, non-immunogenic, biodegradable, inert, have a slow-release mechanism and lastly, it would be convenient if it could be administered as an injectable. Such tissue-engineered constructs would act as temporary scaffolds which maintain cells in-situ whilst inducing neovascularisation.

Eventually, the existing ECM matrix will be replaced by the products of newer cells such as collagen, laminin, elastin, GAGs or fibronectin. These undergo continuous remodelling {Driessen, 2003} as depicted by figure 1.8 and ultimately reorganise into near-normal tissue {Nor, 2001}. Current ECM scaffolds can be classified into natural and synthetic types each with its own advantages and disadvantages. Natural biomaterials are characteristically biodegradable, non-immunogenic and bio-compatible. A list of natural ECM available is summarised in table 1.3.

Figure 1.8. The effect of cell traction on tissue patterns.

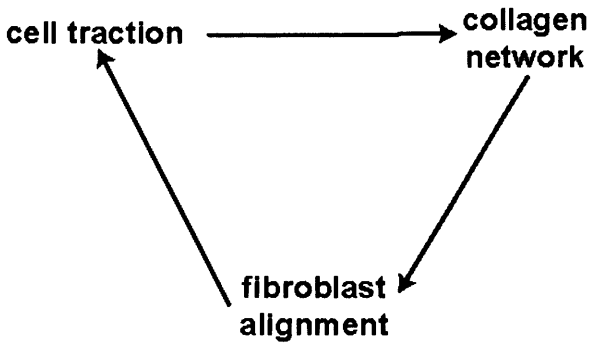

Table 1.3. Natural materials used in ECM constructs

Biomaterials	Composition	Characteristics	Comments	Modifications	References
Alginate	β-D-mannuronic acid + α-L-glucuronic acid	Temperature-independent gel	Burst release	Microsphere / bead incorporation, heparin cross-linkage(controlled release), RGD-peptide sequence incorporation	{Draget, 1997;Halberstadt, 2002;Kikuchi, 2002;Tanihara, 200
Agarose	Agarose	Solid gel	Sub-optimal release	Heparin addition (increase factor load)	{Watanabe, 1998}
Hyaluronic acid (HA)	Glucuronic acid + N-acetyl D-glucosamine (linear GAG)	Biodegradable gel, biocompatible, +/- photopolymerisable	Angio-inhibitory, degradation products are angiogenic, non-adhesive to cells	Chitosan cross-linkage (improves angiogenesis), RGD sequences (improve cell adherence), methacrylate addition	{Slevin, 2002}
Fibrin glue	Fibrin monomers	Injectable gel *	Structurally weak	Heparin cross-linkage(controlled release)	{Shireman, 2000}
Collagen / gelatine	Type I collagen (atelocollagen)	Porous and permeable.	Low factor-loading capacity	Heparin cross-linkage	{Kuberka, 2002}
Matrigel	Collagen type IV + laminin + entactin + proteoglycans	Inert, permeable, injectable gel	Structurally weak	None	{Montanez, 2002}

Keys: * Ideal for local delivery.

1.3.2.1.1. Natural

Alginate is an anionic polysaccharide composed of ß-D-mannuronic acid and α-L-glucuronic acid cross-linked in a gel by non-toxic levels of calcium ions. It has been incorporated with various growth factors like basic fibroblast growth factor (bFGF), VEGF and heparin within microspheres {Kawada, 1999}. Alginate gel is a hydrogel system that is independent of temperature changes {Draget, 1997} but tends to release its chemicals within 4 days {Elcin, 2001}. This can be overcome by incorporating microspheres and peptides {Kikuchi, 2002} or cross-linking with heparin {Tanihara, 2001}. Alginate gels modified with RGD peptide sequences {Halberstadt, 2002} and syngeneic fibroblasts formed strong gels and were more tissue-like {Marler, 2000}. An agarose gel cross-linked with heparin has been used to deliver basic FGF beads to the porcine myocardium but delivery characteristics are still sub-optimal {Watanabe, 1998}.

Hyaluronic acid (HA), a linear glycosaminoglycan (glucuronic acid N-acetyl D-glucosamine) has good biocompatibility and is degraded by hyaluronidase. However, it has poor adherence and inhibits EC proliferation while its degradation products are pro-angiogenic {Slevin, 2002}. To improve this, chitosan; a glycosaminoglycan (N-acetyl D-glucosamine), has been added to HA to form a composite material in the synthesis of endotheliased human skin equivalent {Black, 1999}. Chitosan attracts neutrophils and activates macrophages {Chupa, 2000}. Microspheres filled with FGF within similar constructs were used to improve neovascularisation in rat tissue {Elcin, 1996}. The addition of methacrylate groups to HA, followed by exposure to light of 480 – 520 nm wavelengths could photopolymerise composite HA gels into any given shape with minimal gel swelling. RGD sequences could also be added to the composite to improve cell adherence. *In vitro* studies on this composite showed improved fibroblast viability and proliferation compared to standard HA gels {Park, 2003}.

Fibrin glue derived from blood clots is useful as an injectable medium for the local delivery of growth factors like VEGF. Burst release is a problem which is overcome by the incorporation of heparin for better control {Shireman, 2000}. Collagen type I is highly porous (pore sizes of 50 to 150 μm) and has been seeded with Fb or pre-adipocytes {Kuberka, 2002}. Chondrocytes embedded within three-dimensional collagen gels were found to be viable and capable of synthesising proteoglycans (PG) {Weiser, 1999}. Unfortunately, loading factors onto it is difficult but this can be overcome by cross-linking collagen gels with heparin. This has been shown to increase the incorporation of angiogenic factors sufficiently to culture human umbilical vein cells (HUVEC) *in vitro* {Wissink, 2000}. ECM gel (Matrigel™) that is composed of basement membrane proteins has been used *in vitro* as scaffolds {Montanez, 2002} but has so far few clinical uses. In addition, concerns have been raised regarding its tumourigenic origin {Zisch, 2003}. Other natural substitutes used are porcine intestinal sub-mucosa {Hodde, 2002}, acellular dermis, cadaveric fascia and amniotic membrane {Hodde, 2002}. The most significant drawback of these ECM substitutes is that they are structurally weak with unmodulatable hydraulic conductivity.

1.3.2.1.2. Synthetic

A broad range of polymer have been employed in developing ECM scaffolds into which cells could be seeded. Depending on the site of implanting these tissue engineering constructs, namely cartilage, bone, nerve or vascular grafts, the choice of these polymeric component of the scaffold is made. Current polymers such as poly-(propylene fumarates)/ PPF, poly-anhydrides (PA), polyglycolic acid (PGA), polylactic acid (PLA), poly-carbonates (PC), polylactone (PL), polyurethanes (PU), poly(orthoesters)/POE, polyphosphazenes (PPZ) and poly(ethylene-

terephthalate)/PET have different physical and chemical characteristics which are then optimised for a specific purpose. For instance, PET is suitable for vascular grafts{Kikuchi, 1998}. These are being used with increasing frequency in biomedical devices.

Polyglycolic acid (PGA) is inelastic polyester with high crystallinity (46-50 %). It is degraded by the diffusion of water followed by hydrolysis of the crystalline elements of the polymer into glycolic acid {Chu, 1981}. Polylactic acid (PLA) is less crystalline than PGA but more hydrophobic, making it less susceptible to hydrolysis. Poly(lactide-co-glycolide) / PLGA co-polymer in the amorphous form is a high porosity, open-pore system which degrades in 2 to 6 months by means of hydrolysis of the ester bonds {Vert, 1994}. A significant drawback is that angiogenic factors incorporated within it tend to leach out. This can be rectified using microsphere, beads or bioactive foams {Lenza, 2003} for slower release of chemicals. Experiments using microspheres containing recombinant VEGF within PLGA foams which were then implanted into rat fascial flaps, showed a more controlled release of growth factors {Linn, 2003}.

1, 3 - trimethylene carbonate (TMC) and D, L - lactide (DLLA) (19:81, molecular weight ratio) are amorphous co-polymers of PLA. Salt-leaching these polymers produced foams of high pore interconnectivity and porosity with an average pore size of 100 μm. Cardiomyocytes grown on it were able to adhere and proliferate indicating that TMC-DLLA co-polymers are not cytotoxic. *In vitro* signs of degradation occurred by four months via hydrolysis {Pego, 2003}. When these polymers were implanted subcutaneously in rats, degradation started at three weeks and by one year, 96 % of its mass was lost. These co-polymers also elicited a sterile and acute inflammatory reaction resulting in the formation of a capsule *in vivo* {Pego, 2003}. Degradation was far more rapid in poly-TMC polymers (three weeks). Silica-based poly(dimethylsiloxane)/PDMS has been polymerised with PLA-PGA composites to form PLGA/TEGOMERS which have shown to be biocompatible, supportive to cell growth and non-

toxic {Porjazoska, 2002}.

Experiments with microvascular cell cultures mainly involve PLA, PGA or their composite scaffolds. These are summarised in table 1.4. PLs like poly-CL are biocompatible with prolonged degradation times of up to three years *in vitro* {Middleton, 2000}. Combining CL with TMC slows down degradation of the primary TMC polymer {Pego, 2003}. The mechanism of degradation is hydrolysis with caproic acid, the by-product. Its disadvantage is that it is structurally weak.

Table 1.4. Synthetic materials used for ECM construction in various tissues such as bone, cartilage, skin etc.

Polymer	Compressive strength	Synthesis	DT (months)	By-products	Advantages	Disadvantages	References
PGA	7.5 GPa	E/M/C	6-12	Glycolic acid	Porous, biocompatible, non-toxic, non-inflammatory, natural waste metabolite	Not pliable	{Chu, 1981}
PLA	2.7 GPa	E/M/C	>24	L-lactic acid	Porous, biocompatible, non-toxic, slower degradation, natural waste metabolite	Hydrophobic	{Gunatillake, 2003}
PLGA	1.9 GPa	E/M/C	12-16	D,L-lactic acid	Porous, biocompatible, non-toxic, non-inflammatory	Excessive leakage	{Vert, 1994}
PL	0.4 GPa	E/M/C	>24	Caproic acid	Non-toxic, biocompatible	Weak structure	{Middleton, 2000}
PPF	2-30 MPa	Injection	≈ 30	Fumarate, polyethylene glycol, poly (acrylic-co-fumaric) acid	Non-toxic, biocompatible, minimal inflammation, photo-cross linkage, strong	Not significant	{Peter, 1998;Peter, 1997}
PA	1.3 MPa	Thermoplastic	12 (*in vitro*)	Dicarboxylic acids	Biocompatible, thermoplastic, surface erosion, angioinductive	Weak	{Erdmann, 2000}
PC	Sufficient for load-bearing	Thermoplastic	Very slow	Tyrosine, CO_2 and alcohols	Porous, biocompatible, thermoplastic, osteoconductive	Acidic byproducts	{Muggli, 1999}
PU (LDI)	8-40 MPa	Thermoset	1-2	Lysine, glycolic acid, caproic acid	Biocompatible, strong, pliable	Some PUs (TDI) are toxic	{Gunatillake, 2003}
PPZ	Sufficient for load-bearing	-	-	Phosphates and ammonia	Biocompatible, osteoconductive, strong	Not significant	{Gunatillake, 2003}
POE	Sufficient for load-bearing	-	Regulatable with lactide	Carboxylic acids	Biocompatible, osteoconductive, strong	Not significant	{Ng, 1997}
PEEU	Tensile strain (9-29 MPa)	-	-	-	Biocompatible, strong	Poor cell adhesion	{Guan, 2002}
PPy	-	-	<13	-	Electrical conduction, minimal inflammation	-	{Jiang, 2002}

Keys: C, casting ; DT, Degradation time; E, Extrusion; M, moulding; '-', unknown.

PPFs are polyesters based on fumarates. They can be injected into any space and further photo cross-linked by adding methacrylates {Peter, 1998}. PPFs are structurally strong and capable of withstanding great loads. *In vitro* degradation (up to 200 days) occurs following hydrolysis of its ester bonds to form fumaric acid; a natural metabolite, propylene glycol and poly (acrylic acid-co-fumarate) {Peter, 1997}. Apart from being biodegradable, PPF has also been found to be non-cytotoxic with minimal inflammatory reaction *in vivo* {Peter, 1998}.

PA forms soft tissue constructs being biocompatible, thermoplastic with controlled degradation characteristics (surface erosion). It is a weak polymer limiting its use in load-bearing devices. It may be strengthened by the addition of imide groups {Attawia, 1995}. PAs are degraded by hydrolysis of its anhydride bonds by 12 months *in vitro* into dicarboxylic acid {Erdmann, 2000}. *In vivo* implantation of these polymers, show evidence of good vascularisation of itself by four weeks {Laurencin, 1990}.

PCs are thermoplastic and strong enough to sustain heavy compressive loads. Their advantages are that they are biodegradable, biocompatible and have very low rate of degradation. However, hydrolysis of its carbonate groups culminates in the formation of acidic by-products. This is an undesirable property for an ECM substitute {Gunatillake, 2003}.

Bioelastic materials; monomeric protein polymers which convert heat or chemical energy into mechanical energy represent the next generation of polymers. Heat exchange, hydrophobicity or hydrophilicity induces a mechanical tensile force within the polymer that is mediated by competition between the molecules for hydration. These forces modulate cells within the construct to form micropatterns and secrete new ECM. This process is called cellular tensegrity or mechanotransduction {Urry, 1999}. An example would be poly (N-isopropylacrylamide) which can mechanically reconfigure themselves with changes in

hydrophilicity and temperature {Kikuchi, 1998}.

1.3.2.1.3. Sol-gel systems

Gels are composed of three components namely solute, solution and voids with the three in equilibrium with one another {Aamer, 2004}. A typical gel is poly-ethylene glycol (PEG). As shown in figure 1.9, polymer molecules are initially functionalised with adhesion factors. These are then cross-linked via the formation of reactive termini. Cells migrating into this matrix break down the cross-linking peptide leading to local degradation and hence release of the incorporated factors such as heparin and VEGF {Zisch, 2003}. These synthetic gels need to be bio-degradable and cell-responsive {Lutolf, 2003}. Using a PEG-based polymer, by shortening the block length from a mean molecular weight of 930 to 6090 kDa, biodegradation of the hydrogel could be minimised {Shin, 2003}. The same effect has been shown in triblock co-polymers of poly (L-lactide)/PLLA and poly(ethylene oxide) (PEO) / PLLA-PEO-PLLA {Aamer, 2004}.

Figure 1.9. The synthesis of biomimetic gels.

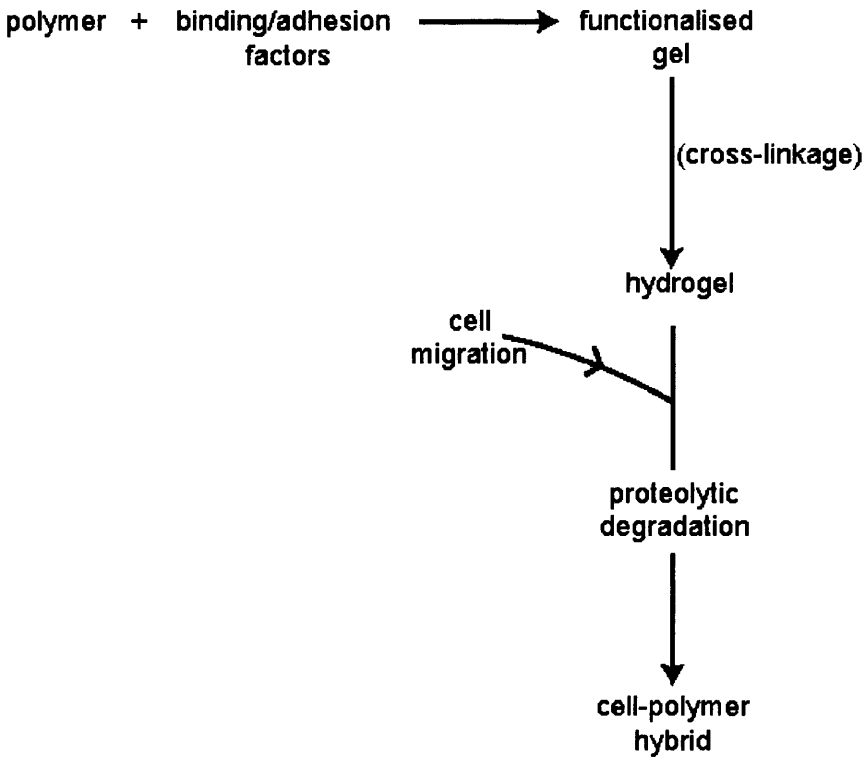

Photo-polymerisable poly-vinyl alcohol (PVA) hydrogels {Nguyen, 2002} are injectable. As such, it is possible to place these gels *in vivo* using minimally invasive procedures and then allowing cross-linkage to occur. This gel was found to be highly elastic and strong. Since cell adherence was poor, these constructs were modified with the RGD peptide sequence {Schmedlen, 2002}. This principle was used by Cao and colleagues to immobilise ovalbumin within a 3-D hydrogel {Cao, 2002}. De Rosa and co-workers proposed a polyelectrolyte gel with a cationic surface charge across it. These charges increased the adhesion of Fb to the gel as well as their proliferation thereby minimising the risk of fibrous encapsulation {De Rosa, 2004}.

1.3.2.2. Superstructure

Superstructure refers to the integration of two-dimensional pores or structures into a three-dimensional (3-D) configuration whereby these overlap in a regular or irregular pattern. In polymers, the former confers crystallinity and the latter, amorphous characteristics. The superstructure of a polymer determines pore characteristics. Studies have shown that cells aggregate less within smaller pores and these smaller aggregates proliferate to a lesser extent {Ma, 1999}. Hence, in scaffolds with smaller pore sizes and volumes, cells spread faster {Li, 2001}.

Superstructures exist in three main forms namely textile (woven/knitted), open-pore and angiopolar systems. The angiopolar principle involves spatially orientating pores within matrices to induce cells, microvessels and nutrients to propagate in a given direction {Wintermantel, 1996}. Pores within biopolymers may be classified into macropores ($\approx$ 500 μm), mesopores (20 -30 μm) and micropores (<10 μm). Macropores regulate the optimum cell type and seeding density within a construct. Mesopores allow microvessels to infiltrate the polymer. It has been observed in early *in vivo* studies on rats that arterioles and venules tend to proliferate on the inner surface of mesopores while capillaries lined its outer surface {Wintermantel, 1996}. Lastly, micropores function as regulator of molecular transport within a polymer system. Pore characteristics may be modulated depending on the method of polymer synthesis like extrusion, leaching, casting, moulding or electrospray.

1.3.2.3. Cells seeded onto matrices

Seeding cells onto a matrix is integral to the formation of a bio-hybrid scaffold as cells like fibroblasts and chondrocytes secrete extra-cellular matrix (ECM). However, long-term cell viability in such artificial constructs is a limiting factor as these cells have to remain viable *in vivo* until neovascularisation occurs. Fibroblasts are the most abundant cells within the ECM but scaffolds seeded with fibroblasts tend to contract following *in vivo* implantation, thus impairing fibroblast migration. In a study comparing pure and GAG-chitosan-collagen sponges, the latter minimally contracted and showed a 300 % increase in fibroblast proliferation at six weeks compared to pure collagen sponges {Vaissiere, 2000}. This was augmented by incorporating RGD-peptide sequences to improve fibroblast attachment and proliferation {Shu, 2004}. Engineered cartilage using chondrocytes has the potential to act as a viable ECM scaffold (as these cells have low metabolic rates and require minimal perfusion), into which micro-vascular networks can actively proliferate and grow. Embedded chondrocytes within fibrin glue showed that these cells can maintain viability in a non-vascularised environment {Sims, 1998} although chondrocytes alone forms rigid tissues. Brown and co-workers developed a hybrid chondrocyte-SMC with a compressive modulus between muscle and cartilage {Brown, 2000}.

Research has demonstrated that fat has potential as a bulking agent, however the difficulties associated with the extraction of adipocytes and their subsequent culture, this being the propensity for intra-cellular lipid vacuole bursting has rendered their usage in tissue engineering to be extremely limited. Pre-adipocytes extracted from the epididymal fat pads of Sprague-Dawley rats proliferated *ex vivo* {Patrick, 1999} on PLGA scaffolds up to two months following implantation but viability decreased thereafter. However, the study did not mention whether these cells survived by neovascularisation or diffusion. Pre-adipocytes attached maximally to hyaluronic acid scaffolds with mean pore sizes of 400 μm {Halbleib, 2003}. Pre-laminating

these cells layer onto layer *in vitro* improved its vascularisation characteristics {Garfein, 2003}. Fatty tissue from lipoaspirate (LPA) has been shown differentiate into many cell lines and hence form a source of stem cells {De Ugarte, 2003}. Injecting the cDNA of VEGF into scaffolds further improves vascularisation prior to actual cell seeding {Soker, 2000}.

1.3.3. VASCULARISATION

While scaffolds and microvessels are essential components of a capillary bed, it is equally important for the tissue-engineered device to connect to the host tissue. This would entail the induction of incoming microvessels into the scaffold (angioinduction) as well as allow the inherent microvessels to grow out and meet these vessels (inosculation).

1.3.3.1. Inosculation

The presence of an inbuilt micro-vascular network itself within a matrix is insufficient unless the intra- and peri-vascular regions are seeded with ECs, SMCs and fibroblasts. Therefore for the growth of vessels within an engineered vascularised tissue construct out into the host tissue, it is necessary for these to either "link" or "hook-up" with the host's vasculature, this process is a term described as inosculation. While ECs confer non-thrombogenicity to the graft, circulating haematopoietic stem cells such as EPCs are capable of stimulating the formation of a vascular network (post-natal vasculogenesis) {Masuda, 2003}. Their sources are the bone marrow, mononuclear cells and the vessel wall. These cells can be harvested by enrichment following extraction or *ex vivo* cultures {Kalka, 2000}. Once these cells are injected into the circulation, EPCs move on to sites of neovascularisation (therapeutic vasculogenesis)

{Murohara, 2000}.

Early studies on vasculogenesis used cells like quail blastodiscs, murine embryonic stem cells, HUVEC and human pulmonary microvascular endothelial cells (HPMEC) grown on collagen, fibrin, gelatin and methylcellulose matrices (table 1.5). These cells have been shown to grow into capillary-like tubes (CLTs) which may be controlled by altering the growth factor gradient or biomechanical tension across the gel. While in culture, tissues can be genetically modified by transfecting them with viral vectors. Over-expression and carcinogenicity are a problem. Alternatively, cells like SMCs could be transduced with multiple genes and then be allowed to repopulate the microenvironment (transgenesis). SMCs were harvested from tissue enzymatically and cultured serially until differential cell adhesion molecules are removed. Next, the SMCs were magnetically extracted and incubated with high-titre retroviral supernatants. 99% of these cells were successfully transfected {von Degenfeld, 2003}.

Table 1.5. *In vitro* developmental models of angiogenesis and vasculogenesis.

Cells	CLS formation (day)	Morphogenesis induction	Matrix	Spatial organisation	References
Bovine Capillary EC	2-3	Spontaneous	Collagen I sandwich	3-D	{Montesano, 1983}
Embryonic Stem Cells	12	Spontaneous embryoid body formation	Culture dish	3-D	{Doetschman, 1985}
Muscular Tissue Fragments Adipose Tissue Frag.	3-12	Spontaneous	Fibrin + Collagen I	3-D	{Montesano, 1987}
Bovine Aortic EC, Adrenal Capillary EC, HUVEC	1	Spontaneous	Fibrin	2-D	{Olander, 1985}
Bovine Capillary EC	5-15	Cytokines	Collagen I	3-D	{Montesano, 1986}
Bovine Capillary EC	2-3	Phorbol ester	Fibrin	3-D	{Montesano, 1987}
Human Umbilical Vein EC, HDMEC	1	Spontaneous	Matrigel	2-D	{Kubota, 1988}
Bovine Capillary EC	1-2	Spontaneous-cytokines	Fn + Collagen IV + Matrigel	2-D	{Ingber, 1989}
Rat Aortic Explants	7	Spontaneous	Fibrin + Collagen I	3-D	{Nicosia, 1990}
Bovine Aortic EC	10-18	Spontaneous	Collagen I	2-D	{Vernon, 1995}
Human Umbilical Vein EC	1	Spontaneous	Fibrin I or II sandwich	3-D	{Chalupowicz, 1995}
Rat Fat Microvessels Fragments	4-6	Spontaneous	Collagen I	3-D	{Hoying, 1996}
Calf Pulmonary Aortic EC	2-7	Spontaneous-cytokines	Fibrin in micro-carriers	3-D	{Nehls, 1996}
Human Umbilical Vein EC, Bovine Retinal EC	1-2	Spontaneous	Fibrin	2-D	{Vailhe, 2001}
Embryonic Stem Cells	11	Spontaneous embryoid body formation	methylcellulose	3-D	{Vittet, 1996}
Human Placental Blood Vessels	7-21	Spontaneous	Fibrin	3-D	{Brown, 1996}
Mice Microvessel Fat Pad	14	Spontaneous-cytokines	Collagen gel	3-D	{Vailhe, 2001}
Bovine Aortic EC, Human HUVEC	3	Spontaneous	Fibrin + Collagen I	3-D	{Korff, 1999}
Human Marrow Microvascular EC	21-50	Spontaneous-cytokines	Fn + Collagen I	2-D	{Pelletier, 2002}
HDMEC	5-7	Spontaneous	Sterilised donor dermis	3-D	{Sahota PS, 2003}

Keys: EC, endothelial cells; HUVEC, human umbilical vein endothelial cells; HDMEC, human dermal microvascular endothelial cells; Fn, fibronectin.

EC have been sourced from arteries, veins, omentum, subcutaneous fat {Tiwari, 2001} and skin {Sahota, 2003}. Using enzymatic degradation, EC are harvested from vein grafts by either the cannulation or eversion technique and cultured for 5 to 6 weeks. Grenier and co-workers have introduced a method of obtaining EC, SMC and fibroblasts from the same vein biopsy {Grenier, 2003}. Isolation of EC from fatty tissue requires it to be minced, enzymatically digested, centrifuged in a Percoll gradient before extracting EC using magnetic beads {Tiwari, 2001}. Alternatively, ECs from the microvascular environment may be derived from skin as HDMECs {Sahota, 2003}.

Prior to *in vivo* implantation, EC or EPCs would need to be seeded onto scaffolds. The seeding density would depend on the scaffold material, its porosity and the method of cell inoculation. The standard mode for promoting cell attachment is to culture cells onto the polymer with or without adhesion molecules. A disadvantage is that cells tend to adhere only to the outer layers of the scaffold. In order to achieve more homogenous implantation throughout a three-dimensional scaffold, other methods like the 'drop on' and low-pressure centrifugation techniques which systematically seed cells onto scaffolds have been introduced {Halbleib, 2003}.

Human adipose stromal cells placed within microcarriers and co-cultured with HUVECs were grown in a serum-free static culture model with the addition of angiogenic factors. By day 16, stable CLTs with patent lumens were formed by outgrowing ECs. Larger loops coalesced while smaller ones regressed, similar to the 'pruning' phenomenon that is observed during embryological development of the vascular system. *In vitro* this is termed 'guided migration'.

Clinically, the larger the microvessel, the greater the perfusion {Hershey, 2001}. An *in vivo* model wherein HDMEC seeded onto biodegradable polymer matrices were put into

immunodeficient mice showed the following characteristics. On day 1 EC migrated through the matrix, on day 5 they formed CLTs and by one week had differentiated into functional microvessels. Maturation occurred by 21 days and these microvessels eventually linked up with the host vessels {Hudon, 2003;Black, 1998}. Immunohistochemical analysis of a murine myocardial model showed that monocytes / macrophages produced holes through the myocardium using proteolytic enzymes, the lumens of which were eventually colonised by EPCs {Moldovan, 2000}.

1.3.3.2. Angioinduction

The process of inducing incoming microvessel formation depends on the growth factors used and the method of delivery. Their angiogenic effects were studied using *in vivo* models like chorio-allantoic membrane (CAM) {Ribatti, 2001;Borges, 2003}. FGF and VEGF are mainly involved in vasculogenesis. Angiogenic sprouting is mediated by transforming growth factor- β (TGF-β) while maturation of vessels is via angiopoietin-1 and -2 (Ang-tie) and platelet-derived growth factor (PDGF) pathways {Van Den, 2003}. Their effects are summarised in table 1.6.

Table 1.6. Role of angiogenic growth factors during vascular development {Van Den, 2003}.

Event	Factor	Receptor	Action
Angioblast induction	FGF	FGFr	Angioblast formation
Conversion of angioblasts to EC	VEGF	VEGFR2 / Flk-1	EC formation
EC formation into tubes	VEGF	VEGFR2 / Flk-1	Primitive vascular plexus
Angiogenic sprouting	VEGF	VEGFR-2 / Flk-1, VEGFR-1/Flt-1	Angiogenesis
EC activation	TGF-β_1	ALK-1, ALK-5	Angiogenic modulation
Vessel thickening	Angiopoietin-1	Tie-1	Vessel stabilisation
Smooth muscle recruitment	PDGF-β	PDGFR-β	Vessel stabilisation
Vessel thinning	Angiopoietin-2	Tie-1 and Tie-2	Antagonistic to Angiopoietin-1
Arterio-venous differentiation	Ephrin B2	Eph B_4	Remodelling

Keys; FGF, fibroblast growth factor; VEGF, vascular endothelial growth factor; TGF-β_1, transforming growth factor beta-1; PDGF-β, platelet-derived growth factor-beta.

The primary stimulus and factor causative for the process of capillary sprouting is hypoxia. Within 30 minutes of its onset, early growth response factors (Egr-1 and -3) are expressed {Lyn, 2000}. VEGF modifies the ECM to allow EC and fibroblast migration {Cassell, 2002; Hershey, 2001}, acting on the venules, it increases their permeability. Subtypes A- and B- are generally involved in EC migration and proliferation while C- and D- subtypes are responsible for venous and lymphatic proliferation {Felmeden, 2003}. FGF is another angiogenic factor used. Derived from SMCs and ECs, FGF is stimulated by EC regeneration, hypoxia and collateral formation to elicit cell induction and proliferation. In pre-fabricated flaps, Bayati and colleagues showed that tissue viability was enhanced by using FGF {Bayati, 1998}.

MCP-1 is released following shear stress to the vessel wall. It attracts circulating and *in-situ* MCs to home in at sites of neovascularisation {Wahlberg, 2003}. GM-CSF acts synergistically with MCP-1 by promoting arteriogenesis, stimulating MC/MP release from the bone marrow as well as prolonging their life span {Buschmann, 2000}. TGF-β described earlier also serves as a growth factor which depending on the receptor, either ALK-1 or ALK-5, stimulates or inhibits angiogenesis respectively {Goumans, 2003}. This illustrates the overlapping functions of these mediators. The slow release of these growth factors would diminish function, while excessive amounts would induce fibrovascular growth.

Control over spatial and temporal patterns of the chemical's release is necessary to form an organised, configured and functional microvascular network. *In vitro*, growth factors may be incorporated by co-culturing them with constructs or placing these factors within bioartificial organs like microcarriers which allow regulated release of

chemicals. *In vivo*, these factors are introduced directly into the bloodstream, incorporated into cells or packed into defects as beads {Berglund, 2003} or bioactive scaffolds {Tabata, 2003}, preferably surface-eroding scaffolds like poly(glycerol sebacate) / PGS {Wang, 2003}.Other methods of delivery include viral transduction {Chang, 2003}, direct inoculation {Springer, 2003} or genetically-modified cells {Von Degenfeld, 2003}.

1.4. CONCLUSION

The biggest hurdle in the construction of tissue-engineered flaps is the inability of existing synthetic or tissue-engineered small-diameter vascular grafts (< 6 mm) to sustain flow through them and more importantly, the absence of any source of an incorporatable capillary bed, natural or otherwise. Current trials on EC-seeded infra-popliteal vessel bypass grafts have only been proven to be as successful as vein grafts in the same setting {Meinhart, 2001} while the development of an artificial capillary bed is limited to *in vitro* models {Brown, 1996;Chalupowicz, 1995;Doetschman, 1985;Hoying, 1996;Ingber, 1989;Kubota, 1988;Montesano, 1983;Montesano, 1986;Montesano, 1987;Montesano, 1987;Nehls, 1996;Nicosia, 1990;Olander, 1985;Vailhe, 2001;Vernon, 1995;Vittet, 1996}. However, a better understanding of microcontact printing {Moldovan, 2002}, microfluidics {Kaihara, 2000}, bioreactors {Mironov, 2003} and further breakthroughs in tissue engineering technology {Ochoa, 2002} may make this more likely. In this thesis, the aim is to identify and develop a polymer as the building block for the creation of a microvascular network. For this purpose, we have chosen a novel nanocomposite which will be discussed in greater detail in chapter 2.

Chapter 2

2. Syntheses and physical characterisation of polyhedral oligometric silsesquioxane integrated poly (carbonate-urea) urethane nanocomposites with single and twin hydroxyl-functionalised diol groups.

2.1. INTRODUCTION

For long now, the researchers have been working towards the development of more biocompatible vascular access devices using conventional silicon-containing poly(dimethylsiloxane) (PDMS) as a coating, a surface modifying end group {Capone, 1992;Mathur, 1997;Ward RS, 1996} and by partial incorporation into the soft segment of the polymer {Chun Y, 1992;Hergenrother, 1994;Shibayama M, 1991;Ward RS, 1995}. The rationale behind this approach has been that silicon has an unstable surface free energy which would repel protein and platelet adhesion as well as increase degradative resistance to hydrolysis and oxidation. As PDMS itself is a rigid polymer, efforts have been made to link silicon with more compliant materials such as rubber so as to better mimic the elastic properties of arteries {Salacinski, 2001c}.

Rubber itself possesses high elastic extensibility. Meyer proposed that the molecular explanation for this property in 1932 when he recognised that the individual atoms of the polymer chain were capable of rotation and vibration thereby allowing crumpled (contact) conformations which represents the equilibrium flexibility. A stretching force allows considerable extension of this chain. Crystalline polymers are harder than rubber but not brittle like glass. They comprise rigid polymer chains (crystallites) embedded in an amorphous gel. However, this latter soft phase is vulnerable to biodegradation in vivo and accordingly, efforts have been made to improve this facet of its property. An example of this is polyurethane.

End-capping of urethanes containing ether segments has resulted in, silicon-enriched surfaces this being due to the low surface free energy coupled with the high mobility of PDMS {Mathur, 1997;Ward RS, 1996}. Mathur and colleagues {Mathur, 1997} showed that PDMS-end capped poly(ether)urethane evidenced no degradation of the PDMS itself, but pitting and cracking was observed when the amorphous polytetramethylene oxide (PTMO) segments of a polyurethane co-polymer in an *in vivo* animal model was strained to 400%. It became obvious that a more flexible, rubber-like composite with even greater elasticity was required.

Subsequent efforts to improve the elasticity of silicon-polyurethane elastomers included the incorporation of PDMS into urethanes by the addition of oligomeric sequences (>500Da) into the amorphous segment. However, even this approach has had poor results both *in vivo* and clinically, as the PDMS does not react with the amorphous segment or crystalline segments resulting in increased macrophase separation due to the hydrophobicity of PDMS sequences. As a consequence of this, current silicon-polyurethane composites have extremely poor mechanical properties, low bio-stability, low clarity and yellowing resulting in a non-aesthetically pleasing material (clinically this being of extreme importance as yellowing materials are not suitable as biomedical interventional devices); all results of poor chemical integration within the polymer composite {Kao, 1994;Shibayama M, 1991}.

Nano-engineered materials integrate with its constituents at the nanoscale level resulting in significantly enhanced physical properties such as increased conductivity, mechanical strength, optical activity and catalytic activity {Merkel, 2002}. Depending on the extent of interaction between its components in the formation of its

ultrastructure, nanocomposites can exist as intercalated or exfoliated. Nanocomposites has been classified by Novak in 1993 {Novak B, 1993} into five groups depending on the presence of a matrix and covalent bonds. The first generation of nanocomposites were predominantly in the form of carbon nanotubes and metal oxides. Over time, it became recognised that silica particles could also behave as nanofillers, making more innovative usage of silicon compounds possible, discoveries with immense potential in the world of vascular biotechnology {Mark JE, 2003} as well as medicine in general {Fong H, 2005}.

In complete difference to siloxane, silsesquioxanes (SQS) exists as ladder- or cage-type nano-structures {Lim, 1994} and have recently generated great interest because of their unique structure. Polyhedral oligomeric silsesquioxane (POSS), a hybrid nanostructured macromer is being used increasingly to synthesise hybrid nanocomposites due to its chemical versatility over other nanofillers such as carbon nanotubes and nanoclays {Joshi M, 2004}. These oligomers are formed by Si_4O_6 monomers with the stoichometric formula $(SiO_{1.5})_n$. These molecules have an inorganic silica-like core surrounded by eight organic corner groups which could be made to react in order to form homosilsesquioxanes {Kao, 1994;Xiang K, 1998} dendrimers or nano-bridges {Dijkstra, 2002;Lichtenhan JD, 1995;Suresh, 2004}. Importantly these nano-composite cubes can be incorporated as building blocks {Moreau, 2003} of controllable shapes {Suresh, 2004} into polymers to form hybrid materials {Wada, 2005} with improved with improved properties {Sanchez C, 2001}. This is achieved as monodispersions in polymers such as epoxide, acrylate, norborne, styrene, acetoxystyrene {Xu H, 2002} and polyurethanes.

Herein as an alternative to siloxane, our original hypothesis was that by using POSS attached by direct reaction onto the urethane segment, a significant improvement in mechanical strength could be achieved as compared to non-POSS integrated poly(carbonate-urea)urethane(PCU). This would then so engender significantly improved bio-stability, but with the attractive anti-protein adsorption qualities of silicon itself previously not possible with siloxane polyurethanes. In this paper, we tested the hypothesis using single and double hydroxyl-functionalised diol side-chained POSS to find which provided the optimal molecular and steric interaction with the urethane grouping. The syntheses, molecular characterisation and mechanical assessment of a series of new nanocomposites was made with particular emphasis placed on the interaction between the polyurethane component and the inorganic POSS cube core to form hybrid POSS-PCU nanocomposites {Pyun J, 2001}. The effect of POSS addition to the polyurethane on the overall bulk thermal properties as well as its mechanical qualities were also studied.

2.2. METHOD & MATERIALS

2.2.1. SYNTHESIS

Poly-carbonate polyol and either propanediol or cyclohexane-diol linked octasiloxane (figure 2.1), depending on whether single- or twin-hydroxyl functionalised diol substituted POSS groups was being synthesised, was mixed and heated to 130°C before adding methylene diisocyanate (MDI), to form a pre-polymer. The diluent N, N-dimethyl-dimethylacetamide (DMAC) was then added with chain

extension at 70 to 80 °C being carried out by ethylenediamine and diethylamine. By simply increasing the ratio of POSS-substituted groups added to polycarbonate polyol, POSS concentrations within the nanocomposite could be proportionately increased. For comparison, a pure PCU was also synthesised. All the chemicals, reagents, glassware and associated relevant equipment were purchased from Sigma-Aldrich Co. Ltd. (New Road, Gillingham, UK).

Figure 2.1. Molecular structure of twin-hydroxyl functionalised cyclohexane-diol side-chain substituted POSS.

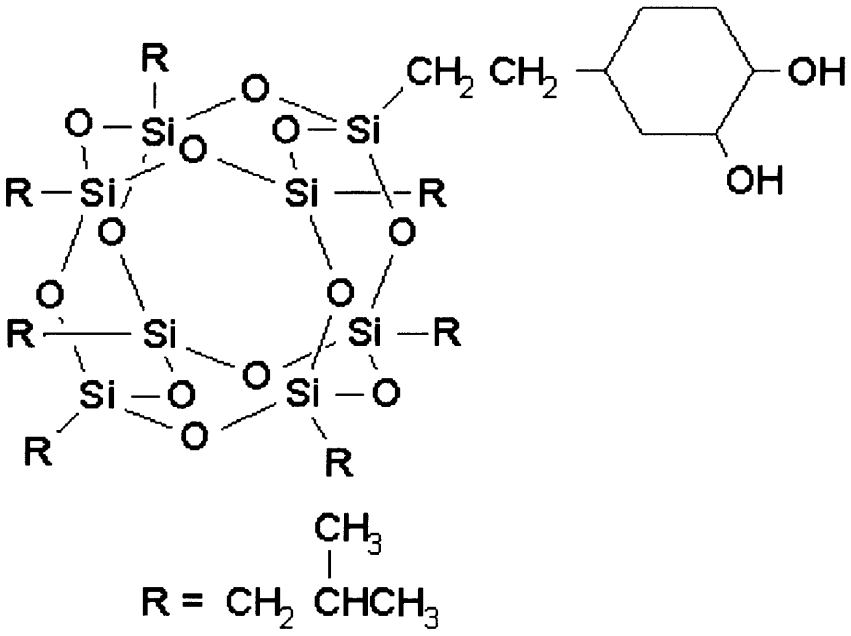

2.2.2. POLYMER CHARACTERISATION

2.2.2.1. Nuclear Magnetic Resonance Spectroscopy (NMR)

Solution state NMR (^{1}H-NMR) on the various types of POSS-PCU

nanocomposites were performed using a solution state spectrometer (Bruker Avance 500 spectrometer, Oxford Instrumentations Ltd, UK) at 500 MHz with 7 mm zirconia rotors. Casted sheets of the various nanocomposites were first dissolved in methyl sulfoxide-d_6 solvent. Analyses were performed using ^{13}C ('H), 'H - 'H correlation; ^{13}C-'H correlation and DEPT – ^{13}C ('H).

Solid state NMR experiments were carried out at room temperature using a Bruker MSL 300 spectrometer with 7mm zirconia rotors (Oxford Instrumentation Ltd, UK). The respective polymers were then pulverised into a fine powder using a dismembranator cup oscillated at 2000 rpm for 2 minutes after being cooled in liquid nitrogen. The NMR glass tubes were then filled with the polymeric powder and subjected to solid-state NMR. The instrument was operated at resonance frequencies of 75 MH_z for ^{13}C, 30 MH_z for ^{15}N, and 59 MH_z for ^{29}Si and the data was then analysed using Fourier-transform and the Cross-Polarisation Magic Angle Spinning Technique (CPMAS). The spectra being run were ^{13}C CPMAS; ^{13}C MAS/Decoupling ride; ^{13}C CPMAS NQS; ^{13}C CPMAS TOSS; ^{29}Si CPMAS and ^{15}N CPMAS. These experiments were conducted by the Department of Chemistry, Univesity College London, UK.

2.2.2.2. Fourier-Transform Infra-Red Spectrometry

Using a spectrophotometric analyser (Advance 2000, Perkins-Elmer Ltd, USA), the surface and bottom surfaces of cast sheets of the various polymers were exposed to infra-red spectra of 4200 cm^{-1} to 600 cm^{-1} wavelengths at an incident angle of 30°, a total of 16 times per scan. Each scan was in turn repeated six times on both surfaces

(n = 6) as well as cut-sections to determine the bond patterns on both surfaces, the intervening bulk regions as well as the effect of incremental concentrations of POSS nanocages to the primary PCU component.

2.2.2.3. Differential Scanning Calorimetry (DSC)

Using a heat-flux DSC thermal analysis system (Shimadzu Ltd., Japan) the glass transition temperature (T_g), specific heat increment (ΔC_p), temperature at which softening occurs and melting temperature (T_m) of the polymers were analysed. The temperature ranges measured were between -100 °C and 270 °C with a heating rate of 10 °C/min. T_g was taken as the 50^{th} percentile of the specific heat increment curve. All samples were compared to blank controls. The crystallisation temperature as well as the point at which softening occurs was looked for in order to determine the percentage crystallinity of the nanocomposite, if present. The samples were also subjected strain-induced crystallisation by first heating them to 210 °C (just prior to heating) and then inducing thermal shock (cooling them at that temperature in liquid nitrogen) before being reheated to 270 °C from -100 °C.

2.2.2.4. Mechanical Testing

Two sheets of each polymer (PCU, 2% POSS-PCU and 6% POSS-PCU) were cast in a vacuum oven (150 mm x 200 mm, 50 °C, 48 h) for evaluation. The tensile properties were assessed according to ASTM D1708. Tests were conducted on a Shimadzu B444 testing machine at a displacement rate of 10 mm/min. The tensile

stress was recorded at 100% elongation and 300% elongation. The tear strength was measured according to ASTN D624, using the die 'C' specimen geometry. Testing was conducted on a Shimadzu B444 test machine at a rate of 500 mm/min. The specimens for both tests were cut from the polymer sheets using a template and a scalpel, rather then using a cutting die. A minimum of five samples of each polymer were tested by each test method. For each test, samples were taken from two different sheets of polymer. All tests were performed at room temperature (21 °C). These tests were conducted at the University of Cambridge, UK.

2.3. RESULTS

2.3.1. SOLUTION-STATE NMR

2.3.1.1. $^{13}C(^{1}H)$ pure PCU/DMSO 298K (Control)

A standard carbon spectrum first group of peaks is at 155.444 – 153.454 ppm shows the joining of four carbonate groups. Carbonyl groups (from urea) (6), (8) carbonyl from urethane where carbonate has reacted with the MDI, the carbonyl for the carbonate itself while the fourth would be the (12) chemically identical carbonyl that has either reacted with urethane again (or related small peak related with chain extender – diethylamine). As shown in figure 2.2, the peaks between 128.8 – 138.5 ppm are the aromatic carbons. Next group of peaks 72.407 – 60.288 ppm are the ones close to polar groups. There are sixteen respective peaks. There are the aliphatic carbons first group marked on spectrum, and corresponding to 9, 9', 5 marked on

chemical structure. The next group of peaks is from 29.131 ppm to 24.833 ppm.

Figure 2.2. ^{13}C-(^{1}H) NMR of control PCU.

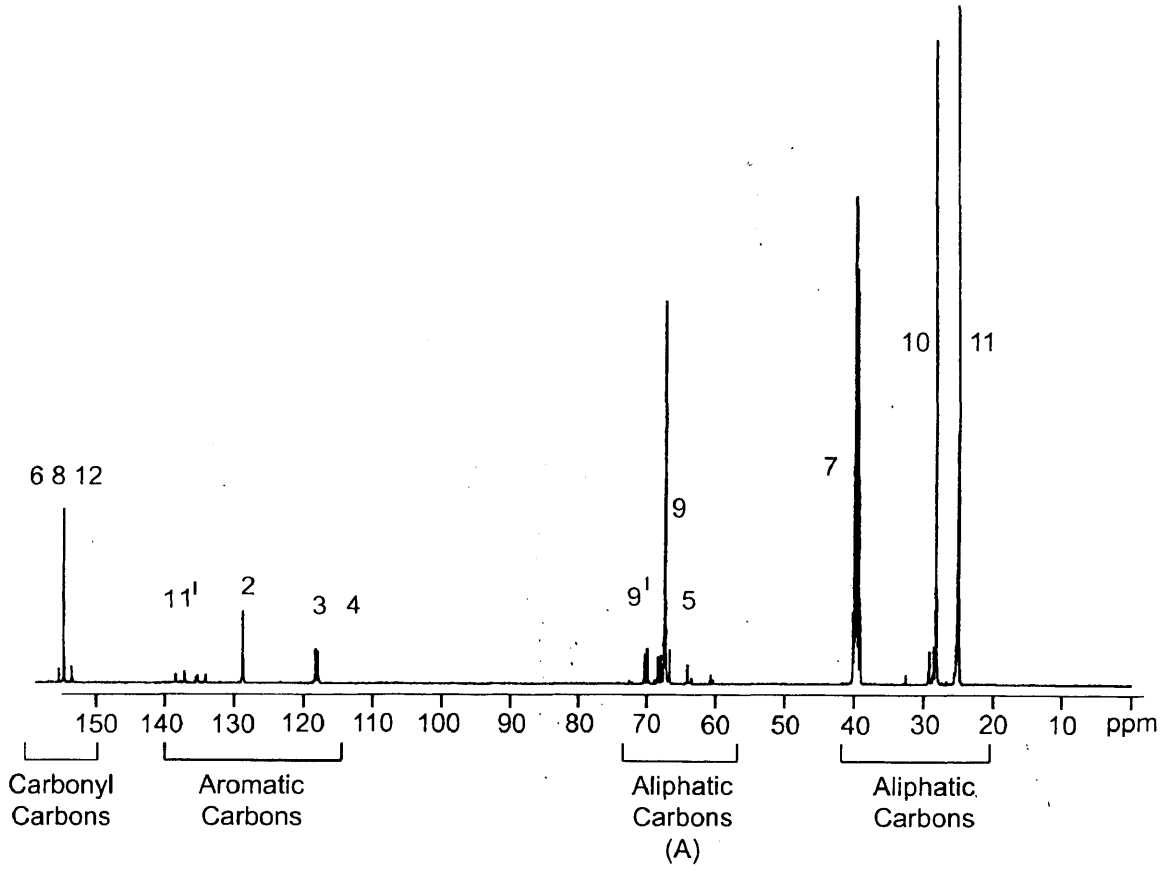

2.3.1.2. ^{1}H pure PCU/DMSO 298K (Control)

The first multiple group of peaks from 7.366-7.020 ppm are the aromatic groups. The peaks are marked on the chemical structure on figure. 2.3. The unusual splitting pattern is the normal one for MDI in urethanes. The carbonate hydrogens are in the area 4.167 ppm which are followed by peaks for ethylene diamine and urethane. The aliphatic hydrogens are marked 8 and 9 on the chemical structure shown in figure 2.3.

Figure 2.3. ^{1}H-NMR spectra of control PCU.

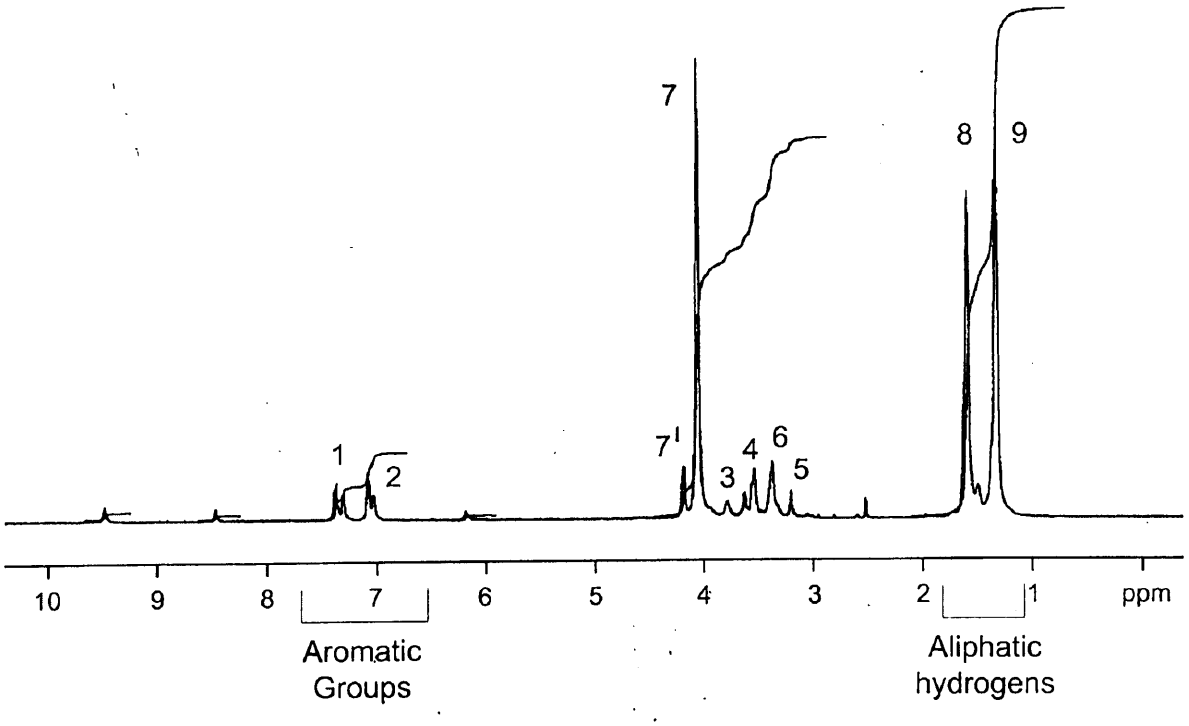

2.3.1.3. ^{13}C (^{1}H) Single hydroxyl functionalised POSS-PCU/DMSO 298K

In figure 2.4, the spectrum corresponds to the solution state carbon. The peaks at 155.408-153.606 ppm correspond to the carbonyl peaks 6, 8 and 12 in that respective order. The next set of peaks are the aromatic carbons, which are from 138.367-117.884 ppm and correspond to the carbons in the MDI 1.1' (a mixture thereof) and 2, 3 and 4 (again a mixture) at 138.367-134.060 ppm, 128.771-128.703 ppm and 118.259-117.884 ppm. The multiple peaks at 1 and 1' are due to conjugation that is isomerism with the urethane group. The group of peaks at 70.078-63.907 ppm correspond to the aliphatic carbons. The peaks correspond to 9 and 9' from the polycarbonate polyol then 13, 14, the CH_2 and CH groups of the pendant arm of the cage. The methylene group associated with the aromatic group is at 5 and is at 63.907

ppm. The group of peaks at 39.963-38.961 ppm correspond to 7 the CH_2 of the ethylene diamine the chain extender and the CH_2 groups of the pendant chain 15 and 16 and 18 and 19 of the cage respectively. The group of peaks at 28.918-27.961 ppm correspond to 10 from the polycarbonate polyol, 19 from the cage and 25.402-24.765 ppm to 11 from the polycarbonate polyol respectively. The smaller peak(s) at 18.5 ppm corresponds to the CH_3 group of the cage.

Figure 2.4. ^{13}C-(^1H) NMR spectra of single-hydroxyl functionalised POSS-PCU.

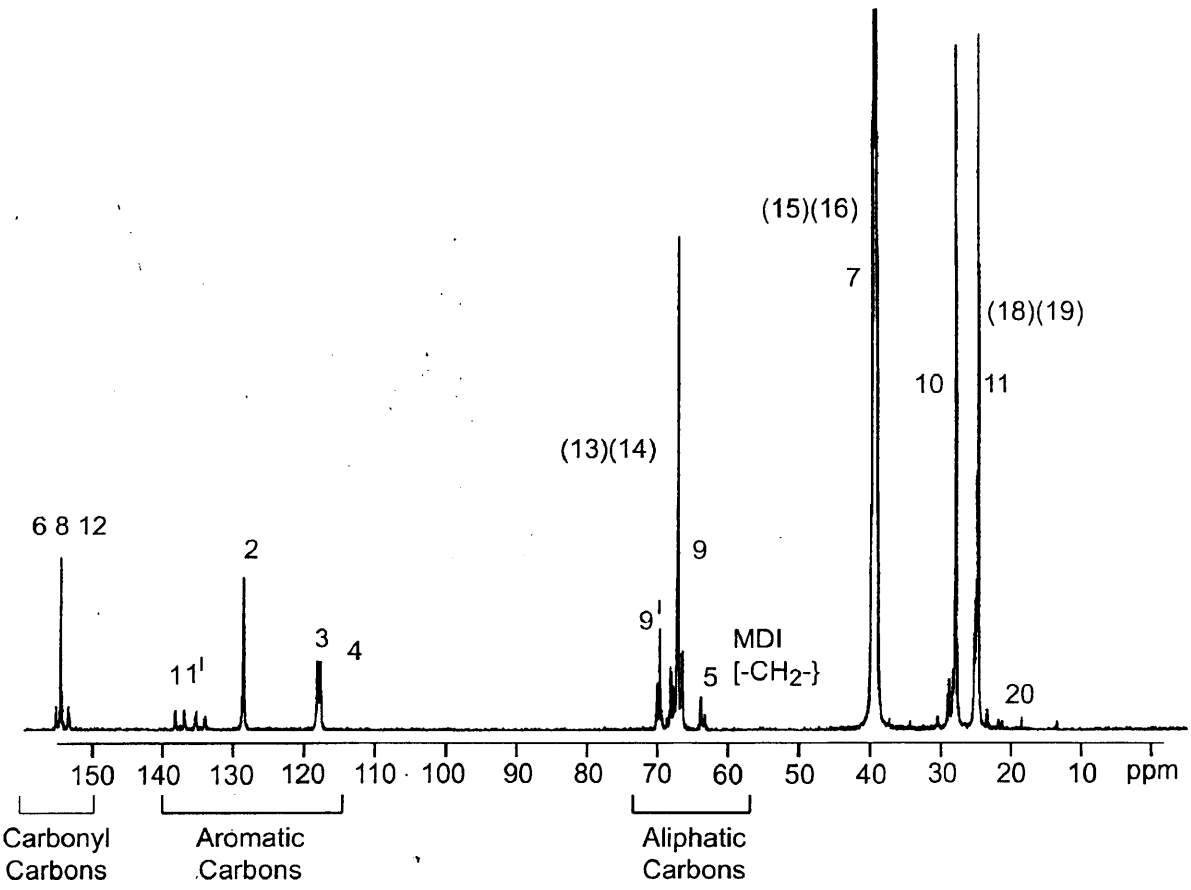

2.3.1.4. *(*^{1}H*)* Single hydroxyl-functionalised POSS-PCU/DMSO 298K

The first set of peaks corresponding to the aromatic groups are from 7.368-7.024 ppm. These correspond to 1 and 2 in figure 2.5. The next set of peaks at 4.174 - 3.924 ppm corresponds to the aliphatic protons. The protons of the carbonate and from the silsesquioxane are numbered 7 and 7' and 10 and 11 respectively, as it is in the same environment. The peaks at 3.766-3.521 ppm correspond to 3 (methylene group) and 4 (urethane NH). The peaks at 3.402-3.370 ppm correspond to 6 of the ethylene diamine chain extender and 12 and 13 of the cage. The peak at 3.370 ppm corresponds to number 5. The peaks at 1.723-1.313 ppm correspond to the numbers 8 and 9. The peaks at 0.515-0.481 ppm to 18 and 16 while the tiny peaks at 0.086-0.0446 ppm correspond to the CH_3 and CH_2 groups of the cage ('R' groups).

Figure 2.5. ^{1}H-NMR spectra of single-diol functionalised POSS-PCU.

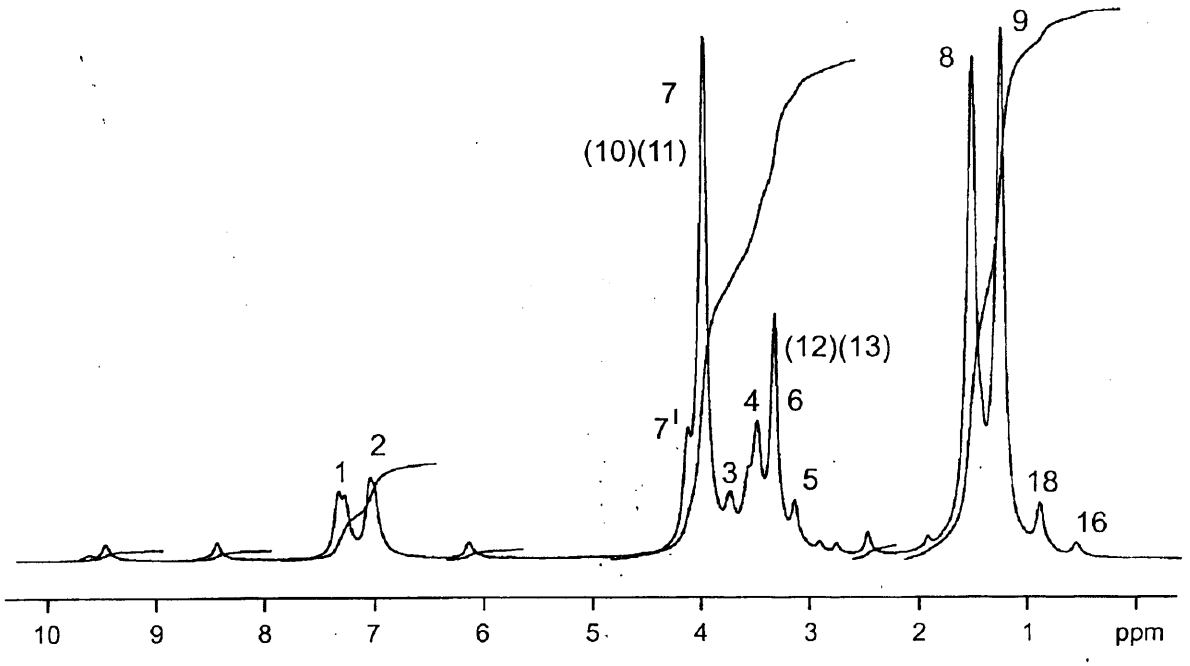

2.3.2. SOLID-STATE NMR

2.3.2.1. ^{13}C CPMAS Single hydroxyl-functionalised POSS-PCU

As in the case of PCU, the group of peaks at 158.092-155.867 ppm are equivalent to the carbonyl groups, urea, urethane and carbonate all clustered at these peaks – order is urea, urethane and carbonate. The next group(s) of peaks is the aromatic carbons numbered 136.292-120.184 ppm. The order respectively is due to the shift being generated at the carbon 1 next to the urethane group. The 1st peak is split due to isomerism; a form of conjugation with the aromatic ring. The 2nd and 3rd peaks should theoretically be equal in intensity but they are not. The next set of peaks are the aliphatic carbons the first being at 68.129 ppm. This corresponds to the carbonate section of the polymer. The methylene peak(s) comes up at 58-60 ppm as a shoulder from the MDI. The next set of peaks is at 40.851 ppm and represents the chain extender, the ethylene diamine. The next group of peaks at 29.241 and 26.110 ppm are of the carbonate chain. In the same environment, but hidden as they are of smaller amplitude. Peaks of the pendant chain are also seen as are the CH_3 groups of the POSS cage at 17 ppm.

2.3.2.2. ^{13}C MAS/Decoupling Ride - Single diol 2% POSS-PCU

The group of peaks at 155.727 ppm are equivalent to the carbonyl groups, urea, urethane and carbonate (all clustered at this peak) in the following order; urea, urethane and carbonate. The next group of peaks are the aromatic carbons numbered

145.234-119.010 ppm. The next set of peaks is the aliphatic carbons, the first being at 70.999 and 68.084 ppm which corresponds to the carbonate section of the polymer. The next set of peaks at 40.702 ppm are from the chain extender; ethylene diamine. The next group of peaks at 29.250-25.984 ppm are from the carbonate chain.

The group of peaks at 158.201-155.872 ppm are equivalent to the carbonyl groups urea, urethane and carbonate all clustered at these peaks order is urea, urethane and carbonate. The next group(s) of peaks is the aromatic carbons numbered 137.680-119-733 ppm. The order is due to the shift being generated at the carbon 1 next to the urethane group. The 1st peak is split due to isomerism a form of conjugation (with the aromatic ring). The 2nd and 3rd peaks in theory should be of identical intensity, but they are not. The next set of peaks is the aliphatic carbon the first being at 70.972 ppm which represents the carbonate section of the polymer. The methylene peak(s) comes up at 59.286 ppm as a distinct shoulder from the MDI. The next set of peaks at 40.867 ppm are from the chain extender; ethylene diamine.

The next group of peaks at 29.228 and 26.010 ppm are of the carbonate chain. In the same environment but hidden, are the peaks of smaller amplitude while the unhidden components of the cage is at 35.241 ppm, 21.810 ppm and at ~1 ppm.

2.3.2.3. ^{13}CPMAS NQS – Single hydroxyl-functionalised POSS-PCU

The group of peaks at 155.806 ppm are equivalent to the carbonyl groups urea, urethane and carbonate (all clustered at these peaks). Their order is as urea, urethane

and carbonate. The next group(s) of peaks is the aromatic carbons numbered 137.518 to 129.479 ppm. The order respectively is due to the shift being generated at the carbon 1, next to the urethane group. The first peak is split due to isomerism a form of conjugation, (with the aromatic ring). The 2nd and 3rd peaks in theory should be of identical intensity but they are not.

The next set of peaks is the aliphatic carbons, the first being at 68.144 ppm of the carbonate component of POSS-PCU. The next group of peaks at 29.244 and 26.134 ppm are of the carbonate chain. No evidence of the silsesquioxane (POSS) is visible.

2.3.2.4. ^{13}C CPMAS NQS – Twin-diol POSS-PCU

The group of peaks at 158.155 and 155.875 ppm are equivalent to the carbonyl groups urea, urethane and carbonate all clustered at these peaks in the following order; urea, urethane and carbonate. The next group(s) of peaks is the aromatic carbons numbered 137.577, 129.710 and 118.966 ppm. The order respectively is due to the shift being generated at the carbon 1, next to the urethane group. The first peak is split due to isomerism a form of conjugation (with the aromatic ring) itself and again as in single-diol POSS-PCU, where in theory the 2nd and 3rd peaks should be equal but again not so in reality.

The next set of peaks are the aliphatic carbons the first being at 70.985 ppm the shoulder and at 68.122 ppm the principal peak. The next group of peaks at 29.240 and 26.086, 21.790 ppm are of the carbonate chain. The fully condensed silsesquioxane

closed cage (POSS) is evidenced by the peak 5 ppm as well as 38.048 ppm, 35.248 ppm and 21.790 ppm.

2.3.2.5. ^{13}C MAS/Decoupling Ride – Twin hydroxyl-functionalised POSS-PCU

The group of peaks at 155.732 ppm are equivalent to the carbonyl groups, urea, urethane and carbonate (all clustered at this single peak) order is urea, urethane and carbonate. The next group of peaks are the aromatic carbons numbered 129.671-118.873 ppm. The next sets of peaks are the aliphatic carbons, the first being at 71.044 and 68.084 ppm. The next set of peaks at 40.7 ppm which arise from the chain extender; ethylene diamine. The next group of peaks at 29.252 and 26.002 ppm are from the carbonate chain. The peak seen at 1.411 ppm is the CH_3 group at the cage itself.

2.3.2.6. ^{13}C CPMAS TOSS – Single hydroxyl-functionalised POSS-PCU

The group of peaks at 155.880 are equivalent to the carbonyl groups urea, urethane and carbonate (all clustered at these peaks). The next groups of peaks are the aromatic carbons numbered 137.695 ppm to 119.813 ppm. These are four peaks are 137.695 ppm, 129.656 ppm, 125.398 ppm and 119.813 ppm of the aromatic group of peaks. The order respectively is due to the shift being generated at the carbon 1, next to the urethane group. The first peak is split due to isomerism a form of conjugation, (with the aromatic ring). The peaks 2 and 3 in theory should be of identical intensity

but they are not.

The next set of peaks are the aliphatic carbons the first being at 68.163 ppm. This corresponds to 9' of the shoulder and 9 of the carbonate section itself of the polymer. The peak at 41.175 ppm corresponds to 7 on both picture and figure and are from the chain extender the ethylene diamine. The next group of peaks at 29.259 ppm and 26.190 ppm are 10 and 11 of the carbonate chain. No evidence of the silsesquioxane is visible.

2.3.2.7. ^{13}C CPMAS TOSS – Twin hydroxyl-functionalisedl POSS-PCU

The group of peaks at 158.244 ppm are equivalent to the carbonyl groups urea, urethane and carbonate all clustered at these peaks in the order of urea, urethane and carbonate. The next groups of peaks are the aromatic carbons numbered 137.749 ppm to 119.699 ppm representing the aromatic peaks. The order respectively is due to the shift being generated at the carbon marked 1, next to the urethane group. As before, the first peak is split while the 2^{nd} and 3^{rd} peaks are of unequal intensity. The next set of peaks are the aliphatic carbons, the first being the shoulder on the principal peak at 68.141 ppm corresponding to the carbonate section of the polymer. The peak at 40.991 ppm is from the chain extender; ethylene diamine.

2.3.2.8. ^{29}Si CPMAS – Single hydroxyl-functionalised POSS-PCU

This is the silsesquioxane cage made whereby within the cage itself, there is an unreacted primary OH group and a secondary OH group. Post reaction, these are no

longer present. There is now only one peak at -67.81 ppm corresponding to the silicon present in the cage (949.64 M_w) as shown in figure 2.6. The peak is shifted to the right hand side (-ve) due to the different environment the silicon atoms are present in and also to the larger number of silicons present as well. As the silicon atoms are present in one similar environment and as the fully condensed POSS cage is symmetrical, this therefore leads to only one signal being evidenced.

Figure 2.6. ^{29}Si-CPMAS NMR of single hydroxyl-functionalised POSS-PCU

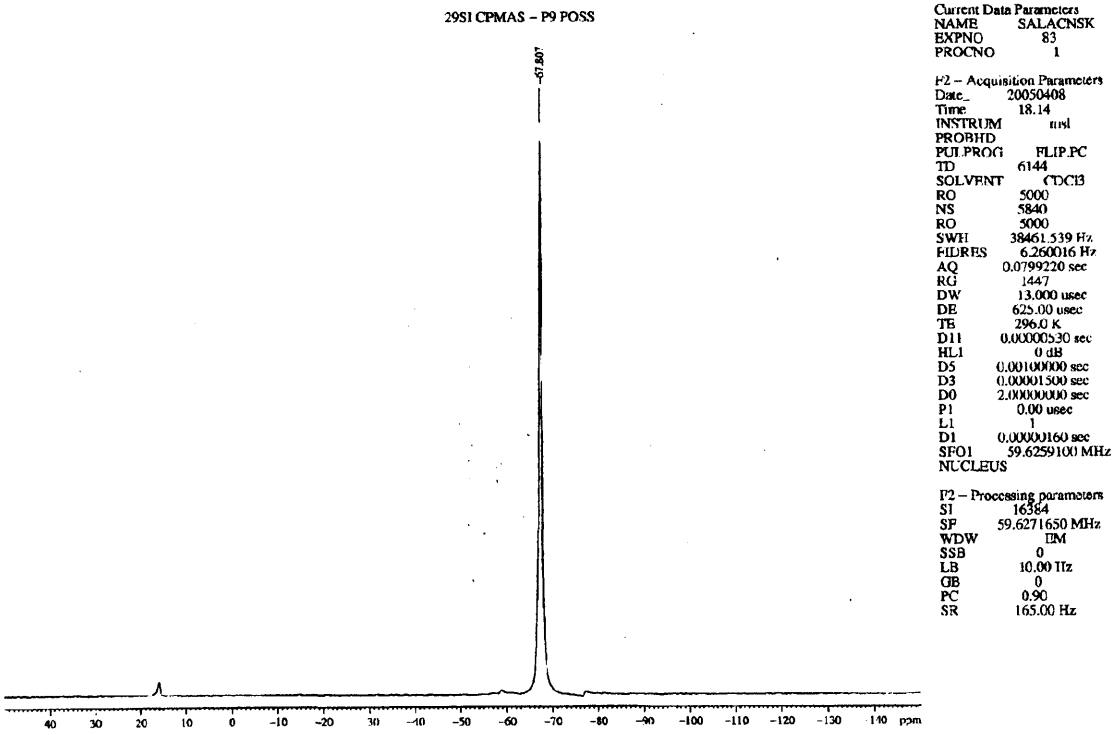

2.3.2.9. ^{29}Si CPMAS – Twin hydroxyl-functionalised POSS-PCU

This is a similar cage core to that of single hydroxyl-functionalised POSS but with two symmetrical secondary OH groups attached via side-chains to the unreacted POSS cage itself, these being no longer present in the final structure as they have been reacted upon. There is only one peak at -67.77 ppm again corresponding to the silicon present in the cage. They are all present in one similar environment and as the cage is symmetrical (a fully condensed POSS cage), this therefore leads to only the one signal being evidenced. The peak is shifted to the right hand side (-ve) due to the different environment the silicons are present in, and also due to the larger number of silicons present as well.

2.3.2.10. ^{15}N CPMAS – Single hydroxyl-functionalised POSS-PCU

In figure 2.7, the first peak has a shoulder and is the nitrogen present in the urea group linked to the aromatic ring, while the peak itself represents the adjacent urea group attached to ethylene diamine. The peak at -299.85 ppm is the other nitrogen in the urea group attached to the ethylene diamine. The urethane group of the POSS-MDI group is not distinguishable.

Figure 2.7. ^{15}N CPMAS NMR of single hydroxyl-functionalised POSS-PCU.

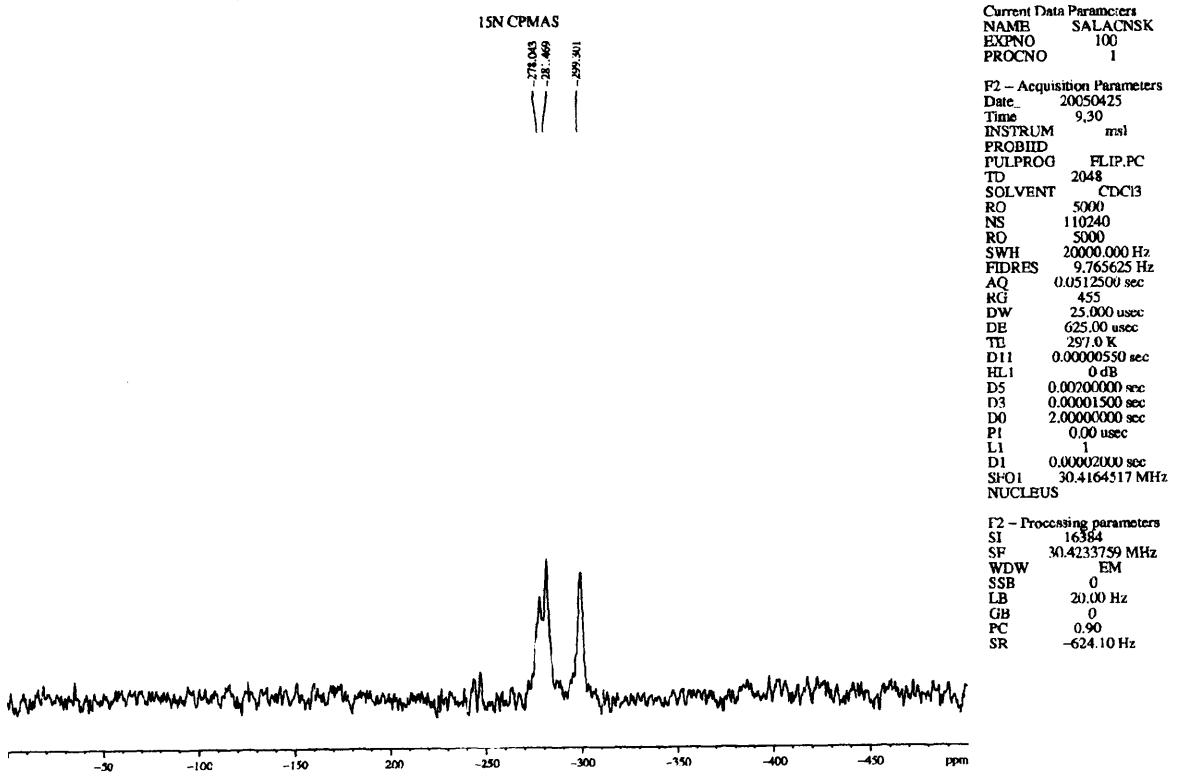

2.3.2.11. ^{15}N CPMAS – Twin hydroxyl-functionalised POSS-PCU

This is the silsesquioxane POSS in which prior to reaction are present two equivalently placed secondary OH groups which are no longer visible in the spectra post reaction synthesis. The second peak at -281.778 ppm is the nitrogen in the urethane group attached to the polycarbonate polyol. The first peak has a shoulder which is the nitrogen present in the urea group adjacent to the aromatic ring with the peak representing urea attached to ethylene diamine. The peak at -299.605 ppm is the nitrogen of the urethane group attached to the polycarbonate polyol.

2.3.2.11. ^{1}H-^{1}H correlation two-dimensional spectra

In all these correlation spectra, the methyl protons attached to the silicon in the silsesquioxane POSS cage(s) shows up strongly at around 0 ppm, P6 = - 0.90 to + 0.10 ppm. This is not observed in the control sample that contains no silicon. This confirms that the POSS nanocage integrates into the polyurethane (PCU) backbone.

2.3.3. FOURIER-TRANSFORM INFRA-RED SPECTROMETRY

Analyses of the PCU control showed a sub-surface bond structure indicative of ν(C=O) bonds at 1740 cm^{-1} with the absence of the hydrogen-bonded variation at 1709 cm^{-1}. Urethane carbonyl groups were present at 1637 cm^{-1} as were the C-O-C=O groups at 1253 cm^{-1} wavelengths. It is this latter absorption peak whereupon that its maximum shifts slightly toward higher frequency when the POSS is incorporated. This pronounced effect is due to the inert diluent effect of the POSS moiety resulting in a distinct reduction of the so termed "self-association" interaction of the PCU chains. An asymmetric broadening of this particular vibration band occurs at the low frequency of the spectrum with an absorption resulting in a lower wave number. As the percentage POSS content increases from 2 to 10%, this absorption shoulder intensity becomes longer in amplitude.

An aromatic reference peak of 1591 cm^{-1} accounted for the C=C bonds of the (MDI hard crystalline) segment of the polyurethane component. The amine groups were also seen consistently at over 3000 cm^{-1} wavelength. All these results are

consistent with our earlier tests with PCU {Seifalian, 2003}. With the addition of POSS nanocages within the nanocomposite, wavelengths at 1109 cm^{-1} appear which indicate the presence of Si-O-Si bonds based on previous studies. The concentration of these molecules increases proportionately with the bandwidth of 'Si-O-Si' group, which confirmed the hypothesis. This indicates that the NH-(C=O)-O of PCU reacts with the hydroxyl groups of the 2,3-proponediol and 2-trans-cyclohexonediol based terminated cores respectively. Namely this being the "so-called" 'R' side chain of the POSS nanocomposites respectively as was hypothesised. Thus the POSS-nanocages form an internal scaffold binding together the polyurethane segments whilst maintaining the chemical composition and hence mechanical properties of the polyurethane. The PCU moiety shows characteristic carbonate and urea vibration bands at 1253 and 1637 cm^{-1} respectively.

'Si-O-Si' bonds; the 'Si' stretching peak [νs(Si-O-Si)] appear at ^1109 cm^{-1} in all of the POSS-PCU nanocomposites which is in the form of silsesquioxane inorganic core cage. Interestingly, as the percentage POSS composition incorporated increases from 2% to 6% the amplitude of this peak significantly increases (figure 2.8a). The continued presence of this Si-O-Si stretching peak confirmed that the cube POSS structure was consistently incorporated into the polyurethane backbone of all the polymers in place of the 'C-O-C=O' groups and urethane 'C=O' bonds at 1253 cm^{-1} and 1740 cm^{-1} wavelengths respectively (figure 2.8b). This analysis also clearly shows that as POSS concentrations increase from 2 to 6 %, it begins to 'infiltrate' rather than 'integrate' with the soft segment of PCU, which would result in increased strength but decreased elastomeric properties. As indicated previously with the increasing amplitude of this peak as an absorption band, the final mole fraction of

POSS present is directly related to the initial feed ratio.

Figure 2.8a. ATR-FTIR analyses of the effect of increasing POSS feed ratios into PCU.

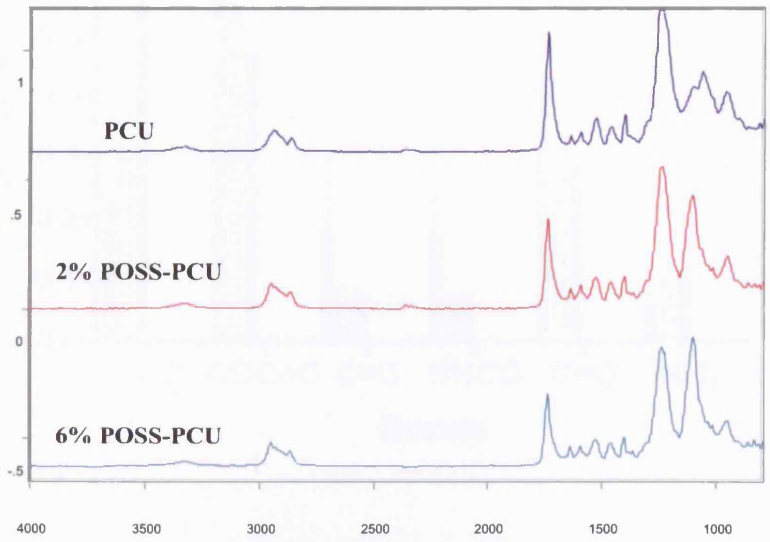

Figure 2.8b. FTIR analysis showing the bond patterns with incremental concentrations of POSS within PCU.

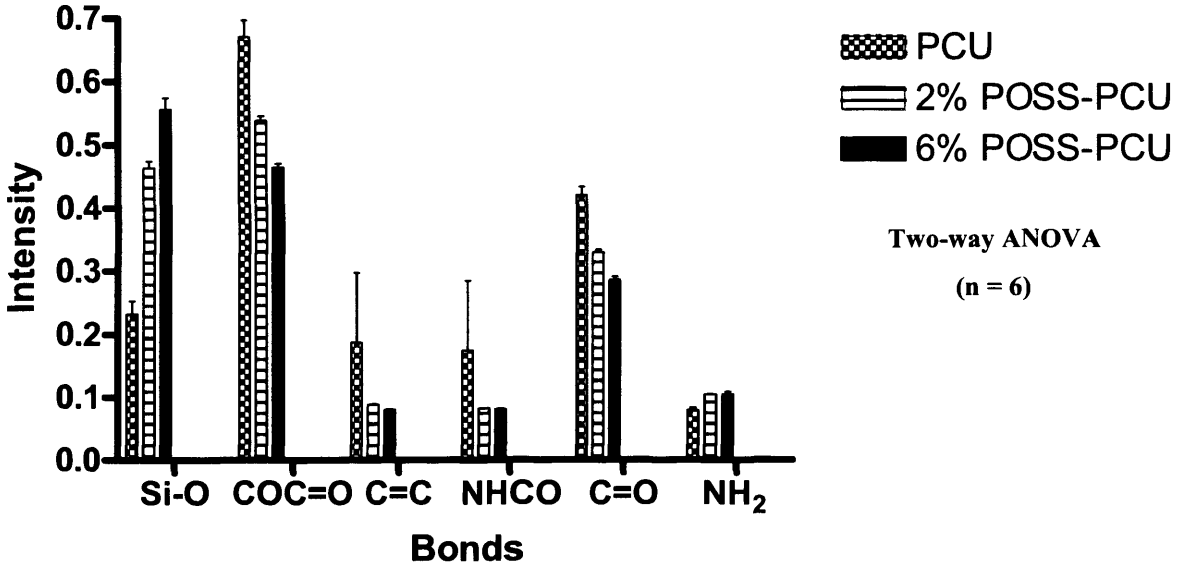

In order to confirm the bonding of POSS to the urethane group of PCU, it was re-dissolved in DMSO to form homogenous, transparent solutions and then added to cyclohexane (a non-solvent for POSS-PCU), but an excellent solvent for pure POSS. The product that was subsequently precipitated was collected by filtering in order to remove any unreacted POSS. These re-dissolution/re-precipitations were undertaken (n = 6) whereby the final product still exhibited the characteristic spectral absorption peak in the region from 1050 to 1150 cm^{-1} with no statistically significant change in amplitude before of after purification. Identical procedures were carried out on mere mixtures of POSS and PCU where the final material showed no characteristic peak at 1050-1150 cm^{-1}. This result indicates bonding by the diol grouping to the urethane segment of the polyurethane.

2.3.4. DIFFERENTIAL SCANNING CALORIMETRY (DSC)

This experiment was performed to assess the bulk characteristics of POSS-PCU. DSC of PCU, 2% POSS-PCU and 6% POSS-PCU nanocomposites revealed glass transition temperatures (T_g) of -35.95 °C, -35.48 °C and -35.08 °C respectively with similar heat capacities of 0.36 J/gK as shown in figure 2.9. These results showed no significant difference in the glass transition temperature (T_g) as well as heat capacity (ΔC_p) of POSS-PCU nanocomposites even at POSS concentrations of up to 6 %. On closer inspection however of the 6% POSS-PCU tracings, it is evident that its T_g is beginning to shift slightly to higher temperatures as well as broaden. There was no evidence of exothermic or endothermic peaks suggestive of crystallinity although this may be a limitation of DSC when studying nanocomposites {Joshi A, 2004}.

Figure 2.9. DSC trace comparing PCU and the incremental doses of POSS to the resulting nanocomposite.

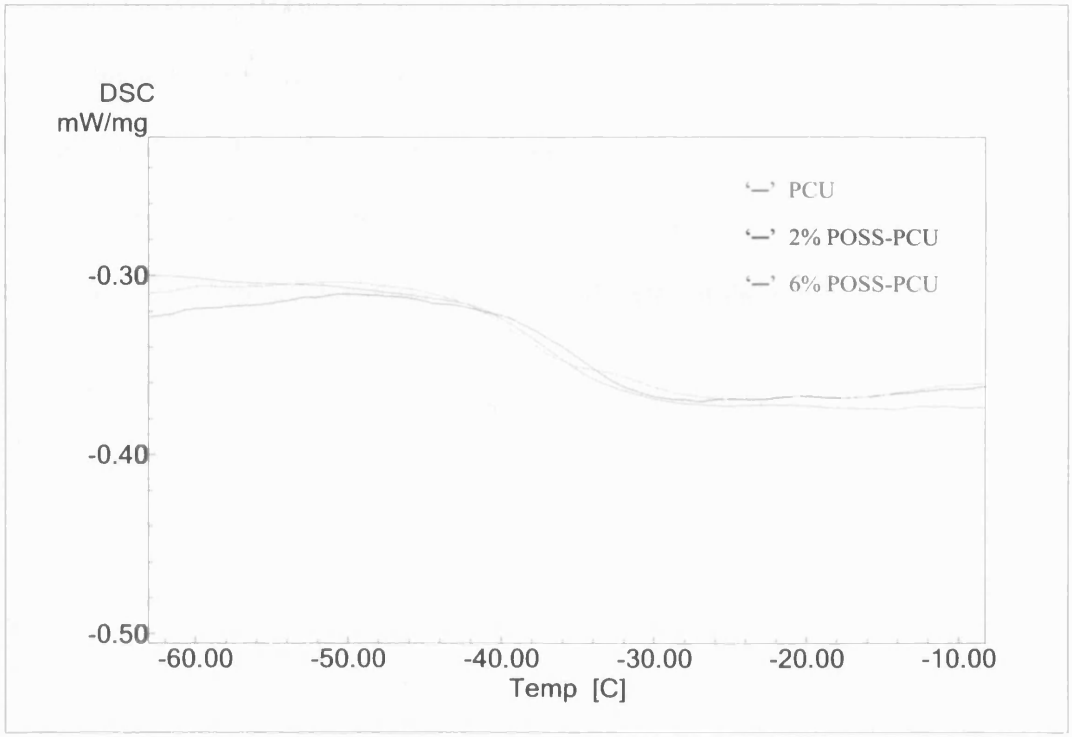

Parameter	*PCU*	*2% POSS-PCU*	*6% POSS-PCU*
Tg	-35.95 °C	-35.48 °C	-35.08 °C
ΔCp	0.36 J/gK	0.36 J/gK	0.36 J/gK

2.3.5. MECHANICAL TESTING

The tensile strength of single-diol 2 % POSS-PCU was found to be significantly increased compared to PCU (Mann-Whitney test, $p < 0.0001$) at 100 % and 300 % elongation (figure 2.10a) while its cross-sectional tear strength was far more consistent at random points along POSS-PCU with coefficients of variation of 7.35 % compared to PCU (24.69 %) as shown in figure 2.10b. The greater tensile strength could be attributed to the efficient nanoscale transmission of force across the matrix of

the polymer in accordance in Griffin's criteria {Kannan RY, 2005}, a finding seen in other POSS hybrid nanocomposites {Li GZ, 2001}. The finer nature of POSS integration and distribution within PCU translates into decreased macrophase separation and hence, more consistent tear strength values in contrast to PCU. A summary of the test results is given in the table below. The values quoted are the mean of a minimum of five results and are accompanied by the standard deviation of the results. The standard deviation was within the size of the symbol used.

Figure 2.10a. Comparison of tensile stress between plain PCU and POSS-PCU nanocomposites stretched at 100% and 300 % normal showing the increased elastomeric property of POSS-PCU due to POSS integration.

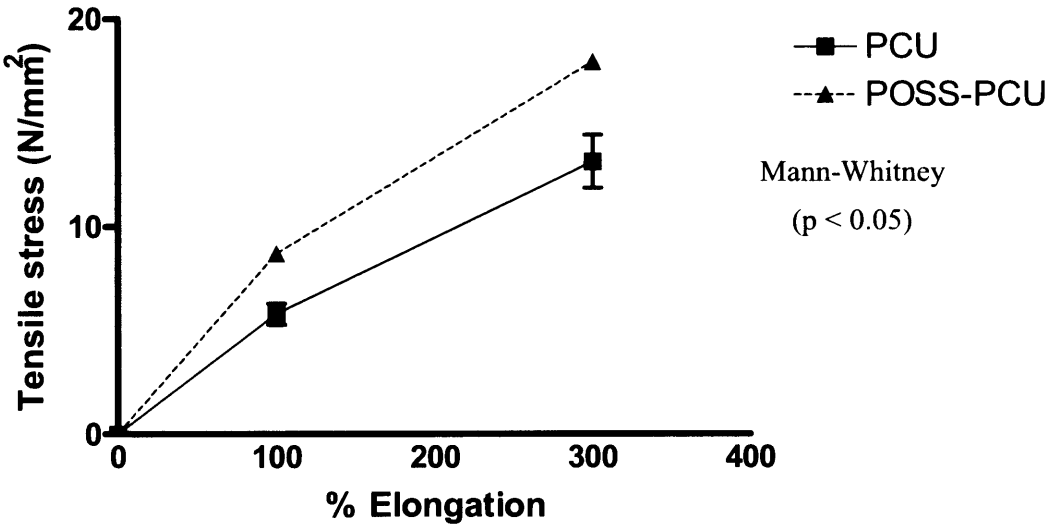

Parameter	*PCU*	*POSS-PCU*
Tensile stress at 100% elongation (N/mm^2)	5.8 +/- 1.24	8.8 +/- 0.29
Tensile stress at 300% elongation (N/mm^2)	13.1 +/- 3.10	17.9 +/- 0.52

Figure 2.10b. The variation in tear strength between PCU and POSS-PCU indicating the improved structural homogeneity of POSS-PCU taken at random points across its cross-section; a characteristic due to the nanoscale integration of POSS into the PCU matrix which decreases phase separation and prevents the formation of focal stress points in PCU.

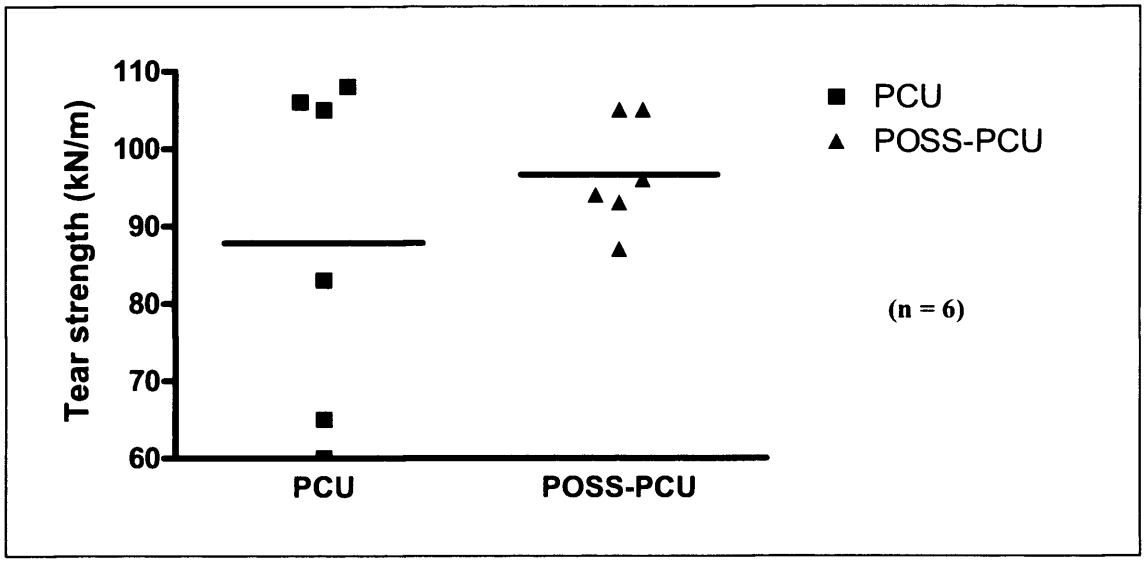

Statistics	*Tear strength (kN/m)*	
	PCU	*POSS-PCU*
Mean	87.83	96.67
Standard deviation	21.68	7.118
Standard error	2.906	8.852
Coefficient of variation	24.69 %	7.36 %
Number	6	6

2.4. DISCUSSION

Nanocomposites may be synthesised by a variety of methods {Calliot T, 2004;Raki L, 2004;Tampieri A, 2004;Meneghetti P, 2004;Benfarhi S, 2004;Pacheco F, 2004;Naka K, 2004;Pal M, 2004;Sharma DR, 2003} depending on the type of nanoparticle used, to form intercalated or exfoliated nanomaterials {Meneghetti P, 2004}. Silica nanoparticles such as POSS are increasingly being used to synthesise hybrid nanocomposites with a variety of polymers. POSS hybrid nanocomposites are usually synthesised by polymerisation techniques at lower concentrations {Lee YJ, 2005} with direct nucleation working only at POSS concentrations in excess of 10 wt% {Joshi A, 2004}. In the polymerisation method, simply increasing the feed ratios would elevate POSS concentrations {Xu HY, 2004}. More recent developments in POSS hybrid synthesis include grafting them onto previously synthesised polymers {Lee A, 2005}.

Monte Carlo simulations on POSS network structures have shown that by increasing linker length between it and the polymer backbone, the reactiveness of their tethers would decreased while increasing its inter-cubic pore sizes resulting in a more even distribution. This prevents large mesopore and bulk cavities but this effect is countered if its tethers are rigid as the level of cross-linking is reduced {Choi, 2001}. In this article, we used two different linkers; propane-diol and cyclohexane-diol with the latter being functionalised with single- and twin-diols. The rationale for this was based on Capaldi's work on POSS-polyurethane hybrids wherein it was found that the orientation of the polymer backbone is dependent upon the linker configuration which is parallel to its surface. From the surface kinetics perspective,

this would mean that surface mobility perpendicular to the surface is minimal while circumferential mobility is enhanced {Capaldi FM, 2005}, a finding that is supported by angle-resolved X-ray photoelectron spectroscopy (XPS) proving that these nanocomposites are lamellar structures {Oaten M, 2005}.

Based on this, we placed the diol groups of the linker cyclohexane in the ortho position in order to modulate the surface kinetics of this nanocomposite such that the conformation of adsorbed proteins would be contorted, thus inhibiting its actions. Concurrent studies on other diol-functionalised nanocomposites by Turri and co-workers have shown a lowering of surface free energy {Turri S, 2005}, possibly as a result of the end-capping property of cyclohexane-diol compacting the POSS nanocage {Anderson SE, 2005}. This finding is corroborated by models based on POSS tethered nanostructures which have shown similarities between POSS hybrids and surfactants {Chan ER, 2005} as well as significant mechanical reinforcement. The POSS nanocage end-groups are of no significance as they do not affect the overall structure of POSS hybrids {Anderson SE, 2005}. NMR analyse(s) on these nanocomposites have shown that increasing POSS concentrations reduce molecular rotation as a whole thereby permitting greater strength.

Existing data shows that POSS should increase the glass transition temperature (T_g) as it would reduce the distance between the inorganic cases so hindering molecular and segment rotation with reference to the polymer. This reduces its dipole interaction potential and makes the polymer stronger {Haddad TS, 1999} mechanically. The extent to which this occurs would however depend on (i) the nature of the host polymer itself and (ii) the degree of interaction between the POSS molecule and the

polymer. In a parallel study, octaaminophenyl-linked POSS-polyurethane hybrids showed significant increase in T_g {Liu HZ, 2005} unlike the POSS-PCU nanocomposite.

In order to explain this, we looked at the thermal characteristics of POSS-polyimide hybrid nanocomposites which have been shown to be unaffected at concentrations of below 15 %, an effect seen only at higher concentrations of POSS (> 20 %) {Li GZ, 2005}. This would explain why the addition of POSS at concentrations of up to 6 % did not impede overall chain motion and preserves the overall thermal characteristics of PCU. We believe that another reason for this behaviour is that when POSS molecules exists as side-chains within the nanocomposite, Schatzki side-chain motion of these molecules would not alter T_g as it does not affect polymer chain reptation unless these POSS molecules were to infiltrate into the polymer matrix to a significant degree. This postulate is supported by a study by Leu and colleagues who found that the thermal characteristics of POSS-polyimide hybrids were preserved on DSC {Leu CM, 2005}. Furthermore, they found increased microphase separation resulting in a more ordered polymer structure, finding which we have replicated during atomic force microscopy (AFM) analysis of these POSS-PCU nanocomposites as well.

The elastomeric properties of POSS-polyurethane hybrids depend on the miscibility of POSS molecules within the base polymer which contributes to increased dispersion within its matrix {Kopesky ET, 2005}, specifically within the hard segment {Hsiao BS, 2000}. On linear deformation, small-angle X-ray diffraction studies indicate that the POSS nanocrystals within the hard segments decreased whilst

elongation-induced crystallisation occurred in the soft segments, TEM analyse(s) showing strain-induced hard segment destruction {Fu BX, 2001}.

In summary, the use of POSS molecules to form hybrid nanocomposites is enhancing the advances in materials sciences with the key issue being the selection of the optimal linker molecule in order to suit its application. In the case of vascular devices, the substitution of one corner group of the POSS nanocage with diol-functionalised cyclohexyl groups linked to carbonate-based polyurethanes has numerous advantages; (i) improved mechanical strength as well as flexibility, (ii) greater resistance to biodegradation, particularly oxidative and (iii) modulation of adsorbed surface proteins. We believe that these basic characteristics of POSS-polyurethane nanocomposites make it the ideal vascular interface in vivo. In the following chapter, the resistance of POSS-PCU nanocomposites to in vitro degradation was studied.

Chapter 3

3. The degradative resistance of polyhedral oligomeric silsesquioxane (POSS) nanocore-integrated polyurethanes.

3.1. INTRODUCTION

Polyurethanes are amorphous co-polymers which consist of a soft phase and a hard phase. The hard segment is formed as a result of the interaction of the isocyanates {Tang, 2002} with either diol or diamine molecules while the soft segment may consist of ether, ester or carbonate groups with the latter being the most resistant to degradation {Salacinski, 2002b}. This dimorphic characteristic of polyurethanes (PU) gives it greater elasticity courtesy of the flexible soft segment while the hard segment contributes strength to the co-polymer. Although PU is being increasingly used in biomedical devices, there have been concerns regarding its resistance to degradation in vivo. Recent studies on pacemaker leads explanted after 10 years have shown ultrastructural evidence of degradation {Schubert, 1997;Wu, 1994} indicating a need to improve the stability of existing PU.

As the soft segment is the most vulnerable {Coury, 1988;Kao, 1999;Labow, 1999;Wu, 1994} component of PU, efforts have been made to improve resistance by varying the soft segment groups. Ester groups impart greater resistance to oxidation but are susceptible to hydrolysis {Coury AJ, 1996} while ether groups have weak oxidative resistance to enzymes such as myeloperoxidase {Stokes K, 1998}. Using carbonate groups instead have been shown to improve the degradative resistance of PU {Edwards, 1998}, an effect due to the increased hydrogen bonding between all of the segments {Tang, 2001;Woo, 2000}, information which we capitalised on when synthesising poly(carbonate-urea)urethane (PCU) {Salacinski, 2002b;Salacinski, 2002c;Seifalian, 2003}. However, both in vitro and in vivo studies by our group on PCU have shown that hydrolysis of the carbonate group is still possible {Salacinski,

2002b;Salacinski, 2002c} under certain circumstances such as peroxidation.

The principal function of the hard segment of a PU is to give mechanical strength by acting as the structural framework of the polymer as well as having a 'shielding' effect on the soft segment {Stokes, 1995} of the PU {Salacinski, 2002b}. According to Stokes, this 'shielding effect' depends on the distribution of the isocyanate molecules within the polymer and the then resulting microstructure. Traditional PU have hard segments composed of urethanes or urea but more recently, there have been alternatives to improve both hydrolytic and oxidative stability with the use of silicon-containing poly(dimethylsiloxane) (PDMS) either as a coating, a surface-modifying end group {Hu, 2002;Werner, 1999} or by its interaction with the soft segment of the polymer {Barbucci, 2003;Mirzadeh, 1995}. The reason for this approach is that PDMS has extreme resistance to hydrolysis and oxidation. However, the incompatibility of PDMS integration into PU has led to poor materials which display low biostability {Salacinski, 2002b;Salacinski, 2002c}.

Recently, a newer generation of polymers have been developed which interact at the nanoscale and hence possess completely different qualities. Nanocomposites are materials whose components interact at a nanoscale level, a characteristic which confers great mechanical strength to these polymers {Zhang, 2004} due to the quantum-scale interaction between these molecules which also gives it an anti-fracture properties. The reason for this according to Griffin is that when a composite has fillers below a critical length, their strength even if cracked, is virtually equivalent to that of a solid crystal. This holds true for nanocomposites and explains the relative immunity of nanocomposites to fracture {Gao H, 2003}.

As illustrated in chapter 2, we have developed a Novak type II nanocomposite {Novak B, 1993} using nano-sized silsesquioxane molecules namely that of polyhedral oligomeric silsesquioxanes (POSS) linked to a previously synthesised polyurethane; poly(carbonate-urea)urethane (PCU). It is our original hypotheses that using these nanocores would hold together all the components of the polyurethane and thus repel degradation.

3.2. METHODS AND MATERIALS

3.2.1. POLYMER SYNTHESIS

Please refer to chapter 2.

3.2.2. GRAFT FABRICATION

Using a novel polymer as synthesised above using a combination of PCU with POSS nanofillers, we have fabricated 5 mm diameter POSS-PCU grafts by the cast-coagulation technique. 5 mm diameter stainless steel mandrels were dip-coated in 14 % (w/v) of the polymer solution using a mechanised dipping device at a rate of 1 cm/s before being coagulated in distilled water (DW) for 24 hours. The grafts were then air-dried for 48 hours at room temperature before being pulled off the mandrels as single-lumen vascular prostheses with a closed-pore microporous vessel wall and

lumen. The degradative resistance of these grafts was determined by keeping them in oxidative, hydrolytic and physiological solutions which replicate all forms of degradation in vitro.

3.2.3. DEGRADATION PROTOCOL

3.2.3.1. Hydrolysis

The degradative mechanisms in vivo were simulated using a set of well-described hydrolytic and oxidative degradative tests {Zhang, 2004}. Polymeric susceptibility to hydrolytic lysosomal action was studied using cholesterol esterase (CE) which was prepared by dissolving CE powder (Sigma Chemical Co., Ltd., Poole, Dorset, UK) in sterile, neutral pH, 0.05 M phosphate-buffered saline (PBS). The other hydrolytic mechanism elicited was using phospholipase A_2 solutions / PLA; (Porcine pancreatic phospholipase, Sigma Chemicals) dissolved in 50 mM Tris with 6.8 mM $CaCl_2$ at pH 8.0 at 0.18 IU/mL concentration where 1 U is its ability to hydrolyse 1 mM/min of phosphatidylcholine at 37 °C and pH 8.0. The sheets and grafts of POSS-PCU nanocomposites exposed to these hydrolytic solutions were incubated for 70 days at 37 °C prior to being rinsed in distilled water, dried and stored before testing.

3.2.3.2. Oxidation and peroxidation

Oxidative and peroxidative degradative solutions involved an oxygen donating

system which was prepared by mixing 1.63 M hydrogen peroxide; H_2O_2 (Stabiliser-free; Fluka Chemicals Ltd., Poole, UK) and 0.1 M $CoCl_2$. $6H_2O$ (Sigma-Aldrich Ltd., UK). A previously described peroxidation system using 1.63 M t-butyl hydroperoxide and 0.10 M $CoCl_2.6H_2O$ (t-but/$CoCl_2$) was prepared as was a thiyl radical peroxidative system with the addition of 0.10 M glutathione solution (Glut/t-but/$CoCl_2$). As with the hydrolytic degradation systems, the grafts and sheets of POSS-PCU were incubated for 70 days before being rinsed and dried, ready for testing.

3.2.3.3. Plasma protein fractions

In this study, we utilised Zhang's technique which used polyethylene glycol (PEG) to extract the different plasma protein fractions. Into a beaker, we placed 200 mL of citrated human plasma (fresh frozen plasma) at 4 °C from the Blood Transfusion Department of the Royal Free Hospital, London, UK to which 20g of PEG at a M_w of 3350 (Sigma-Ultra grade; Sigma Chemical) was added. The 10% mixture (fraction I) was stirred every 15 minutes for an hour, 100 mL of it was removed as fraction I and the remaining 100 mL was centrifuged at 2000 rpm for 30 minutes. The supernatant was then extracted and PEG was added to it to reconstitute a 10% mixture. The process of mixing and centrifugation was then repeated to form four plasma protein fractions (Plasma Fractions I to IV labelled herein as PF I to PF IV). Fraction I (PF I) is rich in fibrinogen, plasminogen, the C-3 component of the complement and IgG, and b-lipoproteins. Fraction II (PF II) is rich in α2-macroglobulin, IgA, prothrombin, and other coagulation factors (prothrombin complex). Fraction III (PF III) contains

mainly acid glycoprotein, transferrin, and 20% PEG. Fraction IV (PF IV) contains principally albumin and transferrin.

3.2.3.4. Control

As the positive control, cumene chloride was used as it is has very strong degradative effect on plastics in general. All degradative solutions contained 10 mg of streptomycin, 10,000 U of penicillin, and 10 mg of neomycin per millilitre to prevent bacterial and fungal infections which could affect the outcome of the results. As above, 6 samples of POSS-PCU nanocomposite sheets were placed in these solutions for 70 days before being washed and dried for testing.

3.2.4. FOURIER TRANSFORM INFRA-RED SPECTROSCOPY

The casted sheets of POSS-PCU (n = 6) were now subjected to infra-red spectrophotometric analysis to assess for evidence of sub-surface bond degradation following simulated in vivo degradation using the technique mentioned in chapter 2. The analysis was repeated six times on both surfaces of the sheets to determine whether there was a significant change in sub-surface bond patterns which indicated the presence and extent of bond scission, if any.

3.2.5. SCANNING ELECTRON MICROSCOPY

The degraded control and polymer sheets were dehydrated with ethanol/distilled water in increments of 10% ethanol at 41 °C and then freeze-dried for 2 days. Following this, pieces of the nanocomposite was cut out and attached to aluminium stubs before being coated with gold using an SC500 (EM Scope) sputter coater. Next, a scanning electron microscope system (Philips SEM Model 501, Netherlands) was used to analyse 10 areas on the surface of the polymer sheets which were chosen at random for any evidence of surface degradation namely pitting, fissuring, cracking {Wiggins, 2001} and crystalline segment shearing ('balding'). More sensitive methods of surface analyses such as AFM and XPS analyses were not used due to the higher probability of artefacts developing on their surfaces following the handling process. All the SEM analyses in this thesis was done at the Electron Microscopy Unit, Royal Free UCL Medical School, London, UK.

3.2.6. RADIAL STRESS-STRAIN ANALYSES

The 5 mm diameter POSS-PCU nanocomposite grafts which were first exposed to degradative solution were placed in series within a flow circuit containing native citrated blood of 0.40 haematocrit which was pumped at 1 Hz and at mean pressures of 70 and 100 mmHg through using a variable speed pump (BioMedicus, Minnetonka, MN, USA) in order to simulate arterial pulsation. The entire system was placed in a water bath at 37 °C to reduce damping. The intraluminal pressures within these grafts were recorded at the mid-section of each graft using a Millar Mikro-tip catheter tip transducer (Millar Instruments, Houston, Texas, USA). The mean pressure was

regulated by varying the height of the blood reservoir while pulse pressure was controlled by regulating the pulsatile pump. In this series of experiments, no pre-clotting was performed as no transmural leakage was observed in spite of high intramural pressures of up to 300 mmHg. In addition, all grafts were stretched to 110 % of their original lengths to simulate biology. The output data was then recorded using an analogue-to-digital data acquisition recording systems (ADC/MacLab; AD instruments, Hastings, UK) via 7.5 MHz linear array probes of a Duplex scanner (Pie 350; Pie Medical Systems, Maastrict, The Netherlands) which kept track of graft wall distension (WallTrack, PieMedical Systems, UK).

From the mechanical perspective, the radial distension experienced by these grafts is directly reflective of the strain under which it has been put while the stress within a cylindrical system is given by Laplace's Law shown here below,

$$\sigma = (pR)/t$$

where, σ refers to the circumferential stress within the graft, p refers to the maximal pressure within the system, 't' is the thickness of the graft wall and R is the radius of the graft. For the purposes of these experiments, 't' and 'R' are constants as all these grafts were fabricated in exactly the same way. In this system, stress (σ) is therefore directly proportional to the maximal/systolic pressure. Based on these assumptions, a stress-strain curve was plotted with strain/vessel wall distension on the x-axis and systolic pressure representing circumferential stress on the y-axis in order to understand the biomechanical behaviour of these degraded polymers and to correlate with classical Hookean laws.

3.2.7. DIFFERENTIAL SCANNING CALORIMETRY

Nanocomposite samples which were found to have suffered the greatest amount of degradation was then studied using differential scanning calorimetry to determine whether the respective samples had undergone a significant change in glass transition temperature (T_g), melting temperature (T_m) and heat capacity at T_g (ΔC_p). 3 by 3 mm sheets of the nanocomposite taken from different parts of the polymeric sheet were then subjected to heat-flux DSC (Shimadzu DSC Ltd., Japan) as described in chapter 3. All samples were weighed pre- (W) and post-test (W') to confirm that there was no change in mass after melting. In order to achieve consistency, all specimens were run thrice (n = 3).

3.3. RESULT

3.3.1. SURFACE DEGRADATION

The control POSS-PCU nanocomposite showed all the characteristic bond patterns of PCU with the typical wavelengths at 1740 cm^{-1} (carbonyl segments of carbonate), the 1640 cm^{-1}wavelengths of urethane carbonyl groups and bonds in the 1240 to 1250 cm^{-1} range indicative of the C–O–C bonds of the CO–O–C segments. In addition, the POSS nanocages resulted in wavelengths at 1100 cm^{-1}, the presence of which did not alter the existing polyurethane bonds.

Polymer degradation of these nanocomposites was classified into three categories namely hydrolytic, oxidative and plasma fractions with each of these samples being analysed by infra-red spectroscopy. FTIR analyses of the nanocomposite exposed to differing plasma fractions I to IV showed no difference in intensity for each bond wavelength as compared to the control ($p = ns$) (figure 3.1). These results indicate that biological proteins have a negligible degradative effect on these POSS-PCU nanocomposites.

Figure 3.1. Sub-surface bond patterns in POSS-PCU nanocomposites following exposure to plasma protein fractions (PF I to IV) showing no difference in the intensities of 'Si-O', 'C-O-C', 'NH-CO'(urea) and '(NHCO)O'(urethane) bonds although on closer inspection of PF III-degraded samples (marked in red), there is a slight left-shift in the C-O=C bond indicating a reduction in hydrogen bonding.

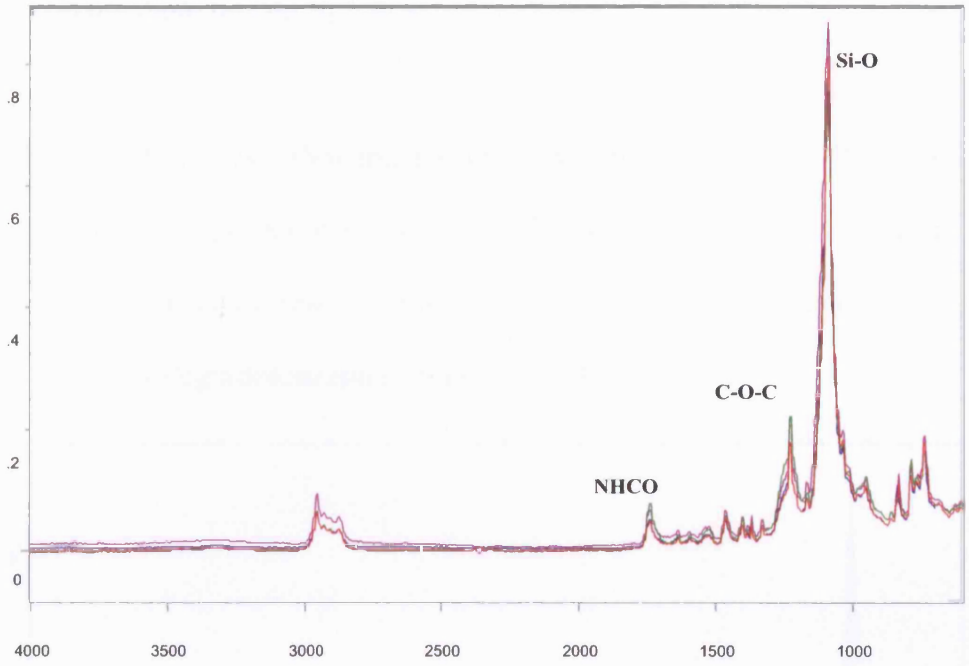

Index:

PF I PF II PF III PF IV

Hydrolytic enzyme degradation and in particular, phospholipase (PLA) had a significant effect on silicon-associated bonds (One way ANOVA, $p < 0.01$) compared to the control. Interestingly, these had no significant effect on the remaining hard

segment as well as the soft segment of the polymer. This suggests that the POSS nanocores integrated into the polyurethane via zones of intercalation which had an overall 'shielding' effect on the structure of PCU (figures 3.2 a&b). The remaining degradative solutions including cumene chloride, a potent degrador of plastics in general were no different from the undegraded polymer. In all of these samples and in particular PLA, we found no evidence of colour change or macroscopic signs of degradation indicating that although 'Si-O' bond were less prominent in this system, for some reason there was no significant degradation.

Figure 3.2a. FTIR analyses showing the sub-surface bond patterns in POSS-PCU nanocomposites after being degraded by hydrolytic solutions with significant decreases in the 'Si-O' bonds of the POSS nanocores in the PLA-degraded samples (marked in red).

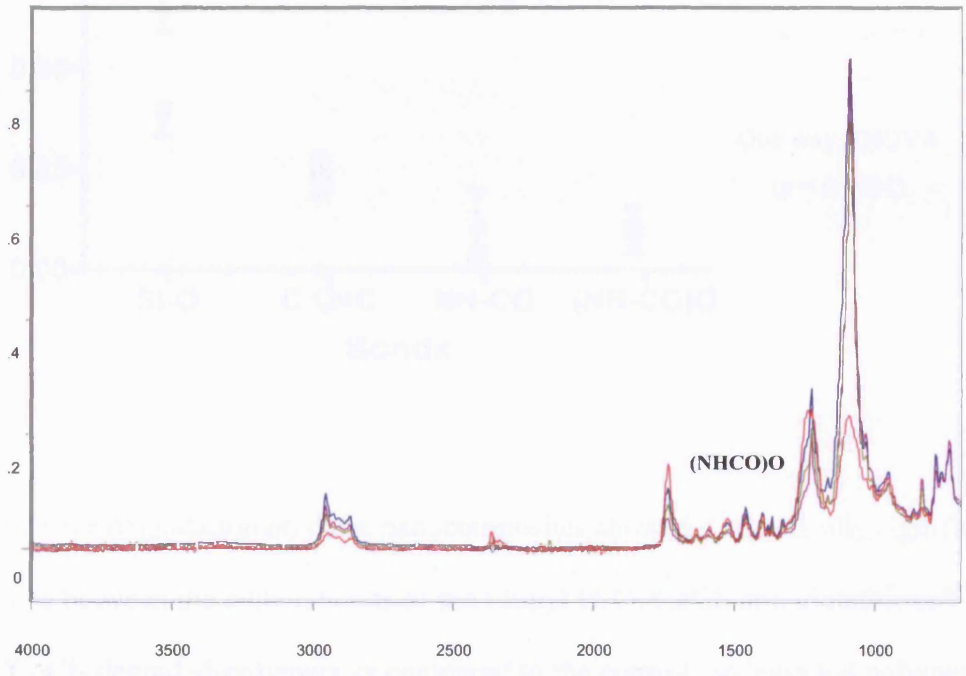

Index:

Control	CE	PLA	Cumene

Figure 3.2b. One-way ANOVA analyses (n = 12) showed a significant decrease in the 'Si-O' bonds of the PLA- degraded samples compared to the control, CE-degraded and cumene-degraded samples ($p < 0.0001$). The remaining bonds did not show any significant difference post-degradation.

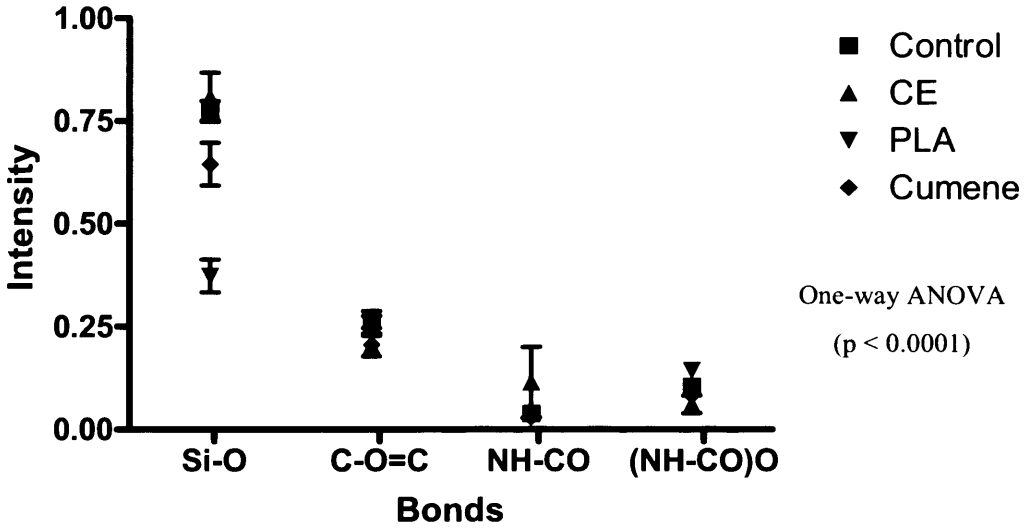

Oxidative degradation on these nanocomposites showed a statistically significant difference between the silicon bonds of the t-butyl $H_2O_2/CoCl_2$ and glutathione/t-butyl H_2O_2 /$CoCl_2$ degraded-polymers as compared to the control, undegraded polymer (figures 3.3 a&b). Detailed analysis of the samples showed a small left-ward shift in the peak of the C-O-C bonds indicating a reduction in overall hydrogen bonding

(figure 3.4) especially with the glut/t-butyl system. The biologically abundant H_2O_2 system did not show any effect on any of the bond structures of the polymer. Based on this, we can see that t-butyl peroxide degrade the 'Si-O' bonds and cause macrophase separation within the nanocomposite as suggested by the yellowing of the t-butyl peroxide degraded solutions {Shibayama M, 1991}.

Figure 3.3a. The effect of oxidative and peroxidative degradative solutions on the POSS-PCU nanocomposite showing a reduction in the intensity of 'Si-O' bonds of t-butyl/$CoCl_2$ degraded samples (marked in red) compared to the control (marked in blue). Please note that there is a leftward shift of the 'C-O-C' bonds indicating a decrease in hydrogen bonding.

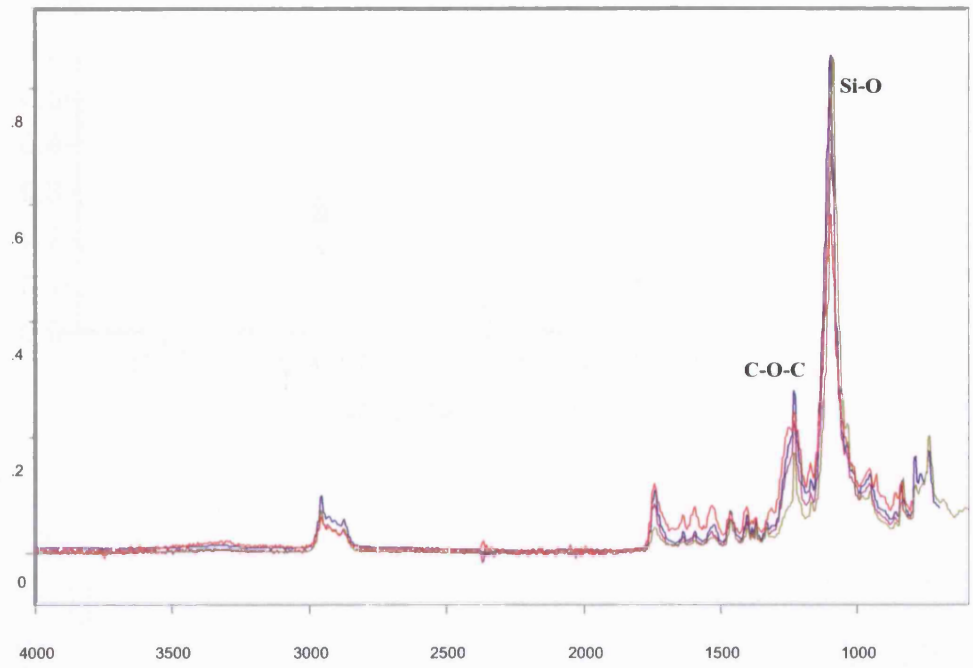

Index:

Control H_2O_2 t-butyl glut/t-butyl

Figure 3.3b. One-way ANOVA analyses of the main bonds within the POSS-PCU nanocomposite showing a significant decrease in 'Si-O' bonds following t-butyl/$CoCl_2$ and Glut/ t-butyl/$CoCl_2$ degradation with an effect on the' C-O=C' bonds as well in the latter.

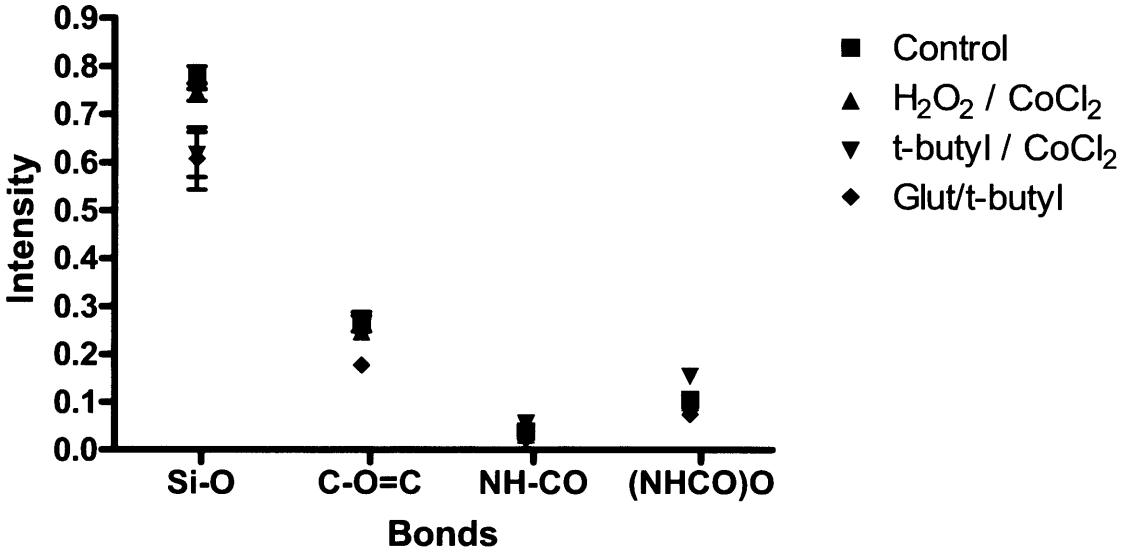

Figure 3.4. Comparisons of PLA-, Glut/t-butyl-peroxide, t-butyl-peroxide degraded and control polymers.

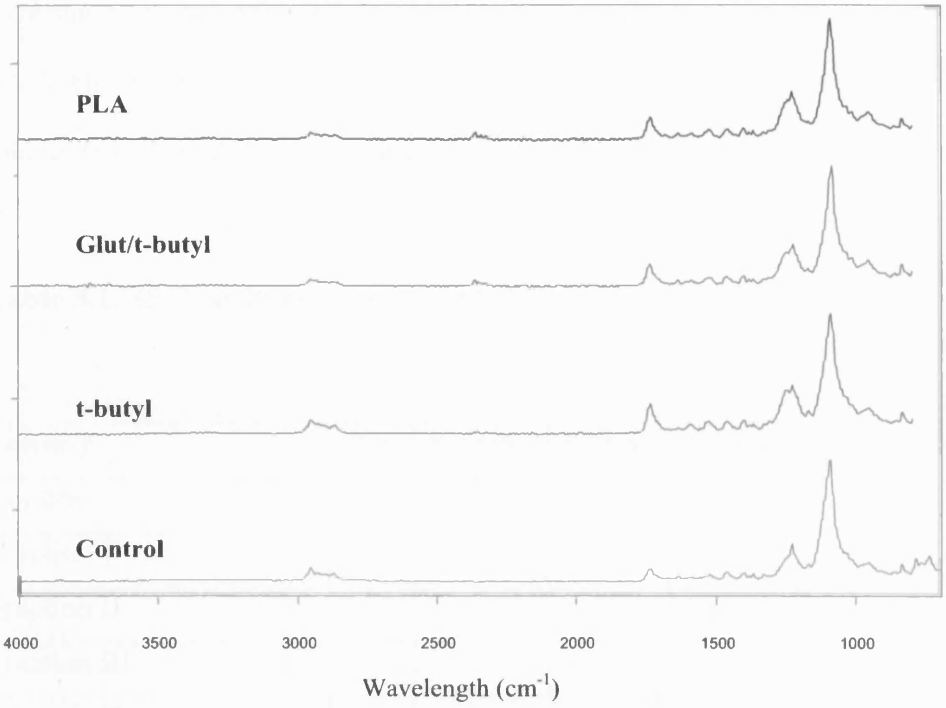

3.3.2. SURFACE TOPOGRAPHY

The surface ultrastructure of the polymer was assessed at ten random sites using SEM (640x magnification). The undegraded polymer characteristically showed a rough surface with numerous crystalline peaks and intervening flat areas, a consistent feature in all the analysed samples (figure 3.5a). Overall as shown in table 3.1, the plasma fractions especially I and II resulted in the formation of minimal pit formation and 'balding' (shearing of the crystalline peaks). These effects were even more pronounced in the hydrolysed samples particularly with PLA (figure 3.5b).

Correlating this observation with FTIR analyses indicate that the weakening of the amide cross-linkages with the POSS segments results in the increased surface degradation (pit formation) with loss of the POSS crystalline peaks (balding). This shearing effect was more pronounced with the t-butyl peroxidation systems (figure 3.5c). The polymer on the whole was found to be resistant to cumene chloride; a potent degrador of plastics in general.

Table 3.1. SEM analyses of the degraded samples.

Polymer	*Pits*	*Fissures*	*Cracks*	*Balding*
Control	-	-	-	-
Fraction I	+	-	-	-
Fraction II	+	-	-	+
Fraction III	-	-	-	-
Fraction IV	-	-	-	+
Cholesterol esterase	+	-	-	+
Phospholipase	+++	-	-	+
$H_2O_2/CoCl_2$	-	-	-	-
t-butyl/$CoCl_2$	+	-	-	++
Glutathione/t-butyl/$CoCl_2$	+	-	-	++
Cumene chloride	-	-	-	+

Figure 3.5a. Surface topography of undegraded POSS-PCU (control)

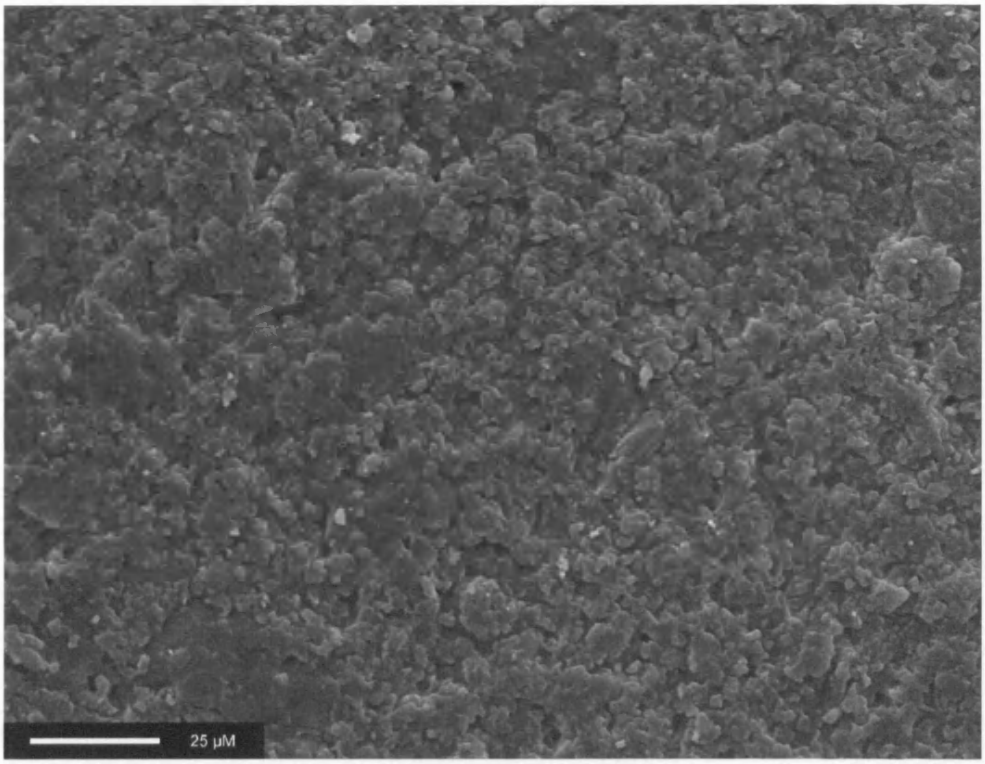

Figure 3.5b. Surface topography of PLA degraded POSS-PCU nanocomposite showing increased pitting and fissuring.

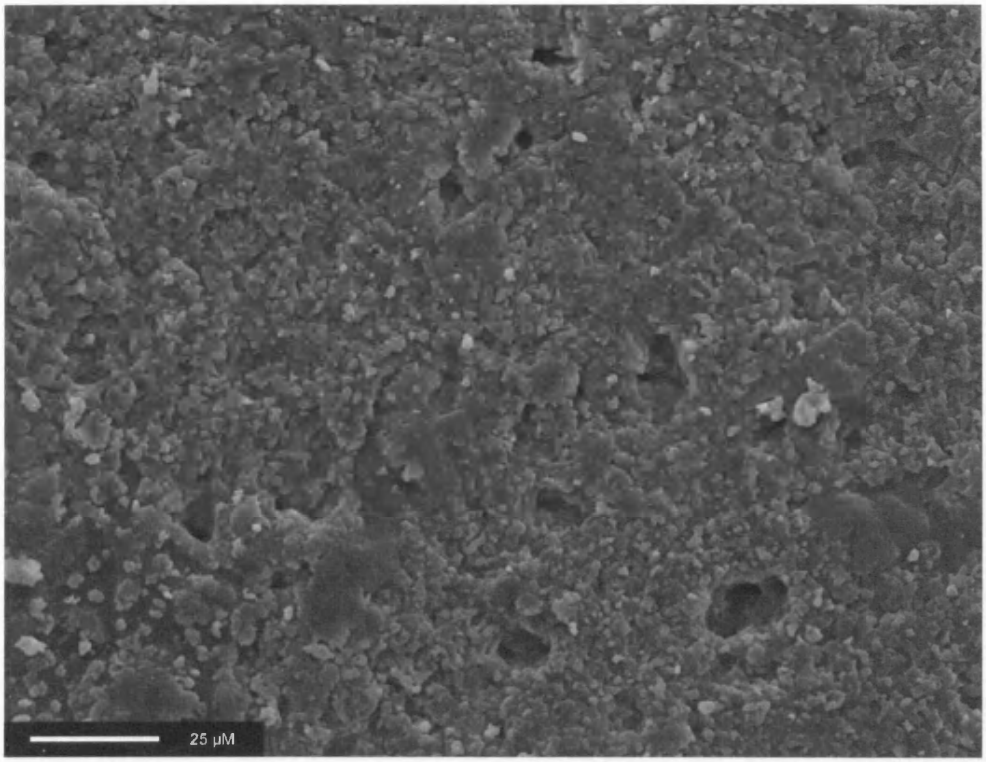

Figure 3.5c. Surface topography of t-butyl peroxide degraded POSS-PCU nanocomposite revealing an increasingly glabrous surface.

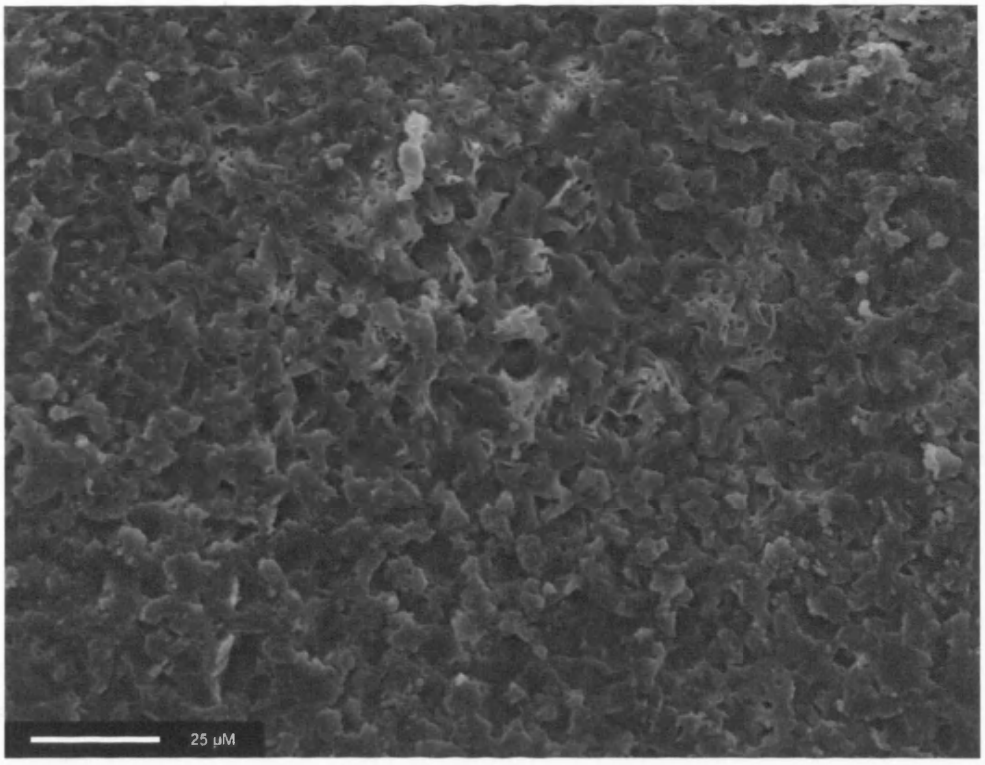

3.3.3. RADIAL STRESS-STRAIN CURVES

Stress-strain curves performed on the polymers which were most affected physically as well as chemically, showed that no significant difference in stress-strain behaviour existed between the control, PLA, CE, t-butyl-peroxide and F2-degraded nanocomposites. This data shows that the soft segment of the polyurethane nanocomposite remains intact in spite of accelerated degradation as illustrated by the preservation of its elasticity in the figure 3.6 below. It is important to note however that in the case of t-butyl-peroxide degraded nanocomposites (marked blue), the

vessels burst at pressures beyond 220 mmHg indicating a decrease in mechanical strength compared to all the other grafts. As FTIR studies have previously shown, t-butyl peroxide and its counterparts affected the 'Si-O' bonds within the graft which are responsible for holding together the nanocomposite by means of intercalating zones between the soft, amorphous and the hard, crystalline segments of the polyurethane which explains its lower burst strength. Thus, t-butyl peroxide seems to affect the functional side-chain of the POSS nanocage which links it to the backbone of the polymer. As there was no difference in the FTIR studies between the t-butyl peroxide/$CoCl_2$ and glut/t-butyl peroxide/$CoCl_2$ solutions, the former was used as the reference degradative solution representing the peroxidation group in all subsequent studies.

Figure 3.6. Radial stress-strain curves of the representative degradation groups showing their similarity in elasticity.

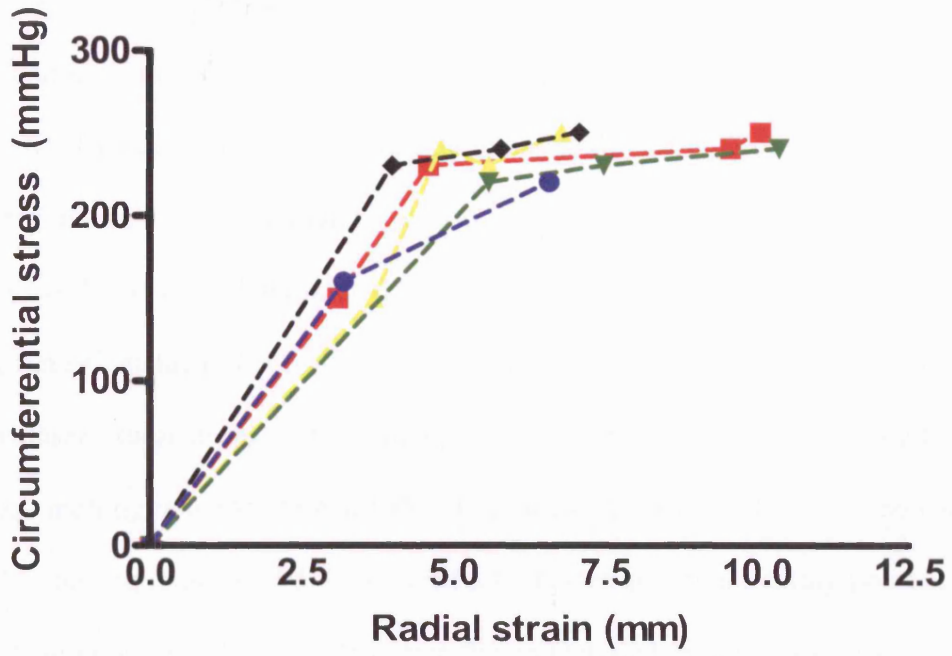

Index :

- Fraction II (PF2)
- Undegraded control
- t-butyl peroxide / $CoCl_2$
- Cholesterol esterase (CE)
- Phospholipase (PLA)

3.3.4. THERMAL CHARACTERISTICS

Glass transition temperature (T_g) gives information on the amorphous segment of the nanocomposite while the heat capacity changes (ΔC_p) at the T_g is a measure of the inter-molecular interaction between these molecules during this transition. In the undegraded samples, we found a mean T_g of -37.34 °C and a mean ΔC_p value of 0.40 J/gK while the t-butyl peroxide degraded samples showed a mean T_g of -37.01 °C and a mean ΔC_p value of 0.42 J/gK, values which are almost similar to the control group. On closer examination of the t-butyl peroxide-degraded samples, we found a double-phase melting range starting at 165.5 °C followed by a second melt phase with softening beginning at 195.42 °C, gradually reaching a final melting point at 255.04 °C. Comparing this to the softening in the undegraded sample starting at 226.12 °C and ending at 265.06 °C, this indicates that t-butyl peroxide causes greater phase separation between the hard and soft segments within the nanocomposite.

Based on this data, we deduced that the POSS nanocore/fillers resulted in closer packaging of the polymer with greater interaction between both phases of the polyurethane particularly at the aforementioned zones of intercalation. From the degradation perspective, although there have been surface degradative changes observed in the peroxidated nanocomposites, the chemicals as such have failed to affect the soft segment of the nanocomposite and dismantle the bulk superstructure of the nanocomposite as a whole since these DSC results showed no macroscopic thermal changes in the degraded nanocomposite versus the control sample. There was however a change in the melting temperature (T_m) between the t-butyl-peroxide containing samples and the control group. As T_m is more reflective of the hard

segment of the polyurethane which constitutes its structural framework, we found that this data correlated with our FTIR studies on these degraded nanocomposites as well as the lower burst strength of the t-butyl peroxide-degraded grafts. This further lends credence to our hypothesis that these POSS nanocores/fillers 'shield' and so essentially protect the soft segments of the polymer via the interlinkages at the zone of intercalation.

In the case of the hydrolytic enzymes, although PLA seemed to show a marked effect on the Si-O bonds of the POSS nanocage on FTIR, this did not translate on DSC into a significant change in T_g or T_m as well as change in elasticity on stress-strain curves. The mean T_g of the nanocomposites was -37.35 °C with a mean ΔCp of 0.40 J/gK, not dissimilar from the control while the mean T_m of these samples was 268.7 °C. These results suggest that the 'Si-O' bonds which were degraded by PLA may not have been functionally involved in cross-linking within the polymer. This may be explained by the fact that the nanocore used in this polymer has seven non-functional side-groups (2,3-propanediol) and one main functional linkage group (dihydroxyl-cyclohexyl pendant chain) connecting it to the main polyurethane backbone. All these results are graphically illustrated in figure 3.7.

Figure 3.7. Comparison of DSC thermal analyses of t-butyl-degraded, PLA-degraded and undegraded polymers showing the stabilising effect of POSS nanocores to PCU degradation.

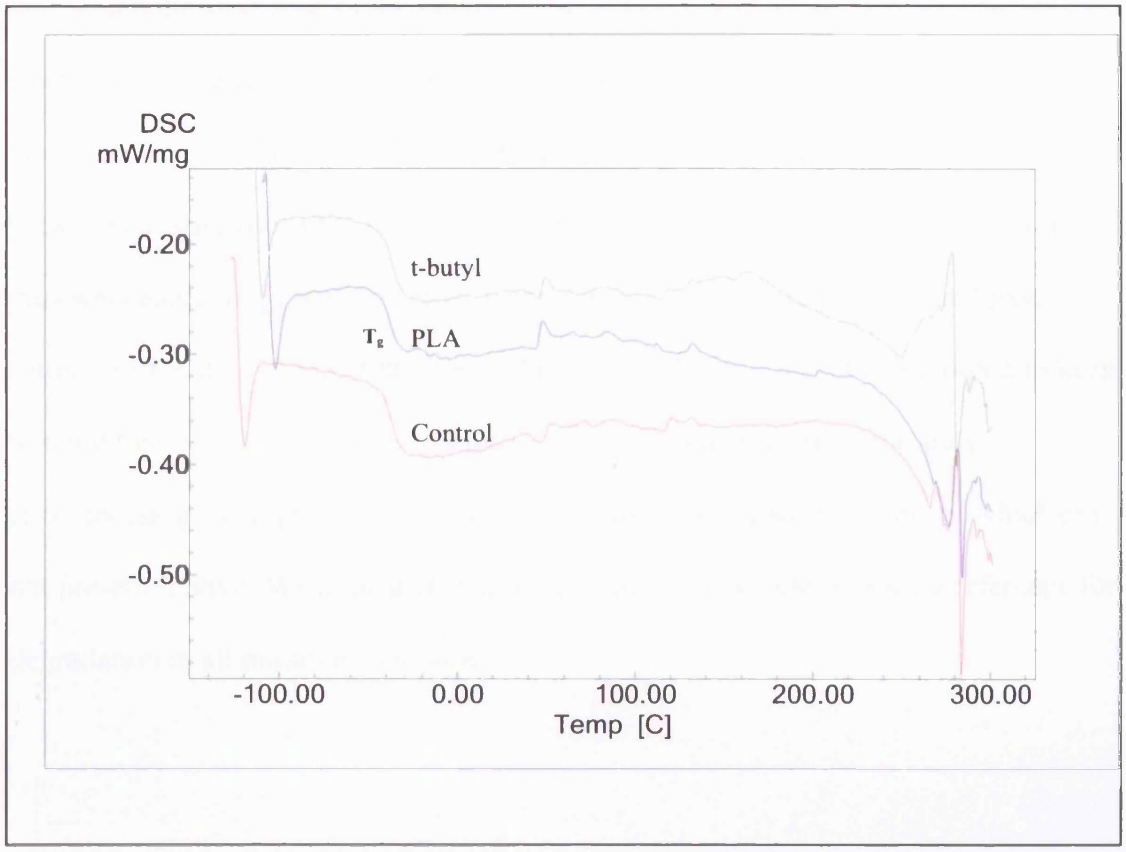

In the CE group, there were physical signs of degradation on these samples ('blistering' effect) but with no colour change indicating no phase separation. Analysis of the T_g showed no significant decrease but the heat capacity at this temperature was decreased (0.28 J/gK) compared to the other samples. This shows that although there was a decrease in the intermolecular bonding strength within the soft phase at this temperature, it remained relatively stable while the T_m did not change on treatment with a single-phase melt process beginning at 193.83 °C, possibly an effect of the reduced intermolecular forces within the soft phase. We

found that the physiological solutions did not cause any significant degradation to the POSS nanocomposite.

As polyurethane degradation begins as a surface phenomenon and gradually creeps into the substance of the polymer {Schubert, 1997}, both FTIR as well as DSC analyses were performed on samples. A summary of the DSC analyses is depicted in table 3.2. We postulate that while t-butyl peroxide affected the linker molecule between the silsesquioxane nanocore and the hard segment polyurethane backbone thus weakening the structural network and causing an alteration of T_m, the lipase action of PLA did not affect this particular linkage. In any case, it is important to keep in mind that the chemicals used represent accelerated degradative solutions encompassing a comprehensive range of degradative mechanisms some of which are not present in vivo. We hope that in this way, this study would become a reference for degradation in all possible situations.

Table 3.2. Summary of DSC results on undegraded, t-butyl-peroxide degraded and PLA-degraded POSS-PCU nanocomposites.

Degradative solution	**Colour change**	**T_g**	**ΔC_p**	**Softening**	**T_m**
None (control)	None	-37.34 °C	0.40 J/gK	226.12 °C	265.06 °C
H_2O_2 / $CoCl_2$	None	-36.4 °C	0.28 J/gK	245.7 °C	266.15 °C
t-butyl H_2O_2 / $CoCl_2$	Yellowing	-37.01 °C	0.42 J/gK	195.42 °C	255.04 °C
Glut / t-butyl H_2O_2 / $CoCl_2$	Yellowing	-37.55 °C	0.34 J/gK	235.13 °C	261.3 °C
Phospholipase (PLA)	None	-37.35 °C	0.42 J/gK	225.2 °C	268.7 °C
Cholesterol Esterase (CE)	None	-36.49 °C	0.28 J/gK	193.83 °C	269.33 °C
Cumene chloride (Cum)	None	-42.26 °C	0.34 J/gK	231.32 °C	257.66 °C
Plasma fraction I (PF 1)	None	-36.34 °C	0.32 J/gK	237.3 °C	267.8 °C
Plasma fraction II (PF II)	None	-37.29 °C	0.38 J/gK	236.1 °C	268.39 °C
Plasma fraction III (PF III)	None	-38.09 °C	0.26 J/gK	238.92 °C	268.9 °C
Plasma fraction IV (PF IV)	None	-39.4 °C	0.42 J/gK	231.83 °C	262.93 °C

3.4. DISCUSSION

PU are currently being used in a variety of medical devices and in the field of cardiovascular medicine, variations of polyurethanes containing ester-, ether- and carbonate-based soft segments have been used as vascular grafts {Eberhart, 1999;Hsu, 2000}. Previous studies have shown that PU has ideal elastic and compliance properties, characteristics which minimise intimal hyperplasia (IH) {Salacinski, 2001c}. As alluded to earlier, there have been some concerns regarding the susceptibility of PU to degradation in vivo. Our previous study on poly(carbonate-urea)urethane (PCU), a new generation PU, showed that these grafts were more biostable in the in vivo environment than its predecessors (Seifalian, 2003}. Nevertheless our experiments on PCU degradation reveal room for improvement in the stability of these polyurethanes. As existing data suggests that nanofillers substantially increase the mechanical strength of the composite, a new variety of nanocore-integrated PU were designed and synthesised by our group {Kannan, 2004;Kannan, 2004}. The stability of these materials as vascular grafts in vivo was therefore of prime importance to prevent aneurysmal formation.

PU degradation begins as a surface phenomenon and in this study, FTIR analysis performed on these samples reveals that in spite of prolonged periods on incubating the nanocomposite, minimal surface changes were elicited. In the t-butyl peroxide degradation systems of t-butyl/$CoCl_2$ and glut/t-butyl/$CoCl_2$, which had shown a significant degradative effect on MyoLink® {Salacinski, 2002b}, apart from a small drop in the intensity of the 'Si-O' bonds in the nanocomposite which correlated visually with a loss of silicon-rich POSS segments on SEM studies, the bonds

particularly within the soft segment were virtually unharmed. These changes included the development of 'pits' as well as a 'balding' effect on the nanocomposite. Based on this, we deduced that POSS-PCU nanocomposites extended from the hard domain of the polymer into the soft domains at transitory zones of intercalation akin to a 'wire mesh' which holds together the various components of the nanocomposite and causes a reduction in phase separation within the polymer.

Strength and toughness/elasticity analysis of these nanocomposite vascular grafts revealed that in spite of accelerated degradation, all samples had shown no significant difference in their elastic properties. This is an indicator of the stability of the soft phase of the nanocore-integrated PU to all forms of in vitro degradation. When compared to the similar experiments on MyoLink®, these nanocomposite grafts showed greater stability in a degradative environment. These results were further explained on performing DSC to assess both the soft and hard phases of the nanocomposite.

Thermal analysis of even the most severely degraded POSS-PCU nanocomposites showed that the glass transition temperature; an indicator of the soft phase of a polymer, did not vary significantly between the non-degraded and degraded samples, thus seconding the data on stress-strain analysis of the nanocomposite grafts. We found that the addition of POSS nanocore/fillers to PCU increased the final melting temperature of the nanocomposite by approximately 30 °C while the T_g remains the same, for reasons which are explained in chapter 2. This is in line with the published literature of fillers in microcomposites, which show the negligible action of fillers on T_g {Turi EA, 1981}. The similarity of these values to MyoLink® following POSS

degradation by t-butyl systems reveal that in the absence of these nanofillers, the thermal properties of the nanocomposite are not dissimilar from PCU.

The increase in T_m and the lesser phase separation on the other hand are attributable to the increased nanoscale interactions between its constituents binding together the polymer. Furthermore, these nano-core integrated PU unlike MyoLink® which show three-phase melting, exhibited a single phase melting process with higher temperatures at which softening occurs. In the t-butyl degraded samples, the melt process was two-phased with lower softening temperatures. These results again signal that both hard and soft phases of the polymer integrate to a far greater extent than in PCU due to the nanoscale interaction of the POSS-nanocages with the soft phase.

In summary, the addition of POSS nanocore/fillers to the PU imparts a type of 'shielding' effect on the soft phase of the nanocomposite thereby preserving its elasticity and compliant properties via zones of intercalation. In addition, the extensions of these nanofillers from the hard phase into the soft phase help cross-link and bind together the entire composite as a single elastic unit, not unlike vulcanised rubber. This is exemplified by the increase in T_m compared to PCU or MyoLink®. These results herein indicate the immense potential of POSS nanoparticles in improving the degradative resistance of polymers.

Chapter 4

4. The in vivo biocompatibility and biostability of silsesquioxane nanocomposites

4.1. INTRODUCTION

Having now confirmed the increased degradative resistance of this nanocomposite in vitro, two additional objectives were identified (a) Is it safe in a biological host ? and (b) Would its degradative pattern be altered in an in vivo environment ? This is a pertinent issue as parallel experience with silicon-based breast implants has shown us. The most important property of any of these tissue implants is interfacial biocompatibility; the inter-relationship between the implant and its biological host {Eberhart, 1987}. A biomaterial conventionally elicits a foreign-body reaction once implanted in vivo. However, when there is minimal interaction and bioadhesion {Weiwei Du, 2000} at its interface (figure 4.1) once in vivo, it is said to have improved biocompatiblity. Hence, understanding the behaviour of this nanocomposite at the biological interface is essential prior to developing it as a microvascular prostheses.

Figure 4.1. Schematic representation of the interplay between the biological host and the implant.

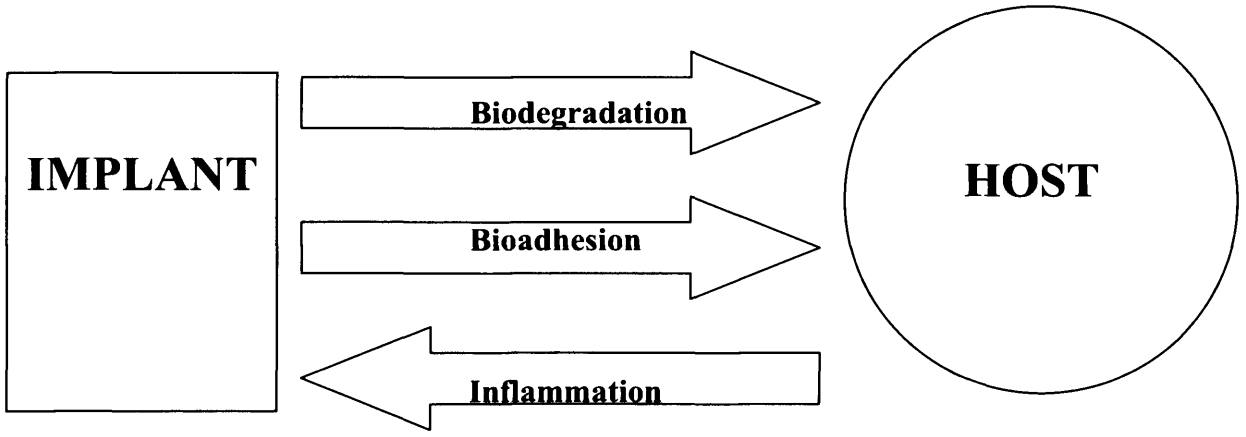

Silicone is a favoured material particularly as breast implants and finger joint replacements. First introduced in breast surgery during the 1960s, it is an inert biomaterial thought to cause minimal inflammation. However, long-term studies are now revealing that silicone delays wound healing {Shanklin, 1999}, causes capsular contracture {Wagner, 1977;Ersek, 1997;Batra, 1995;Kasper, 1994;Siggelkow, 2003}, is immunogenic {Bar-Meir, 1995} and in joint prostheses {McCarthy, 1988}, causes severe inflammation {Peters W, 1996}. Alternatively, porous polyurethane breast implants allow better tissue fixation {Cohney, 1997}. There have been reports that these implants reduce the incidence of capsular contracture {Sinclair, 1993}. A possible explanation is that fibroblasts proliferate into numerous pores and when they contract, they counterbalance one another to minimise the occurrence of painful contractures {Pennisi, 1990}. This prompted the creation of silicone breast implants coated with porous polyurethane but its use was limited due to poor biocompatibility {Brohim, 1992}. Nevertheless, polyurethane implants have not gained much popularity because of carcinogenic risks {Brinton, 1995}, difficulty in removing infected prostheses {Berrino, 1986} and significant foreign body reaction {Wagner, 1977}. All this has caused some degree of confusion with different implants being used in different parts of the world {Muller GH, 1996}.

While it is true that silicone is relatively inert, its tendency to fragment into miniscule particles {Copeland, 1994} limits its interfacial biocompatibility and this holds true for polyurethanes as well. A solution to this problem could be the incorporation of biocompatible silicon molecules as a cage-like structure; silsesquioxanes. Following the encouraging results from the in vitro degradative analyses of the nanocomposite discussed in chapter 3, we tested the biocompatibility

and biostability of these nanocomposites in vivo in order to ascertain its biocompatibility.

4.2. METHODS AND MATERIALS

4.2.1. POLYMER SYNTHESIS

As described in chapters 2 and 3.

4.2.2. IMPLANTATION IN SHEEP

A 23 % (w/v) solution of 2% POSS-PCU was casted into sheets of equal dimensions, heated at 70 °C and the resultant sheets were then autoclaved prior to being placed subcutaneously into the back of normal, healthy adult sheep for 18 months as shown in figure 4.2. A control polymer as mentioned above, consisting of linear siloxane molecules integrated with PCU of the same dimensions, was also implanted in similar conditions at the same setting. After 18 months, the implants were removed from the animals under general anaesthesia and the surrounding tissue and capsule if any, was taken for histopathological examination, performed at the Department of Pathology, Royal Free Hospital, London, UK. Throughout the period of implantation, the sheep were monitored for signs of illness or physiological dysfunction and international animal research guidelines were strictly adhered to. The implantation of the polymer sheets was done by the Dept. of Surgery, University of

Tehran, Iran.

Figure 4.2. Subcutaneous insertion of POSS-PCU casted sheets into the back of sheep (n = 6).

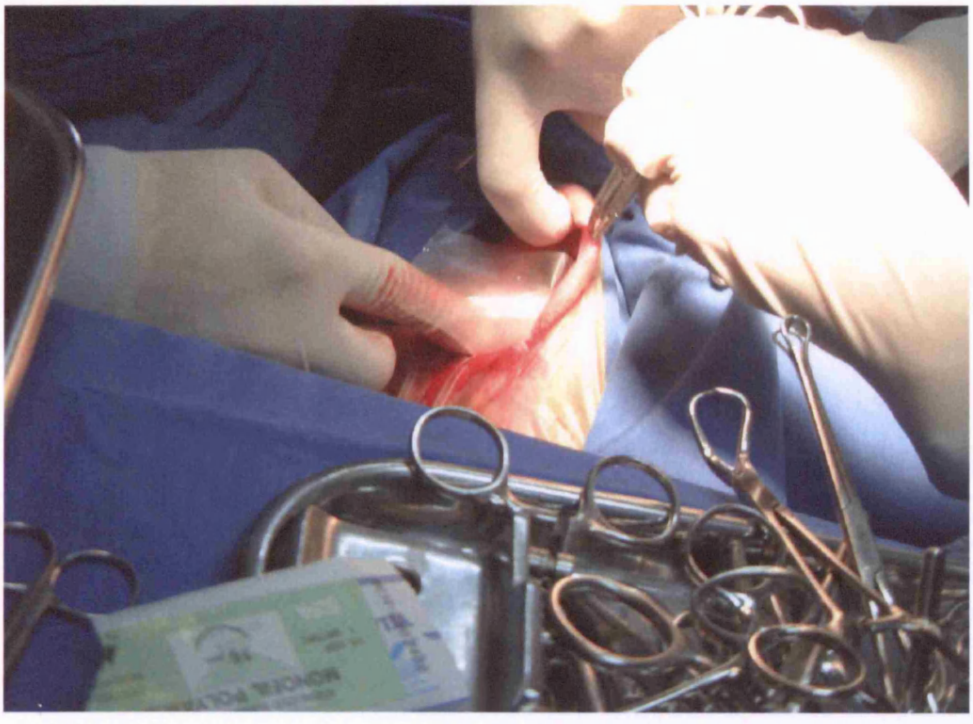

4.2.3. HISTOPATHOLOGY

In the presence of a capsule surrounding the implant, it was removed and a gross morphological assessment was performed. The specimens were then kept in 10 % formalin for histopathological examination using haematoxylin-eosin and an abridged version of the Van Tiernen classification system (table 4.1) (excluding tissue ingrowth as these sheets were non-porous) for inflammatory capsules was used to assess the extent of implant-host interaction {Van Tienen, 2002}. As the nanocomposite did not elicit any capsule formation, further tests using immunocytochemistry and enzyme

histochemistry were not performed.

Table 4.1. An abridged version of the Van Tiernen classification system for inflammatory capsules.

PARAMETER	GRADING	CHARACTERISTIC
H&E matrix staining	Grade I	Weakly red
	Grade II	Red
	Grade III	Deep red/pink
Neovascularisation	Grade 0	No vascular tissue
	Grade I	Minimal vascular tissue
	Grade II	Fibrovascular tissue
Capsule thickness (cell layers)	Grade 0	Nil
	Grade I	1 to 5 layer
	Grade II	6 to 10 layers
	Grade III	11 to 15 layers
	Grade IV	> 15 layers
Inflammatory cell distribution	Grade 0	No inflammatory cells
	Grade I	Few macrophages & giant cells (GCs)
	Grade II	Many macrophages & GCs but no neutrophils
	Grade III	Grade II & few neutrophils
	Grade IV	Numerous macrophages, GCs & neutrophils

4.2.4. FOURIER TRANSFORM INFRA-RED SPECTROSCOPY

The explanted polymers (n = 6) and the control siloxane both of which were kept in 10 % formalin solution were washed in saline and dried before assessment using the infra-red spectrophotometric analysis described in chapter 2 to determine whether any bonds had degraded during the period of in vivo implantation.

4.2.5. SCANNING ELECTRON MICROSCOPY (SEM)

Simultaneously, samples of the explanted nanocomposites and control polymers were subjected to SEM observation at magnifications of up to 640x magnification as described in chapter 3 at 10 randomly selected points on the surface of the polymer sheets for any signs of surface degradation such as pitting, fissuring, cracking {Wiggins, 2001} and crystalline segment shearing ('balding'). AFM and XPS analyses on the samples were not performed as these methods are so surface-sensitive that the results would have been affected polymer handling peri-operatively.

4.2.6. MEASUREMENT OF EQUILIBRIUM CONTACT ANGLE

Using the sessile drop method, pure distilled water (DW) was introduced via a syringe onto the surface of the nanocomposite and the dynamic contact angle of the POSS-PCU nanocomposite was measured with a Rame-Hart contact angle goniometer (New Jersey, USA). Advanced contact angles (θ_a) were measured by increasing the volume of the drop in increments of 2 μl while receded angles (θ_b) were measured by decreasing the volume of droplets in a similar fashion. Four independent measurements were performed on each sample (n = 4) and the hysteresis angles ($\Delta\theta$) were calculated as the difference between θ_a and θ_b. The values for $\Delta\theta$ were then plotted on the x-axis against the contact angles on the y-axis to determine Young's angle for water on this POSS-PCU nanocomposite at the y-intercept. This work was conducted at the Polymer Research Centre, Sheffield, UK.

4.2.7. FIBRINOGEN DIRECT ELISA

A comparison of fibrinogen adsorption to both POSS-PCU and its siloxane counterpart was performed using direct ELISA. 100 μL of bovine fibrinogen was placed in 0.28 cm^2 wells and left at 37 °C for 60 minutes to allow fibrinogen adsorption before being rinsed away and replaced with 100 μL of a 1:1600 rabbit anti-bovine fibrinogen HRP-tagged conjugated antibody (Dako Ltd, USA) in 2% serum bovine albumin for a further 120 minutes. After removing the enzyme complex, a solution of ortho-phenylamine diamine (ODP) in acid citrate buffer was added to the wells and left for 3 minutes to allow for a colour change. The reaction was finally terminated with 100 μL of 1% sulphuric acid. The mixture was then exposed to an absorption spectrum of 490 nm to assess the amount of fibrinogen adsorbed to the polymer surface (Dynex MRV, Prior Laboratory Supplies Ltd, UK). This experiment was performed with 6 repeats (n = 6).

4.3. RESULTS

4.3.1. GROSS MORPHOLOGY

The implanted nanocomposites exhibited no evidence of an inflammatory layer or capsule formation (figure 4.3a) even after 18 months of implantation. This was very clearly evident in all 6 samples following explantation. In the case of POSS-PCU samples, there was no gross morphological evidence of a capsule. Unfortunately, no surrounding tissue was taken for histology to confirm this . In stark contrast, the

control siloxane resulted in the formation of a thick, fibrous and vascular capsule as shown in figure 4.3b which completely engulfed and was adherent to the polymer. As far as the nanocomposite samples were concerned, there were no overt signs of physical degradation such as fragmentation or cracking. On the other hand, the control siloxane polymers showed gross thinning and signs of decreased mechanical strength compared to its undegraded version.

Figure 4.3a. POSS-PCU nanocomposites implanted subcutaneously for 36 months exhibited no significant capsule formation.

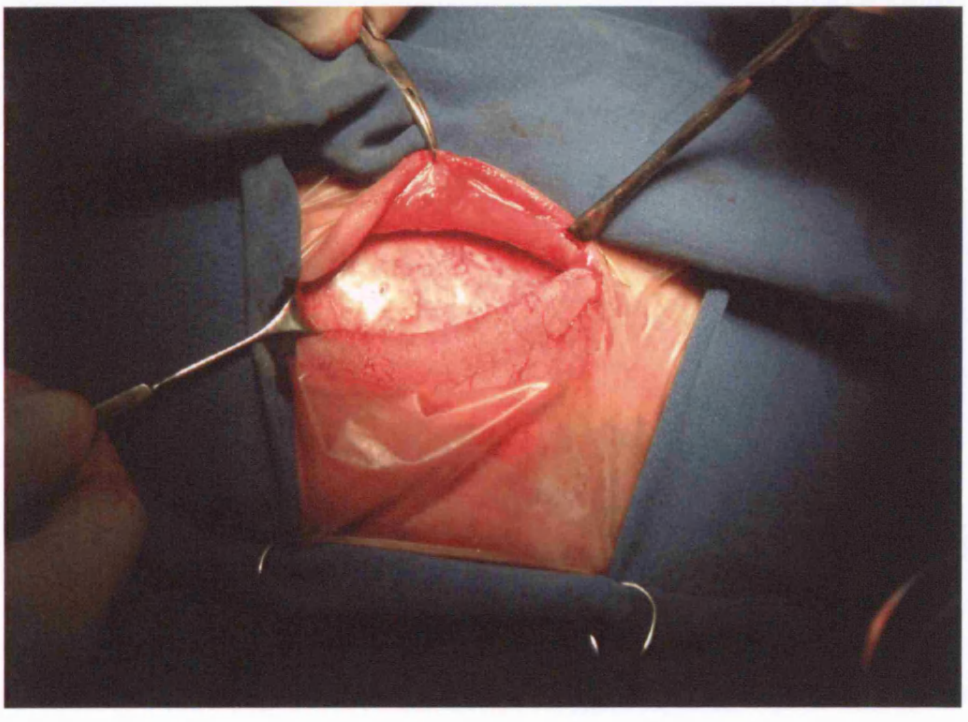

Figure 4.3b. The control siloxane implant and its surrounding capsule indicating a severe foreign body reaction.

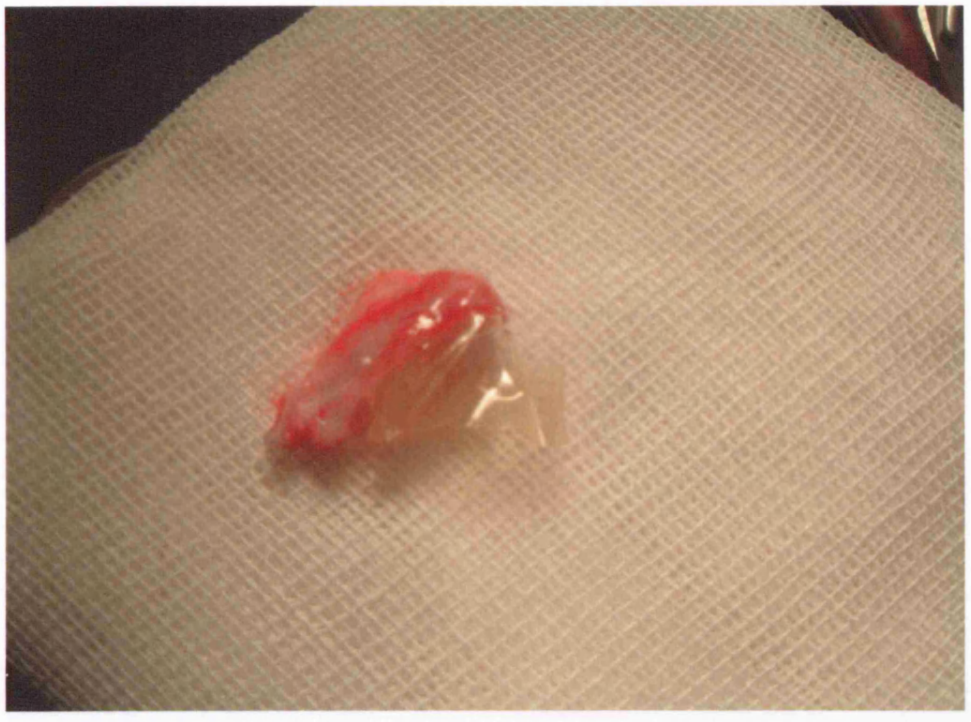

4.3.2. HISTOPATHOLOGY

In this series of experiments, we found that the casted sheets of 2% POSS-PCU nanocomposites did not exhibit any capsule formation, indicating that the inflammatory cascade did not affect it as compared to the degree endured by its siloxane (figure 4.4) which elicited a massive foreign body reaction in one of six samples. The innermost capsular layer was formed by multiple layers of fibrin which initiated the influx of inflammatory macrophages. In this region, numerous eosinophils as well as foreign body giant cells (GCs) are present which suggest a foreign body reaction due to a persistent stimulus, probably microscopic fragments of

degraded silicon. The continuing presence of the offending stimulus contributed to a chronic inflammatory state characterized by incoming vessels that constituted a vascularised capsule with a high likelihood to cause painful contractures necessitating removal later.

Figure 4.4. 10x magnification of the H&E-stained inflammatory capsule surrounding the siloxane control showing the innermost fibrin layer followed by inflammatory macrophages, fibroblasts and vascularisation.

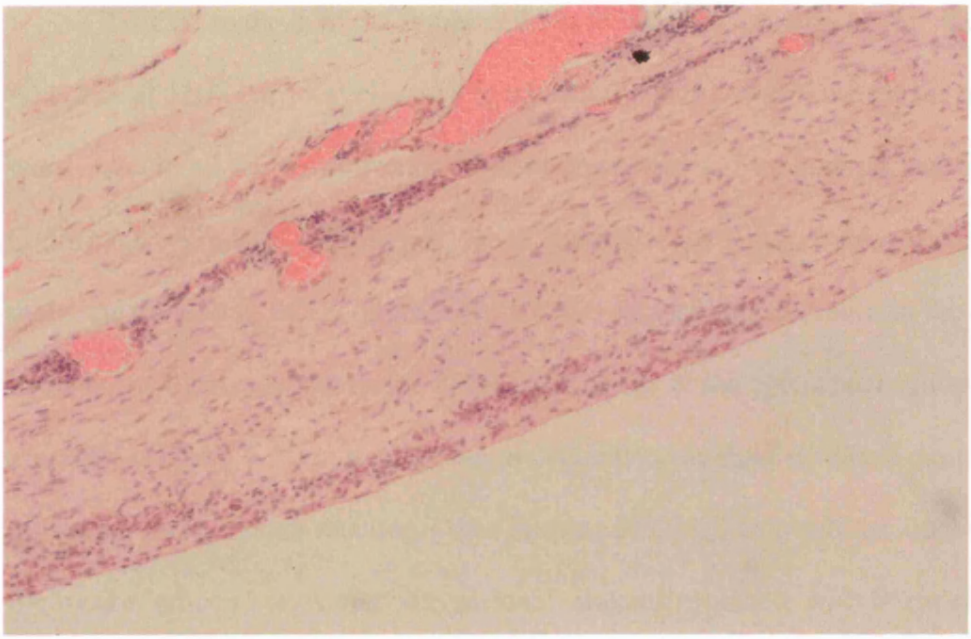

Using van Tiernen's classification system, the control siloxane microcomposite revealed a highly eosinophilic specimen (Grade III) with evidence of neovascularisation (grade II) as well as capsular thickness of greater than 15 cells (Grade III). In addition, the inflammatory cell distribution was a mixture of numerous macrophages, giant cells and even neutrophils (Grade IV), all of which indicate a severe foreign body reaction. Although there was no visible capsule surrounding

POSS-PCU sheets, we could not conclude on its interaction with the immune system due to the lack of histology in this specific instance. Nevertheless, current literature points to nanocomposites in general having diminised foreign-body reaction in vivo {Tanaka, 2002}. In any case, we are conducting further in vivo studies on these nanocomposites. nHopefully, this would shed more light on this matter.

4.3.3. SURFACE DEGRADATION

ATR-FTIR analysis of the implanted 2% POSS-PCU sheets showed that the 'Si-O' bonds at 1109 cm^{-1} wavelengths {Marcolli C, 1999} within the closed nanocage were intact in all the 6 samples of the nanocomposite and on both surface and bottom in different regions of the polymer. 'Si-O' bonds of the control linear siloxane molecule bonded to PCU (figure 4.5b) and showed a mean decrease in the intensity of its Si-O waveforms as compared to the Si-O bonds in the cyclic silsesquioxane molecules (figure 4.5a) indicating that its silicon-containing elements degraded and initiated a foreign body reaction {Van Tienen, 2002}. This would be attributable to the weaker silicon bonds in a conventional siloxane molecule with linear silicon atom configuration. Closed POSS-nanocages on the other hand are more compact and have increased bond strengths due to Van der Waals bonds, all of which make it more resistant particularly to the oxidative enzyme; myeloperoxidase (MPO) that accounts for 95 % of the macrophage digestive enzymes {Hu, 2001;Voronkov MG, 1982}.

Figure 4.5a. ATR-FTIR analysis of implanted 2% POSS-PCU nanocomposites before and after implantation showing no difference in amplitude at the Si-O group wavelength of 1109 cm^{-1}.

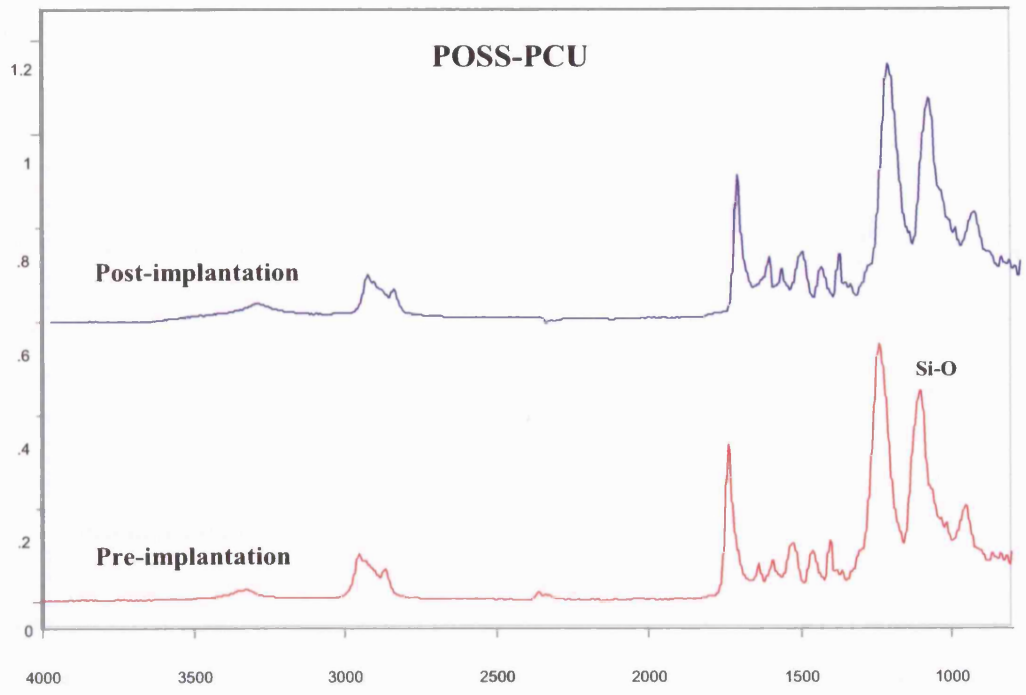

Figure 4.5b. ATR-FTIR analysis of the degraded control siloxane following implantation showing a significant decrease in 'Si-O' wavelength amplitude.

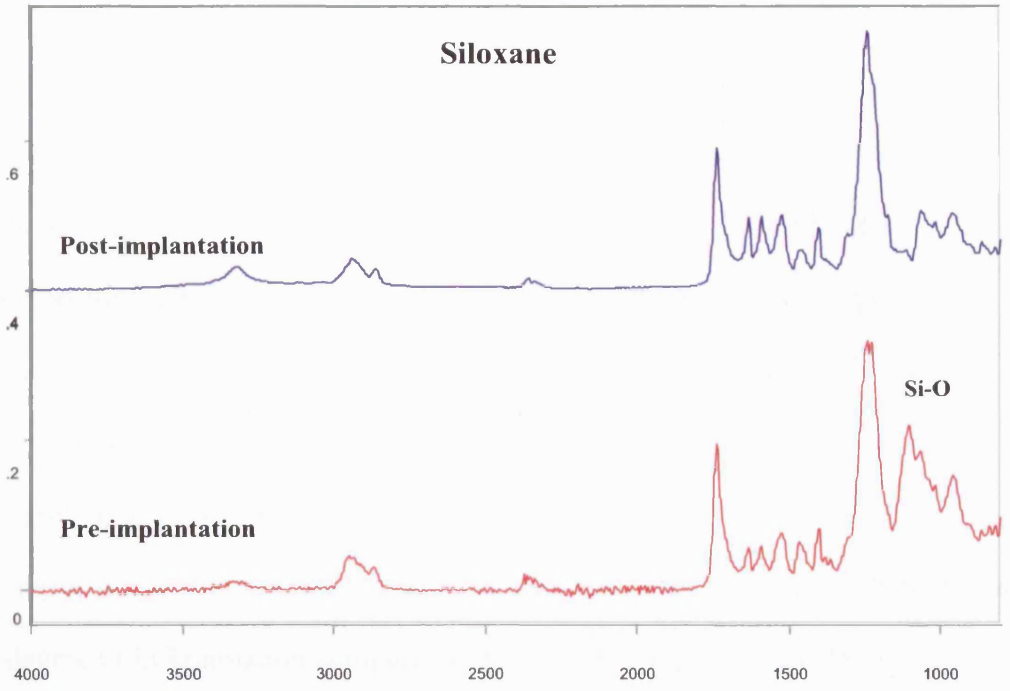

The polyurethane component within the POSS-nanocomposite also exhibited far greater resistance to *in vivo* degradation with no alteration to the carbonate carbonyl groups υ(C=O) at 1740 cm^{-1} and the absence of its hydrogen-bonded variation at 1709 cm^{-1}. Urethane carbonyl groups at 1637 cm^{-1} were also resistant as were the C-O-C=O groups at 1253 cm^{-1} wavelengths {Seifalian, 2003} all which showed no difference between the pre-and post-degraded sample (figure 4.5a). An aromatic reference peak of 1591 cm^{-1} accounted for the C=C bonds of the methylene di(p-phenyl isocyanate) (MDI) hard segment. ATR-FTIR analysis of the control siloxane-polyurethane co-polymer showed hydrolysis of the soft, amorphous segment carbonate carbonyl groups (C=O) and the 'C-O-C=O' groups with evidence of chain scission. These

results indicate that the silicon molecules configured as POSS-nanocages form a protective network holding together all the constituents of the nanocomposite thus improving resistance to biodegradation and fragmentation.

SEM analyses on the explanted nanocomposite samples showed no significant difference in its surface morphology as compared to the undegraded control POSS-PCU nanocomposite. As shown in figure 4.6a, the surface of the implanted nanocomposite showed a 'cobblestone' appearance with no evidence of pitting, fissuring or cracking compared to the obvious signs of surface degradation in the control siloxane polymer which also showed significant fibrinogen adsorption to its surface (see figure 4.6b). The significantly decreased degradation of the nanocomposite may be explained by two factors. Firstly, these implants elicited a far lesser degree of inflammation compared to the controls and secondly, POSS nanocages are known to have high resistance to oxidative degradation. This is an advantage of this biomaterial in vivo as the primary degradative enzyme of macrophages is myeloperoxidase (MPO). Based on all the available data, we hypothesised that the addition of POSS nanocages to the polyurethane gave it a protective effect by (1) denaturing inflammatory protein cognition of the polymer and (2) greatly augmenting its biostability in the face of oxidative enzyme degradation. This would explain its optimal interfacial biocompatibility.

Figure 4.6a. Surface morphology of degraded 2% POSS-PCU nanocomposites showing minimal evidence of surface degradation and the absence of fibroblast attachment compared to the control (shown in figure 4.6b).

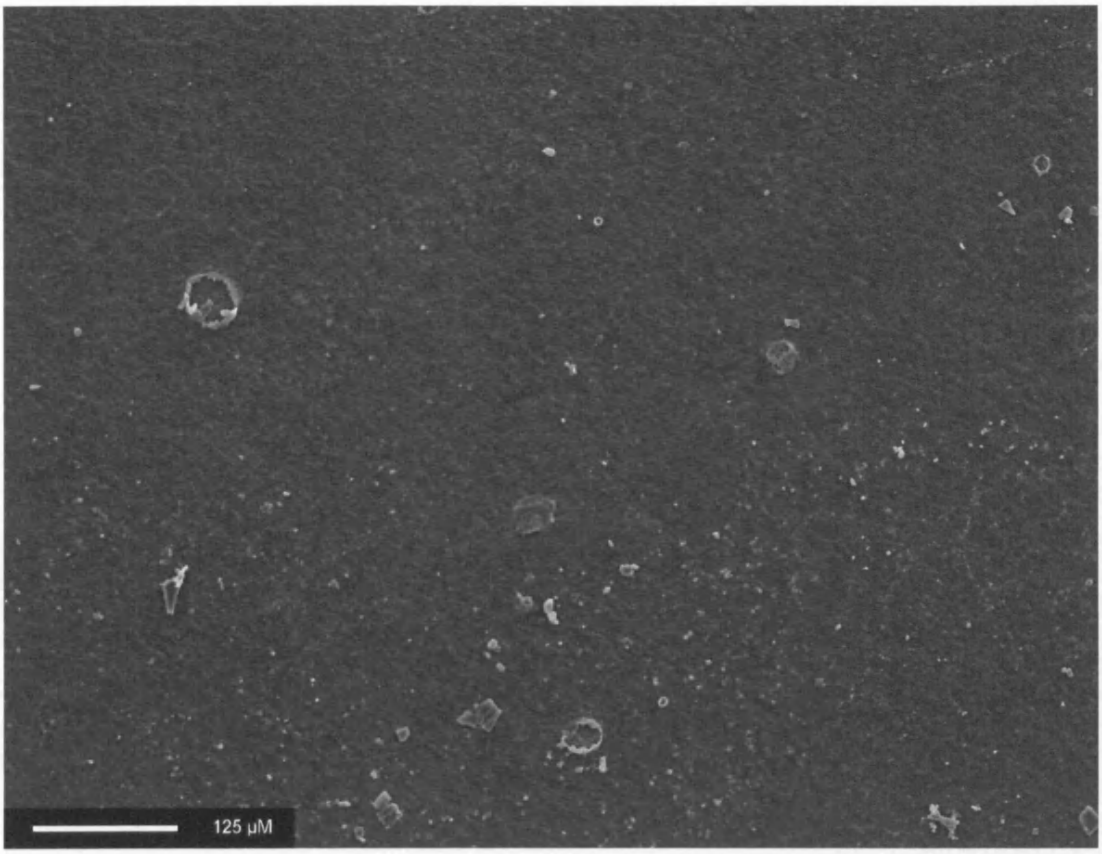

Figure 4.6b. Surface morphology of siloxane showing significant surface degradation with evidence of fissures, cracks a heavy deposition of stellate-shaped fibroblasts. .

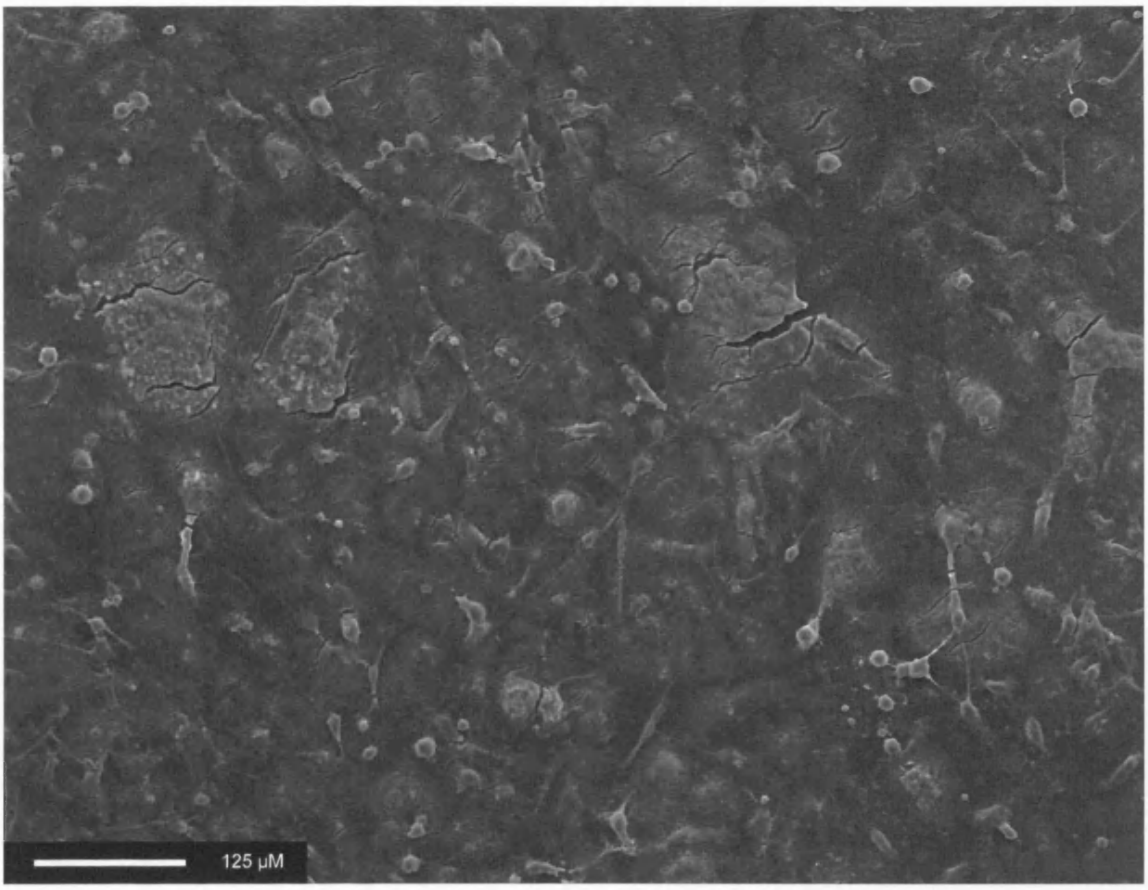

4.3.4. YOUNG'S EQUILIBRIUM CONTACT ANGLE

A Young's angle of less than 90 ° is suggestive of a hydrophilic surface while values greater than 90 ° indicate hydrophobicity {Riedel, 2001}. As shown in figure 4.7, we found that the equilibrium contact angle on 2% POSS-PCU nanocomposite was 82.6 ° as compared to 110° for siloxane {Mata, 2005}. This reveals the hydrophobic character of the nanocomposite. However, the receding contact angle (θ_r)

values also indicate a hydrophilic component as well. This combination of both hydrophobicity and hydrophilicity indicates that this nanocomposite is amphiphilic in nature. This is in line with concurrent with published literature which show the surfactant activity of POSS molecules {Deng, 2002}. The standard deviations for this is not apparent as they lie very close to the mean values. In addition, the hysteresis angle is large, indicating the unstable surface free energy of the nanocomposite. This is a measure of the degree of surface roughness of the nanocomposite {Muller B, 2001}.

Figure 4.7. Derivation of Young's equilibrium contact angle using dynamic contact angle analyses showed the amphilic (combined hydrophobic and hydrophilic) nature of the POSS-PCU nanocomposite.

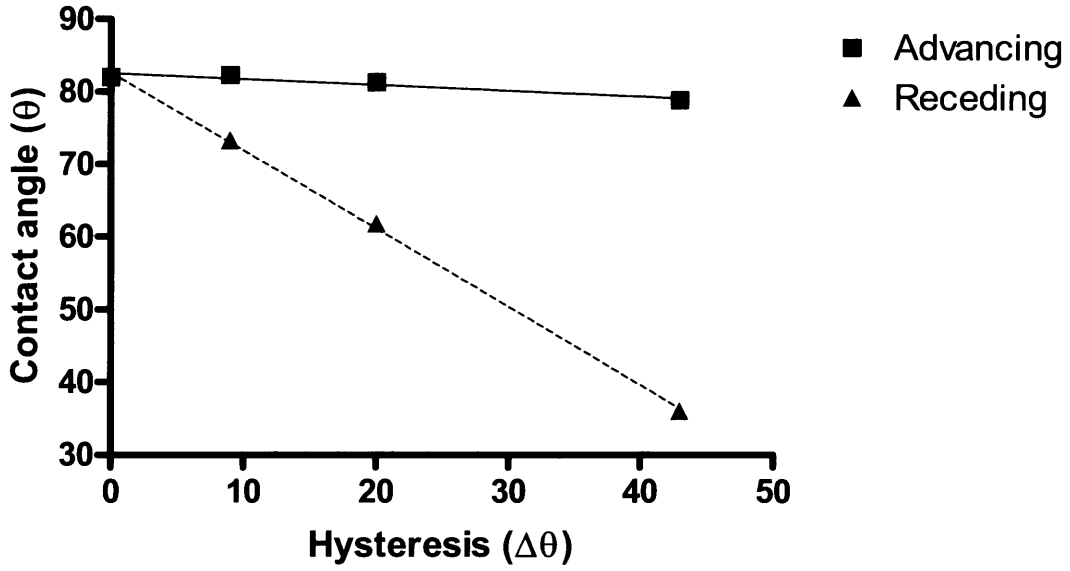

Receding angle; $y = (-1.075 \pm 0.009847)x + (82.60 \pm 0.2377)$; $r^2 = 0.8000$

Advancing angle; $y = (-0.08221 \pm 0.01099)x + (82.54 \pm 0.2651)$; $r^2 = 0.9988$

Equilibrium contact angle = 82.6°

4.3.5. FIBRINOGEN ADSORPTION

The in vitro fibrinogen adsorption tests performed to explain the minimal inflammatory behaviour of these nanocomposites showed a significant increase in fibrinogen adsorption to its surface as compared to the siloxane control (One-way ANOVA, $p < 0.01$) as shown in figure 4.8. This corresponds to the existing literature which showed that nanocomposites proportionately adsorb proteins with increasing surface roughness {Muller B, 2001;Riedel, 2001}. This could in turn be due to the effect of an increase in surface area and therefore it would be logical to assume that the formation of an inflammatory capsule in the case of nanocomposites would be accentuated. Paradoxically however, nanocomposites have been shown to cause minimal inflammation in vivo both in this study as well as others {Tanaka, 2002}. The prevalent hypothesis is that proteins such as fibrinogen undergo conformational changes upon adsorption to these surfaces as a result of large hysteresis angles as we have shown above.

Figure 4.8. Fibrinogen direct ELISA showing significantly increased fibrinogen adsorption to siloxane as compared to POSS-PCU (One-way ANOVA, $p < 0.01$).

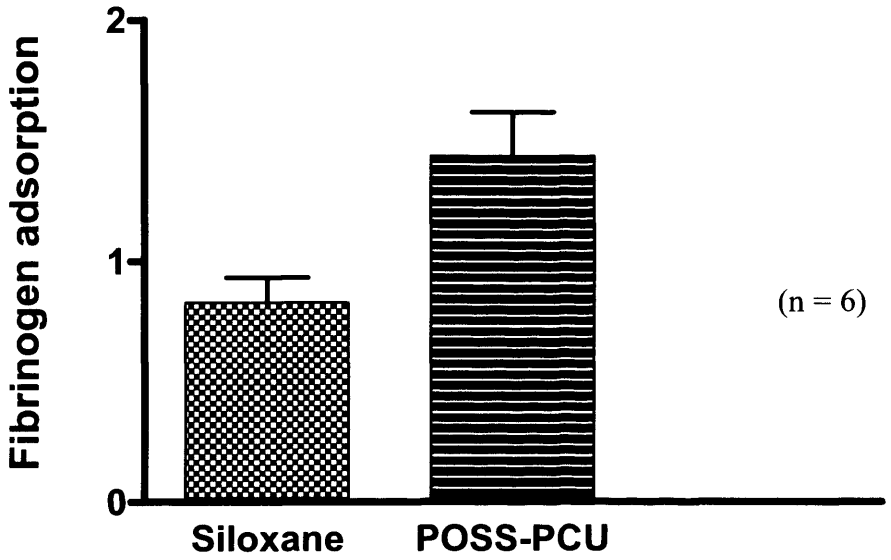

4.4. DISCUSSION

Protein adsorption represents the first stage of the interaction between implants and their biological interface. This is determined by the rate of formation and thickness of these protein layers as well as their conformation. The adsorbed proteins act as an information source for the immune system and are thus pivotal in minimising interfacial biocompatibility {Eberhart, 1987}. When silicone implants are placed in a biological system, thrombin converts soluble fibrinogen into an adsorbable form which adheres to the biomaterial. The integrin Mac-1 (CD-11b/18) on macrophages then interact with the exposed P1 and P2 epitopes on the D-domain of the denatured, adsorbable fibrinogen which acts as an opsonin once critical levels are reached {Hu, 2001}. The chronic inflammatory reaction {Hu, 2001} is further propelled by tumour necrosis factor-alpha (TNF-α) and interleukin-6 (IL-6) {Mena, 1995} and culminates in a foreign body reaction. The activated macrophages and tissue monocytes then produce angiogenic factors which form a thin vascular layer which sustains capsular proliferation {Rubino, 2001}. This causes an increased mucopolysaccharide and collagen production by the incoming fibroblasts {Robert A.Freitas Jr., 2003}. Subsequently, a third layer of external vascularity develops to sustain this capsule.

The resultant capsule becomes acellular within 4 weeks leaving only a fibrous framework to separate the implant from living tissue {Liu, 1992}. The extent to which this capsule is formed depends on the rate of release of its constituents and how they react with the surrounding cells. The other factors are surface, shape {Carpaneda, 1997}, differing elasticity, location and duration of implantation {Robert A.Freitas Jr.,

2003}. Once formed, a biological capsule can have four major outcomes; resorption, extrusion, integration or encapsulation with the latter being the most common outcome. Studies on peri-prosthetic tissue have found that initially, an inflammatory capsule is formed by proliferating CD-68 negative and vimentin-positive mesenchymal cells {Friemann, 1997} of macrophage / histiocyte origin {Luke, 1997}. On subsequent capsular contracture, the cells found were CD3/CD68 positive macrophages which correlated clinically with Baker's classification {Kamel, 2001}. In long-standing cases, dystrophic calcification {Peters, 2001;Yeoh, 1996} occurs.

In the case of these POSS-PCU nanocomposites, we hypothesise that the two main factors responsible for the minimal capsular reaction seen in vivo with them are (a) a large contact angle hysteresis causing a conformational change in adsorbed fibrinogen (b) minimal POSS-PCU nanocomposite degradation and an absence of fragmentation. In this experiment, both sample and control polymers were matched for surface and shape with both specimens implanted subcutaneously in sheep for 18 months. Having accounted for these confounding factors, the only remaining cause for the difference in foreign-body reaction between both groups was the biological interactions of the nanocomposite.

By the chemical integration of POSS nanocores with the polymer, this increases its surface roughness and contact angle hysteresis as well. Previous studies on germanium-silicon (Ge-Si) nanopyramids showed that globulin conformation altered on contact with these surfaces due to a large contact angle hysteresis loop {Muller B, 2001}, a similar result to the dynamic contact angle analysis on these POSS-PCU nanocomposites. It was postulated in these previous studies that this is due to the

'edges' seen on the glabrous nanocomposite surface {Riedel, 2001}. This characteristic would have caused a conformational change in opsonic fibrinogen adsorption and affected macrophage recognition of the P1 and P2 epitopes on the fibrinogen molecule {Hu, 2001}. As macrophages barely recognised these nanocomposites, the process of inflammation was not carried through and no biological capsules were thus formed. In a parallel in vivo study, carbon nanocomposites implanted subcutaneously into the back of Wistar rats as tissue implants showed almost no inflammation {Tanaka, 2002} further supporting the theorical basis for its use at the tissue interface.

In both silicone and conventional polyurethane breast implants, polymeric particles have been found to be engulfed by inflammatory macrophages which eventually migrate to the lymph node {Katzin, 2005} and cause systemic manifestations; 'silicone-osis' {Englert, 2004}. At a more local level, a study by Lesesne and colleagues on breast implants found silicone fragments {Lesesne, 1997} mainly localised to the peri-implant tissue. These particles would explain some of the systemic manifestations which persisted in patients even after implant removal. This remains a problem with silicone implants.

On the other hand, nanocomposites have far greater mechanical strengths {Zhang, 2004} than their constituents with its strength based on the arrangement of quantum-scale sizes of its nanocores {Alivisatos AP, 1996} within the matrix. These nanocores confer tensile strength to the composite as a result of its nanoscale interfacial shear with the surrounding molecules to allow for efficient load transfer. According to the Griffin criterion, nanocomposites with cores below a critical length have mechanical

strengths equivalent to a solid crystal, in spite of being cracked or fissured. This holds true for nanocomposites and explains the relative immunity of nanocomposites to fracture {Gao H, 2003} and would explain its diminished propensity to cause capsular formation.

With reference to this POSS-PCU nanocomposite, there was no significant fall in the FTIR wavelength intensities of both the soft and POSS-integrated hard segments of the polymer after in vivo implantation. This suggests that this polymer is highly resistant to biological degradation. Our concurrent in vitro degradation experiments however suggests that even under accelerated hydrolytic and oxidative stresses, these POSS-PCU nanocomposites remained completely intact. This data conforms to current beliefs regarding nanocomposite behaviour in vivo.

In summary (table 4.2), POSS-PCU nanocomposites are ideal for use at the biological interface as tissue implants, biomedical devices and even vascular grafts due to the very low levels of inflammation elicited by the host to it. We hypothesise that this is due to the intrinsic surface roughness of the polymer causing increased contact angle hysteresis and conformational change in adsorbed surface fibrinogen; a key initiator for foreign-body reactions. We hope that these results would stimulate an entirely new generation of bioartificial implants with 'stealth-like' properties, possibly undetected by the immune system.

Table 4.2. Summary of the experimental study.

Parameter	**POSS-PCU nanocomposite**	**Siloxane control**
Capsule	Absent	Significant
Degradation	No obvious macro- or microscopic signs of degradation.	Thinning of polymer sheets with microscopic evidence of pitting, fissuring and cracking.
Si-O bonds	Negligible effect	Significant decrease in 'Si-O' bonds.
Fibrinogen adsorption	Significantly higher adsorption to POSS-PCU nanocomposites compared to siloxane. (One-way ANOVA, $p < 0.001$).	
Wettability	Amphilic (Hydrophobic + Hydrophilic)	Hydrophobic

Chapter 5

5. Endothelialisation of polyhedral oligomeric silsesquioxane nanocomposites for microvascular tissue engineering: An in vitro study

5.1. INTRODUCTION

Tissue-engineered vascular grafts can be constructed by using biopolymers coated with heparin, endothelial cells etc. or as truly biological grafts tissue-engineered *in vitro* prior to re-implantation {Teebken, 2001}. Polyethylene teraphthalate (Dacron™) and expanded polytetrafluoroethylene (ePTFE) have been the biopolymers of choice in the construction of synthetic vascular grafts to date. However, poor elastic properties {Salacinski, 2001c;Tai, 2000} and graft thrombogenicity have limited its clinical potential particularly at lower flow rates where patency has been shown to bear an inverse relationship to the internal diameter of the grafts {Brossollet, 1992;Lau, 2001;Suma, 1999}. This may be reversed by lining these bypass grafts with ECs {Salacinski, 2000;Salacinski, 2001b}. Randomised clinical trials using endothelialised 7 mm internal diameter PTFE vascular grafts have shown primary patency rates of 83.7 % in lower limb bypass grafts at four years {Deutsch, 1999;Meinhart, 2001}. Its success however depends on the initial seeding density, duration of culture and the capacity of the cells to proliferate on the biopolymer {Seifalian, 2002}.

Given the importance of endothelialisation in vascular grafts, we sought to study the ability of these nanocomposites to sustain endothelialisation. The work described in chapter 4, is indicative of the fact that this nanocomposite elicits minimal inflammation, probably due of the conforming effects of POSS on surface fibrinogen adsorption. However, optimising the surface concentration of POSS is essential in order to promote endothelialisation following implantation as excessive amounts of silica-based molecules could hinder endothelialisation. This was the question which

needed to be answered.

Another concern is that at lower flow rates, the compliance mismatch between current bypass grafts and the native vessels has been hypothesised to be a cause of intimal hyperplasia; a major cause of long-term graft occlusion {Zilla, 1987}. PU are polymers with similar radial compliance characteristics to native vessels {Tai, 2000}. Of these, carbonate-based PU, unlike earlier generations of PU, do not possess ether or ester linkages and are hence less susceptible to degradation. Our own study using PCU grafts on the aorto-iliac vessels of four beagle dogs over 36 months showed 100 % patency, minimal intimal hyperplasia and no signs of aneurysmal dilatation and most importantly, an ability to sustain endothelialisation {Seifalian, 2003}.

The latter characteristic prompted the linking of POSS to PCU in order to achieve the synergy of the compliance characteristics of PCU and the platelet repelling action of silica-based polymers {Berrocal, 2001}, which confers an anti-thrombogenic effect {Park, 2002}. Previous experience with this includes the use of co-polymers of PU and siloxanes in intra-aortic balloons which have relative haemocompatibility due to the dispersive force fields on its surface which maintains any adsorbed proteins in an unstable state {Nyilas, 1977}. However, siloxane-based vascular grafts have not been successful as the formation of an EC lining on these constructs is sub-optimal {Hoffman, 1993}.

In this study, we assessed whether this nanocomposite is safe and compatible with in vitro cell cultures. Apart from indicating its safety as a biomaterial at the cellular level, such information would also serve as a measure of its potential for developing

bio-hybrid vascular grafts. As shown in figure 5.1, developing bio-hybrid vascular grafts would require the ECs to undergo four phases. These cells have to first remain viable within the culture medium exposed to POSS-PCU as well as on direct contact with the polymer (Phase I). Next, the ECs would have to adhere to the polymer surface, preferably within a short time, to minimise the complications associated with long-term cell cultures (Phase II). These adherent ECs would then need to proliferate at a steady rate (phase III) in order to achieve a confluent EC monolayer (Phase IV).

Figure 5.1. Schematic representation of the stages of cell seeding on biomaterials.

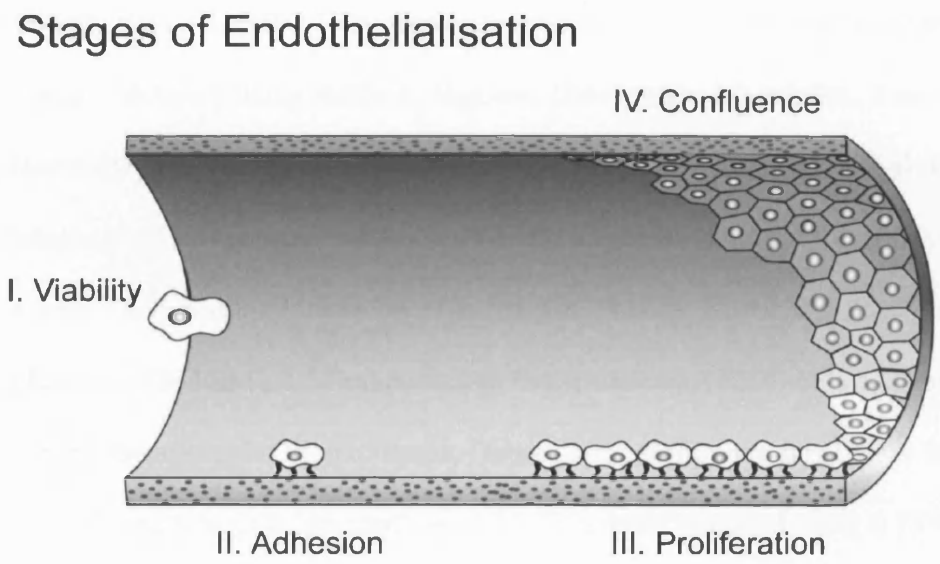

5.2. MATERIALS AND METHODS

5.2.1. POLYMER SYNTHESIS

Please refer to chapter 2.

5.2.2. PRIMARY ENDOTHELIAL CELL CULTURE

Using a previously described method {Seifalian, 2001}, Human Umbilical Vein Endothelial Cells (HUVECs) were extracted from umbilical cords procured within 24 hours of delivery using sterile collagenase (Boehringer Mannheim; from Clostridium Haemolyticum). HUVECs were then grown in tissue culture using Cell Culture Medium (CCM) consisting of 157 ml of M199 medium, 40 ml foetal bovine serum, 4.8 ml 7.5 % sodium bicarbonate (Invitrogen, Paisley, Scotland, UK), 5 ml L-glutamine (200mM), 1.57 ml penicillin / streptomycin (5000 units of penicillin and 5 mg/ml streptomycin (Sigma, Poole, Dorset, UK). Following incubation for 48 hours at 37 °C and 5 % CO_2, the confluent HUVECs were removed using 0.25% Trypsin – EDTA (Sigma-Aldrich Company Ltd., Poole, UK) and split in a 1:4 ratio. In our experiments, confluent HUVECs from passages 4 to 5 were used.

5.2.3. CELL VIABILITY ANALYSIS

5.2.3.1. Direct contact method

1.0 x 10^5 fourth passage (P4) HUVEC suspensions in CCM were each placed in sterile 24-well culture plates (Helena Biosciences, Sunderland, UK) coated with circular sheets of casted POSS-PCU with its edges sealed off with POSS-PCU liquid using a micropippete. This was then incubated at 37 ^{0}C and 5 % CO_2 for 24 hours and 48 hours respectively. Alamar Blue™ analysis (Serotec Ltd., Kidlington, Oxford, England) was then performed and its absorption spectra at 570 nm and 630 nm wavelengths were measured using a Multiscan MS spectrophotometer (Labsystem Multiskan MS; Labsystem, Helsinki, Finland) {Seifalian, 2001}. All tests were repeated four times in duplicate (n = 4) with uncoated standard polystyrene tissue culture wells serving as controls. In this experiment, the cell seeding density was higher than normal so as to optimise the sensitivity of the Alamar Blue™ analysis system {Seifalian, 2001}.

5.2.3.2. Diluent extraction method

POSS-PCU was pulverised using a dismembranator (Mikro-dismembranator u, B.braun biotech international gmbh). The powder was autoclaved, placed in CCM to constitute a 100 mg/mL solution of POSS-PCU and then shaken at 200 rpm for 19 days at 37 °C. Following exposure, the mixture was sieved, rinsed and centrifuged to extract the remnant CCM. 24-well plates seeded with 5.0 x 10^4 HUVECs were then incubated at 37 °C and 5% CO_2 for 48 hours in 25, 50, 75 and 100 mg/ml of the

polymer-exposed CCM with plain CCM acting as the control. Following incubation for 0,6,12 and 24 hours, AlamarBlue™ analysis was performed as mentioned earlier (n = 4).

5.2.3.3. High permeation liquid chromatography (HPLC)

HPLC analysis was performed to assess whether any component of POSS-PCU leached out into the media following incubation. Powdered polymer was placed in sterile PBS for 90 days to allow for leaching of the polymer if any, before being centrifuged and filtered. The filtrated PBS was then subjected to HPLC analysis using a 30 mm gradient with the sample run at 20 cms/hr, through a C_{18} reverse plate to assess hydrophobicity (Varian Ltd., USA). The sample was run for 30 minutes using buffer solutions of (A) 0.1 % tri-fluroacetic acid/TFA in water and (B) 0.1 % TFA in acetonitrile. Plain PBS controls were used as the control group. This experiment was performed by the Department of Biochemistry, Royal Free UCL Medical School, London, UK.

5.2.4. CELL ADHESION ASSAY

Fourth passage (P4) HUVECs were seeded at 3.5 x 10^5 cells/cm^2 on sterile POSS-PCU sheets placed within standard 96-well plasma-treated polystyrene wells (Helena Biosciences Ltd., Sunderland, UK) as per ISO 10993 specifications {ISO part 5, 1992}. HUVECs were then allowed to incubate at 37 °C and 5% CO_2 before being subjected to AlamarBlue™ assays at 30, 60, 120, 180 and 240 minutes respectively (n = 4). As before, spectroscopic analysis at 570 and 630 nm was performed using the Multiscan MS spectrophotometer (Labsystem Multiskan MS; Labsystem, Helsinki, Finland). A parallel experiment was performed using plasma-treated polystyrene culture plates as the gold standard and conventional siloxane to elicit the difference in

EC adhesion between linear siloxanes and caged silsesquioxanes as well as to compare the endothelialising properties of silsesquioxanes to standard cell culture plates. Alamar Blue™ was the preferred technique in this instance as it is non-cytotoxic, independent of polymer, allows continous monitoring of cells, assesses viability and is user-friendly. Moreover, it is the preferred assay in our laboratory as we have optimised the technique over time.

As a measure of the hydrophilicity of the polymer, the water absorption index (WAI) of POSS-PCU was determined. Thin strips of PTFE, PCU and POSS-PCU of equal dimensions were immersed in pure distilled water (Sigma Ltd., Dorset, UK) for 1, 3 and 7 days. Their respective pre-immersion (m_0) and post-immersion weights (m_1) were measured and the WAI was determined using the formulae,

$$\text{Water Absorption Index} = (m_1 - m_0)/ m_0 \times 100\%$$

5.2.5. CELL PROLIFERATION ASSAY

Proliferation of HUVECs on POSS-PCU over time was determined using PicoGreen® DNA quantisation assay (Molecular Probes Co., OR, USA); a vital dye which stains DNA fluorescent green. HUVECs were seeded onto glass petri dishes at 1.0×10^3 cells/cm^2 containing culture media and incubated for 1, 3, 7, 11 and 14 days. The HUVECs were then extracted and reconstituted in 1 mL mixtures of 10 mM tris-HCl with 1 mM EDTA at pH 7.5 (1x TE) to form the sample while serially diluted calf thymus DNA served as the standards {Singer, 1997}. 100 µl aliquots of these solutions were then mixed with 100 µl 1: 400 (v/v) dilution of PicoGreen® dye in 1x TE and incubated for 5 minutes. This was then excited at 485 nm and the emissions at 538 nm were read. The amount of DNA in the sample was then determined from the standards (data not shown) and based on the assumption that each cell contains 7.7 pg of DNA, the number of cells was calculated.

5.2.6. CELL CONFLUENCE MORPHOLOGY

5.2.6.1. Light microscopy

Fifth passage (P5) HUVECs were cultured on sterile, flat sheets of the POSS-PCU for 48 hours at a seeding density of 3.5 x 10^5 cells/cm^2 to assess cell confluence morphology. The cultured cells were then fixed with 4 % paraformaldehyde for 10 minutes and carefully rinsed with PBS and stained with 0.1 % Toluidine Blue (TB) stain (Sigma Chemical Company, Poole, Dorset, UK) for 10 minutes before being washed off with PBS. The sheets were then examined under a confocal microscope (Nikon D-Eclipse C1, Japan) at 20x magnification to assess cell confluence on POSS-PCU qualitatively assess cell attachment to the polymer.

5.2.6.2. Electron microscopy

The morphology of the proliferating ECs was studied using electron microscopy using the method alluded to in chapter 3 using P5 HUVECs cultured on sterile, flat sheets of POSS-PCU for 48 hours again at a seeding density of 3.5 x 10^5 cells/cm^2. The parameters assessed were the presence of cell retraction, loss of filopodia and a rounded cell appearance; indicators of impaired cell motility and morphogenesis {Park, 2002}.

5.3. RESULTS

5.3.1. CELL VIABILITY

Cell viability on the polymer was assessed using both the direct contact and diluent extraction methods {Park, 2002}. Direct contact involved exposing HUVECs directly to the polymer while the indirect technique involved using CCM exposed to the polymer to culture cells. Analysis was performed using a vital dye; Alamar Blue® (AB) which viable cells metabolised from blue resazurin to pink resarufin and the change in colour was detected spectroscopically {Park, 2002}. Leaching from POSS-PCU into CCM was assessed using high performance liquid chromatography (HPLC).

5.3.1.1. Direct effect of POSS-PCU

Direct contact studies showed that there was no significant difference between HUVEC viability on POSS-PCU and standard tissue culture plates following measurement with AlamarBlue™ assay at 24 and 48 hours of cell culture (Two-way ANOVA; p = ns) as is shown in figure 5.2. This shows that HUVECs cultured directly onto POSS-PCU exhibited optimal cell viability for up to 48 hours.

Figure 5.2. Direct contact analysis using Alamar Blue™ spectral absorption (ABSA) which showed no significant difference in cell viability between standard cell cultures and those on POSS-PCU (Two-way ANOVA, p = ns).

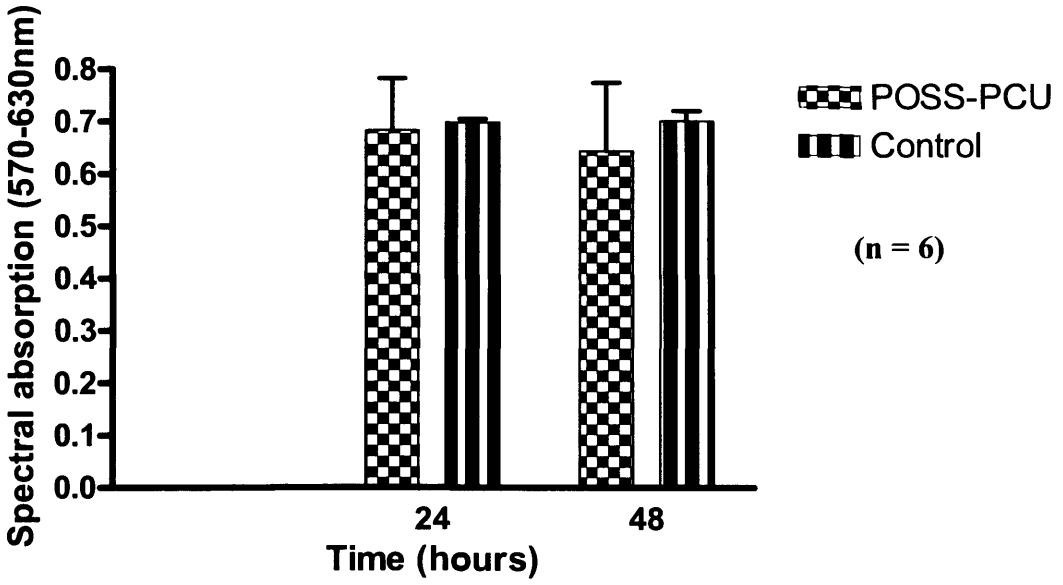

5.3.1.2. Indirect effect of POSS-PCU

AlamarBlue™ analysis of the diluent extract of POSS-PCU showed no significant difference (p = ns) in cell viability between the control group and cell cultures with varying concentrations of the polymer extract (0, 25, 50, 75 and 100 mg/ml) at 6, 12 and 24 hours respectively as is shown in figure 5.3. This indicates that no cytotoxic substance leaches out of POSS-PCU *in vitro* as ECs can remain viable on the polymer for the prolonged *in vitro* culture period that is necessary for two-stage seeding procedures.

Figure 5.3. Diluent extraction analysis using Alamar Blue™ spectral absorption (ABSA) showing no significant differences between varying doses of cell media incubated with the nanocomposite at 0, 6, 12 and 24 hours (Two-way ANOVA, p = ns). Mean and standard deviation values are tabulated below.

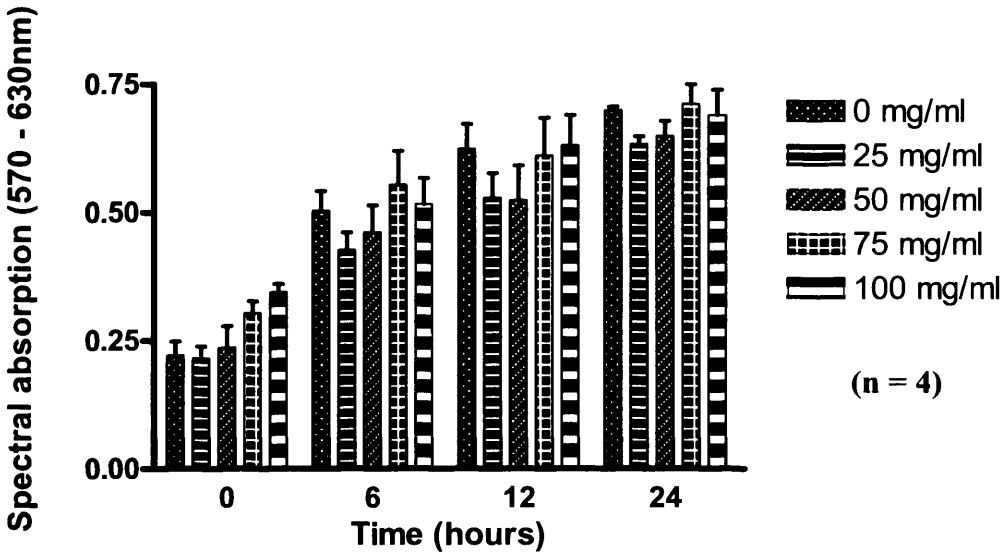

Time	0 mg/ml	25 mg/ml	50 mg/ml	75 mg/ml	100 mg/ml
0 hrs	0.2215 ± 0.053791	0.2215 ± 0.045886	0.2365 ± 0.083983	0.30375 ± 0.047407	0.34475 ± 0.031135
6 hrs	0.50325 ± 0.076049	0.50325 ± 0.066745	0.461125 ± 0.104772	0.553375 ± 0.131563	0.51575 ± 0.101276
12 hrs	0.623375 ± 0.09665	0.623375 ± 0.09591	0.52325 ± 0.134906	0.610375 ± 0.147749	0.6305 ± 0.117397
24 hrs	0.69825 ± 0.013623	0.69825 ± 0.030119	0.6485 ± 0.134906	0.711 ± 0.075825	0.68925 ± 0.098872

5.3.1.3. HPLC

HPLC analysis showed here was no evidence of any substance leaching out the polymer on prolonged contact. This was in line with the results showing optimal cell viability in the diluent extraction method performed above.

5.3.2. CELL ADHESION

EC adhesion to the POSS-PCU sheets showed a significant increase in adherent viable cells to the polymer (53 % increase in spectral absorption over baseline values) within 30 minutes of contact (student's t-test, $p < 0.05$). Subsequent adhesion of viable ECs to the polymer reached saturation within 2 hours of cell culture on the polymer (figure 5.4a). Compared to the minimal cell adhesion to medical-grade siloxane these results indicate that when silicon molecules are incorporated as closed-cage silsesquioxanes, they allow for improved EC adhesion to its surface and hence, endothelialisation. Two-way ANOVA analysis showed a very significant difference in EC adhesion between POSS-PCU and siloxane ($p < 0.0001$). There was no difference in EC adhesion between POSS-PCU and standard polystyrene cell culture plates.

Figure 5.4a. Alamar Blue™ assay showing significant endothelial cell adhesion to POSS-PCU within 30 minutes of contact (student's t-test, $p < 0.05$) and reaching saturation after 2 hours of incubation. These values were significantly greater than endothelial cell adhesion to medical-grade siloxane (Two-way ANOVA, $p < 0.0001$). There was no statistical difference in EC adhesion between POSS-PCU and standard cell culture plates.

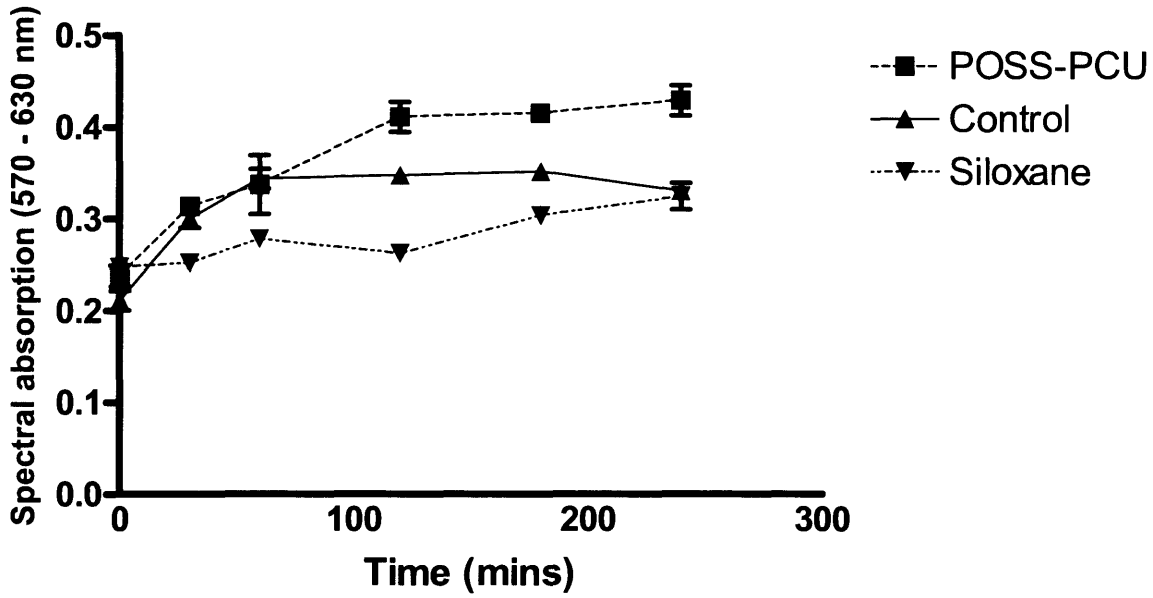

The WAI of silica nanocomposites was 28.54 % +/- 3.216 % as compared to PCU (6.194 % +/- 1.985 %) and PTFE (3.978 % +/- 3.218 %). Two-way ANOVA analysis (figure 5.4b) showed a statistically significant difference between these values ($p < 0.0001$) indicating the greater hydrophilicity of the nanocomposites compared to PTFE and PCU. WAI tests on medical-grade siloxane were not performed as the hydrophobicity of siloxane per se is well documented. These results suggest that the

improved endothelialising property of the nanocomposite is attributable to its improved hydrophilic behaviour.

Figure 5.4b. Water absorption index (WAI) assays which show significantly higher water absorption indices and hence hydrophilicity of POSS-PCU as compared to ePTFE and PCU (One-way ANOVA, $p < 0.0001$).

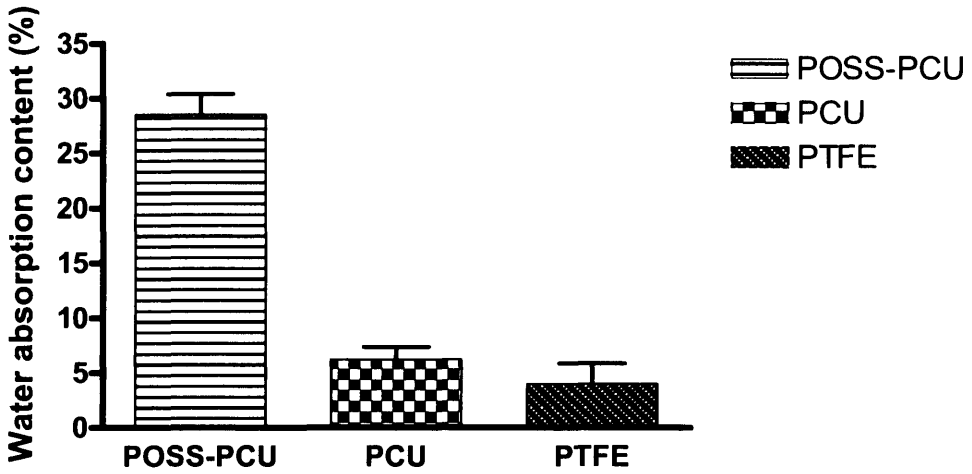

5.3.3. CELL PROLIFERATION

Quantitative analysis of HUVEC proliferation on POSS-PCU polymers studied with PicoGreen®, showed a significant increase in mean EC proliferation at 1, 3, 7, 11,14 and 21 days over baseline values (One-way ANOVA, $p < 0.0001$). There was no significant difference found between different repeats of ECs for a given time (One-way ANOVA, p = ns). This study shows that the growth pattern of ECs on the nanocomposite (initial seeding density of 1.0×10^3 cells per cm^2) reached the exponential phase of growth beyond one week in culture which was sustained at two

weeks with a 60-fold increase in EC surface density finally reaching saturation beyond 14 days (figure 5.5). These results show that ECs are able to proliferate on the polymer even from very low seeding densities over the prolonged periods of time necessary for two-stage seeding procedures.

Figure 5.5. PicoGreen assay showing significant increases in cell proliferation on POSS-PCU over 21 days (One-way ANOVA, $p < 0.0001$).

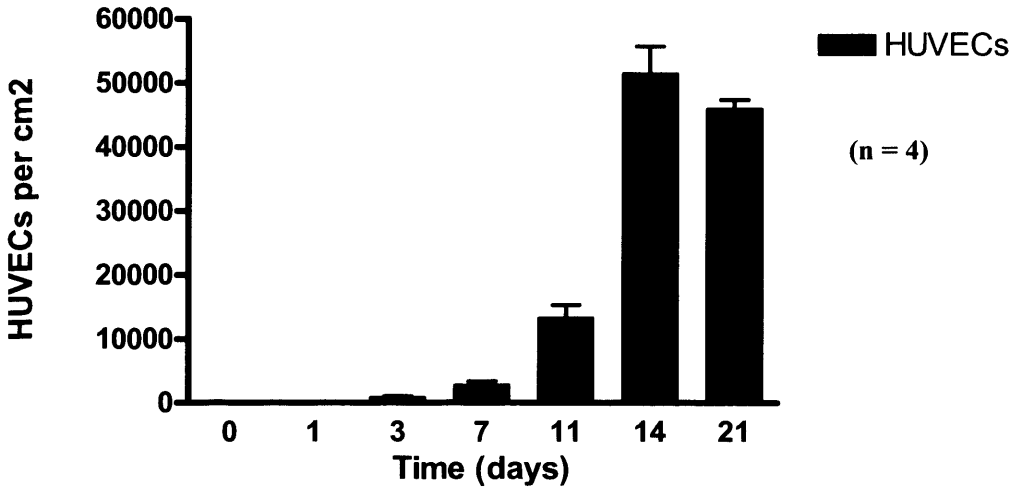

Here, cell viability refers to the ability of the cells to survive both in direct contact with or in the presence of culture media in contact with the nanocomposite. On the other hand, cell adhesion referred to the number of cells actually adherent to the nanocomposite after the culture media was removed and the wells were gently rinsed with PBS.

In order to differentiate between these two parameters, AlamarBlue™ was added to the cell adhesion assay wells only after the original culture medium had been removed and gently rinsed at specified time periods to ensure that only those cells

which were adherent, were present. Our previous studies have shown that the amount of dye metabolised by the cells is an indicator of the number of cell adherent in this case {Seifalian, 2001}.

As for the cell viability assays, all wells contained AlamarBlue™ to begin with and the media was not changed for the 24 to 48 hour duration. The colour change from blue to pink was taken as a measure of the overall metabolising capacity of these cells; an indicator of their viability. If these cells were physiologically dysfunctional then accordingly the amount of dye metabolised would have been decreased. In this manner, AlamarBlue™ assays were used to distinguish between cell viability and adhesion.

5.3.4. CELL MORPHOLOGY

Light microscopic examination of TB-stained ECs on POSS-PCU showed a reticulate pattern of confluence morphology by 48 hours of culture (figures 5.6a & b). Higher magnification of these cells with a scanning electron microscope (SEM) showed morphological features of proliferating cells, with the formation of numerous cellular filopodia as well as the absence of cell retraction and 'rounded' cells (figure 5.7). These data suggest that ECs are ultimately capable of forming confluent EC layers within POSS-PCU microvessels once implanted in vivo, through the process of neo-endothelialisation (endothelial cell proliferation into the graft from beyond the anastomotic site. Comparing these results with the published data on gelatine-coated plates (current gold standard), ECs on POSS-PCU had comparable characteristics

although the presence of apoptotic bodies in this case suggests that POSS-PCU supports endothelialisation but not as significant as gelatine {Prasad Chennazhy K, 2005}. Nevertheless, the use of silicon atoms as POSS instead of siloxane does improve its endothelialisation.

Figure 5.6a. Light microscopic analysis (20x magnification) of Toluidine Blue-stained endothelial cells showing their confluence morphology on POSS-PCU at 48 hours.

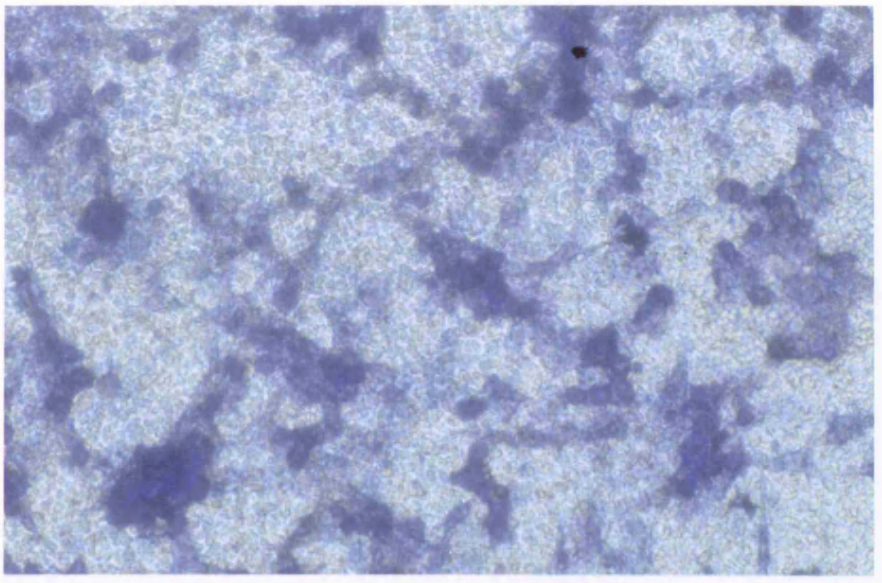

Figure 5.6b. Toluidine Blue-stained HUVECs on POSS-PCU showing improved cellular confluence by 6 days, compared to 48 hours (20 x magnification).

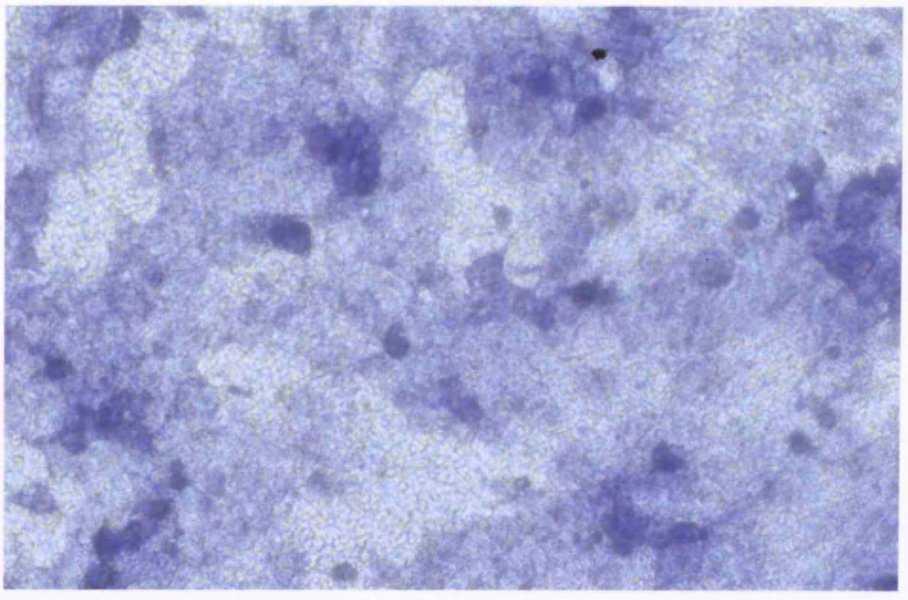

Figure 5.7. Scanning electron microscope pictures of endothelial cell adsorption morphology on POSS-PCU showing the presence of a flat, spindle-shaped cells with numerous filopodia and the absence of cell retraction. This indicates the presence of viable, proliferating cells on POSS-PCU at 48 hours (320x magnification).

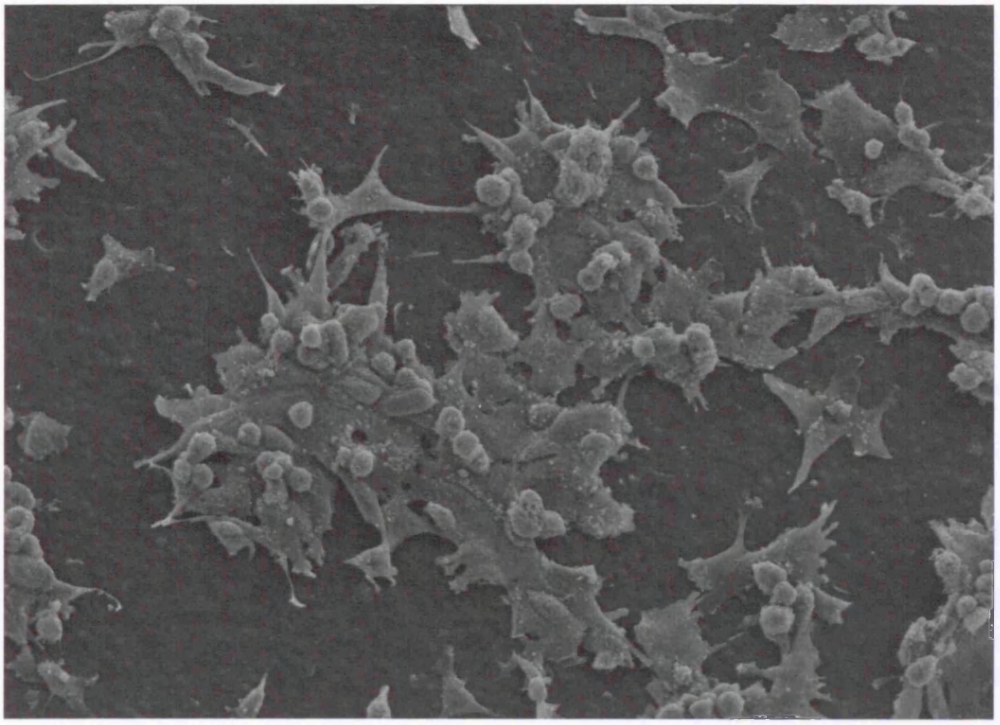

5.4. DISCUSSION

Studies have shown the clinical benefit of lining PTFE vascular grafts with endothelial cells, particularly in lower limb arterial bypass grafts {Zilla, 1987} unlike native, uncoated polyethylene terephthalate grafts. Studies on the latter grafts have been shown to be a result of decreased expression of the fibronectin receptor; VLA-5 {Cenni, 2001}. This has seen the increasing use of fibronectin motifs namely, RGD-peptides {Kidane, 2003}, cell adhesion peptides such as P-15 {Hamm, 2003} and titanium coatings which promote endothelial cell confluence on the surfaces of conventional vascular prostheses {Lehle, 2003}.

Current generations of siloxane co-polymers have two main limitations namely (a) stiffness {Ai, 2003} and (b) poor endothelial cell adhesion due to its high hydrophobicity {Zilla, 1991} One answer to this problem, is coating these surfaces with gelatine-glutaraldehyde cross-linkages{Ai, 2002}, titanium carboxonitride{Lehle, 2003} and peptides{Lateef, 2002}. All these surface modifications have been shown to enhance EC seeding onto the graft surface but this involves a secondary coating procedure. An alternative is to incorporate low-adhesive silicon into higher adhesive polymers such as polyurethanes {Zilla, 1987} in a way which would improve overall EC adhesion whilst maintaining its viscoelasticity. Even so, seeding of these grafts would require prolonged culture times with increasing risks of infection to the graft.

This necessitates the development of a vascular interface with optimal cell seeding and cytocompatibility in the cell culture environment as well {Wilsnack, 1976}. The cytocompatibility of the entire nanocomposite may be explained by the inherent stability of the nanocomposite as all 8 of its reactive side-groups (R) of POSS are fully reacted with PCU.

The polyhedral nature of the POSS molecule ensures greater integration between both soft and hard domains of the polyurethane with a lesser chance of substance degradation and leaching. All polymer sheets were casted at 70 °C which was well above the boiling point of dimethyl acetamide (DMAC). This technique thus allows for complete evaporation of the diluent; DMAC and would further minimise the probability of substance leaching into the media.

Thus, compared to existing silicone co-polymers {Ai, 2003;Hesse, 2003}, we found that the use of a POSS-based nanocomposite improves cell adhesion characteristics. As these nanocages occupy minimal volumes within the polymer {Lichtenhan, 1995}, relatively greater surface areas of PU are available which allows for improved endothelialisation. This would also confer a greater degree of polarity to the polymer which could explain its superior hydrophilicity to PCU.

These experiments also indicate that once adherent to its surface, ECs are also capable of proliferating manifold in order to form a confluent monolayer. While the PicoGreen® assay showed the excellent proliferating characteristics of ECs on the polymer, light microscopic analysis revealed how this occurred. Prior to achieving cellular confluence, the ECs aligned in a reticular manner. The intervening areas were

subsequently filled in to achieve cellular confluence as shown in figures 5.6a & b.

Our data also showed that the quality of cell adhesion and proliferation on the polymer was excellent. Qualitative data using SEM analysis clearly visualised the presence of optimal cell–polymer interactions with the formation of numerous filopodia at its surface, flattened ECs and no rounded cells. This suggests that these ECs are capable of morphogenesis and have the ability to proliferate well.

As these set of experiments have found ECs to be compatible with this polymer, further tests need to be performed on the optimal conditions of cell seeding on this polymer. This would also include seeding smooth muscle cells (SMCs) and eventually, co-cultures of ECs and SMCs onto the polymer. Nevertheless, further tests using in vivo conditions would need to be performed before concluding on its overall biocompatibility and for its potential use in biomedical devices. In conclusion, POSS-PCU nanocomposites are compatible for seeding cardiovascular devices.

Chapter 6

6. The anti-thrombogenic potential of a polyhedral oligomeric silsesquioxane (POSS) nanocomposite.

6.1. INTRODUCTION

In the microvascular setting, the interplay between the components of Virchow's triad is essential. {Conte, 1998}. From the experimental standpoint, this has been exemplified thus far by many studies {Budd, 1991;Demiri, 1999;Harris, 2002}. For instance, polyethylene terephthalate has high platelet adsorption characteristics {Desai, 1991} while PTFE microvessels are far inferior to vein grafts {Schmedlen, 2003;Teebken, 2001}. The initiation of the coagulation cascade in these cases is due to significant fibrinogen adsorption {Balasubramanian, 1999} with the resulting thrombus activation {Lin, 2004} in the short term and intimal hyperplasia (IH) {Ballyk, 1998;Perktold, 2002}in the long term.

For now, autologous vein grafts are the grafts of choice for microvascular repairs {Kannan, 2005} but in the case of microvascular networks, the technical impossibility of dissecting out a capillary bed rule this out as an option in microvascular networks {Bourassa, 1994}. This has prompted us to develop a synthetic vascular interface which is anti-thrombotic and with the capacity to be microfabricated into a microvascular network.

While PTFE and Dacron™ have limitations, certain groups have turned to PU as they possess optimal physico-mechanical properties and are resistant to flex-fatigue {Lelah MD, 1986}. We have previously worked on PCU was shown to have superior resistance to both hydrolytic and oxidative degradation {Salacinski, 2002b} as well as similar compliance characteristics to biological vessels in both in vitro {Tai, 2000} and in vivo conditions {Seifalian, 2003}. However, even these polymers only have

moderate haemocompatibility which need to be improved upon before use as small-diameter and micro-vessels.

As such, efforts are currently being made to improve upon the surface haemocompatibility of conventional polymers {Wetzels, 1999}. Studies by Silver and colleagues revealed that the haemocompatibility of a surface depends on the wettability characteristics of its surface head-groups {Silver, 1999}. Therefore incorporating silicon, which repels platelet and fibrin adsorption due to their unstable surface free energy, onto a vascular interface would confer to it increased thromboresistance {Silver, 1999}. A disadvantage of silicon-containing vessels however is that they are rigid and would have minimal radial compliance with a tendency to form intimal hyperplasia more rapidly. Further studies have also revealed that shorter and more mobile surface moieties have increased thromboresistance {Park, 2002;Silver, 1999} thus strengthening the need for the use of nanoparticles.

As mentioned earlier, POSS {Lichtenhan JD, 1995} is a nanoparticle which can assemble at the atomic scale as they are larger than ions and smaller than macroscopic material {Fukushit, 2005}.

Researchers have since shown that these nanocomposite cubes may be incorporated as building block fillers or cores {Sanchez C, 2001} into other polymers to form hybrid inorganic-organic co-polymers with improved miscibility and hence, elasticity {Haddad TS, 1999}. In addition, optimal POSS dispersion within the polymer {Ribot F, 1999} serves as a reinforcing nanofiller with high surface coverage. Our hypothesis is that POSS-based nanocomposites would interact with coagulant

proteins and platelets in such a manner as to repel them. Such prostheses would not need systemic anti-coagulation such as heparinisation, ideal in a microvascular network.

Prior studies have shown that POSS nanocomposites have the ability to self-assemble once mixed with other polymers {Lee YJ, 2004}. As we have combined POSS with a PU, the surface mobility of the co-polymer should improve and hence reduce the urethane group's functionality of both protein and platelet adsorption responsible for activating coagulation .

This improves the surface mobility of the co-polymer and hence potentially reduces the urethane group's functionality of both protein and platelet adsorption responsible for activating coagulation {Groth, 1995}. Our postulate is that a pendant silicon nanocage with foci of silicon-rich areas serving as the scaffold would preserve the PU architecture sufficiently so as to maintain its compliant properties whilst conferring anti-thrombogenic properties. In this chapter, we focus on the luminal behaviour of the nanocomposite (Kannan, 2006) whilst chapter 7 would be based on its bulk characteristics namely compliance and permeability.

6.2. METHODS AND MATERIALS

6.2.1. POLYMER SYNTHESIS

As mentioned in chapters 2 and 3.

6.2.2. SURFACE CHARACTERISATION

Polymer samples for transmission electron microscopy (TEM) were prepared using thin slivers of 2% POSS-PCU which were removed from the glass slide and placed in plastic moulds which were then filled with Lemix epoxy resin and polymerised in an oven at 70 °C overnight. 0.5 μm sections were cut using a diamond knife (Diatome) on a Reichert-Jung ultracut microtome and collected on 200HS, 3.05mm copper grids (Gilder) coated with Butvar support film. The sections were viewed and photographed at up to 53,000 x magnification using a Philips CM120 transmission electron microscope at 80 kV to understand the composition of the polymer. The elemental composition of these regions were then analysed using energy dispersion X-ray analysis (EDXA). X-ray spectra and maps were also acquired using an EDXA DX-4 EDS X-ray microanalysis system. This test was done at the EM unit, Royal Free UCL Medical School, London, UK.

Using the data from the contact angle measurement alluded to in chapter 4 {Kim, 2003}, the equilibrium angle was calculated.

The surface topography of the 2% POSS-PCU nanocomposite was studied with a commercial Atomic Force Microscope (AFM) (Nanowizard, JPK Instruments, Berlin) using both contact and intermittent contact mode. For this purpose the nanocomposite was prepared by casting it on new glass cover slips and left to dry at 70 °C for 72 hours before being carefully peeled off using fine forceps and wrapped in aluminium foil to avoid surface contamination. Contact imaging was performed with a commercial AFM cantilever (gold-coated Microlevers™, type C, Veeco Metrology Group, Sunnyvale, CA) at a scan speed of 1 Hz at scan speed of 2.5 Hz. Intermittent contact imaging was performed at a scan speed of 1 Hz with a commercial non-contact silicon cantilever (Ultrasharp, NSC12/50, type A, MikroMasch, Talinn, Estonia). These experiments were done in conjunction with the London Nanotechnology Centre, UCL, London, UK.

X-ray photoelectron spectroscopy (XPS) was performed by mounting pieces of the nanocomposite onto stainless steel stubs with double sided adhesive tape, leaving their surfaces exposed. Using a VG CLAM2 spectrometer (East Grinstead, UK) with a (non-monochromated) Mg Kα source (photon energy 1253 eV), survey scans were taken at a pass energy of 100 eV and core level spectra at 20 eV with an electron take off angle of 60°. Elemental peak areas were used, with appropriate sensitivity factors to determine relative atomic concentrations. The sampling depth (into the surface) under the conditions employed for this work was approximately 5 nm. This experiment was performed at the Polymer Research Centre, Sheffield, UK.

SEM analyses of the nanocomposite, was performed as described in chapter 3.

6.2.3. THROMBOELASTOGRAPHY

Using a Thromboelastograph Coagulation Analyser (TEG®, Niles, IL, USA) calibrated at 37 °C, 4.5 ml of blood was collected using the two-syringe technique in a citrated tube to constitute 3.8 % citrated whole blood (CWB) at 1:10 v/v, pH 7.4. The CWB is then gently inverted thrice to mix it and incubated for 15 minutes. In the meantime, 0.2 M calcium chloride was left to thaw at room temperature for 10 minutes. TEG cups were coated with a thin, uniform layer of 2% POSS-PCU in DMAC and incubated at 50 °C to remove DMAC. These cups were then mounted onto the TEG analyser and 20μL calcium chloride was added to each cup followed by 340 μL of blood. The mixture was then coated with 6 drops of mineral oil to prevent blood evaporation and finally mixed by gently lowering and raising the pin {Horacek, 2002}.

Similarly, parallel analysis using poly (carbonate-urea) urethane (PCU) with empty polystyrene TEG cups as control was performed in comparison to 2% POSS-PCU. Each of these tests were performed using blood from healthy volunteers (n = 6). TEG tests on PTFE were not done as these high extrusion polymers did not allow the casting of a thin, uniform layer on the cups. Any other method of coating the TEG cups with these polymers would have significantly altered the outcome and was hence not attempted. Tests on polyethylene terephthalate (Dacron™) were not performed in any of these experiments as it is known that it is not the optimal material for smaller diameter grafts and microvessels {Schmedlen, 2003;Teebken, 2002}.

6.2.4. FIBRINOGEN ADSORPTION

Fibrinogen adsorption to POSS-PCU was determined using direct ELISA. The bases of 24-well polystyrene plates were coated with flat sheets of 2% POSS-PCU, PCU and PTFE (Goretex®, WL Gore Ltd., USA) with plain, uncoated polystyrene wells as controls. 100 μL of 5 % semi-skimmed milk (Marvel™) in PBS solution was then placed in each well for 2 hours at 37 °C to block non-specific antibody binding. This solution was removed and the wells rinsed with 0.01% Tween in PBS solution. 100 μL of human fibrinogen solution (310 mg/mL) was then placed in each well and incubated at 37 °C for an hour to allow fibrinogen adsorption to the polymers. This was then carefully rinsed again and replaced with 100 μL of a 1:1600 rabbit anti-human fibrinogen HRP-tagged conjugated antibody (Dako Ltd, USA) in 2% serum bovine albumin for a further two hours. This enzyme complex was then removed and a solution of ortho-phenylamine diamine (ODP) in acid citrate buffer was then added to the wells and the colour change allowed for 3 minutes before the reaction was terminated with 100 μL of 1% sulphuric acid. The wells were then exposed to an absorption spectrum of 490 nm to determine the readings (Dynex MRV, Prior Laboratory Supplies Ltd, UK.). This experiment was performed with 4 repeats (n = 4). No experiments were performed on polyethylene terephthalate for the reasons mentioned above.

6.2.5. ANTI-FACTOR XA ACTIVITY

Blood collected from healthy, normal volunteers without the use of tourniquets was citrated with 3.8% (w/v) tri-sodium citrate. The samples were then centrifuged at 250 g for 10 minutes and then re-centrifuged at 13,000 g for 30s using a microcentrifuge. This was followed by snap-freezing 250 ml aliquots of the plasma in liquid nitrogen before being stored at -80 °C. Prior to thrombogenicity analysis, these aliquots of platelet-poor plasma (PPP) were pre-warmed at 37 °C {Williams, 2004}.

The anti-factor Xa activity of 2 and 6 % POSS-poly(carbonate-urea)urethane(PCU) was studied using a factor X assay kit (AMAX ACCUCOLOR™ kit, Trinity Biotech, USA) with plain PCU and PTFE (Goretex Ltd., USA) as the controls. The base of 0.28 cm^2 well plates were sealed with solid flat sheets of POSS-PCU, PCU and PTFE. Heparin standards were prepared by diluting heparin in PPP to form decreasing concentrations of 1.0, 0.5, 0.25 and 0.125 IU/mL, constituting the heparin reference standard. The heparin solutions and PPP were diluted 1:2 in PBS to be used in the control and sample groups respectively. To this, 75 μL of human anti-thrombin III was initially added to each well followed by 25 μL of the 1:2 heparin solutions, in case of the control and PPP, in case of the sample. This was allowed to incubate for 2 minutes at 37 °C before adding another 75 μL of bovine factor Xa and incubating it a further one minute in the same setting. Next, 75 μL of factor Xa substrate (MeO-CO-D-CHG-Gly-Arg-pNA) was added and re-incubated for 10 minutes at 37 °C. Activated factor X (FXa) hydrolysed this substrate to release the chromophobe, para-nitro anilide (pNA). Thus, the amount of pNA released is inversely proportional to the extent of factor Xa inactivation. The reaction was terminated by the addition of 75 μL

of glacial acetic acid. Then 100 μL of this mixture was analysed at 420 nm absorption band to detect pNA and compared to the blank reagent. The latter was prepared in the same manner except that the wells were filled with acetic acid first {Saito, 1997}. The anti-factor Xa property of POSS-PCU was expressed as heparin equivalents per unit area (IU per cm^2). All experiments were repeated 6 times and in duplicate (n = 6).

6.2.6. PLATELET ADHESION

The bases of 24-well polystyrene plates were sealed with flat sheets of the polymer and then hydrated in PBS for 24 hours. Next, 1.0 ml of platelet rich-precipitate (PRP) at a concentration of 1.3 x 10^6 platelets / µl was added and incubated at 37 °C for 30, 60 and 120 minutes in a shaker. The PRP was then removed and each container was then rinsed with PBS. The extract was counted immediately in a Coulter counter. PRP were also incubated in wells with PCU and PTFE while uncoated polystyrene wells were used as controls {Park, 2002}

The number of platelets attached to POSS-PCU was calculated from the difference between the number of platelets in the PRP control and those left in the extract. The quantitative analysis of platelets attaching to POSS-PCU was expressed using Salzman's platelet retention index (PRI) {Salzman EW, 1963} as shown below.

$$PRI = \frac{(PLTi - PLTe)}{PLTi} \times 100\ \%$$

Where PLTi represents the concentration of the platelet precipitate prior to adsorption and PLTe represents its concentration after adsorption.

Platelet adsorption morphology was analysed using scanning EM (SEM as described in chapter 3.

6.3. RESULTS

6.3.1. POSS NANOCAGE DISTRIBUTION

In this thesis, we preferred to describe TEM analysis in this chapter as opposed to chapter 2 (synthesis and characterisation) as we felt that it would better illustrate surface behaviour patterns. TEM analyses on casted polymer sheets revealed that the darker areas of the nanocomposite correspond to the hard segment of the nanocomposite whereas the soft segment was optically less dense. EDXA mapping on these samples showed three specific regions; yellow silicon and oxygen-rich POSS segment(s) immediately surrounded by light purple areas of urethane which together constitute the hard segment and a dark purple area corresponding to the carbon-rich carbonate soft segment (figure 6.1a). TEM also showed that the silicon-rich POSS regions were distributed evenly throughout the hard segments of the nanocomposite while the presence of yellow speckled dots (silicon) within the amorphous domain also suggested POSS incorporation into the soft segment at the nanoscale. These POSS groups residing within the hard segment of PCU extended into the soft segment to form nebulous patterns as shown in figure 6.1b indicating an exfoliated type of nanocomposite {Giannelis EP, 1999}. This shows that POSS nanocages act as cross-linkers which form a 3-D net-like internal scaffold within the existing structural framework of the polyurethane hard segment, binding together the remaining constituents not unlike a 'wire mesh'.

Figure 6.1a. EDXA map of 2% POSS-PCU showing the distribution of POSS (yellow) within the hard segment of the polymer (light purple) while softer segments correlate to purple areas of carbon. The red line represents the copper grid. On closer inspection, speckled yellow dots may also be seen within the soft (purple) segments of the polymer indicating that POSS molecules also interact with the amorphous carbonate segment.

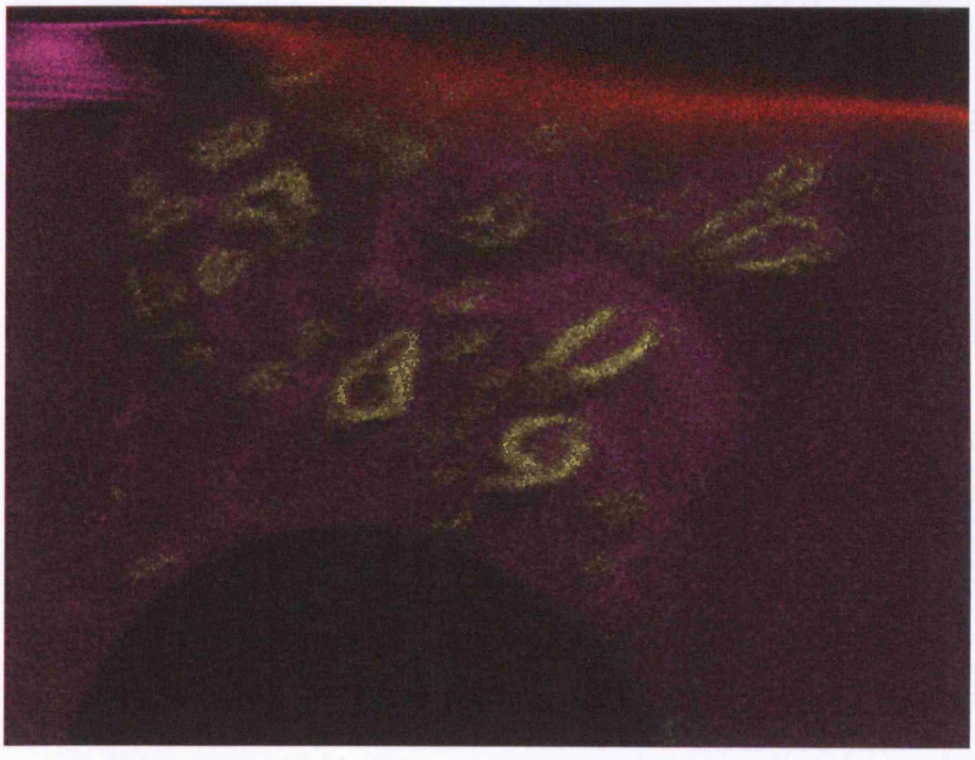

Figure 6.1b. TEM analysis of a cross-section of 2% POSS-PCU casted sheets showing the distribution of silicon-rich POSS segments within the darker, hard segments of the nanocomposite whilst gradually encroaching the soft segments, typical of an exfoliated nanocomposite.

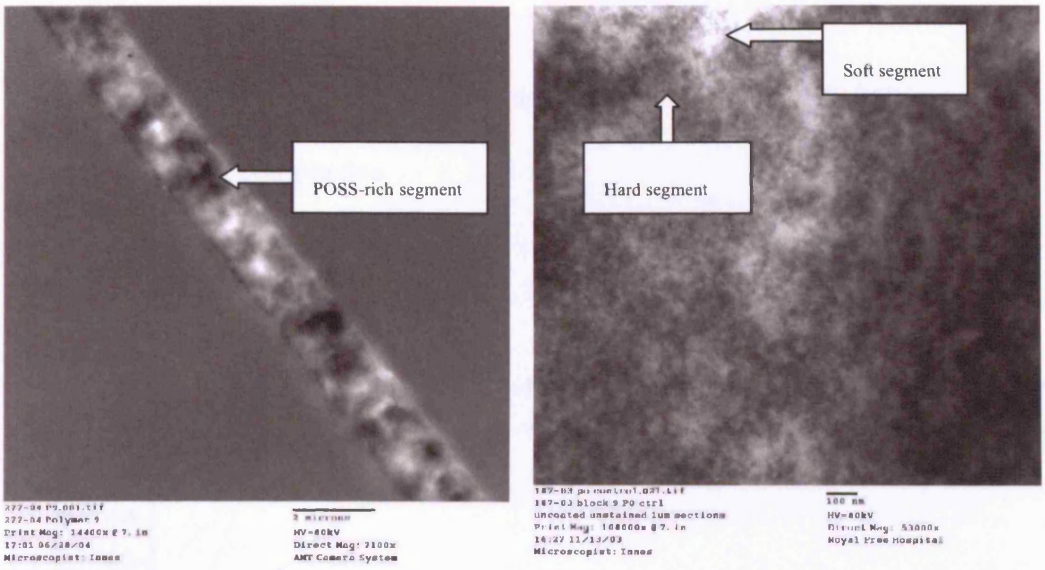

6.3.2. WATER CONTACT ANGLE MEASUREMENT

2% POSS-PCU had an advanced contact angle of 81 ± 2° and a receded angle of 36 ± 5° which reveals a large difference between the advanced and receded angles; contact angle hysteresis (see figure 6.2) compared to conventional polyurethanes which is known to be in the region of 80 ± 1° without significantly large contact angle hysteresis. Known causes of a large hysteresis loop include surface roughness, microscale chemical heterogeneity and surface fabrication in an aqueous environment. All samples were dried and casted in a hot air oven at 70 °C which excludes an aqueous environment. TEM studies show chemical heterogeneity then the advanced

angle is thought to be typical of the low energy surface component and the receded angle typical of the high energy surface component. As such, atomic force microscopy (AFM) was performed to determine if there was a significant topographic contribution.

Figure 6.2. The large contact angle hysteresis loop of 2 % POSS-PCU nanocomposites.

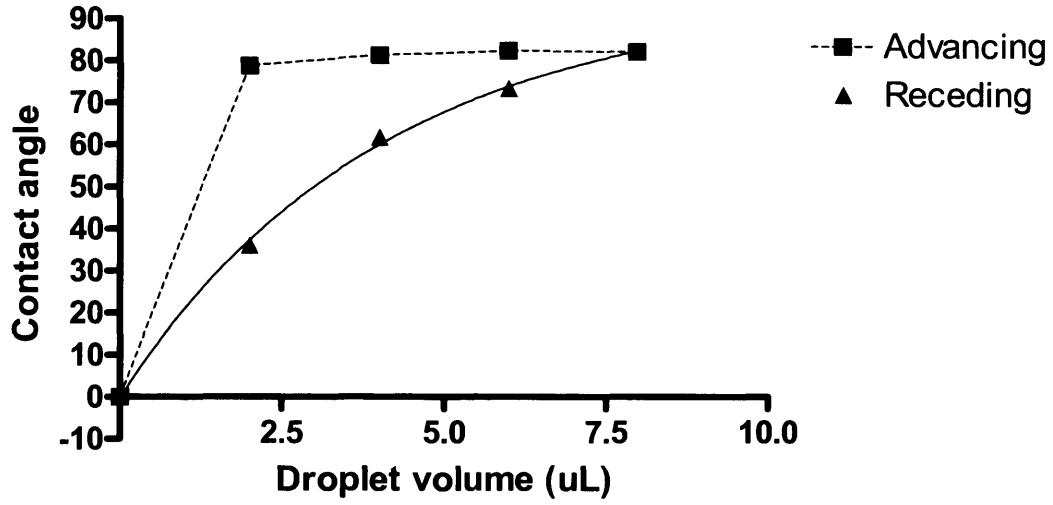

6.3.3. SURFACE TOPOGRAPHY

Surface visualisation of the nanocomposite with SEM at 5000x magnification (figure 6.3a) shows an uneven surface ultrastructure at the nanoscale with crystalline peaks protruding as obelisk-like structures. Corroborating evidence with AFM in contact mode shows that 2% POSS-PCU has three different phases: a crystalline-like

phase and a two phase "pebble stone" blend. The smooth crystalline phase consists of domains that are 5-20 μm in size with a height of 1-6 μm compared to base level (figure 6.3b). The crystalline phase consists of well-defined peaks with some existing as nanopyramids {Riedel, 2001}. The pebble stone blend can only be observed at higher magnifications (figure 6.3c) and consist of elevated domains that are 200-500 nm in size and 100-200 nm in height ('mushroom-like' domes) {G.J.Fleer, 1993}, characteristic of an extended surface configuration {Jonsson, 2004}. The friction image shows that the elevations and depressions have different visco-elastic properties {Duan, 2002} and therefore can be considered as two separate phases.

Figure 6.3a. SEM image of the microvessel lumen showing its surface ultrastructure with the crystalline hard segments projecting out of its surface.

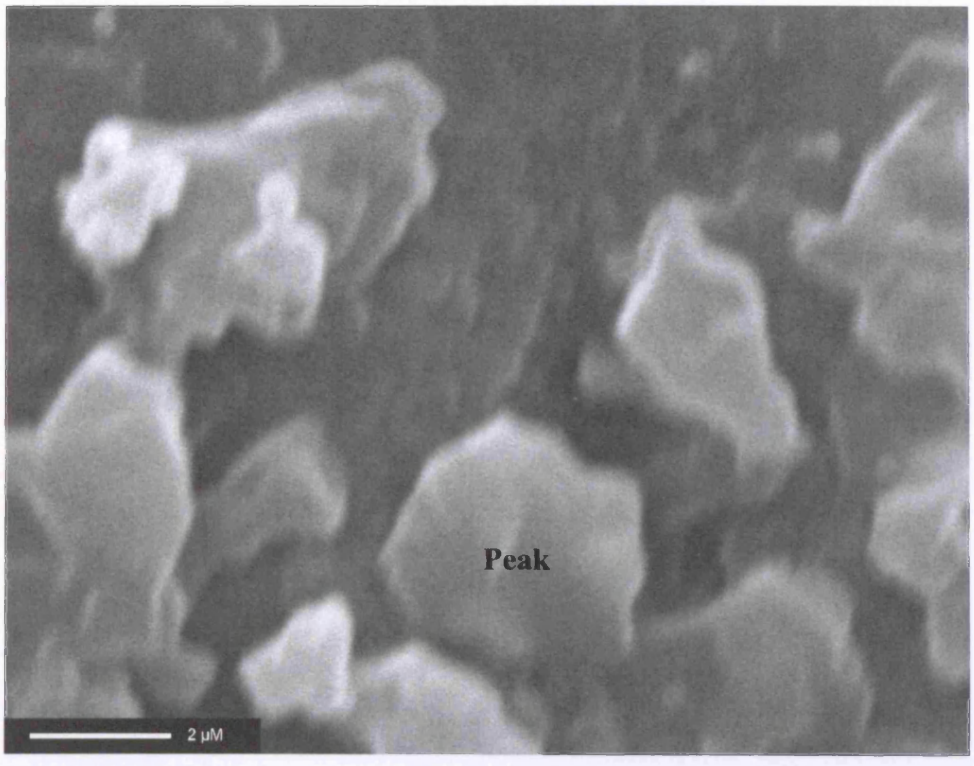

Figure 6.3b. AFM image of 2% POSS-PCU at 25 x 25 μm resolution showing large peaks of up to 8000 nm high within the crystalline segment showing increased geometrical definition. The domes (300 to 500 nm high) and troughs are suggestive of POSS nanocage interaction with the amorphous, soft segment.

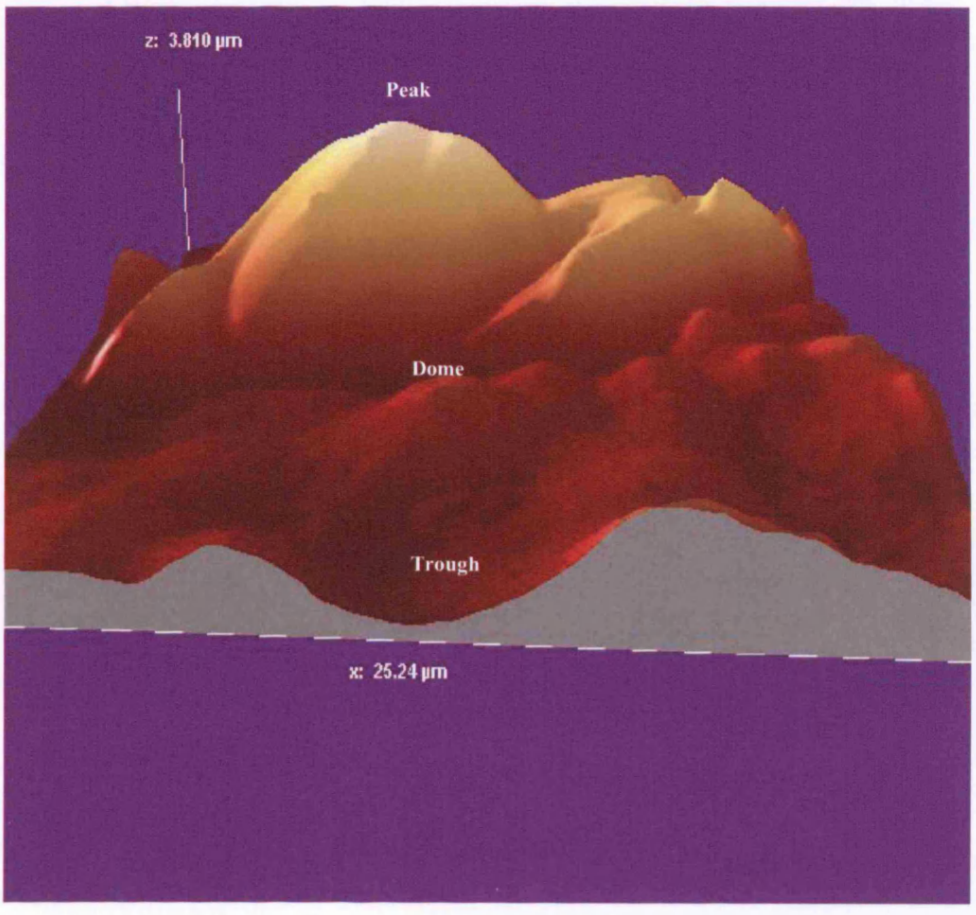

Figure 6.3c. Microphase images of 2% POSS-PCU at the nanoscale revealing its extended surface ('mushroom' configuration) with 100 nm high elevations and corresponding depressions.

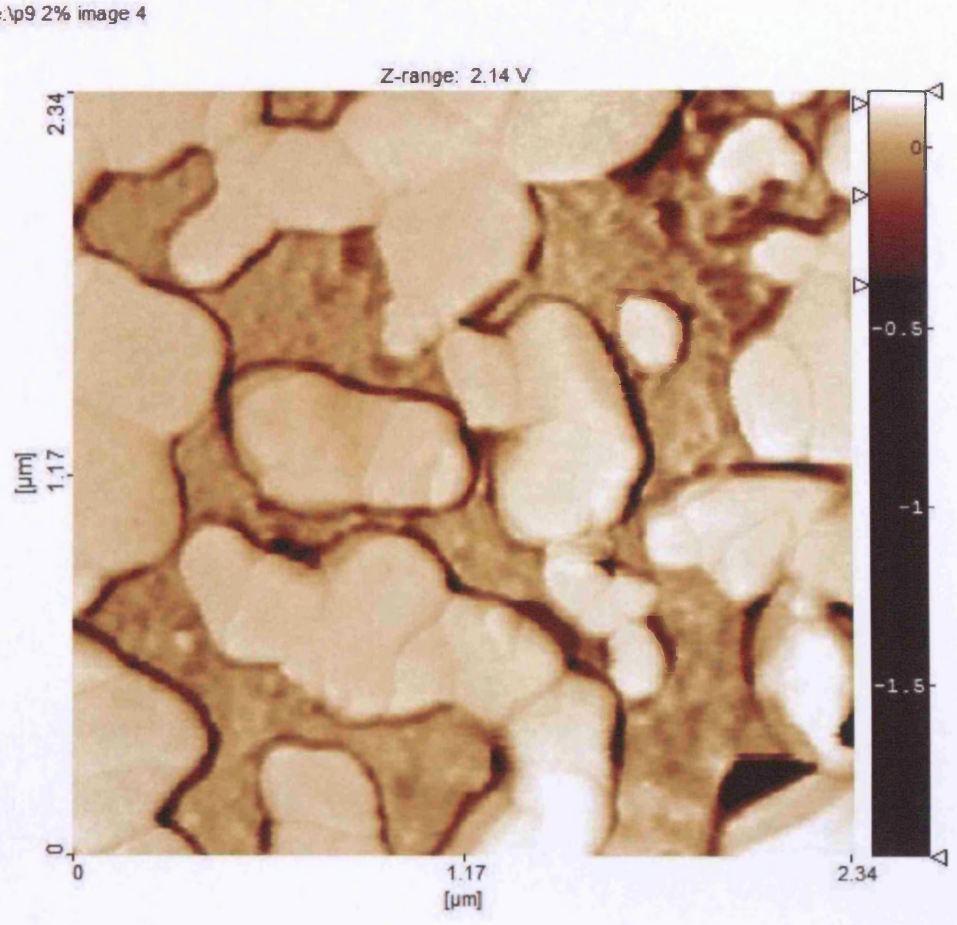

Friction image maps are obtained by the twisting of the cantilever that arises from forces on the AFM cantilever parallel to the plane of the sample surface. Further images were obtained in intermittent contact mode from transition zones between elevations and depressions. In intermittent contact mode the phase image shows the relative adhesion between the tip and sample in addition to height information. The depressions have lower adhesion compared to the elevations and therefore appear darker in figure 6.3d. This figure also shows the presence of transitional intercalating zones between the POSS nanocore and the polyurethane matrix which possesses

intermediate adhesion characteristics compared to the other domains. This is in contrast to the PCU control which shows the diminished presence of a nanopyramid crystalline phase and the absence of a two-phase 'pebble stone' blend (figure 6.3e).

Figure 6.3d. AFM on the 2% POSS-PCU nanocomposite surface showing the nanoscale interaction between the POSS-rich dark segments and the brighter areas with relatively less POSS content specifically in the intermediate 'zone of intercalation'.

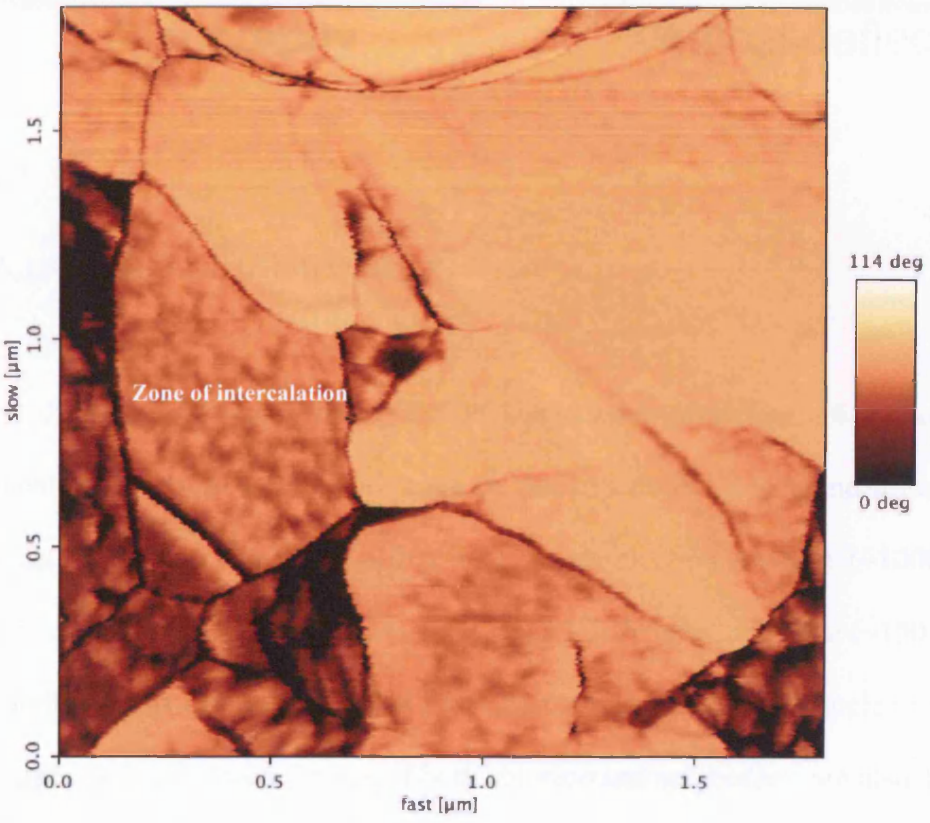

Figure 6.3e. Surface topography of control PCU showing the absence of crystalline nanopyramids and a two-phase pebble-stone phase.

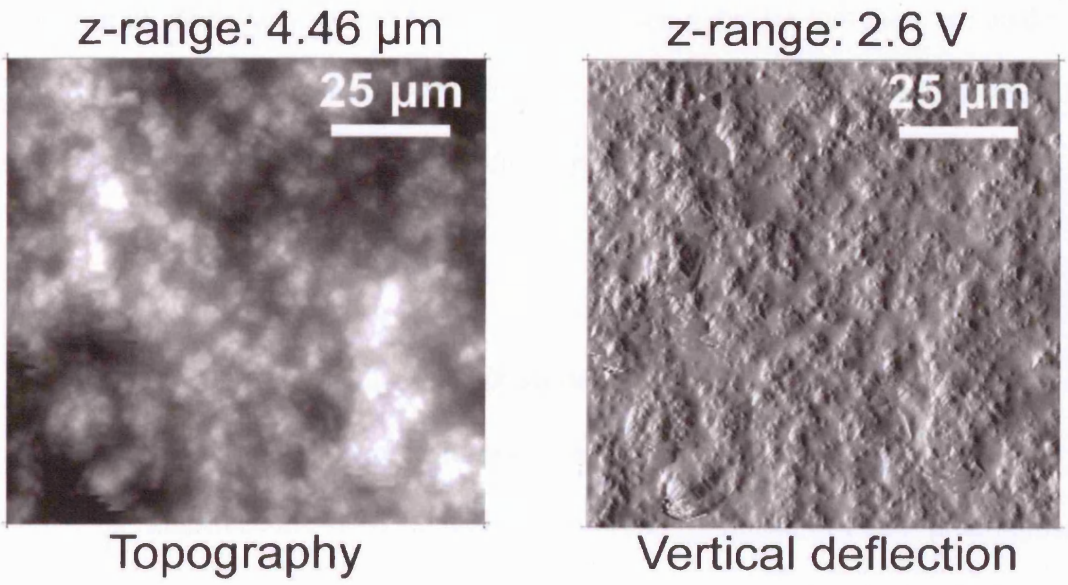

6.3.4. SURFACE COMPOSITION

XPS survey spectra from POSS-PCU nanocomposite (figure 6.4) showed that the most prominent photoelectron peaks are due to carbon, oxygen and silicon. Unlabelled peaks are due to carbon KLL Auger electron emission (~1000 eV), oxygen KLL Auger electron emission (~720 eV) and Si *2s* photoemission (~150 eV). X-ray satellite peaks are evident on the low binding energy side of photoelectron (but not Auger electron) peaks. Traces of both chlorine and magnesium are also detected. Accurately assigning the latter is potentially questionable as its peak is rather weak, and may be due to another element, such as the selenium, ruthenium or iodine (the binding energy of Se *3d*, Ru *4p* and I *4d* are very close to that of Mg *2p*). However, no other peaks typical of these elements were observed and therefore the most likely

candidate is magnesium. The elemental concentrations are tabulated along with figure 6.4 for the two samples, the error in the quantification being in the order of 1 atomic %. Additional narrow scans of the carbon, silicon and oxygen peaks demonstrated no evidence of chemically shifted environments, which indicates that there are no direct bonds between oxygen and carbon. The oxygen is therefore bound predominantly to silicon atoms which indicate the significant presence of closed POSS cages (Si_8O_{12}).

Figure 6.4. XPS surface analysis at 30° angle of incidence showing an elemental silicon surface composition of the luminal surface of POSS-PCU microvessels of 16 %. As the silicon (Si 2p) bonds of POSS predominantly reside on the surface of POSS-PCU, this indicates that the luminal surfaces of the microvessels are POSS - enriched.

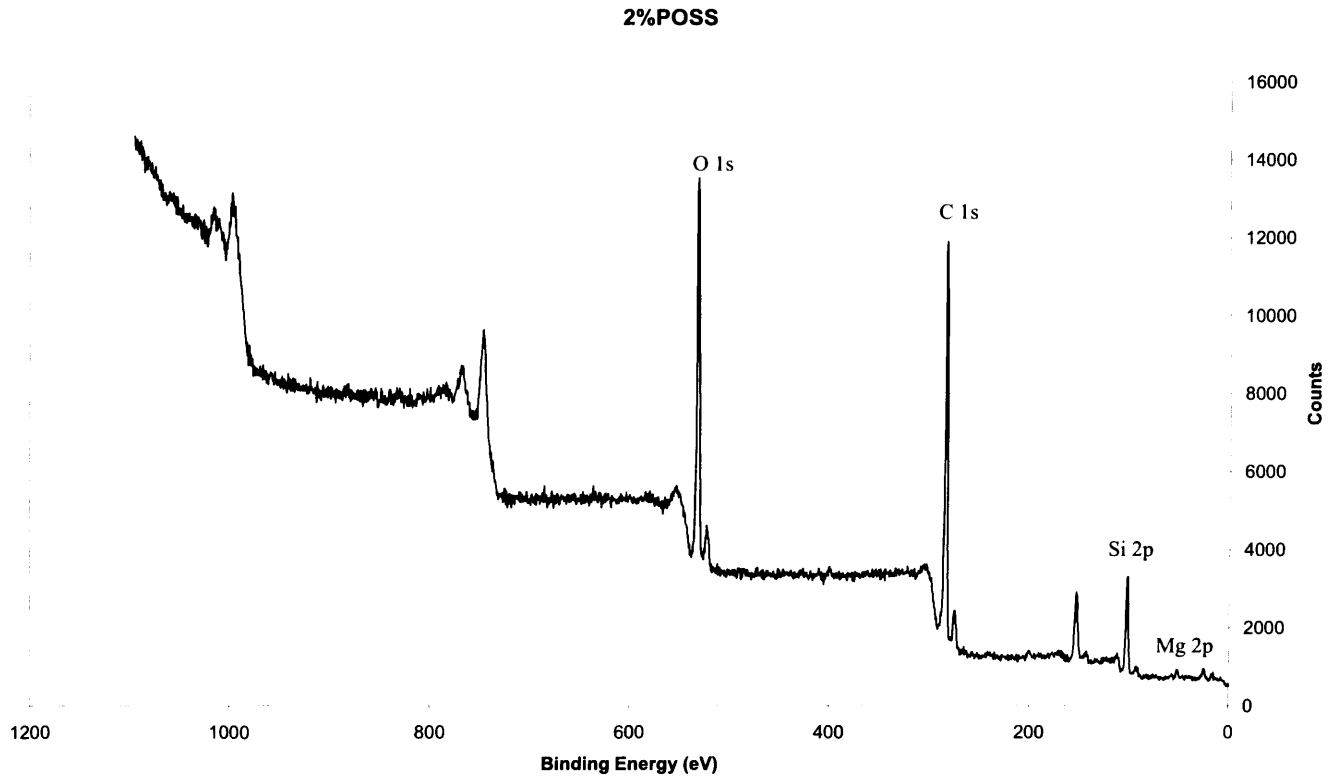

Bond	Position	Area	Atomic (%)
C 1s	284.70	60714.7	59.238
O 1s	532.70	62058.0	21.245
Si 2p	102.20	14154.5	15.966
Cl 2p	200.70	1048.0	0.433
Mg 2p	52.20	1534.0	3.118

The binding energy of POSS nanocages [102.5 eV] in this case is similar to a polydimethylsiloxane (PDMS) polymer [102.4 eV] as compared to silicon metal [99.6 eV] and silicon oxide [103.4 eV] {Briggs, 1983}. In order to rule out surface contamination by PDMS; a highly surface active contaminant commonly found in laboratories in the form for example, of greases for vacuum joints. Working under the assumption that PDMS was a surface contaminant, we attempted to remove it by washing with *n*-hexane. The XP spectra did not change significantly after this treatment. The binding energy which resembles PDMS may be explained by the cyclohexyl side-groups attached to the primary POSS nanocage.

6.3.5. THROMBOELASTOGRAPHY (TEG)

TEG is a sensitive indicator of thrombogenicity and we used these as screening tests to ascertain the anti-thrombogenic properties of POSS-PCU. We found that the polymer had a significantly lower maximum amplitude (MA) value(s) indicative of decreased platelet bonding strength ($p < 0.001$, One-way ANOVA) as compared to control polystyrene and PCU. In addition, it was also found that the clots which formed on POSS-PCU were significantly unstable and lysed by 60 minutes compared

to PCU or the control polystyrene polymer ($p < 0.0001$, One-way ANOVA). Both MA and LY60 results are shown in figure 6.5. These results may be due to either decreased fibrin binding strength to the polymer or lower fibrin adsorption to the TEG cup or a combination of both. In the following series of experiments, we sought to determine the cause of this behaviour. As mentioned earlier, these tests were not performed with PTFE and polyethylene terephthalate as it is not possible to evenly coat onto the TEG cups as is the case with PCU and POSS-PCU since PTFE and Dacron™ are high extrusion-based polymers.

Figure 6.5. Tests showing lower maximum amplitude values and increased clot lysis at 60 minutes of 2% POSS-PCU compared to PCU and the polystyrene control ($n = 6$).

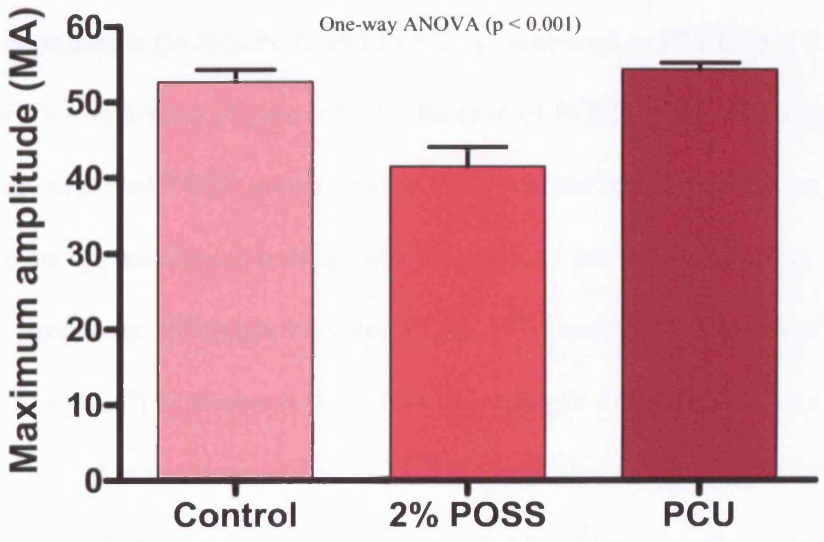

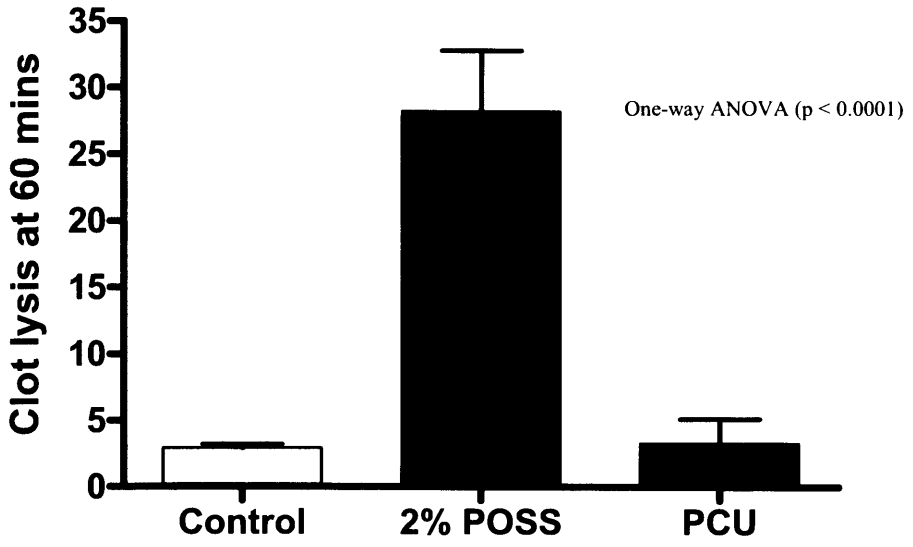

6.3.6. FIBRINOGEN ADSORPTION TESTS

Direct ELISA fibrinogen adsorption analyses (n = 4) to the various polymers showed that there was a significantly decreased fibrinogen adsorption to the polyurethanes (POSS-PCU and PCU) as compared to PTFE ($p < 0.01$, One-way ANOVA analysis) (figure 6.6). In the case of POSS-PCU, this may again be attributed to the effect of POSS groups on the PCU surface which possess an unstable surface free energy and hence reduce both platelet and protein adsorption. Although we found no significant difference between POSS-PCU and PCU in terms of fibrinogen adsorption, TEG analyses show that the strength of the fibrin clot in POSS-PCU is much weaker as compared to PCU. This indicated that while the amount of fibrinogen adsorbing to both polymers are similar, the binding strength is weaker in POSS-PCU compared to PCU alone. No comparisons were done with polyethylene terephthalate for the reasons discussed above.

Figure 6.6. Fibrinogen adsorption direct ELISA tests on 2% POSS-PCU, PCU and PTFE (n = 4).

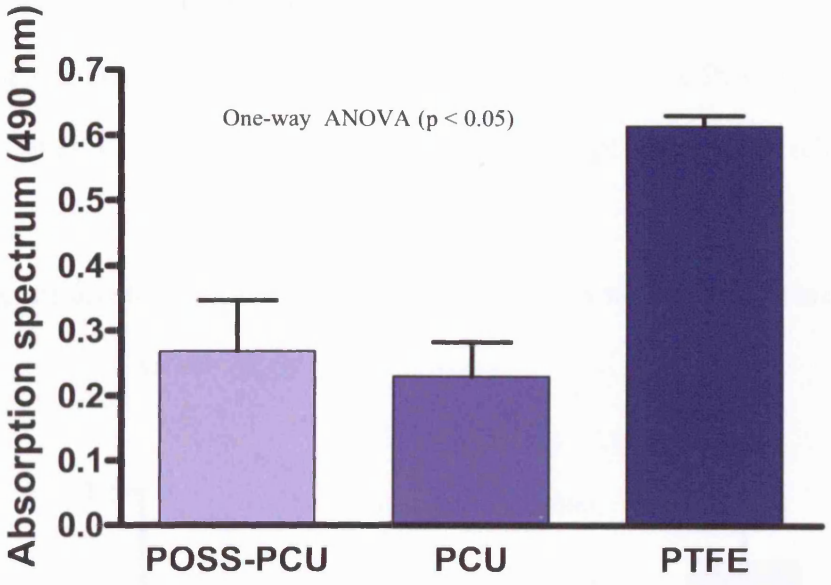

6.3.7. ANTI-FACTOR XA ACTIVITY

Factor X (FX) is a crucial element of both the intrinsic and extrinsic coagulation pathways. Using the methods described earlier, we first compared the surface anti-FXa activity of 2% POSS-PCU to PCU and PTFE. On increasing the concentrations of POSS in PCU to 2% and then 6%, we found a proportionate increase in the anti-FXa activity of the co-polymer as compared to both PCU and PTFE (figure 6.7) which was statistically very significant (One-way ANOVA, $p < 0.0001$). These findings indicate that POSS-PCU nanocomposites inactivate FXa to a greater extent than PTFE {Seifalian, 2002} and PCU. It is important to note that PCU also exhibited some if not as significant, FXa inactivation. Correlating this with the AFM data suggests that increasing the nanoscale surface roughness of the polymer would

enhance FXa denaturation and inactivation {Riedel, 2001}. Since we are primarily interested in graft material for smaller diameter (< 6 mm) and microvessels (< 1mm), no tests on polyethylene terephthalate were performed. It must be mentioned that here that 2 % POSS-PCU gained precedence over 6 % POSS-PCU as a vascular graft since the latter was markedly stiffer during radial compliance studies (chapter 7).

Figure 6.7. Incremental concentrations of POSS within PCU conferring greater anti-FXa activity (n = 6).

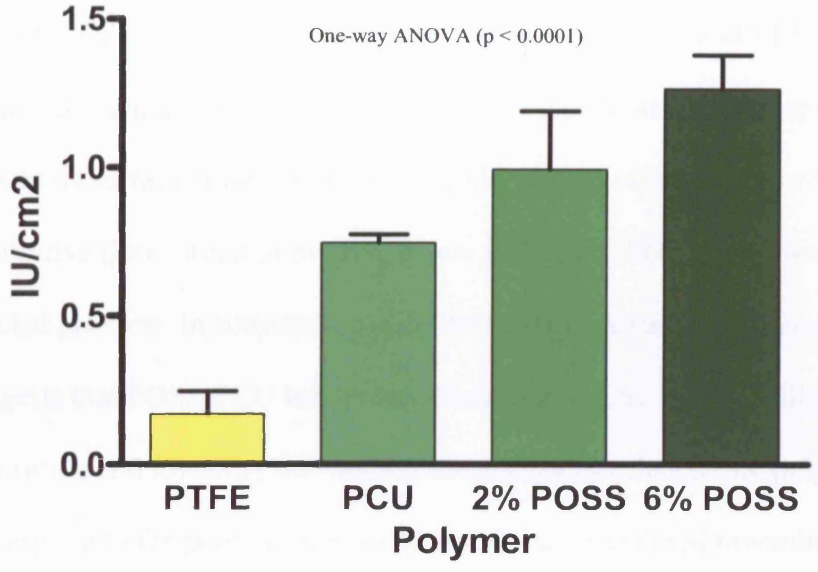

6.3.8. PLATELET ADSORPTION TEST

Platelet adsorption onto casted sheets of POSS-PCU was significantly less than both PCU and PTFE sheets *in vitro* after 120 minutes in contact. Statistical analysis using two-way ANOVA showed significant difference (Two-way ANOVA, $p < 0.05$) in platelet adsorption by 120 minutes between POSS-PCU, PCU and PTFE as shown in figure 6.8. Given that the actual difference between POSS-PCU and the rest is less than 10 %, it also has to be noted that POSS-PCU does not significantly minimise adsorption quantitatively but the difference is the qualitative decrease in binding strength. This deduction is in keeping with both the TEG and ELISA results. These results indicate that POSS-PCU significantly repels platelet adsorption with increasing time to its surface compared to PTFE and PCU, an effect which would be amplified in a pulsative flow circuit or in vivo, where increased shear would wash away weakly-bonded platelets. In conjunction with the lower MA values obtained on TEG, this suggests that POSS-PCU has an anti-platelet effect by both repelling their surface adsorption and lowering the binding strength of platelets to the polymer which correspond to the poor adsorption characteristics exhibited towards fibrinogen discussed above.

Figure 6.8. Platelet retention indices on 2% POSS-PCU, PCU and PTFE at 30, 60 and 120 minutes (n = 6) showing significant decrease in platelet adsorption to 2% POSS-PCU compared to PCU and PTFE.

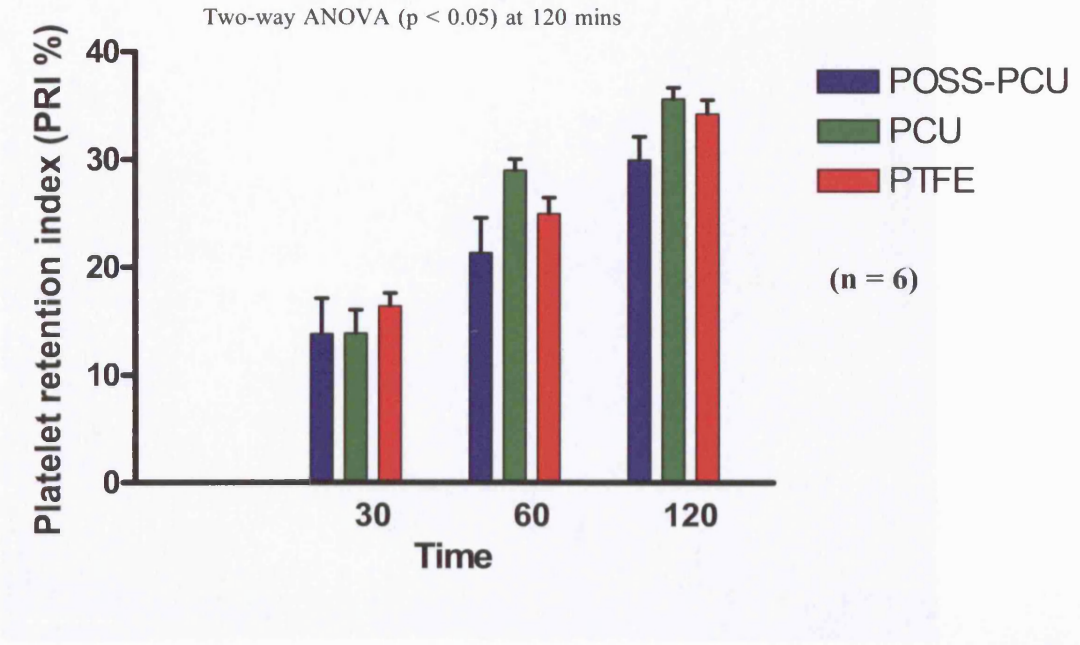

SEM analysis performed on these samples at 120 minutes to assess platelet adsorption morphology revealed very few platelets adhering to POSS-PCU (figure 6.9b) compared to the uniform, thick layer of platelets deposited on PTFE as shown in figure 6.9a. Against the 'cobblestone' background of the nanocomposite, it can be clearly seen that even the very few platelets which did adhere to the polymer, did so to the elevated POSS-poor 'domes' seen earlier on AFM. These images supported the PRI studies conducted on polymer-platelet adhesion which showed decrease adhesion to the nanocomposite.

Figures 6.9a. SEM images of platelet adsorption on PTFE at 1250x magnification reveal uniform platelet adsorption on PTFE (Stage IV) after incubation for 120 minutes.

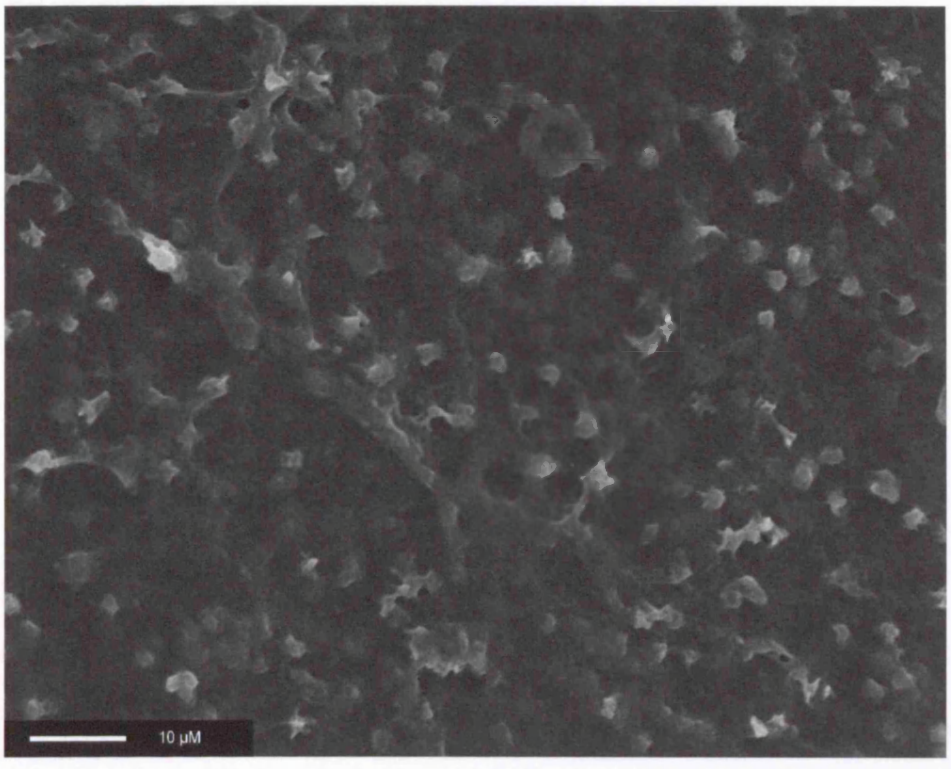

Figures 6.9b. SEM images of platelet adsorption on 2% POSS-PCU at 640x magnification showing minimal platelet adsorption at 120 minutes (Stage I) on 2 % POSS-PCU.

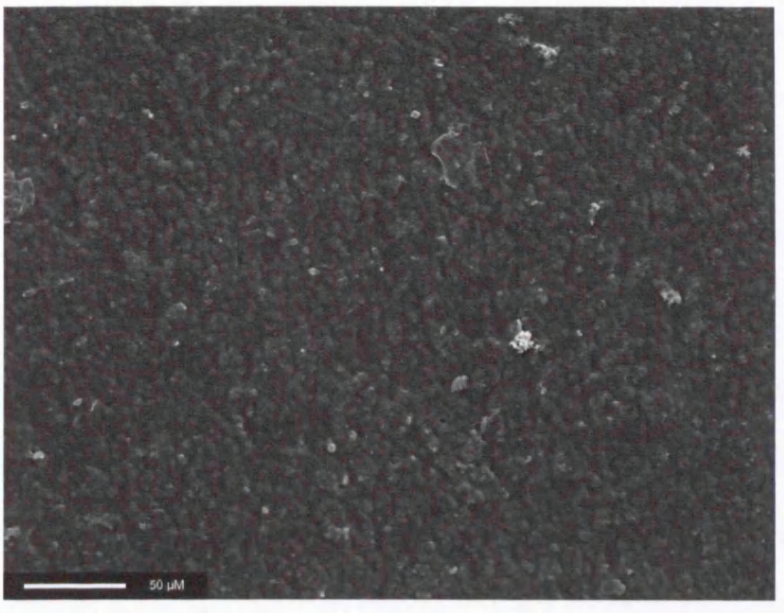

Figures 6.9c. SEM images of the control POSS-PCU 'without' any platelets, showing the basic undulating morphology of the nanocomposite. Each bar code represents 10 µm. Figure 6.3c graphically depicts this undulating morphology better.

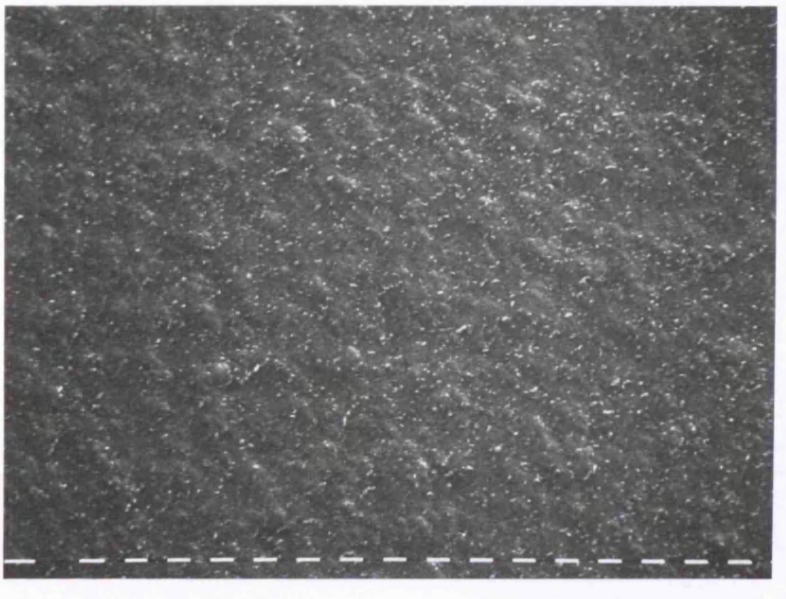

Platelet adsorption patterns were then graded based on Cooper's arbitrary classification scheme (table 6.1) {Ko, 1993}. According to this scheme, there was very minimal platelet adsorption to the POSS-PCU nanocomposite and even those platelets that did adsorb, showed stage I patterns; round platelets with no pseudopodia. In contrast, platelet adsorption to PTFE was far greater with multiple layers of adherent platelets visualised even at lower magnifications. These platelets exhibited stage IV adsorption patterns in over 50 % of its surface area. These findings show that integrin activation on platelets {Groth, 1995} occurs to a lesser extent in POSS-nanocomposites as compared to PTFE. This improved haemocompatibility corroborates with previous studies on silicon-containing polymers {Silver, 1999}. Platelet adsorption tests on Dacron™ were not performed since they are known to possess relatively high platelet adsorption characteristics {Desai, 1991}, even significantly higher than PTFE.

Table 6.1. Cooper's classification scheme for platelet adsorption {Ko, 1993}.

Stage	Description
I	Rounded platelets with no pseudopodia.
II	Dendritic, rounded platelets with early pseudopodia formation.
III	Spreading, dendritic platelets.
IV	Spreading platelets and their hyaloplasms with prominent pseudopodial formation.
V	Fully spread platelets over the entire surface.

6.4. DISCUSSION

In the past, the anti-protein and anti-platelet actions of silicon {Silver, 1999} have been negated by its relative stiffness to native vessels {Desai, 1991}, a contributory factor to intimal hyperplasia {Seifalian, 2003;Tai, 2000}. Combining it with more compliant polymers such as rubber {White, 1987} have been attempted but results have been suboptimal. On the other hand, nanoscale POSS {Lichtenhan JD, 1995} inclusion as a side-chain group {Nishino, 2004} should preserve the compliance of the co-polymer whilst further lowering its surface free energy (SFE), as nanocomposites have been shown in the past to have SFEs of less than 20 mJ/m {Schmidt, 2001;Schidmt, 1995}. These results are even lower than the SFE values of the fluorinated PTFE molecule, the current biomaterial(s) of choice for small diameter {Nishino T, 1999} and microvascular grafts. A further advantage is that as experiments on dental materials have shown, unstable SFEs could also lower bacterial adhesion thereby creating an anti-bacterial surface action as well {Quirynein M, 1995;Knorr, 2005}.

The factors which determine particle adsorption to a polymeric interface are (1) SFE, (2) surface morphology/configuration and (3) particle size. The SFE so often confused with hydrophobicity, {Blunden, 1994} is defined as the amount of work required to increase the surface area of a substance by 1 cm^2 and is a measure of its surface reactivity. For instance, air has a low SFE while water possesses high SFE values {Nagasawa A, 2004}. SFE measurements involve analysing the static and dynamic contact angles of surfaces using a variety of liquids {Gu GT, 2002}. Monte Carlo simulation studies have shown that hydrophobic surfaces are better at repelling

larger particles and vice versa for hydrophilic ones. These researchers have also proved that polymers with extended surface configurations wherein its monomeric units overlap one another have lower particle adsorption particularly for larger-sized molecules such as proteins {Jonsson, 2004}. With respect to haemocompatibility, the primary proteins in question are fibrinogen and the coagulating proteins.

In the past, Feng and co-workers showed that the haemocompatibility of low-temperature isotope carbon (LTIC) is greater than conventional silicone polymers as it denatures or alters the conformation of adsorbed fibrinogen to a greater extent {Feng, 1994}. Our contact angle measurements however indicate that unlike earlier silicones, these nanocomposites possess large contact angle hysteresis which has been shown to affect the conformation of particles such as fibrinogen adsorbed to its surface {Tengvall, 1998}. Subsequent tests showed that fibrinogen also had decreased quantitative and qualitative adsorption to POSS-PCU surfaces as exemplified by direct ELISA and TEG respectively. While there was no significant difference in fibrinogen adsorption between PCU and POSS-PCU, there exist a marked difference in clot lysis times ($p < 0.01$) between the two polymers. This indicated that although the number of adsorbed fibrin molecules is similar in quantity, their binding strength to the nanocomposite is much lower, possibly due to a conformational change in adsorbed proteins over time. Studies are currently underway to quantify the exact conformational change utilising ellipsometry and neutron scattering. This may also explain the lower platelet adsorption and maximum amplitude (MA) values to the nanocomposite compared to PCU because platelet adsorption requires a stable configuration of fibrinogen formation {Hynes, 1991;Sixma, 1991}.

Using polyurethaneureas based on 4,4'-diphenylmethane diisocyanate and polytetramethylene glycols, Groth and co-workers had reported that platelet and protein adsorption increases proportionately with urethane and urea concentrations {Groth, 1995} within the hard segments. This study shows that platelet and protein adsorption to the POSS-PCU nanocomposite was low in all regions including the crystalline segment. This is corroborated by the undulating platelet adsorption topography and the evidence of low-grade platelet adsorption (Cooper grades I and II) to the nanocomposite that was observed with SEM. This reversal is attributable to the presence of silicon-rich POSS nanocages occupying the hard segment of the nanocomposite and concurrently replacing both urethane and urea and so reducing its concentration.

While the protein-/platelet-repellent nature of this nanocomposite is due to its high contact angle hysteresis, the cause for the degree of hysteresis can be attributed to either its nanoscale chemical heterogeneity and/or surface topography. TEM and EDXA analyses reveal the heterogenous nature of the polymer surface at the nanoscale with the POSS-nanocages preferentially residing within the hard segments of the nanocomposite with extensions to the soft segment as well. Based on X-ray photoelectron spectroscopy (XPS) analyses on silicon-germanium nanocomposites, Muller and co-workers believed that nanoscale surface roughness or topography was the prime factor responsible for this hysteresis {Muller B, 2001} as compared to surface composition. Based on this background, XPS surface analyses of was performed on 2 % and 6 % POSS-PCU wherein there was an increase in elemental surface silicon content from 16 % to 18 %. Interestingly, there was no difference in contact angle hysteresis between the two nanocomposites, suggesting that surface

topography due to the POSS-induced surface reorientation was the main determinant of contact angle hysteresis in this case.

Surface topography may be broadly classified into the mushroom-, brush- or pancake- profiles {G.J.Fleer, 1993}. The former two varieties have extended configurations wherein they rise out of the surface whereas pancake-type profiles have collapsed or flattened surfaces with the highest monomer density within two lattice spaces of the surface. Extended surfaces can extend up to ten lattice spaces (A lattice space may be defined as the space bounded by atoms/molecules with identical surroundings to one another) from the surface with the self-attractive hydrophobic constituents closer to and the hydrophilic constituents further away from the surface {Jonsson, 2004}, the degree to which depends on the nature of the contacting surface. Monte Carlo simulation studies indicate that polymers with extended configurations would repel particle adsorption better than collapsed ones as long as the ratio of particle size to polymer layer is 4 or greater {Malmsten, 1998}. This strengthens the argument for the inclusion of nanofillers onto interfaces in contact with large molecules such as proteins. The use of such nanomaterials would increase this ratio significantly and so improve protein repulsion and in case of blood, platelets as well. Interestingly, such nano-engineered surfaces would be able to better adsorb very small particles such as low-molecular weight heparin whilst repelling the larger coagulant proteins, making them ideal at the vascular interface. In this case, the extremely small size of silicon in the form of POSS nanocages (1-3 nm) {Xiang K, 1998} would further increase the ratio of particle size to polymer layer and thereby accentuate both platelet and protein repulsion.

Tapping mode AFM studies on these POSS-PCU nanocomposites revealed a nanoscale extended surface configuration with a 'mushroom/dome-like' profile. Its surface nanoarchitecture is such that POSS-rich hard segments were found to reside closer to the surface as depressions while the more hydrophilic soft segments rise from the surface as elevations which is in keeping with existing data on polymers possessing both hydrophobic and hydrophilic elements namely be being amphilic in nature. The lower adhesion exhibited between the contact probe of the AFM and the darker, depressed areas also corresponded to the decreased platelet and protein adsorption behaviour on SEM to the depressed areas of the nanocomposite while the brighter, elevated regions show relatively higher adhesion characteristics.

As a significant proportion of this 2% POSS-PCU nanocomposite surface consist of peaks at the microscale and domes at the nanoscale, it would be not be wrong to expect increased overall surface protein adsorption. Similar studies on globulin {Muller B, 2001} and macrophage {Riedel, 2001} using silicone-germanium nanocomposites had shown that although these so-called peaks or 'nano-pyramids' {Riedel, 2001} exhibited increased protein adsorption, the adsorbed proteins were actually inactive as this nanoscale roughness contributes to large contact angle hysteresis {Muller B, 2001}. This would also explain why FXa inhibition is present although to a lesser extent, in the control polymer (PCU) as it showed microscale surface roughness on AFM studies. Interestingly, there is a proportionate increase in FXa inhibition on increasing POSS nanocage concentrations as this would increase surface nanostructure density and contact angle hysteresis further which would in turn accelerate protein denaturation.

While we agree with previous work that this anti-thrombogenic effect is a result of the surface morphology of nanocomposites, AFM experiments on these POSS-PCU nanocomposites and the PCU controls also reveal that the addition of nanofillers is necessary in creating these nanostructures in the first place. In all, both surface composition and morphology are a must in order to elicit this protein-repellent activity.

Assays to show irreversible protein adsorption to the polymers were not performed as we felt that testing them in a dynamic setting using pulsatile flow was more physiological. These tests are currently under way as further investigations on these nanomaterials are performed in addition to the surface ellipsometry and neutron

scattering studies described earlier. In any case, if all our results thus far hold true *in vivo*, thrombus formed on POSS-PCU grafts would be unstable and weak with lower propensity for thrombus propagation and vessel occlusion. Animal studies using the rabbit central ear artery microvascular model are also being performed to establish this fact.

This represents the first reported literature of the anti-thrombogenic effect of POSS-PCU nanocomposites. This group of polymers are only now being commercialised in industry, principally within aerospace-based applications and has thus far, few if any practical biomedical applications as of yet. It not only possesses the anti-platelet and anti-protein effects of existing siloxane co-polymers but in addition behaves as a surface anticoagulant as well. POSS-incorporated macro- and micro-vascular interfaces could remove the necessity to heparinise devices like the heart -lung machines and artificial capillary beds. This approach could also provide a simpler chemical alternative compared to current methods of improving small diameter and microvascular graft patency. There even is the possibility of tagging molecules such as nitric oxide (NO) {Duan, 2002} as side-chains directly to the POSS nanostructure to enhance its haemocompatibility even further. These findings could open entire vistas of use for silicon nanocomposites in medicine particularly as thromboresistant macro- and micro-vascular interfaces *in vivo*.

Encouraged by our results, we fabricated 2% POSS-PCU as microvessels for use as interpositional microvascular grafts and the building blocks of an artificial capillary bed {Kannan, 2005}. As far as vessel fabrication is concerned, the ability of POSS to self-assemble predominantly on the surface would mean that the bulk of the polymer would consist of polyurethane molecules cross-linked by POSS nanocages which preserves radial compliance and should hypothetically enhance its resistance to degradation {Salacinski, 2002b}. This is could be a further advantage of POSS-PCU nanocomposites. From the manufacturing point of view, polyurethanes being low-extrusion polymers remain as stable liquids with the ability of either dip-coating or extruding them into prostheses. These are still early days to comment on the clinical success of these nanomaterials but for certain, the future is very bright.

Chapter 7

7. Smart biomimetic nanocomposite microvessels: Building blocks of an artificial capillary bed.

7.1. INTRODUCTION

Vein grafts are the current microvascular graft of choice but as a component of a microvascular network, it is limited by donor-site morbidity and the technical impossibility of dissecting it out as a microvascular network {Bourassa, 1994}. While current prosthetic materials are not suitable, we believe that the answer lies with a new generation of nanocomposites incorporating silicon in the form of POSS molecules.

POSS molecules may be incorporated as building blocks {Sanchez C, 2001} into other polymers to form hybrid inorganic-organic co-polymers with improved miscibility and hence elasticity {Haddad TS, 1999}, an effect demonstrated by previous studies {Lee YJ, 2004}. Optimal POSS dispersion within the polymer {Ribot F, 1999} imparts greater mechanical strength to the co-polymer by virtue of its surface coverage {Hays JN, 2000} and mobility {Sanchez Munoz, 2003}.

Based on the previous chapters, we have found that this translates into resistance to degradation, improved biocompatibility, and anti-thrombogenicity. In this final chapter, we combine all the attributes of this nanocomposite in order to identify the optimal design for microvascular prostheses. This microvessel would (a) serve as a substitute for small arteries (Zdrahala RJ, 1996) and (b) allow for diffusion-limited exchange when placed into a microvascular network. This chapter emphasises primarily on the bulk properties of the microvessel namely, permeability and radial compliance.

7.2. METHODS AND MATERIALS

7.2.1. POLYMER SYNTHESIS

Please refer to chapter 2.

7.2.2. FABRICATION

Polyurethanes are low extrusion polymers with the ability to remain stable in the liquid state for prolonged periods. While extruding these polymers have proved successful in vessels of above 3 mm in internal diameter, dip-coating remains the primary method of fabricating microvessels (< 1mm) {Chen, 1999}. This technique depends upon the homogeneity, viscosity and concentration of the coating polymer as well as the type of mandrel used {Arcaute K, 2003}. When using this method, achieving a uniform coating on the mandrel depends upon consistent polymer flow patterns on the mandrel.

Previous studies have proven that polyurethanes may be made porous by placing them in non-solvent solution like water which leach into it and create pores as shown in figure 7.1a. The objective of this study was to determine the ideal method of fabricating microvessels with similar compliance characteristics to native small arteries using a combination of dip-coating and coagulation. By varying the concentration of POSS-PCU mixtures, the ideal viscosity and homogeneity for dip-coating with the polymer was ascertained in the first phase of fabrication as well as

the technique of dip-coating. In the second phase, the polymer-coated mandrels were coagulated in a variety of solutions to achieve ideal compliance and porosity characteristics.

Figure 7.1a. The principle of solvent and non-solvent/weak solvent exchange during the coagulation of POSS- PCU nanocomposite in dimethylformamide (DMF) to form porous, viscoelastic microvessels.

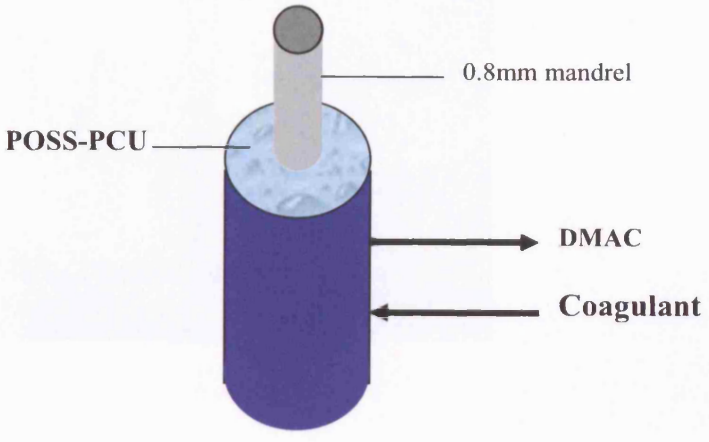

Figure 7.1b. The mechanised device used to dip-coat POSS-PCU microvessels at the rate of 10 mm/s (B).

7.2.2.1. Dip coating

When a mandrel is dip-coated into a viscous polymer solution, the thickness of its coating (e) depends on the equilibrium between its viscosity and capillary retention forces occurring at its meniscus. In Landau's Law, this value is symbolised by the term 'capillary number (N_{Ca})' which is the ratio of the liquid viscosity (η) and dipping velocity (υ) to the surface tension of the liquid (γ). Using an extension of this law for higher velocity dipping of cylindrical conformations (equation 1), the N_{Ca} of the varying polymer concentrations used to dip-coat was indirectly derived to assess the ideal setting for dip-coating POSS-PCU microvessels {Rebouillat S, 2000}. In this case, higher dipping velocities referred to the dipping velocities being greater than

polymer flow subject to gravity.

$$e/(e + R) = 1.32\,(\eta\upsilon/\gamma)^{2/3} = 1.32\,(N_{ca})^{2/3}$$ Equation 7.1 {Rebouillat S, 2000}

where R is the radius of the mandrel.

In order to determine the optimal solute concentration of POSS-PCU to dip-coat these microvessels, a 23 % (w/v) working nanocomposite solution of POSS-PCU was diluted in DMAC to form 17, 14, 11 and 6 % (w/v) solutions of POSS-PCU. These mixtures were then stirred to form homogenous solutions and left to stand in air-tight containers for 3 months at room temperature. 800 μm diameter stainless steel mandrels (Venflon BD Ltd., UK) were then dip-coated vertically into varying polymer concentrations at a rate of 1cm/s using the mechanised device as shown in figure 7.1b. The mandrels were then left to stand for a further 5 minutes to allow excess polymer to flow away. They were then coagulated in distilled water (DW) at 50 °C for 24 hours {Chen, 1999} before being dried in an oven at 70 °C for 48 hours. The completeness and uniformity of these microvessels were then studied on gross morphologic examination and later, scanning electron microscopy (SEM).

In a parallel experiment, the 800 μm cylindrical stainless steel mandrels were dip-coated with a standard solution of 11.5 % (w/v) POSS-PCU solutions using either the single- or double-dipping technique and pre-coating the mandrels with either the non-solvent dimethyl formamide (DMF) or oil. This was to ascertain the ideal technique of mandrel preparation necessary to fabricate these microvessels.

7.2.2.2. Coagulation

Once a thin layer of POSS-PCU was deposited onto the mandrels, it was placed in different non-solvent or slow solvent solutions at 25 °C for 24 hours to form grafts of varying porosities. The coagulants used were 100 % distilled water (DW), 10 to 50 % (w/w) DMF-water mixtures, 10 to 90 % (w/w) ethanol-water mixtures and 2.5 to 10 % (w/w) sodium bicarbonate ($NaHCO_3$). Following immersion in these solutions, the mandrels were left to dry for 7 days in an incubator at 37 °C before being peeled off as a whole to form complete single-lumen, porous microvascular prostheses.

7.2.2.3. Quality control

Using a scanning electron microscope system (Philips SEM Model 501, Netherlands) the surface and cross-sections of all the fabricated 800μm diameter 2 % POSS-PCU microvessels were analysed in order to determine their vessel wall thicknesses, external diameters, internal diameters, mean pore sizes, pore size distributions and pore morphologies. The wall thickness of these microvessels were taken at four perpendicular points on four different microvessels fabricated in the same way (n = 4). The mean wall thickness with its standard deviation was calculated for each corresponding method of graft fabrication. Only microvascular grafts consistently fabricated with uniform diameters throughout its length and relatively smooth inner lumen without bulk cavities {Chen, 1999} were selected for further testing.

7.2.3. VESSEL WALL ANALYSIS

7.2.3.1. Hydraulic conductivity (K)

The hydraulic conductivity of optimal, quality-controlled, unused fabricated 800 μm POSS-PCU microvessels was determined by connecting them to a permeameter; a closed circuit consisting of a vertical pressure column of distilled water (DW) at 37 °C. The microvessels were clamped at one end and placed at the bottom the water column. By adjusting the height of the water column, the pressures within the system were regulated with the help of an intraluminal Millar Mikro-tip pressure transducer. The microvascular grafts were then exposed to these pressures and the seepage of DW at the mean physiological pressures of 70 mmHg and 100 mmHg through the walls of the microvessels (n = 6) {Miyamoto, 1999} were measured over one minute. The mean hydraulic conductivity and standard deviations were calculated based on Darcy's Law {Baish, 1997} shown below. All values were expressed as $cm/s/cmH_2O$.

$$Q = -K.A.(\Delta h / t) \qquad \text{Equation 7.2}$$

Where 'Q' represents the quantity of water seepage in mL, 'K' is the hydraulic conductivity, 'A' is the surface area exposed in cm^2, 'Δh' is the height of the water column in cms and 't' is the microvessel wall thickness in cm.

7.2.3.2. Radial compliance

Radial compliance of these microvessels was determined using a flow circuit consisting of a fluid reservoir, a temperature regulator, flexible medical-grade tubings, an electromagnetic pump, an arterial flow waveform conditioner, a Transonic medical flowmeter system (HT207; Transonic Medical System, Ithaca, NY, USA) and a Millar Mikro-tip catheter transducer (Millar Instruments, Houston, Texas, USA) via a Y-connection port {Salacinski, 2002a} to measure the intraluminal pressures in mmHg. 40 mm long segments of 800 μm internal diameter POSS-PCU microvessels were then longitudinally stretched by 10 %, so as to mimic conformational changes expected within an in vivo system, before being connected to the flow circuit using commercially available 21G intravenous cannulae (Venflon BD Ltd, UK) and placed in a water bath. The flow circuit was then filled with clinical-grade native citrated blood (0.40 haematocrit) at 37 °C maintained using a heat exchanger (Portex, Hythe, UK) taking care to evacuate any air within the system which could cause damping. On initiating pulsatile flow at a frequency of 1 Hz, physiological mean pressures of 30 to 70 mmHg were achieved whilst maintaining the pulse pressure at 39.633 (± 3.952) mmHg throughout the tests. Both anterior and posterior microvessel wall motion with each pulse was assessed using a 7.5 MHz linear array Duplex probe and an echo-locked wall tracking system (Walltrack; Pie Medical Systems). The data was then interpreted using analogue-to-digital data acquisition recording system (ADC/Maclab; AD Instruments, Hastings, UK).

As the control, freshly harvested arteries (aorta and femoral artery) and veins (inferior vena cava and femoral vein) from cadaveric rats were used in comparison to these POSS-PCU microvessels. These grafts were obtained in accordance with animal research guidelines. All experiments were repeated 6 times for each pressure range using different sets of microvessels (n = 6). Unlike our previous experiments with the MyoLink® vascular grafts {Salacinski, 2002a;Tai, 2000}, we found no need to pre-clot these POSS-PCU microvessels as there was no significant leakage of blood through their walls. This may be explained by the microporous nature of the microvessel walls. The radial compliance {Tai, 2000} of the microvessel walls were calculated using the formula,

$$\text{Radial compliance} = \frac{(D_s - D_d)}{(P_s - P_d).\, D_d} \times 10^4 \qquad \text{Equation 7.3}$$

Where D_s refers to the systolic diameter, D_d is the diastolic diameter and $(P_s - P_d)$ represent the pulse pressure within the pulsatile flow circuit.

7.2.3.3. Burst strength

Using unused quality-controlled 800 μm diameter POSS-PCU microvessels fabricated in the same manner as those used in the water permeability experiment, the microvessels were clamped at one end and connected to a pressure system. The graft was subjected to increasing pressures of up to 300 mmHg using a syringe driver connected to a DW column to determine whether excessively high blood pressure within physiological limits would cause rupture of these nanocomposite microvessels.

All experiments were repeated 6 times using different microvessels (n = 6).

7.3. RESULTS

7.3.1. MICROVESSEL FABRICATION

The uniform thickness of a fabricated microvessel affects its radial compliance and hydraulic conductivity which in turn affects flow-limited nutrient exchange {Levick, 2000}. The factors affecting microvessel wall thickness during any dip-coating process are as follows,

i) Polymer dispersion

ii) Polymer viscosity

iii) Dipping technique

iv) Mandrel preparation

v) Coagulating solution

vi) Molecular weight (M_w) of polymer

As only one type of polymer; 2% POSS-PCU nanocomposites were used for all fabricating purposes, the effect of molecular weight (M_w) in this case is redundant.

7.3.1.1. Polymer dispersion

On leaving to stand at room temperature in a sealed container for 90 days, POSS-PCU nanocomposite solutions at 23 % (w/v) in dimethyl acetamide (DMAC) remained stable and exhibited no evidence of clumping, degradation, change in flow characteristics or colour change. This held true for all its dilutions in DMAC; 17, 14, 11 and 6 % (w/v).

7.3.1.2. Polymer viscosity

Effect of the concentration of polymer POSS-PCU used to dip-coat was assessed by diluting the working 23 % (w/v) solution of the polymer in DMAC to form 17, 14 and 11 % POSS-PCU in DMAC solutions. As shown in figure 7.2, vessel wall thickness, assessed by SEM at 640 x, decreased significantly once the polymer was diluted to a 17 % solution but with a great degree of variation. On further diluting the polymer, the vessel wall formed was of more predictable thickness and uniformity with lesser degrees of variation. Using a version of Landau's Law meant for high speed dipping of cylindrical mandrels, the capillary number (N_{ca}) of the polymer was derived for these varying solutions. It was found that the ideal N_{ca} for dip-coating POSS-PCU was between 0.0136 and 0.0146. At concentrations below this, we found that the polymer did not sufficiently coat the mandrel to form complete vessels as its intrafacial surface tension was greater than its interfacial tension.

Figure 7.2. Effect of dip-coating POSS-PCU concentration (% w/v) on vessel wall thickness showing that when the capillary number (N_{Ca}) (derived from Landau's Law) is between 0.0136 to 0.0146, a mean microvessel wall thickness of 32 to 34 μm with the least standard deviation can be consistently obtained (n = 16).

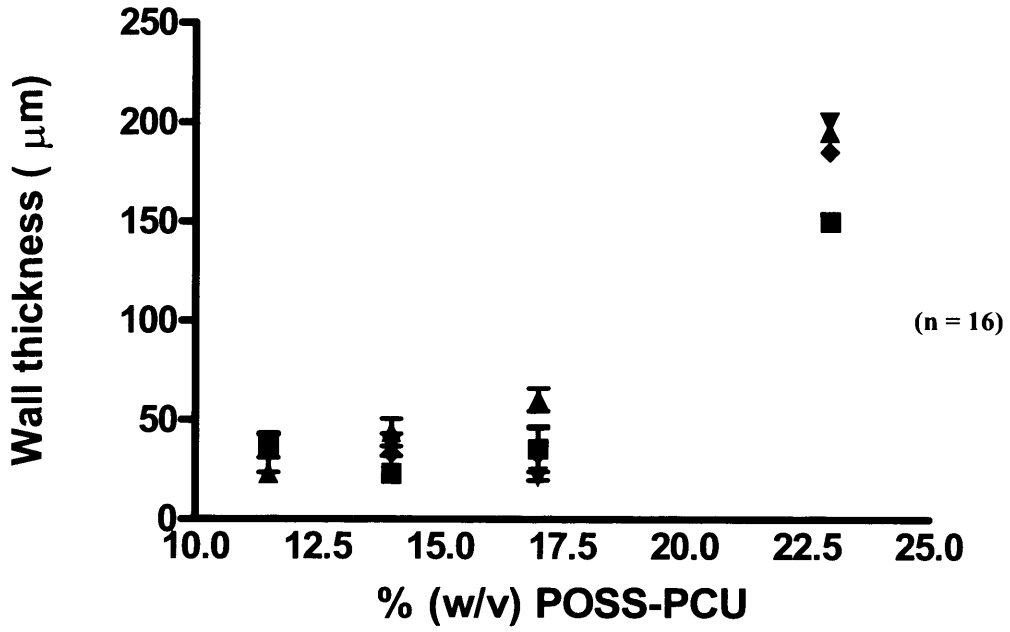

POSS-PCU concentration	11 %	14 %	17 %	23 %
Capillary No. (Landau's Law)	0.013655	0.01464	0.01662	0.1156

7.3.1.3. Dipping technique

We compared single and double dip-coating of these grafts using a standard concentration of the polymer and at a dipping velocity of 1 cm/s in all cases. SEM studies showed that double dip-coating these grafts resulted in excessively thickened and non-uniform walls with poor coagulation particularly towards its inner lumina. As the compliance improves with the formation of a porous graft, double dip-coating would affect graft compliance. Hence in all subsequent cases, single dip-coating was the preferred method.

7.3.1.4. Mandrel preparation

Using standard stainless steel 800 μm mandrels manufactured industrially, we assessed whether pre-coating these mandrels with hydrophilic and hydrophobic liquids such as DW and oil respectively would affect the polymer deposition on the mandrel with non- precoated mandrels as controls. SEM analyses of these grafts showed that pre-coating these mandrels increased the non-uniformity of its walls compared to the control group. This may be attributed to rapid surface coagulation of the uneven pre-coated mandrel on contact with the polymer thus creating a glabrous template for further coagulation. The uneven surface pre-coating was caused by the fact that the pre-coating solution was not sufficiently viscous to evenly coat the mandrel. Therefore, we found no need to pre-coat these mandrels prior to dip-coating.

7.3.1.5. Coagulating solution

When the nanocomposite solution was placed in a weak coagulating solvent such as DMF or ethanol, DMAC which is the diluent in this case, seeped out into the solution in exchange for this weak solvent thus creating a porous structure. The solubility of the coagulating solution was directly proportional to the rate and magnitude of pore formation and hence wall thickness. SEM analysis of POSS-PCU coagulated by different solvents revealed that ethanol/DW mixtures from 10 to 50 % (v/v) as well as DMF/DW mixtures greater than 20 % (v/v) did not form complete, porous and uniform microvessels. Porous POSS-PCU grafts were formed only with those coagulated with DW, $NaHCO_3$ or lower concentrations of DMF. Thus greater the solubility, the more rapid coagulation occurs, thereby improving graft porosity. As this was a relatively rapid process compared to coagulation at higher DMF concentrations, it prevented increased 'creep' of the polymer and the formation of lop-sided, non-uniform vessel walls as shown in figure 7.3 whereby wall thickness variance was greater with slower coagulation.

Figure 7.3. The effect of coagulating solvent (DMF) solubility on the wall thickness and radial uniformity of POSS-PCU microvessels. Bartlett's test for equal variances indicated a significant variation ($p < 0.001$) in microvessel wall thickness with decreasing coagulant solubility while microvessel wall thickness was significantly lower (One-way ANOVA, $p < 0.0001$) when coagulated with weaker solvents.

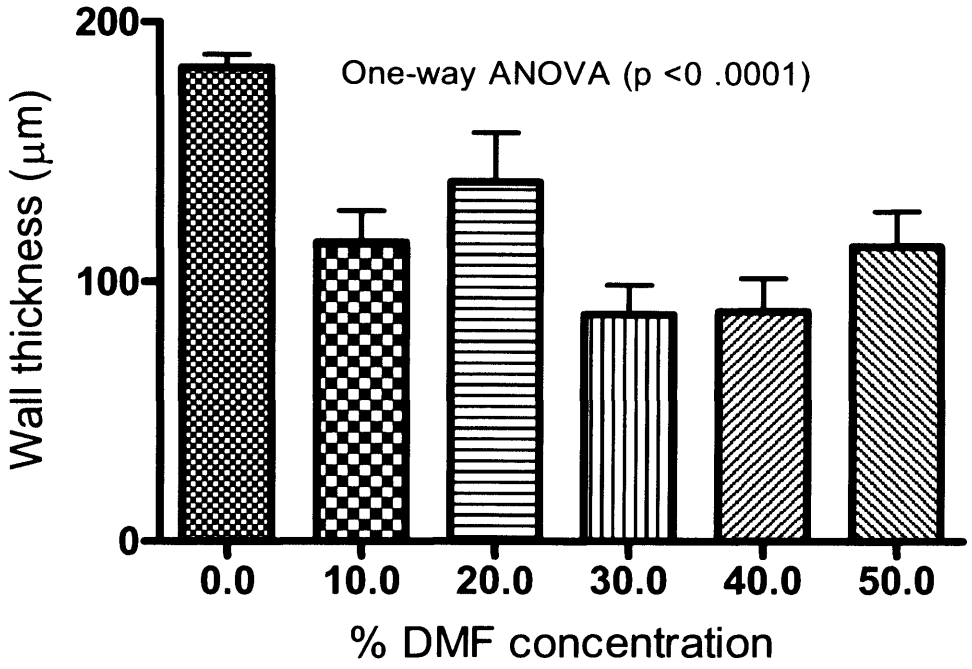

Of all the dip-coated grafts, only coagulation in DW, 10 %DMF and $NaHCO_3$ formed complete, porous microvessels. SEM analyses of these surfaces showed the effect of differing coagulating solutions on luminal architecture. DMF-coagulated vessels exhibited pore sizes between 8 to 40 μm with interpore distances. These pores were non-uniform, irregular with large bulk cavities (figure 7.4a). Unlike microcomposites such as conventional polyurethanes {Chen, 1999}, acidic coagulants such as DMF induced varying capillary pressures within the nanocomposites, which

contribute to the 'wrinkled' surface appearance when coagulated with acidic salts {Harrup M, 2002}. Such a surface would cause turbulent flow and would be unsuited as vascular grafts.

DW is a rapid coagulator of the polyurethane component of the polymer. Once dip-coated in DW, pore formation in exchange for DW occurs within minutes. As mentioned above, this prevents excessive polymer creep (sagging) and forms a porous sponge-like material. Pore formation was found to be more uniform compared to DMF with regular interpore distances, pore sizes and shapes. However, as shown in figure 7.4b, excessive coagulation in certain areas leads to the formation of bulk cavities on the lumen {Chen, 1999}. In clinical practice, such graft lumina would again increase turbulence as in the case of DMF and be more thrombogenic. This should be avoided as far as possible.

Coagulating the POSS-PCU dipped microvessels in 5 % $NaHCO_3$ solutions at 50 °C were found to create uniform micropores between 0.5 and 2 μm with regular interpore distances as shown in figure 7.4c. In addition, there was no evidence of bulk cavity formation {Li, 2001}, unlike DW coagulation, on SEM with 5 % $NaHCO_3$-coagulated POSS-PCU. This is due to the more controlled release of DMAC into the 5 % $NaHCO_3$ solution to form a microporous graft with greater pore inter-connectivity. For the second part of this experiment, we utilised only POSS-PCU microvessels which were fabricated by single dip-coating followed by coagulation in 5% $NaHCO_3$ as only these microvessels had passed our stringent quality control criteria; (a) uniform wall thickness, (b) uniform pore formation and (c) smooth inner lumina devoid of bulk cavities to minimise turbulence.

Figure 7.4a. SEM images of the luminal architecture of 14 % (w/v) solution of POSS-PCU coagulated in 10 % DMF

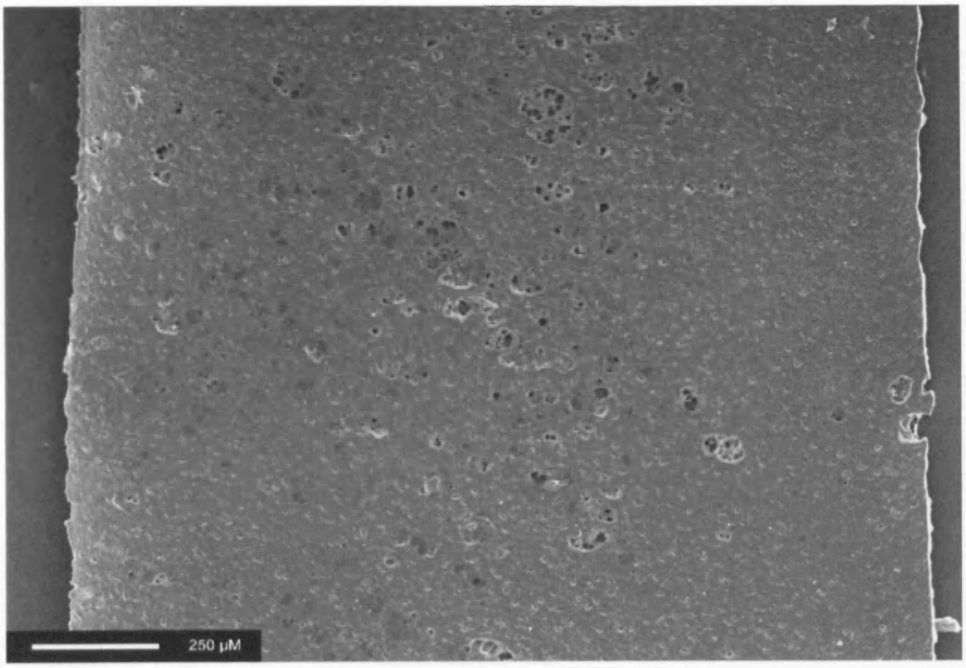

Figure 7.4b. SEM images of the luminal architecture of 14 % (w/v) solution of POSS-PCU coagulated in DW

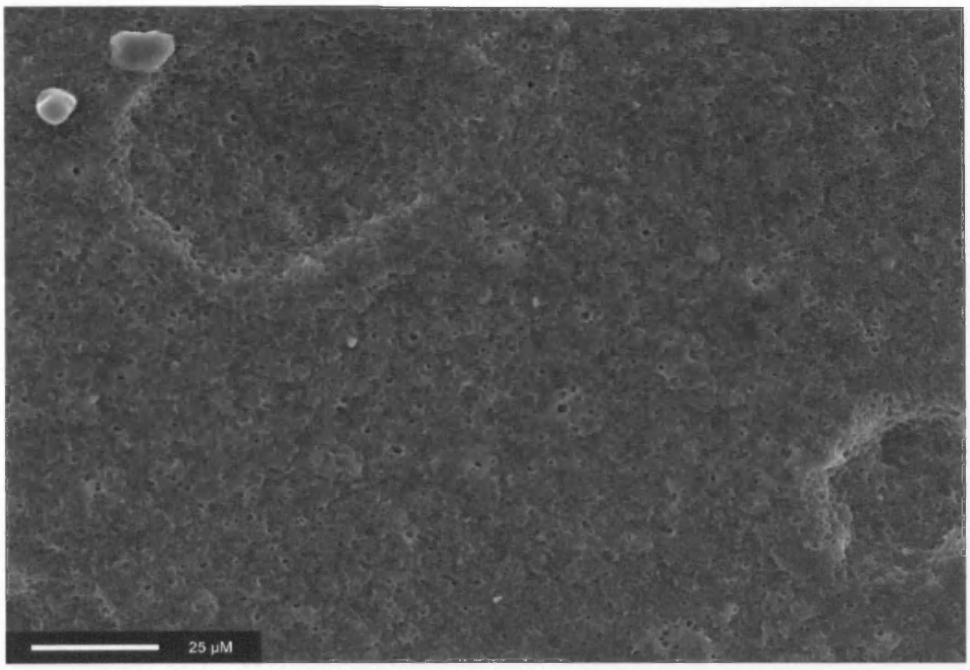

Figure 7.4c. SEM images of the luminal architecture of 14 % (w/v) solution of POSS-PCU coagulated in 5% $NaHCO_3$ solution.

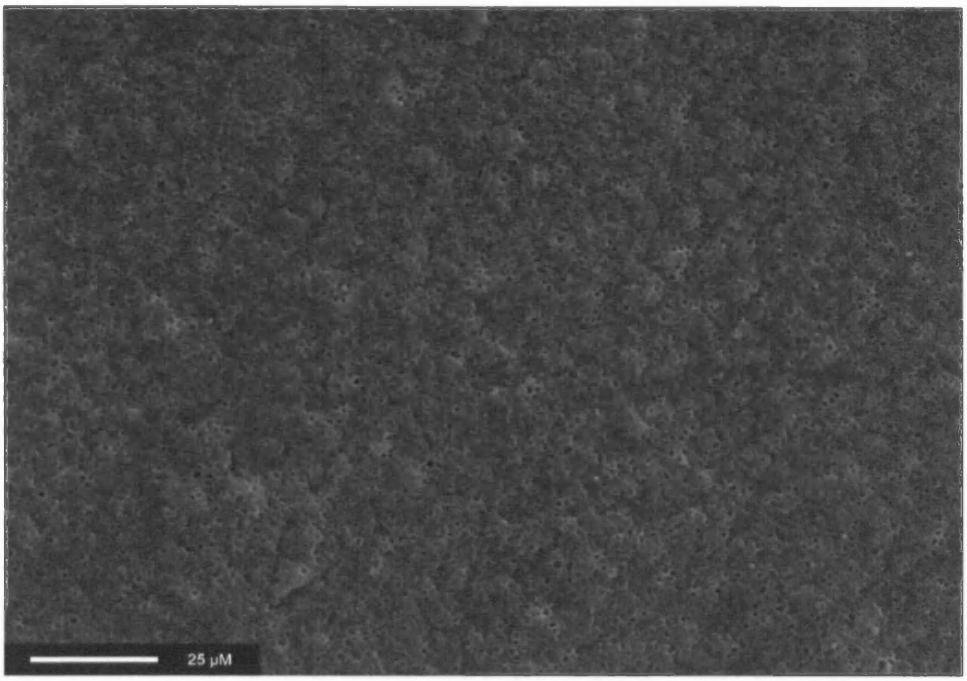

7.3.2. MICROVESSEL WALL

7.3.2.1. Hydraulic conductivity

The hydraulic conductivity of these 800 µm diameter POSS-PCU microvessels was measured using a water-column permeameter at mean pressures of 70 and 100 mmHg respectively. At 70 mm Hg, their mean hydraulic conductivity was found to be 9.0 (± 1.789) x 10^{-7} cm/s/cmH_2O while at the higher pressure of 100 mmHg, the measured values were 8.833 (± 1.602) x 10^{-7} cm/s/cmH_2O. The absence of any significant difference between these two values suggests that hydraulic permeability

of these microvessels were independent of wall shear stresses, similar to arterioles {Williams, 1999}. Furthermore, these results mirror the *in vivo* hydraulic permeability of biological capillary beds which are in the region of 2.4 to 9.8 x 10^{-7} cm/s/cmH_2O {Neal, 2002;Pocock, 2001}.

7.3.2.2. Radial compliance

We found that 0.8 mm diameter POSS-PCU microvessels coagulated with 5% $NaHCO_3$ aqueous solution exhibited very similar compliance characteristics at varying pressures of 30 to 70 mmHg (pulse pressure of 40 mmHg) to rat arteries (internal diameter 1mm). The overall mean compliance values of the synthetic microvessels was 4.478 (± 0.09095) % per mmHg x 10^{-2} as compared to 4.605 (± 1.166) % per mmHg x 10^{-2}, which were very similar. In stark contrast, rat veins exhibited very low compliance values with no evidence of increasing radial compliance with increasing pressures. The pulsatile waveform obtained throughout the physiological pressure ranges (figure 7.5a) was also found to be very similar to rat arteries indicating similar visco-elastic properties between the two.

Figure 7.5a A typical pulse waveforms distension of POSS-PCU microvessels at low-pressure, low-flow states (30 mmHg)

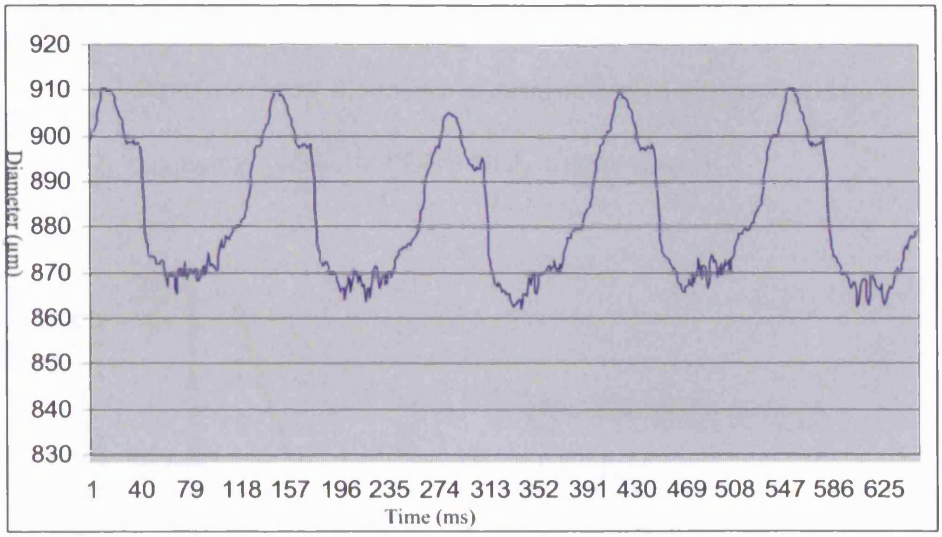

On further analysing the data, the compliance curves of these synthetic POSS-PCU microvessels mirrored the pressure-responsive (anisotropic) patterns {Tai, 2000} of rat arteries with high values at lower pressure and gradually reaching a plateau at mean pressures in excess of 50 mmHg. Two-way ANOVA analysis showed that there was no statistical difference between the 5% $NaHCO_3$-coagulated POSS-PCU microvessels and the rat arteries although on extrapolation of the curve towards even lower pressures, the difference between the biological and synthetic microvessels would eventually have become significant. Unlike the non-pressure responsive (isotropic) compliance characteristics of MyoLink® grafts, the more uniform and homogenous pore sizes and structure within these nanocomposites {Wang RZ, 2001} do not follow the linear correlation associated with Hooke's Law, a characteristic which may be explained by this porous system behaving like a 'net'. This would

further decrease the likelihood of intimal hyperplasia, particularly at low-flow states as these 'smart' microvessels virtually mirror the pressure-responsive radial compliance characteristics of biological microvessels (figure 7.5b).

Figure 7.5b Mimicking the micro arterial pressure-responsive compliance curve using synthetic POSS-PCU microvessels.

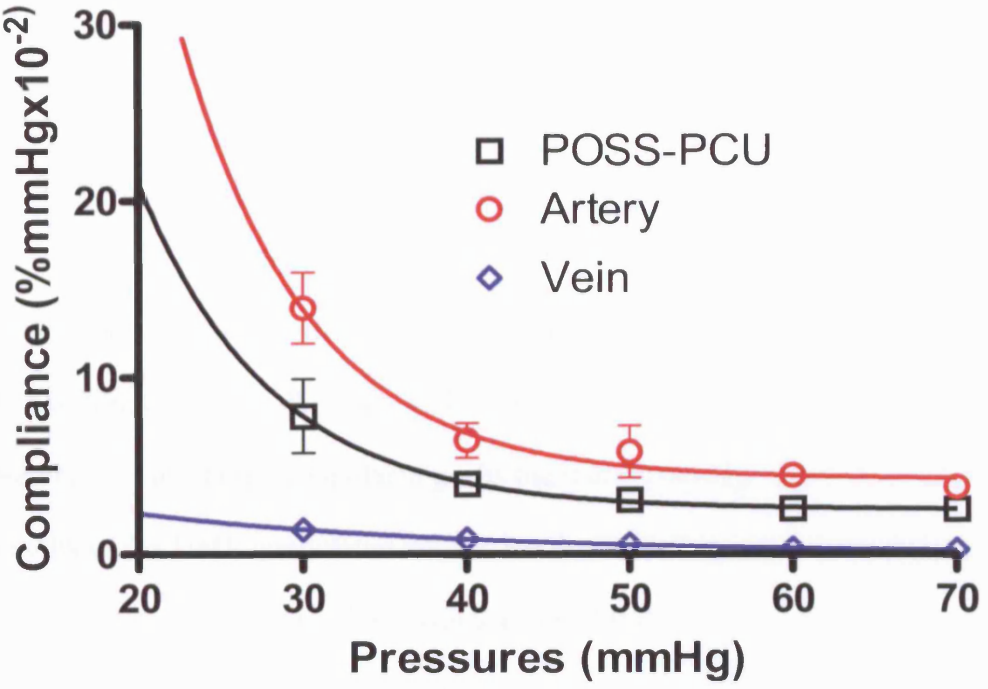

The curve equations for both synthetic and biological microvessels are given below,

POSS-PCU microvessels; $y = 228e^{(-0.126x)} + 2.56$

Rat artery; $y = 485e^{(-0.131x)} + 4.3$

Rat vein; $y = 6.321e^{(-0.052x)} + 0.093$

We postulate that the reason for the anisotropic compliance characteristics of the POSS-PCU microvessels is due to the deformation of the POSS nanofillers within the

polyurethane matrix. As the 'Si'-containing materials such as polydimethylsiloxane (PDMS) and POSS have a lower glass transition temperature (T_g) than polyurethanes , the difference in visco-elasticity at 37 °C contributes to bi-axial deformation of the POSS nanofillers into an ellipsoid {Mark JE, 2003;Mark JE, 2003}. Superadded by the fact, that the Si-O bonds are very flexible and able to bend from 110° to 180° {Mark JE, 2004}, ellipsoid deformation of POSS nanofillers occurs and hence, the similarity of its compliance trends to elastin-rich arteries.

7.3.3.3. Burst strength

We found that the 35 μm thick vessel walls of POSS-PCU microvessels treated with 5% $NaHCO_3$ and DW could withstand pressures of up to 200 mmHg while the more porous 10% DMF-coagulated grafts burst at 60 mmHg. The lower vessel wall strengths of the DMF-coagulated vessels are due to its large and non-uniform pores acting as stress-points along the vessel wall resulting in rupture in these areas. On the other hand, DW and $NaHCO_3$ coagulation ensure more uniform pore formation and hence greater wall strength. In addition, these microvessels have increased radial compliance and hence ability to accommodate rising pressures.

7.4. DISCUSSION

Studies have shown that porosity is inversely proportional to the molecular weight of the polymer {Wan ACA, 2001}. This would mean that POSS-PCU grafts have lesser porosity than MyoLink® grafts and hence radial compliance for the same wall thickness. Therefore in order to preserve radial compliance, POSS-PCU grafts have to be thinner-walled but not excessively permeable. Achieving this depends on the amount and method of polymer deposition on the mandrel as well as the method of coagulation to form a porous microvessel.

Once the POSS-PCU coated mandrels were immersed in a coagulating medium such as water, it underwent demixing and gelation. Demixing refers to the separation of the domains within the polymer while gelation fixes these domains in their separated phases thus creating a porous system {Wijmans JG, 1983}. The pore morphology of the graft depends on the type of coagulant and its solubility. As mentioned earlier the slower the exchange of the diluent (DMAC) for the coagulant molecule, the less porous the microvessel would be. This was exemplified in the experiment with varying concentrations of DMF. Furthermore when coagulation was more controlled following base-catalysis with $NaHCO_3$ solutions, optimal pore characteristics with the absence of bulk cavities were obtained compared to DW (rapid coagulator); a result supported by existing data on nanocomposites.

In nanocomposites, pore formation is accentuated as a result of the increase in the quantity of dynamic voids due to thermally-induced polymer chain rearrangement {Pope EJA, 1986}. Nitrogen sorption studies on metallic silsesquioxanes have also

shown via the Hovarth-Kawazoe equation that nanocomposites can possess very high pore volumes of up to 0.22 ml/g and yet have tiny pores of 6 Å {Maxim N, 2001}. Therefore although its pore sizes may be small, permeability would still be maintained, compared to a larger-pored material. This would explain the reason for the significant water permeability (table 7.1) in these POSS-PCU structures. Although their pore sizes were less than 1.6 μm in diameter, the presence of a nanoporous network in these polymers would allow fluids to traverse through it. Interestingly, water permeability of DMF-coagulated POSS-PCU grafts was lesser in spite of them having greater pore sizes of up to 24 μm further emphasising the importance of pore interconnectivity. We thus fabricated microvessels with very thin walls (30 to 40 μm) using a weakly basic coagulant solution of 5 % $NaHCO_3$ in order to optimise its porosity and compliance in order to simulate nature.

Table 7.1. The effect of coagulating solutions on the pore morphology of POSS-PCU microvessels was studied using neutral (DW), basic (5% $NaHCO_3$) and acidic (DMF) solutions respectively. Our data shows that coagulating in basic 5% $NaHCO_3$ solutions during fabrication allows for arteriolar-like hydraulic permeability within the POSS-PCU microvessels with the most uniformly distributed pores.

Coagulating solvent	Pore sizes	Water permeability	Luminal pore morphology
POSS-PCU in DW	0.4 – 2.0 μm	1.494 +/- 0.5828 ml/min/cm^2	Random micropore formation. Bulk cavities of up to 60 μm present. Rugged and glabrous luminal surface.
POSS-PCU in 5% $NaHCO_3$	0.4 – 1.6 μm	2.645 +/- 0.8436 ml/min/cm^2	Even, uniform micropore distribution with no bulk cavities.
POSS-PCU in 10% DMF	8 – 40 μm	Nil	Variable larger pores with no evidence of bulk cavities.

Hydraulic conductivity (HC) of a porous medium, the microvascular graft wall in this case, is the measure of water efflux through its pores per unit time and pressure. Studies have shown that the capillary filtration coefficient (CFC) in a capillary bed depends on the HC of its constituent microvessels and independent of its vascular tone and number {Bentzer, 2001}. Bates and colleagues found that the mean microvascular HC in single perfused frog mesenteric microvessels was 2.4 to 2.6 x 10^{-7} cm/s/cmH_2O {Neal, 2002}. These values increased significantly with the action of vascular endothelial growth factor (VEGF) up to 9 x 10^{-7} cm/s/cmH_2O {Pocock, 2001}. A more in-depth analysis of the HC of frog mesenteric microvessels by Williams showed that there was no significant difference in HC between the venular and

arteriolar component of the capillary bed at very low-flow states. However, when these microvessels were exposed to higher pressures of up to 30 cm H_2O, there was an exponential increase in the HC of venules compared to the arterioles with maximal values of up to 96.8 x 10^{-7} cm/s/cmH_2O in the former. It was hence deduced that venular HC is proportional to wall shear stress while arteriolar HC is virtually independent {Williams, 1999}.

Based on Darcy's Law, the HCs of these POSS-PCU microvessels which were measured based on the principles of a permeameter, were found to be similar to existing HC data on biological microvessels. In addition, their HC values were independent of mean pressure and wall shear stress, similar to arteriolar HC and unlike the post-capillary venules. Given that the summative HC of a microvascular network depends on the HCs of its component microvessels, these nanocomposite microvessels are ideal as the building blocks of a microvascular network.

We postulate that as the pore sizes in these polymers are miniscule, nutrient exchange is diffusion-limited and not flow-limited which should permit oxygen diffusion and glucose mass transport across this man-made vascular interface. These experiments were performed at higher pressures of 70 and 100 mmHg as in an artificial tissue flap, these microvessels would need to be anastomosed directly to a high pressure arterial system and should function physiologically in such high–flow environments. The high pressures of above 200 mmHg required to rupture these microvascular grafts also support its feasibility to be used within a high pressure arterial system. Further tests will now be carried out to assess whether these microvessels obey Krogh's diffusion model as well {Piiper, 1986}.

In terms of radial compliance, MyoLink® (PCU) grafts exhibit isotropic radial compliance characteristics independent of the pressure applied {Tai, 2000} whereas with the addition of a nanofiller to PCU, improved dynamic compliance is conferred. This is a result of the formation of uniform pore sizes which are well interconnected and spaced leading to the formation of a three-dimensional scaffold which behaves like a 'garter stocking'. This is augmented by the ability of POSS nanocages to conform to an ellipsoid configuration {Mark, 2004} at the molecular level. These factors thus allow the POSS-PCU microvessels to function similarly to the elastin network of biological arteries {Burton AC, 1954} and in this experiment, rat arteries. Just as in biological microvessels, these synthetic microvessels exhibited anisotropic compliance {Roach MR, 1957;Caro CG, 1978} with its value progressively decreasing with increase in mean pressures. However, rat veins had dismal radial compliance values possibly due to the very low amounts of elastin within these biological microvessels. Parallel studies involving DMF coagulation with the same nanocomposite showed poor compliance values with no consistent pattern over the ranges tested. This underlines the importance of both material and fabrication in determining the overall behaviour of vascular grafts {Li, 2001}. In the long-term, such microvessels would also prevent the formation of intimal hyperplasia.

From a surgeon's perspective, there is no need of pre-clotting {Salacinski, 2002a; Tai, 2000} these microvessels to form a fibrin mesh or potentially heparinising them which makes it very convenient as it is virtually ready for use as an off-the-shelf prosthesis. Moreover, such fibrin clots within an already very small lumen would almost occlude it and precipitate thrombosis. This is due to the fact that the pore size

of these microvessels (< 1.6 μm) is much smaller than the average diameter of a red blood cell (RBC). Its nanoporous nature should also exclude vessel wall scarring by connective tissue invasion {Uchida, 1989} as well as reduce vessel wall tethering, thus preserving its radial compliance in vivo, provided they do not degrade.

Our results in chapter 3 on in vitro degradation of this POSS-PCU nanocomposite indicates greater resistance to degradation compared to PCU alone. Nevertheless, these are facts which can only be proved conclusively in a microvascular animal model to study degradation, biocompatibility and compliance characteristics. The effect of vascular tone and its regulation within the microcirculation will also need to be elicited. These nanocomposite microvessels have since been implanted into an in vivo model to elicit its patency rate.

The goal of any researcher fabricating an artificial vascular graft is to mimic nature's vessels. While the surface should prevent thrombus formation (thromboresistance), the bulk of the graft must provide strength (burst strength) to the conduit and allow the continued propagation of a pulse waveform (compliance) throughout the vessel. To this end, these nanocomposite grafts address the fundamental problems limiting contemporary grafts by providing a thrombus-repelling surface (chapter 6) and a biomimetic bulk, simulating arterial pulsations. In addition, from the tissue engineering perspective, they would serve well as components of a microvascular network due to its permeability characteristics.

Chapter 8

8. Summary & Future Prospects

The reconstructive ladder in reconstructive surgery has always been the rubicon by which surgeons have adhered to. At the pinnacle of that hierarchy is free tissue transfer, a successful method of achieving soft-tissue cover. However, it has attendant morbidities such as loss of function, donor-site defects and in some cases, sub-optimal cosmesis. To this end, the development of an artificial capillary network as a forerunner of artificial tissue is a very exciting prospect as (1) it would provide an ideal vascular bed for chronic non-healing wounds and (2) make possible an off-shelf-alternative to free tissue transfer without the associated morbidity.

As alluded to earlier, the creation of an artificial capillary bed is currently limited by the absence of viable microvascular prostheses as the patency rates of PTFE and Dacron graft are dismal at lower flow rates. In this thesis, I sought to identify and develop a suitable material for the fabrication of microvessels as the first stage in a broader effort to create a man-made capillary bed. A nanocomposite of silsesquioxane and carbonate-based polyurethane (POSS-PCU) was chosen for this purpose as nanocomposites have potentially improved degradative resistance and reduced protein adsorption, an advantage when attempting to decrease thrombogenicty. In order to negate the relative non-elasticity of silica-based polymers, silsesquioxane was linked to an elastic polymer; polyurethane. In particular, carbonate-based polyurethane (PCU) was chosen as the absence of toluene diamine, a component of conventional polyurethanes, in PCU minimises the risk of carcinogenicity.

The development of an ideal microvascular graft involves identifying the right polymer and then optimising its fabrication into the graft itself. I began this process by bulk and surface characterising POSS-PCU using DSC, stress strain studies, NMR

and FTIR spectroscopy. NMR showed that the POSS nanocube linked up to the hard segment of PCU by the simple addition of POSS during the polymerisation of PCU. The point of linkage was at the diol side-chain of the POSS nanocube and the NH-CO component of PCU. By varying the amount of POSS added, its concentration increased arithmetrically. This consistently held true for both single- and twin-diol side-chain variants of the POSS molecule. Mechanical experiments indicated that the incorporation of POSS into the primary polymer; PCU conferred greater structural homogeneity throughout the POSS-PCU nanocomposite as compared to PCU alone.

In vitro degradation studies revealed that POSS-PCU was resistant to an entire range of oxidative and hydrolytic enzymes whilst retaining its visco-elastic properties. FTIR, scanning electron microscopy, stress-strain studies and DSC demonstrate that the POSS nanocores shield the soft segment(s) of the polyurethane, responsible for its compliance and elasticity, from all forms of degradation principally oxidation and hydrolysis. POSS incorporation hence provides an optimal method by which polymers may be strengthened whilst maintaining their elasticity, making them ideal as vascular prostheses particularly at low flow states.

When placed in an in vivo environment for 36 months, POSS-PCU exhibited minimal degradative changes on FTIR with no capsule formation in all 6 samples as compared to the siloxane control in 16.7 % of cases. This was corroborated with SEM studies which showed stress cracks, fissures and pits on the siloxane control whereas POSS-PCU had none of these changes. Contact angle analyses indicated that POSS-PCU is an ampiphilic polymer with a large contact angle hysteresis which could theoretically cause proteins such as fibrinogen to undergo conformational changes

thereby altering epitope-macrophage interaction; the initiator of the inflammatory cascade. Ellipsometric studies are currently under way to study this in greater detail.

At a cellular level, cytocompatibility studies were conducted using endothelial cells. The parameters studied were viability, adhesion, proliferation and confluence morphology. Cells were able to survive for up to 3 weeks in a POSS-PCU medium without any evidence of toxicity. HPLC confirmed the absence of any leaching from POSS-PCU in an aqueous environment. These results suggest that once placed in vivo, POSS-PCU grafts would be able to neo-endothelialise without causing any adverse effects on the host.

On studying the behaviour of POSS-PCU at the vascular interface, it was found that POSS confers an anti-thrombogenic surface action by inhibiting fibrin formation. Screening tests with TEG suggested a decrease in fibrin clot strength which was corroborated with fibrinogen ELISA, indicating significantly decreased fibrin adsorption compared to PTFE. However, there was no significant difference in fibrin adsorption between PCU and POSS-PCU. Interestingly, factor Xa assays revealed that with increasing concentrations of POSS, its surface anti-coagulant properties increased compared to PCU alone. Based on this, it was deduced that the unstable clot formation on POSS-PCU was due to a qualitative alteration in protein adsorption as opposed to a quantitative decrease. Based on information garnered on contact angle analysis earlier, I postulated that this behaviour was attributable to its inherent surface roughness as a result of POSS integration. This was confirmed on AFM studies which showed that surface roughness was directly proportional to POSS content. A potential application would be the obviation of the need for systemic anti-coagulation when

using POSS-PCU as vascular access devices.

Having identified POSS-PCU as a suitable material for microvascular prostheses, we sought to determine the optimal design and fabrication technique. Using the 800 μm internal diameter microvessel graft model as a starting point, different methods including electrospraying and dip-coating were used to coat the mandrels. In addition, the coagulating solution necessary to create a microporous lumen was determined. Each fabrication model was then subjected to radial compliance, burst strength and hydraulic permeability testing to optimise a consistent and reproducible fabrication technique. It was found that single dip-coating of the mandrel in a 14 (w/v) % solution of POSS-PCU in DMAC at a speed of 1 cm/s followed by coagulation in a 5 % $NaHCO_3$ solution created the 'ideal' microvessel, closely mimicking micro-arterial compliance and hydraulic permeability. Achieving these attributes was possible due to the POSS-mediated reorganisation within the polymer composite. We are currently awaiting the final results from an animal model study using these microvascular prostheses.

With the culmination of this work, the first phase in our effort to build an artificial capillary bed is completed. Having developed a polymer suitable as the building blocks of a synthetic microvascular network, efforts are now being concentrated on using microfabrication technology to recreate the microvascular environment using POSS-PCU and fuse it into the host using tissue-engineered scaffolds, stem cells and angiogenic factors. As these materials are safe, resistant to degradation, compliant, allow neo-endothelialisation, bio-compatible and anti-thrombogenic, the probability of microvascular occlusion is lower. If successful in the long run, the clinical

implications would be tremendous as the ability to 'grow' tissue in vitro would do away with tissue transfers and even, transplantation.

BIBLIOGRAPHY

International Standards Organization (ISO). Biological evaluation of medical devices: Part 5: Tests for cytotoxicity: In vitro methods. Part 5. 1992.

Aamer K A, Sardinha H, Bhatia S R, Tew G N. Rheological studies of PLLA-PEO-PLLA triblock copolymer hydrogels. Biomaterials 2004; (25): 1087-1093.

Abraham G A, de Queiroz A A, San Roman J. Immobilization of a nonsteroidal antiinflammatory drug onto commercial segmented polyurethane surface to improve haemocompatibility properties. Biomaterials 2002; (23): 1625-1638.

Adams R H, Klein R. Eph receptors and ephrin ligands. essential mediators of vascular development. Trends Cardiovasc Med 2000; (10): 183-188.

Ai H, Mills D K, Jonathan A S, Jones S A. Gelatin-glutaraldehyde cross-linking on silicone rubber to increase endothelial cell adhesion and growth. In Vitro Cell Dev Biol Anim 2002; (38): 487-492.

Ai H, Lvov Y M, Mills D K, Jennings M, Alexander J S, Jones S A. Coating and selective deposition of nanofilm on silicone rubber for cell adhesion and growth. Cell Biochem Biophys 2003; (38): 103-114.

Akers D L, Du Y H, Kempczinski R F. The effect of carbon coating and porosity on early patency of expanded polytetrafluoroethylene grafts: an experimental study. J Vasc Surg 1993; (18): 10-15.

Alexander H., Brunski J.B., Cooper S.L., Hench L.L., Hergenrother R.W., Hoffman A.S., Kohn J., Langer J., Peppas NA, Ratner B.D., Shalaby S.W., Visser S.A., Yannas I.V. Classes of materials used in medicine. In: Biomaterials Science: An introduction to materials in medicine. (Eds.Ratner BD, Hoffman A.S., Schoen F.J., Lemons J.E.). New York: Academic Press, 1996; 37-130.

Alivisatos AP. Synthesis of nanoparticles. Science 1996; (271): 933.

Amato I. Candid cameras for the nanoworld. Science 1997; (276): 1982-1985.

Anderson JM. Recent advances in biomedical polyurethane biostability. Polym Int 1998; (46): 163-171.

Anderson SE, Baker ES, Mitchell C, Haddad TS, Bowers MT. Structure of hybrid polyhedral oligomeric silsesquioxane propyl methacrylate oligomers using ion mobility mass spectrometry and molecular mechanics. Chem Mater 2005; (17): 2537-2545.

Andriano K P, Tabata Y, Ikada Y, Heller J. In vitro and in vivo comparison of bulk and surface hydrolysis in absorbable polymer scaffolds for tissue engineering. J Biomed Mater Res 1999; (48): 602-612.

Angelini G D, Newby A C. The future of saphenous vein as a coronary artery bypass conduit. [Review]. European Heart Journal 1989; (10): 273-280.

Arcaute K, Palafox GN, Medina F, Wicker RB. Complex silicone aorta models manufactured using a dip-spin coating technique and water-soluble molds. 2003. Key Biscayne, Florida, Summer Bioengineering Conference. 25-6-2003.

Armstrong J, Salacinski HJ, Mu Q, Seifalian AM, Peel L, Freeman N, Holt CM, Lu JR. Interfacial adsorption of fibrinogen and its inhibition by RGD peptide: a combined physical study. J Phys : Condens Matter 2004; (16): S2483-S2491.

Arthur W T, Vernon R B, Sage E H, Reed M J. Growth factors reverse the impaired sprouting of microvessels from aged mice. Microvasc Res 1998; (55): 260-270.

Attawia M A, Uhrich K E, Botchwey E, Fan M, Langer R, Laurencin C T. Cytotoxicity testing of poly(anhydride-co-imides) for orthopedic applications. J

Biomed Mater Res 1995; (29): 1233-1240.

Aukland K, Reed R K. Interstitial-lymphatic mechanisms in the control of extracellular fluid volume. Physiol Rev 1993; (73): 1-78.

Aziz C A, Sefton M V, Anderson J M, Ziats N P. Preparation of purified atactic polypropylene and polyvinyl methyl ether surfaces for thrombogenicity studies. J Biomed Mater Res 1996; (32): 193-202.

Babensee J E, McIntire L V, Mikos A G. Growth factor delivery for tissue engineering. Pharm Res 2000; (17): 497-504.

Badylak S F. The extracellular matrix as a scaffold for tissue reconstruction. Semin Cell Dev Biol 2002; (13): 377-383.

Baguneid M, Murray D, Salacinski H J, Fuller B, Hamilton G, Walker M, Seifalian A M. Shear stress preconditioning and tissue engineering based paradigms for generating arterial substitutes. Biotechnol Appl Biochem 2003.

Baier L J, Bivens K A, Patrick C W, Jr., Schmidt C E. Photocrosslinked hyaluronic acid hydrogels: natural, biodegradable tissue engineering scaffolds. Biotechnol Bioeng 2003; (82): 578-589.

Baier R E, Loeb G I, Wallace G T. Role of an artificial boundary in modifying blood proteins. Fed Proc 1971; (30): 1523-1538.

Baier R E. Selected methods of investigation for blood-contact surfaces. Ann N Y Acad Sci 1987; (516): 68-77.

Baish J W, Netti P A, Jain R K. Transmural coupling of fluid flow in microcirculatory network and interstitium in tumors. Microvasc Res 1997; (53): 128-141.

Baker ES, Gidden J, Fee DP, Kemper PR, Anderson SE, Bowers MT. Synthesis and modelling of Polyhedral Oligomeric Silsesquioxane(POSS) systems. 2004.

Balasubramanian V, Grusin N K, Bucher R W, Turitto V T, Slack S M. Residence-time dependent changes in fibrinogen adsorbed to polymeric biomaterials. J Biomed Mater Res 1999; (44): 253-260.

Ballyk P D, Walsh C, Butany J, Ojha M. Compliance mismatch may promote graft-artery intimal hyperplasia by altering suture-line stresses. J Biomech 1998; (31): 229-237.

Baquey C. [New polymers, surface treatments, bioactive materials: value of vascular access devices]. Nephrologie 2001; (22): 399-402.

Bar-Meir E, Teuber S S, Lin H C, Alosacie I, Goddard G, Terybery J, Barka N, Shen B, Peter J B, Blank M, . Multiple autoantibodies in patients with silicone breast implants. J Autoimmun 1995; (8): 267-277.

Barbucci R, Lamponi S, Magnani A, Pasqui D. Micropatterned surfaces for the control of endothelial cell behaviour. Biomol Eng 2002; (19): 161-170.

Barbucci R, Magnani A, Lamponi S, Pasqui D, Bryan S. The use of hyaluronan and its sulphated derivative patterned with micrometric scale on glass substrate in melanocyte cell behaviour. Biomaterials 2003; (24): 915-926.

Batra M, Bernard S, Picha G. Histologic comparison of breast implant shells with smooth, foam, and pillar microstructuring in a rat model from 1 day to 6 months. Plast Reconstr Surg 1995; (95): 354-363.

Baty AM, Suci PA, Tyler BJ, Geesey GG. Investigation of adhesive protein adsorptin on polystyrene and poly(octadecyl methacrylate) using angle-dependent XPS, ATR-FTIR and AFM. J Colloid Interface Sci 177, 307-315. 996.

Bayati S, Russell R C, Roth A C. Stimulation of angiogenesis to improve the viability of prefabricated flaps. Plast Reconstr Surg 1998; (101): 1290-1295.

Belloque J, Smith G M. 1H-nuclear magnetic resonance studies on the conformational changes related to the foaming properties of beta-lactoglobulin. J Dairy Sci 1998; (81): 2580-2587.

Belu A M, Graham D J, Castner D G. Time-of-flight secondary ion mass spectrometry: techniques and applications for the characterization of biomaterial surfaces. Biomaterials 2003; (24): 3635-3653.

Bendahl L, Hansen S H, Olsen J. A new sheathless electrospray interface for coupling of capillary electrophoresis to ion-trap mass spectrometry. Rapid Commun Mass Spectrom 2002; (16): 2333-2340.

Benesch J, Svedhem S, Svensson S C, Valiokas R, Liedberg B, Tengvall P. Protein adsorption to oligo(ethylene glycol) self-assembled monolayers: experiments with fibrinogen, heparinized plasma, and serum. J Biomater Sci Polym Ed 2001; (12): 581-597.

Benfarhi S, Decker C, Keller L, Zahouily K. Synthesis of clay nanocomposite materials by light-induced crosslinking polymerization. Eur Polym Journal 2004; (40): 493-501.

Bennett J P. Aspects of the history of plastic surgery since the 16th century. J R Soc Med 1983; (76): 152-156.

Benoist LJ, Le Parlouer P. Integrated circuit thermal analysis. A new thermal technique for polymer characterization. J Thermal Anal Calorim 2000; (59): 351-358.

Bentzer P, Kongstad L, Grande P O. Capillary filtration coefficient is independent of number of perfused capillaries in cat skeletal muscle. Am J Physiol Heart Circ Physiol 2001; (280): H2697-H2706.

Berger K, Sauvage L R, Rao A M, Wood S J. Healing of arterial prostheses in man: its incompleteness. Ann Surg 1972; (175): 118-127.

Berglund J D, Galis Z S. Designer blood vessels and therapeutic revascularization. Br J Pharmacol 2003; (140): 627-636.

Berman D E, Lineweaver W, Vasconez B, Buncke H. Microvascular silicon replamineform grafts of 2- and 5-cm lengths: experimental studies. Microsurgery 1986; (7): 132-134.

Berrino P, Galli A, Rainero M L, Santi P L. Long-lasting complications with the use of polyurethane-covered breast implants. Br J Plast Surg 1986; (39): 549-553.

Berrocal M J, Badr I H, Gao D, Bachas L G. Reducing the thrombogenicity of ion-selective electrode membranes through the use of a silicone-modified segmented polyurethane. Anal Chem 2001; (73): 5328-5333.

Beyer G. Nanocomposites: a new class of flame retardants for polymers. Plastics Additives and Compounding 2002;22-28.

Black A F, Berthod F, L'Heureux N, Germain L, Auger F A. In vitro reconstruction of a human capillary-like network in a tissue-engineered skin equivalent. FASEB J 1998; (12): 1331-1340.

Black A F, Hudon V, Damour O, Germain L, Auger F A. A novel approach for studying angiogenesis: a human skin equivalent with a capillary-like network. Cell Biol Toxicol 1999; (15): 81-90.

Blaker J J, Gough J E, Maquet V, Notingher I, Boccaccini A R. In vitro evaluation of novel bioactive composites based on Bioglass-filled polylactide foams for bone tissue engineering scaffolds. J Biomed Mater Res 2003; (67A): 1401-1411.

Blandamer M J, Cullis P M, Gleeson P T. Three important calorimetric applications of a classic thermodynamic equation. Chem Soc Rev 2003; (32): 264-267.

Blunden R E, Oliver R G, O'Kane C O. Microbial growth on the surfaces of various orthodontic bonding cements. Br J Orthod 1994; (21): 125-132.

Boland T, Ratner B D. Direct measurement of hydrogen bonding in DNA nucleotide bases by atomic force microscopy. Proc Natl Acad Sci U S A 1995; (92): 5297-5301.

Borges J, Tegtmeier F T, Padron N T, Mueller M C, Lang E M, Stark G B. Chorioallantoic membrane angiogenesis model for tissue engineering: a new twist on a classic model. Tissue Eng 2003; (9): 441-450.

Bos G W, Poot A A, Beugeling T, van Aken W G, Feijen J. Small-diameter vascular graft prostheses: current status. Arch Physiol Biochem 1998; (106): 100-115.

Bostman O, Partio E, Hirvensalo E, Rokkanen P. Foreign-body reactions to polyglycolide screws. Observations in 24/216 malleolar fracture cases. Acta Orthop Scand 1992; (63): 173-176.

Bourassa M G. Long-term vein graft patency. Curr Opin Cardiol 1994; (9): 685-691.

Brey E M, King T W, Johnston C, McIntire L V, Reece G P, Patrick C W, Jr. A technique for quantitative three-dimensional analysis of microvascular structure. Microvasc Res 2002; (63): 279-294.

Briggs D, Seah M P ,eds. *Practical Surface Analysis*. Wiley, (New York) 1990.

Brinton L A, Toniolo P, Pasternack B S. Epidemiologic follow-up studies of breast augmentation patients. J Clin Epidemiol 1995; (48): 557-563.

Brohim R M, Foresman P A, Hildebrandt P K, Rodeheaver G T. Early tissue reaction to textured breast implant surfaces. Ann Plast Surg 1992; (28): 354-362.

Brossollet L J. Mechanical issues in vascular grafting: a review. Int J Artif Organs 1992; (15): 579-584.

Brown M E, Maciejewski M, Vyazovkin S. Computational aspects of kinetic analysis Part A: The ICTAC kinetics project - data, methods and results. Thermochim Acta 2000; (355): 125-143.

Brown A N, Kim B S, Alsberg E, Mooney D J. Combining chondrocytes and smooth muscle cells to engineer hybrid soft tissue constructs. Tissue Eng 2000; (6): 297-305.

Brown K J, Maynes S F, Bezos A, Maguire D J, Ford M D, Parish C R. A novel in vitro assay for human angiogenesis. Lab Invest 1996; (75): 539-555.

Budd J S, Allen K E, Hartley G, Bell P R. The effect of preformed confluent endothelial cell monolayers on the patency and thrombogenicity of small calibre vascular grafts. Eur J Vasc Surg 1991; (5): 397-405.

Buehler FU, Seferis JC. Effect of sample thickness in TMDSC measurements. Thermochim Acta 2000; (348): 161-168.

Bukatina A E, Morozov V N, Gusev N B, Sieck G C. Mechano-chemical effects of Ca(2+) in cross-linked troponin-C films. FEBS Lett 2002; (524): 107-110.

Burnham AK. Computational aspects of kinetic analysis Part D: The ICTAC kinetics

project multi-thermal-history model-fitting methods and their relation to iso-conversional methods. Thermochim Acta 2000; (355): 165-170.

Burns N L, Emoto K, Holmberg K, Van Alstine J M, Harris J M. Surface characterization of biomedical materials by measurement of electroosmosis. Biomaterials 1998; (19): 423-440.

Burri P H, Djonov V. Intussusceptive angiogenesis--the alternative to capillary sprouting. Mol Aspects Med 2002; (23): S1-27.

Burton AC. Relationship of structure to function of the tissues of the wall of blood vessels. Physiol Rev 1954; (34): 619-642.

Busby W, Cameron N R, Jahoda C A. Emulsion-derived foams (PolyHIPEs) containing poly(epsilon-caprolactone) as matrixes for tissue engineering. Biomacromolecules 2001; (2): 154-164.

Buschmann I, Schaper W. The pathophysiology of the collateral circulation (arteriogenesis). J Pathol 2000; (190): 338-342.

Byrne J, Darling R C, III, Chang B B, Paty P S K, Kreienberg P B, Lloyd W E, Leather R P, Shah D M. Infrainguinal arterial reconstruction for claudication: is it worth the risk? An analysis of 409 procedures. J Vasc Surg 1999; (29): 259-267.

Cai Q, Yang J, Bei J, Wang S. A novel porous cells scaffold made of polylactide-dextran blend by combining phase-separation and particle-leaching techniques. Biomaterials 2002; (23): 4483-4492.

Calliot T, Pourroy G, Stuerga D. Microwave hydrothermal flash synthesis of nanocomposites Fe-Co alloy/cobalt ferrite. J Solid State Chem 2004; (177): 3843-3848.

Can Z, Apaydin I, Ercocen A R, Demirseren M E, Sabuncuoglu B. Prefabrication of a high-density porous polyethylene implant using a vascular induction technique. Ann Plast Surg 1998; (41): 264-269.

Cao X, Shoichet M S. Photoimmobilization of biomolecules within a 3-dimensional hydrogel matrix. J Biomater Sci Polym Ed 2002; (13): 623-636.

Capaldi FM, Rutledge GC, Boyce MC. Structure and dynamics of blends of polyhedral oligomeric silsesquioxanes and polyethylene by atomistic simulation. Macromolecules 2005; (38): 6700-6709.

Capone C D. Biostability of a non-ether polyurethane. J Biomater Appl 1992; (7): 108-129.

Caro CG, Pedley TJ, Schroter RC, Seed WA. The mechanics of circulation. Oxford University Press, Oxford 1978.

Carpaneda C A. Inflammatory reaction and capsular contracture around smooth silicone implants. Aesthetic Plast Surg 1997; (21): 110-114.

Cassell O C, Hofer S O, Morrison W A, Knight K R. Vascularisation of tissue-engineered grafts: the regulation of angiogenesis in reconstructive surgery and in disease states. Br J Plast Surg 2002; (55): 603-610.

Celina M, Wise J, Ottesen DK. Correlation of thermal and mechanical property changes during oxidative degradation of neoprene. Polym Degrad Stab 2000; (68): 171-184.

Cenni E, Granchi D, Verri E, Remiddi G, Cavedagna D, Di Leo A. Evaluation of endothelial cell integrins after in \ vitro contact with polyethylene terephthalate. J Mater Sci Mater Med 2001; (12): 345-349.

Chalupowicz D G, Chowdhury Z A, Bach T L, Barsigian C, Martinez J. Fibrin II induces endothelial cell capillary tube formation. J Cell Biol 1995; (130): 207-215.

Chan ER, Zhang X, Lee CY, Neurock M, Glotzer SC. Structure and dynamics of blends of polyhedral oligomeric silsesquioxanes and polyethylene by Simulations of tetra-tethered organic/inorganic nanocube-polymer assemblies. Macromolecules 2005; (38): 6168-6180.

Chandy T, Das G S, Wilson R F, Rao G H. Use of plasma glow for surface-engineering biomolecules to enhance bloodcompatibility of Dacron and PTFE vascular prosthesis. Biomaterials 2000; (21): 699-712.

Chang D S, Su H, Tang G L, Brevetti L S, Sarkar R, Wang R, Kan Y W, Messina L M. Adeno-associated viral vector-mediated gene transfer of VEGF normalizes skeletal muscle oxygen tension and induces arteriogenesis in ischemic rat hindlimb. Mol Ther 2003; (7): 44-51.

Chapman DL. A contribution to the theory of electrocapillarity. Phil Mag 1913; (25): 475-483.

Cheam TC, Krimm S. Transition dipole interaction in polypeptides - Abnitio calculation of transition dipole parameters. Chemical Physics Letters 1984; (107): 613-616.

Chen IIH, Prewitt RL. A mathematical representation for vessel network. J Theor Biol 1982; (98): 211-219.

Chen G, Ushida T, Tateishi T. Preparation of poly(L-lactic acid) and poly(DL-lactic-co-glycolic acid) foams by use of ice microparticulates. Biomaterials 2001; (22): 2563-2567.

Chen J H, Laiw R F, Jiang S F, Lee Y D. Microporous segmented polyetherurethane vascular graft: I. Dependency of graft morphology and mechanical properties on

compositions and fabrication conditions. J Biomed Mater Res 1999; (48): 235-245.

Chen K Y, Kuo J F, Chen C Y. Synthesis, characterization, and platelet adhesion studies of novel aliphatic polyurethaneurea anionomers based on polydimethylsiloxane-polytetramethylene oxide soft segments. J Biomater Sci Polym Ed 1999; (10): 1183-1205.

Chen Z, Zhang R, Kodama M, Nakaya T. Preparations and properties of a novel grafted segmented polyurethane-bearing glucose groups. J Biomater Sci Polym Ed 1999; (10): 901-916.

Cheng WD, Xiang KH, Pandey R, Pernisz UC. Calculations of Linear and Nonlinear Optical Properties of H-Silsesquioxanes. J Phys Chem B 2000; (104): 6737-6742.

Chilkoti A, Schmierer A E, Perez-Luna V H, Ratner B D. Investigating the relationship between surface chemistry and endothelial cell growth: partial least-squares regression of the static secondary ion mass spectra of oxygen-containing plasma-deposited films. Anal Chem 1995; (67): 2883-2891.

Chilkoti A, Boland T, Ratner B D, Stayton P S. The relationship between ligand-binding thermodynamics and protein-ligand interaction forces measured by atomic force microscopy. Biophys J 1995; (69): 2125-2130.

Chittur K K. FTIR/ATR for protein adsorption to biomaterial surfaces. Biomaterials 1998; (19): 357-369.

Chnari E, Lari H B, Tian L, Uhrich K E, Moghe P V. Nanoscale anionic macromolecules for selective retention of low-density lipoproteins. Biomaterials 2005; (26): 3749-3758.

Choi J, Harcup J, Yee A F, Zhu Q, Laine R M. Organic/inorganic hybrid composites from cubic silsesquioxanes. J Am Chem Soc 2001; (123): 11420-11430.

Christenson E M, Dadsetan M, Wiggins M, Anderson J M, Hiltner A. Poly(carbonate urethane) and poly(ether urethane) biodegradation: in vivo studies. J Biomed Mater Res A 2004; (69): 407-416.

Chu C C. The in-vitro degradation of poly(glycolic acid) sutures--effect of pH. J Biomed Mater Res 1981; (15): 795-804.

Chun Y. Synthesis and characterisation of poly(siloxane-urethane)s. Polymer Int 1992; (27): 177-185.

Chung K C, Pillsbury M S, Walters M R, Hayward R A. Reliability and validity testing of the Michigan Hand Outcomes Questionnaire. J Hand Surg [Am] 1998; (23): 575-587.

Chung S, Hazen A, Levine J P, Baux G, Olivier W A, Yee H T, Margiotta M S, Karp N S, Gurtner G C. Vascularized acellular dermal matrix island flaps for the repair of abdominal muscle defects. Plast Reconstr Surg 2003; (111): 225-232.

Chupa J M, Foster A M, Sumner S R, Madihally S V, Matthew H W. Vascular cell responses to polysaccharide materials: in vitro and in vivo evaluations. Biomaterials 2000; (21): 2315-2322.

Cohney B C, Mitchell S. An improved method of removing polyurethane foam-covered gel prostheses. Aesthetic Plast Surg 1997; (21): 191-192.

Collier J H, Camp J P, Hudson T W, Schmidt C E. Synthesis and characterization of polypyrrole-hyaluronic acid composite biomaterials for tissue engineering applications. J Biomed Mater Res 2000; (50): 574-584.

Conte M S. The ideal small arterial substitute: a search for the Holy Grail? FASEB J 1998; (12): 43-45.

Cook A D, Pajvani U B, Hrkach J S, Cannizzaro S M, Langer R. Colorimetric analysis of surface reactive amino groups on poly(lactic acid-co-lysine):poly(lactic acid) blends. Biomaterials 1997; (18): 1417-1424.

Cooper D K. Xenoantigens and xenoantibodies. Xenotransplantation 1998; (5): 6-17.

Copeland M, Choi M, Bleiweiss I J. Silicone breakdown and capsular synovial metaplasia in textured-wall saline breast prostheses. Plast Reconstr Surg 1994; (94): 628-633.

Coury AJ. Biomaterials Science: An Introduction to Materials in Medicine. Academic Press, San Diego 1996.

Coury A J, Slaikeu P C, Cahalan P T, Stokes K B, Hobot C M. Factors and interactions affecting the performance of polyurethane elastomers in medical devices. J Biomater Appl 1988; (3): 130-179.

Cui D, Tian F, Ozkan C S, Wang M, Gao H. Effect of single wall carbon nanotubes on human HEK293 cells. Toxicol Lett 2005; (155): 73-85.

Cunningham J J, Nikolovski J, Linderman J J, Mooney D J. Quantification of fibronectin adsorption to silicone-rubber cell culture substrates. Biotechniques 2002; (32): 876, 878, 880.

Curry F R, Huxley V H. Comparison of the capillary membrane properties determining fluid exchange in single capillaries and whole organs. Int J Microcirc Clin Exp 1982; (1): 381-391.

Dal Ponte D B, Berman S S, Patula V, Kleinert L, Williams S K. Abdominal aortic healing associated with a thin-walled Dacron-covered endovascular graft in a canine model. J Endovasc Ther 2002; (9): 333-343.

Danov K D, Valkovska D S, Kralchevsky P A. Hydrodynamic instability and coalescence in trains of emulsion drops or gas bubbles moving through a narrow capillary. J Colloid Interface Sci 2003; (267): 243-258.

Davenas J, Thevenard P, Philippe F, Arnaud M N. Surface implantation treatments to prevent infection complications in short term devices. Biomol Eng 2002; (19): 263-268.

Davies P F, Remuzzi A, Gordon E J, Dewey C F, Jr., Gimbrone M A, Jr. Turbulent fluid shear stress induces vascular endothelial cell turnover in vitro. Proc Natl Acad Sci U S A 1986; (83): 2114-2117.

Dawson J, Hill G, Fitzpatrick R, Carr A. The benefits of using patient-based methods of assessment. Medium-term results of an observational study of shoulder surgery. J Bone Joint Surg Br 2001; (83): 877-882.

De Rosa M, Carteni' M, Petillo O, Calarco A, Margarucci S, Rosso F, De Rosa A, Farina E, Grippo P, Peluso G. Cationic polyelectrolyte hydrogel fosters fibroblast spreading, proliferation, and extracellular matrix production: Implications for tissue engineering. J Cell Physiol 2004; (198): 133-143.

De Ugarte D A, Ashjian P H, Elbarbary A, Hedrick M H. Future of fat as raw material for tissue regeneration. Ann Plast Surg 2003; (50): 215-219.

Demiri E C, Iordanidis S L, Mantinaos C F. Experimental use of prosthetic grafts in microvascular surgery. Handchir Mikrochir Plast Chir 1999; (31): 102-106.

Deng J, Polidan J T, Hottle J R, Farmer-Creely C E, Viers B D, Esker A R. Polyhedral oligomeric silsesquioxanes: a new class of amphiphiles at the air/water interface. J Am Chem Soc 2002; (124): 15194-15195.

Desai N P, Hubbell J A. Biological responses to polyethylene oxide modified polyethylene terephthalate surfaces. J Biomed Mater Res 1991; (25): 829-843.

Deschamps A A, van Apeldoorn A A, de Bruijn J D, Grijpma D W, Feijen J. Poly(ether ester amide)s for tissue engineering. Biomaterials 2003; (24): 2643-2652.

Deutsch M, Meinhart J, Fischlein T, Preiss P, Zilla P. Clinical autologous in vitro endothelialization of infrainguinal ePTFE grafts in 100 patients: a 9-year experience. Surgery 1999; (126): 847-855.

Devine C, Hons B, McCollum C. Heparin-bonded Dacron or polytetrafluoroethylene for femoropopliteal bypass grafting: a multicenter trial. J Vasc Surg 2001; (33): 533-539.

Dias J J, Bhowal B, Wildin C J, Thompson J R. Assessing the outcome of disorders of the hand. Is the patient evaluation measure reliable, valid, responsive and without bias? J Bone Joint Surg Br 2001; (83): 235-240.

Diederich A, Losche M. Novel biosensoric devices based on molecular protein hetero-multilayer films. Adv Biophys 1997; (34): 205-230.

Dijkstra T W, Duchateau R, Van Santen R A, Meetsma A, Yap G P. Silsesquioxane models for geminal silica surface silanol sites. A spectroscopic investigation of different types of silanols. J Am Chem Soc 2002; (124): 9856-9864.

Ding Z, Fournier R L. Oxygen and inulin transport measurements in a planar tissue-engineered bioartificial organ. Tissue Eng 2002; (8): 25-36.

Doetschman T C, Eistetter H, Katz M, Schmidt W, Kemler R. The in vitro development of blastocyst-derived embryonic stem cell lines: formation of visceral yolk sac, blood islands and myocardium. J Embryol Exp Morphol 1985; (87): 27-45.

Dollimore D. Thermal analysis. Thermal Analysis Anal Chem 1994; (66): 17R-25R.

Dolores W, Christian R, Harald N, Hildegunde P, Georg W. Cellular and molecular composition of fibrous capsules formed around silicone breast implants with special focus on local immune reactions. J Autoimmun 2004; (23): 81-91.

Dong HB, Hunt JD. A novel single pan scanning calorimeter. Measurement of thermophysical properties of metallic alloys. J Thermal Anal Calorim 2001; (64): 341-350.

Draget K I, Skjak-Braek G, Smidsrod O. Alginate based new materials. Int J Biol Macromol 1997; (21): 47-55.

Driessen N J, Peters G W, Huyghe J M, Bouten C V, Baaijens F P. Remodelling of continuously distributed collagen fibres in soft connective tissues. J Biomech 2003; (36): 1151-1158.

Drude P. Ann Phys Chem 1889; (36): 865.

Du H, Xu GQ, Chin WS. Synthesis, characterization and optical properties of hybridized CdS-polystyrene nanocomposites. Chem Mater 2002; (14): 4473-4479.

Duan X, Lewis R S. Improved haemocompatibility of cysteine-modified polymers via endogenous nitric oxide. Biomaterials 2002; (23): 1197-1203.

Dunn R, Watson S. Why climb a ladder when you can take the elevator? Plast Reconstr Surg 2001; (107): 283.

Eberhart A, Zhang Z, Guidoin R, Laroche G, Guay L, De La F D, Batt M, King M W. A new generation of polyurethane vascular prostheses: rara avis or ignis fatuus? J Biomed Mater Res 1999; (48): 546-558.

Eberhart R C, Munro M S, Frautschi J R, Lubin M, Clubb F J, Jr., Miller C W, Sevastianov V I. Influence of endogenous albumin binding on blood-material interactions. Ann N Y Acad Sci 1987; (516): 78-95.

Edwards A, Carson R J, Szycher M, Bowald S. In vitro and in vivo biodurability of a compliant microporous vascular graft. J Biomater Appl 1998; (13): 23-45.

Elcin Y M, Dixit V, Gitnick G. Controlled release of endothelial cell growth factor from chitosan-albumin microspheres for localized angiogenesis: in vitro and in vivo studies. Artif Cells Blood Substit Immobil Biotechnol 1996; (24): 257-271.

Elcin Y M, Dixit V, Gitnick G. Extensive in vivo angiogenesis following controlled release of human vascular endothelial cell growth factor: implications for tissue engineering and wound healing. Artif Organs 2001; (25): 558-565.

Elzein T, Nasser-Eddine M, Delaite C, Bistac S, Dumas P. FTIR study of polycaprolactone chain organization at interfaces. J Colloid Interface Sci 2004; (273): 381-387.

Englert H, Joyner E, Thompson M, Garcia H, Chambers P, Horner D, Hunt C, Makaroff J, O'Connor H, Russell N, March L. Augmentation mammoplasty and "silicone-osis". Intern Med J 2004; (34): 668-676.

Erdmann L, Macedo B, Uhrich K E. Degradable poly(anhydride ester) implants: effects of localized salicylic acid release on bone. Biomaterials 2000; (21): 2507-2512.

Ersek R A. Molecular impact surface textured implants (MISTI) alter beneficially breast capsule formation at 36 months. J Long Term Eff Med Implants 1991; (1): 155-169.

Ersek R A, Salisbury A V. Textured surface, nonsilicone gel breast implants: four years' clinical outcome. Plast Reconstr Surg 1997; (100): 1729-1739.

Ertel S I, Chilkoti A, Horbett T A, Ratner B D. Endothelial cell growth on oxygen-containing films deposited by radio-frequency plasmas: the role of surface carbonyl groups. J Biomater Sci Polym Ed 1991; (3): 163-183.

Esegbona N, Odlyha M. Thermal analysis of silsesquioxane nanofillers. 2005 MRes University College London.

Fabri P J, Mirtallo J M, Ebbert M L, Kudsk K A, Powell C, Ruberg R L. Clinical effect of nonthrombotic total parenteral nutrition catheters. JPEN J Parenter Enteral Nutr 1984; (8): 705-707.

Fang Q, Hanna M A. Preparation and characterization of biodegradable copolyester-starch based foams. Bioresour Technol 2001; (78): 115-122.

Fare S, Petrini P, Motta A, Cigada A, Tanzi M C. Synergistic effects of oxidative environments and mechanical stress on in vitro stability of polyetherurethanes and polycarbonateurethanes. J Biomed Mater Res 1999; (45): 62-74.

Fellah Z E, Depollier C, Berger S, Lauriks W, Trompette P, Chapelon J Y. Determination of transport parameters in air-saturated porous materials via reflected ultrasonic waves. J Acoust Soc Am 2003; (114): 2561-2569.

Felmeden D C, Blann A D, Lip G Y. Angiogenesis: basic pathophysiology and implications for disease. Eur Heart J 2003; (24): 586-603.

Feng L, Andrade J D. Protein adsorption on low-temperature isotropic carbon: I. Protein conformational change probed by differential scanning calorimetry. J Biomed Mater Res 1994; (28): 735-743.

Fernandez P, Bordenave L, Celerier C, Bareille R, Brouillaud B, Basse-Cathalinat B. A novel potential application for 99mTc-HMPAO: endothelial cell labeling for in

vitro investigation of cell-biomaterial interactions. J Nucl Med 1999; (40): 1756-1763.

Fields C, Cassano A, Allen C, Meyer A, Pawlowski K J, Bowlin G L, Rittgers S E, Szycher M. Endothelial cell seeding of a 4-mm I.D. polyurethane vascular graft. J Biomater Appl 2002; (17): 45-70.

Flynn JH. Thermal Analysis. Academic Press New York, New York 1969.

Fong H, Dickens SH, Flaim GM. Evaluation of dental restorative composites containing polyhedral oligomeric silsesquioxane methacrylate. Dental Mater 2005; (21): 520-529.

Frank J L, Garb J L, Halla B, Reed W P, Jr. Ionic implantation of silicone chronic venous access devices does not alter thrombotic complications: a double-blinded, randomized clinical trial. Surgery 2001; (129): 547-551.

Frerich B, Kurtz-Hoffmann J, Lindemann N, Muller S. [Tissue engineering of vascularized bone and soft tissue transplants]. Mund Kiefer Gesichtschir 2000; (4 Suppl 2): S490-S495.

Frerich B, Lindemann N, Kurtz-Hoffmann J, Oertel K. In vitro model of a vascular stroma for the engineering of vascularized tissues. Int J Oral Maxillofac Surg 2001; (30): 414-420.

Friemann J, Bauer M, Golz B, Rombeck N, Hohr D, Erbs G, Steinau H U, Olbrisch R R. [Physiologic and pathologic patterns of reaction to silicone breast implants]. Zentralbl Chir 1997; (122): 551-564.

Fu BX, Zhang WH, Hsiao BS, Rafailovich M, Sokolov J, Johansson G, Sauer BB, Phillips S, Balnski R. Synthesis and characterization of segmented polyurethanes containing polyhedral oligomeric silsesquioxanes nanostructured molecules. High Performance Polymers 2000; (12): 565-571.

Fu BX, Hsiao BS, Pagola S, Stephens P, White H, Rafailovich M, Sokolov J, Mather PT, Jeon HG, Phillips S, Lichtenhan J, Schwab J. Structural development during deformation of polyurethane containing polyhedral oligomeric silsesquioxanes (POSS) molecules. Polymer 2001; (42): 599-611.

Fu BX, Lee A, addad TS. Styrene-butadiene-styrene triblock copolymers modified with polyhedral oligomeric silsesquioxanes. Macromolecules 2004; (37): 5211-5218.

Fu H, Li S, Li J, Xie X, Zhong Y. [Applications of biodegradable polyurethane in medical field]. *Sheng Wu Yi Xue Gong Cheng Xue Za Zhi* 2003; (20): 348-351.

Fukushit K, Sato T. Using a surface complexation model to predict the nature and stability of nanoparticles. Environ Sci Technol 2005; (39): 1250-1256.

G.J.Fleer, M.A.Cohen Stuart, J.M.H.M.Scheutjens, T.Cosgrove, B.Vincent. Polymers at interfaces. Chapman & Hall, London 1993.

Galwey AK, Brown ME. Solid state decompositions - stagnation or progress ? Thermal Anal Calorim 2000; (60): 863-877.

Gamlin C, Dutta N, Roy-Choudury N. Influence of ethylene-propylene ratio on the thermal degradation behaviour of EPDM elastomers. Thermochim Acta 2001;367-368.

Gao H, Ji B, Jager IL, Arzt E, Fratz P. Materials become insensitive to flaws at nanoscale: Lessons from nature. Proceedings of the National Academy of Science 2003; (100): 5597-5600.

Garfein E S, Orgill D P, Pribaz J J. Clinical applications of tissue engineered constructs. Clin Plast Surg 2003; (30): 485-498.

Ghanbari-Siahkali A, Almdal K, Kingshott P. Limitations of using Raman microscopy for the analysis of high-content-carbon-filled ethylene propylene diene monomer rubber. Appl Spectrosc 2003; (57): 1482-1486.

Ghosh B, Banerjee S, Chakravorty D. Electrical properties of Fe-Fe3O4-SiO2 gel nanocomposites. J Nanosci Nanotechnol 2004; (4): 849-854.

Giannelis EP, Krishnamoorti R, Manias E. Polymer-Silicate Nanocomposites: Model Systems for Confined Polymers and Polymer Brushes. dvances in Polymer Science 1999; (138): 108-147.

Bumstead HA, Van Name RG, eds. *Scientific Papers of J Willard Gibbs*, (1961)

Gill I, Ballesteros A. Bioencapsulation within synthetic polymers (Part 1): sol-gel encapsulated biologicals. Trends Biotechnol 2000; (18): 282-296.

Gillen G, Roberson S. Preliminary evaluation of an SF5+ polyatomic primary ion beam for analysis of organic thin films by secondary ion mass spectrometry. Rapid Commun Mass Spectrom 1998; (12): 1303-1312.

Glenn G M, Klamczynski A P, Takeoka G, Orts W J, Wood D, Widmaier R. Sorption and vapor transmission properties of uncompressed and compressed microcellular starch foam. J Agric Food Chem 2002; (50): 7100-7104.

Goessl A, Garrison M D, Lhoest J B, Hoffman A S. Plasma lithography--thin-film patterning of polymeric biomaterials by RF plasma polymerization I: Surface preparation and analysis. J Biomater Sci Polym Ed 2001; (12): 721-738.

Gooding J J, Shapter J G. Carbon nanotube systems to communicate with enzymes. Methods Mol Biol 2005; (300): 225-242.

Gorna K, Gogolewski S. Biodegradable polyurethanes for implants. II. In vitro degradation and calcification of materials from poly(epsilon-caprolactone)-poly(ethylene oxide) diols and various chain extenders. J Biomed Mater Res 2002; (60): 592-606.

Gorna K, Gogolewski S. Preparation, degradation, and calcification of biodegradable polyurethane foams for bone graft substitutes. J Biomed Mater Res 2003; (67A): 813-827.

Goumans M J, Lebrin F, Valdimarsdottir G. Controlling the angiogenic switch: a balance between two distinct TGF-b receptor signaling pathways. Trends Cardiovasc Med 2003; (13): 301-307.

Graham S W, Hercules D M. Surface spectroscopic studies of Biomer. J Biomed Mater Res 1981; (15): 465-477.

Granke K, Ochsner J L, McClugage S G, Zdrahal P. Analysis of graft healing in a new elastomer-coated vascular prosthesis. Cardiovasc Surg 1993; (1): 254-261.

Grenier G, Remy-Zolghadri M, Guignard R, Bergeron F, Labbe R, Auger F A, Germain L. Isolation and culture of the three vascular cell types from a small vein biopsy sample. In Vitro Cell Dev Biol Anim 2003; (39): 131-139.

Griep M A, Fujikawa K, Nelsestuen G L. Possible basis for the apparent surface selectivity of the contact activation of human blood coagulation factor XII. Biochemistry 1986; (25): 6688-6694.

Grobe G L, III, Gardella J A, Jr., Hopson W L, McKenna W P, Eyring E M. Angular dependent ESCA and infrared studies of segmented polyurethanes. J Biomed Mater Res 1987; (21): 211-229.

Groth T, Campbell E J, Herrmann K, Seifert B. Application of enzyme immunoassays for testing haemocompatibility of biomedical polymers. Biomaterials 1995; (16):

1009-1015.

Grundke K, Bogumil T, Gietzelt T, Jacobasch H J, Kwok DY, Neumann AW. Wetting measurements on smooth, rough and porous solid surfaces . Progr Colloid Polym Sci 1996; (101): 58-68.

Gu GT, Zhang ZJ, Dang HX. Synthesis and surface properties of a soluble low surface free energy polymer. Acta Polymerica Sinica 2002; (6): 770-774.

Guan J, Sacks M S, Beckman E J, Wagner W R. Synthesis, characterization, and cytocompatibility of elastomeric, biodegradable poly(ester-urethane)ureas based on poly(caprolactone) and putrescine. J Biomed Mater Res 2002; (61): 493-503.

Guidoin R, Maurel S, Chakfe N, How T, Zhang Z, Therrien M, Formichi M, Gosselin C. Expanded polytetrafluoroethylene arterial prostheses in humans: chemical analysis of 79 explanted specimens. Biomaterials 1993; (14): 694-704.

Guidoin R, Marois Y, Zhang Z, King M, Martin L, Laroche G, Awad J. The benefits of fluoropassivation of polyester arterial prostheses as observed in a canine model. ASAIO J 1994; (40): M870-M879.

Gunatillake P A, Adhikari R. Biodegradable synthetic polymers for tissue engineering. Eur Cell Mater 2003; (5): 1-16.

Haddad TS, Stapleton R, Jeon HG, Mather PT, Lichtenhan JD, Phillips S. Nanostructured hybrid organic/inorganic materials. Silsesquioxane modified plastics. Abstracts of papers of the American Chemical Society 1999; (217): 246-POLY part 2 Mar 21.

Hakvoort GJ, Hol CM, van Ekeren CJ. DSC calibration during cooling. A survey of possible compounds. J Thermal Anal Calorim 2001; (64): 367-375.

Halberstadt C, Austin C, Rowley J, Culberson C, Loebsack A, Wyatt S, Coleman S, Blacksten L, Burg K, Mooney D, Holder W, Jr. A hydrogel material for plastic and reconstructive applications injected into the subcutaneous space of a sheep. Tissue Eng 2002; (8): 309-319.

Halbleib M, Skurk T, de Luca C, von Heimburg D, Hauner H. Tissue engineering of white adipose tissue using hyaluronic acid-based scaffolds. I: in vitro differentiation of human adipocyte precursor cells on scaffolds. Biomaterials 2003; (24): 3125-3132.

Hamm C W, Schaachinger V, Munzel T, Maikowski C, Bonzel T, Koster R, Rau M, Zeiher A M. Peptide-treated stent graft for the treatment of saphenous vein graft lesions: first clinical results. J Invasive Cardiol 2003; (15): 557-560.

Han B, Lenggoro I W, Choi M, Okuyama K. Measurement of cluster ions and residue nanoparticles from water samples with an electrospray/differential mobility analyzer. Anal Sci 2003; (19): 843-851.

Hanlon E B, Manoharan R, Koo T W, Shafer K E, Motz J T, Fitzmaurice M, Kramer J R, Itzkan I, Dasari R R, Feld M S. Prospects for in vivo Raman spectroscopy. Phys Med Biol 2000; (45): R1-59.

Hansen-Smith FM. Capillary network patterning during angiogenesis. Clinical and Experimental Pharmacology and Physiology 2000; (27): 830-35.

Harris J R, Seikaly H. Evaluation of polytetrafluoroethylene micrografts in microvascular surgery. J Otolaryngol 2002; (31): 89-92.

Harris N R. Arteriovenous pairing: a determinant of capillary exchange. News Physiol Sci 2003; (18): 83-87.

Harrup M, Wertsching A, Jones M. Preparation and Characterization of Novel Polymer/Silicate Nanocomposites. 2002.

Harzallah B, Aguie-Beghin V, Douillard R, Bosio L. A structural study of beta-casein adsorbed layers at the air-water interface using X-ray and neutron reflectivity. Int J Biol Macromol 1998; (23): 73-84.

Hauben D J, Baruchin A, Mahler A. On the history of the free skin graft. Ann Plast Surg 1982; (9): 242-245.

Hays JN, Shaw SJ. A review of nanocomposites. Nanocomposites 2000 conference . 2000.

Hergenrother R W, Yu X H, Cooper S L. Blood-contacting properties of polydimethylsiloxane polyurea-urethanes. Biomaterials 1994; (15): 635-640.

Hershey J C, Baskin E P, Glass J D, Hartman H A, Gilberto D B, Rogers I T, Cook J J. Revascularization in the rabbit hindlimb: dissociation between capillary sprouting and arteriogenesis. Cardiovasc Res 2001; (49): 618-625.

Hesse Y, Kampmeier J, Lang G K, Baldysiak-Figiel A, Lang G E. Adherence and viability of porcine lens epithelial cells on three different IOL materials in vitro. Graefes Arch Clin Exp Ophthalmol 2003; (241): 823-826.

Hile D D, Amirpour M L, Akgerman A, Pishko M V. Active growth factor delivery from poly(D,L-lactide-co-glycolide) foams prepared in supercritical CO(2). J Control Release 2000; (66): 177-185.

Hodde J. Naturally occurring scaffolds for soft tissue repair and regeneration. Tissue Eng 2002; (8): 295-308.

Hodde J P, Record R D, Tullius R S, Badylak S F. Retention of endothelial cell adherence to porcine-derived extracellular matrix after disinfection and sterilization. Tissue Eng 2002; (8): 225-234.

Hodgkin J H, Heath G R, Norris W D, Donald G S, Johnson G. Endothelial cell response to polyvinyl chloride-packaged GORETEX: effect of surface contamination. Biomaterials 1990; (11): 9-12.

Hoefer I E, van Royen N, Buschmann I R, Piek J J, Schaper W. Time course of arteriogenesis following femoral artery occlusion in the rabbit. Cardiovasc Res 2001; (49): 609-617.

Hoet P H, Bruske-Hohlfeld I, Salata O V. Nanoparticles - known and unknown health risks. J Nanobiotechnology 2004; (2): 12.

Hoffman D, Gong G, Pinchuk L, Sisto D. Safety and intracardiac function of a silicone-polyurethane elastomer designed for vascular use. Clin Mater 1993; (13): 95-100.

Holy C E, Dang S M, Davies J E, Shoichet M S. In vitro degradation of a novel poly(lactide-co-glycolide) 75/25 foam. Biomaterials 1999; (20): 1177-1185.

Hongyao Xu, Hiao-Wei Kuo, Eng-Chih Chang. Preparations, Thermal Properties and *Tg* Increase Mechanism of Inorganic/Organic Hybrid Polymers Based on Polyhedral Oligomeric Silsequioxanes. Macromolecules, 35, 8788-8793 (2002) 2002; (25): 8788-8793.

Horacek M, Cvachovec K. The effects of cardiopulmonary bypass with hollow fiber membrane oxygenator on blood clotting measured by thromboelastography. Physiol Res 2002; (51): 145-150.

Houlne M P, Sjostrom C M, Uibel R H, Kleimeyer J A, Harris J M. Confocal Raman microscopy for monitoring chemical reactions on single optically trapped, solid-phase support particles. Anal Chem 2002; (74): 4311-4319.

Hoying J B, Boswell C A, Williams S K. Angiogenic potential of microvessel fragments established in three-dimensional collagen gels. In Vitro Cell Dev Biol Anim 1996; (32): 409-419.

Hsiao BS, White H, Rafailovich M, Mather PT, Jeon HG, Phillips S, Lichtenhan J, Schwab J. Nanoscale reinforcement of polyhedral oligomeric silsesquioxane (POSS) in polyurethane elastomer. Polym Int 2000; (49): 437-440.

Hsu S, Tseng H, Wu M. Comparative In vitro evaluation of two different preparations of small diameter polyurethane vascular grafts. Artif Organs 2000; (24): 119-128.

Hsu Y Y, Gresser J D, Stewart R R, Trantolo D J, Lyons C M, Simons G A, Gangadharam P R, Wise D L. Mechanisms of isoniazid release from poly(d,l-lactide-co-glycolide) matrices prepared by dry-mixing and low density polymeric foam methods. J Pharm Sci 1996; (85): 706-713.

Hu WJ, Wunderlich B. Data analysis without Fourier transformation for saw tooth-type temperature-modulated DSC. Thermal Anal Calorim 2001; (66): 677-697.

Hu J, Hu P, Li T, Jiang L, Chen J, Tao Z. [The adhesion and seeding of NIH3T3 fibroblast on PHB surfaces]. Sheng Wu Yi Xue Gong Cheng Xue Za Zhi 2001; (18): 541-3, 551.

Hu S, Ren X, Bachman M, Sims C E, Li G P, Allbritton N. Surface modification of poly(dimethylsiloxane) microfluidic devices by ultraviolet polymer grafting. Anal Chem 2002; (74): 4117-4123.

Hu W J, Eaton J W, Ugarova T P, Tang L. Molecular basis of biomaterial-mediated foreign body reactions. Blood 2001; (98): 1231-1238.

Hu Y, Grainger D W, Winn S R, Hollinger J O. Fabrication of poly(alpha-hydroxy acid) foam scaffolds using multiple solvent systems. J Biomed Mater Res 2002; (59): 563-572.

Huang H, Yuan Q, Yang X. Morphology study of gold-chitosan nanocomposites. J Colloid Interface Sci 2005; (282): 26-31.

Huang X, Li J, Zhang Y, Mascarenhas A. From 1D chain to 3D network: tuning hybrid II-VI nanostructures and their optical properties. J Am Chem Soc 2003; (125): 7049-7055.

Hudak P L, Amadio P C, Bombardier C. Development of an upper extremity outcome measure: the DASH (disabilities of the arm, shoulder and hand) [corrected]. The Upper Extremity Collaborative Group (UECG). Am J Ind Med 1996; (29): 602-608.

Hudon V, Berthod F, Black A F, Damour O, Germain L, Auger F A. A tissue-engineered endothelialized dermis to study the modulation of angiogenic and angiostatic molecules on capillary-like tube formation in vitro. Br J Dermatol 2003; (148): 1094-1104.

Hudson TW, Evans GR, Schidmt CE. Engineering strategies for peripheral nerve repair. Clin Plast Surg 1999; (26): 617-628.

Hughes D. Transvascular fluid dynamics. Veterinary Anaesthesia and Analgesia 27, 63-69. 2000.

Hynes R O. The complexity of platelet adhesion to extracellular matrices. Thromb Haemost 1991; (66): 40-43.

Ingber D E, Folkman J. Mechanochemical switching between growth and differentiation during fibroblast growth factor-stimulated angiogenesis in vitro: role of extracellular matrix. J Cell Biol 1989; (109): 317-330.

Ishihara K, Hanyuda H, Nakabayashi N. Synthesis of phospholipid polymers having a

urethane bond in the side chain as coating material on segmented polyurethane and their platelet adhesion-resistant properties. Biomaterials 1995; (16): 873-879.

Ishihara K, Fukumoto K, Iwasaki Y, Nakabayashi N. Modification of polysulfone with phospholipid polymer for improvement of the blood compatibility. Part 1. Surface characterization. Biomaterials 1999; (20): 1545-1551.

Iurlaro M, Sanders J E, Zhu W H, Scatena M, Mitchell S B, Nicosia R F. Use of vascular explants for ex vivo neovascularization of biomaterials. Microvasc Res 2002; (64): 398-404.

Iwasaki Y, Tojo Y, Kurosaki T, Nakabayashi N. Reduced adhesion of blood cells to biodegradable polymers by introducing phosphorylcholine moieties. J Biomed Mater Res 2003; (65A): 164-169.

J.Willard Gibbs. The scientific papers of J.Willard Gibbs. 1961. New York. (Catalog)

Jabarin SA. Strain-induced crystallization of poly(ethylene-terephthalate). Polym Eng Sci 1992; (32): 1341.

Jansson E, Tengvall P. In vitro preparation and ellipsometric characterization of thin blood plasma clot films on silicon. Biomaterials 2001; (22): 1803-1808.

Jenkins M E, Friedman H I, von Recum A F. Breast implants: facts, controversy, and speculations for future research. J Invest Surg 1996; (9): 1-12.

Jenney C R, DeFife K M, Colton E, Anderson J M. Human monocyte/macrophage adhesion, macrophage motility, and IL-4-induced foreign body giant cell formation on silane-modified surfaces in vitro. Student Research Award in the Master's Degree Candidate Category, 24th Annual Meeting of the Society for Biomaterials, San Diego, CA, April 22-26, 1998. J Biomed Mater Res 1998; (41): 171-184.

Jenney C R, Anderson J M. Alkylsilane-modified surfaces: inhibition of human macrophage adhesion and foreign body giant cell formation. J Biomed Mater Res 1999; (46): 11-21.

Jeong S W, Corapcioglu M Y. A micromodel analysis of factors influencing NAPL removal by surfactant foam flooding. J Contam Hydrol 2003; (60): 77-96.

Jeschke M G, Hermanutz V, Wolf S E, Koveker G B. Polyurethane vascular prostheses decreases neointimal formation compared with expanded polytetrafluoroethylene. J Vasc Surg 1999; (29): 168-176.

Ji J, Feng L, Barbosa M A. Stearyl poly(ethylene oxide) grafted surfaces for preferential adsorption of albumin. Biomaterials 2001; (22): 3015-3023.

Jiang Z, Imrie CT, Hutchinson JM. Temperature-modulated differential scanning calorimetry - Part IV. The effect of heat transfer on the measurement of heat capacity using quasi-isothermal ADSC. J Thermal Anal Calorim 2001; (64): 85-107.

Jiang X, Marois Y, Traore A, Tessier D, Dao L H, Guidoin R, Zhang Z. Tissue reaction to polypyrrole-coated polyester fabrics: an in vivo study in rats. Tissue Eng 2002; (8): 635-647.

Jonsson M, Johansson H O. Effect of surface grafted polymers on the adsorption of different model proteins. Colloids Surf B Biointerfaces 2004; (37): 71-81.

Joshi A, Butola BS. Studies on nonisothermal crystallization of HDPE/POSS nanocomposites. Polymer 2004; (45): 4953-4968.

Joshi M, Butola BS. Polymeric nanocomposites - Polyhedral oligomeric silsesquioxanes (POSS) as hybrid nanofiller. J Macromol Sci-Polym Rev 2004; (C44): 389-410.

Kaihara S, Borenstein J, Koka R, Lalan S, Ochoa E R, Ravens M, Pien H, Cunningham B, Vacanti J P. Silicon micromachining to tissue engineer branched vascular channels for liver fabrication. Tissue Eng 2000; (6): 105-117.

Kalka C, Masuda H, Takahashi T, Kalka-Moll W M, Silver M, Kearney M, Li T, Isner J M, Asahara T. Transplantation of ex vivo expanded endothelial progenitor cells for therapeutic neovascularization. Proc Natl Acad Sci U S A 2000; (97): 3422-3427.

Kamel M, Protzner K, Fornasier V, Peters W, Smith D, Ibanez D. The peri-implant breast capsule: an immunophenotypic study of capsules taken at explantation surgery. J Biomed Mater Res 2001; (58): 88-96.

Kannan RY, Salacinski HJ, Sales KM, Butler PE, Seifalian AM. The endothelialization of polyhedral oligomeric silsesquioxane nanocomposites: an invitro study. Cell Biochem Biophys 2005;(in print).

Kannan RY, Salacinski HJ, Narula A, Riddell A, Butler PE, Seifalian AM. Silsesquioxanes as tissue implants. Plast.Reconstr.Surg . 2005. (in print)

Kannan RY, Salacinski HJ, Butler PE, Seifalian AM. Polyhedral oligomeric silsesquioxane nanocomposites: The next generation material for biomedical application. Acc.Chem Res . 2005.

Kannan R Y, Sales K M, Salacinski H J, Butler P E, Seifalian A M. Cytotoxicity analysis of poly (carbonate-siloxane-urea) urethane. Med J Malaysia 2004; (59 Suppl B): 99-100.

Kannan R Y, Sales K M, Salacinski H J, Butler P E, Seifalian A M. Endothelialisation of poly (carbonate-siloxane-urea) urethane. Med J Malaysia 2004; (59 Suppl B): 107-108.

Kannan R Y, Salacinski H J, Sales K, Butler P, Seifalian A M. The roles of tissue

engineering and vascularisation in the development of micro-vascular networks: a review. Biomaterials 2005; (26): 1857-1875.

Kannan R Y, Salacinski H J, Vara D S, Odlyha M, Seifalian A M. Review paper: the principles and applications of surface analytical techniques at the vascular interface. J Biomater Appl 2006; 21(1): 5 – 32.

Kao W J. Evaluation of protein-modulated macrophage behavior on biomaterials: designing biomimetic materials for cellular engineering. Biomaterials 1999; (20): 2213-2221.

Karajanagi S S, Vertegel A A, Kane R S, Dordick J S. Structure and function of enzymes adsorbed onto single-walled carbon nanotubes. Langmuir 2004; (20): 11594-11599.

Karatas O, Atabey A, Demirdover C, Barutcu A. Delayed prefabricated arterial composite venous flaps: an experimental study in rabbits. Ann Plast Surg 2000; (44): 44-52.

Kasper C S. Histologic features of breast capsules reflect surface configuration and composition of silicone bag implants. Am J Clin Pathol 1994; (102): 655-659.

Katti KS, Mohanty B, Katti DR. Nanomechanical properties of nacre. Materials Research Society 2006; 21: 1237-1245.

Katti D S, Lakshmi S, Langer R, Laurencin C T. Toxicity, biodegradation and elimination of polyanhydrides. Adv Drug Deliv Rev 2002; (54): 933-961.

Katzin W E, Centeno J A, Feng L J, Kiley M, Mullick F G. Pathology of lymph nodes from patients with breast implants: a histologic and spectroscopic evaluation. Am J Surg Pathol 2005; (29): 506-511.

Kawada A, Hiura N, Tajima S, Takahara H. Alginate oligosaccharides stimulate VEGF-mediated growth and migration of human endothelial cells. Arch Dermatol Res 1999; (291): 542-547.

Kawakami Y, Imae I. Functionality and stereochemical design of silicon-containing polymers. Macromolecular Chemistry And Physics 1999; (200): 1245-1256.

Kawakami Y, Li Y, Liu Y, Seino M, Pakjamsai C, Oishi M, Cho YH, Imae I. Control of molecular weight, stereochemistry and higher order structure of siloxane-containing polymers and their functional design. Macromolecular Research 2004; (12): 156-171.

Kenny L C, Bowry A, Crook B, Stancliffe J D. Field testing of a personal size-selective bioaerosol sampler. Ann Occup Hyg 1999; (43): 393-404.

Kent K C, Oshima A, Whittemore A D. Optimal seeding conditions for human endothelial cells. Ann Vasc Surg 1992; (6): 258-264.

Khattab M A, Farr S J, Taylor G, Kellaway I W. The in vitro characterisation and biodistribution of some non-ionic surfactant coated liposomes in the rabbit. J Drug Target 1995; (3): 39-49.

Kidane A G, Salacinski H J, Punshon G, Ramesh B, Srai K S, Seifalian A M. Synthesis and evaluation of amphiphilic RGD derivatives: uses for solvent casting in polymers and tissue engineering applications. Med Biol Eng Comput 2003; (41): 740-745.

Kidd K R, Patula V B, Williams S K. Accelerated endothelialization of interpositional 1-mm vascular grafts. J Surg Res 2003; (113): 234-242.

Kikuchi A, Okuhara M, Karikusa F, Sakurai Y, Okano T. Two-dimensional manipulation of confluently cultured vascular endothelial cells using temperature-responsive poly(N-isopropylacrylamide)-grafted surfaces. J Biomater Sci Polym

Ed 1998; (9): 1331-1348.

Kikuchi A, Okano T. Pulsatile drug release control using hydrogels. Adv Drug Deliv Rev 2002; (54): 53-77.

Kim K, Yu M, Zong X, Chiu J, Fang D, Seo Y S, Hsiao B S, Chu B, Hadjiargyrou M. Control of degradation rate and hydrophilicity in electrospun non-woven poly(D,L-lactide) nanofiber scaffolds for biomedical applications. Biomaterials 2003; (24): 4977-4985.

King B. Suitable dressings for toenail bed wounds: a literature review. J Wound Care 2003; (12): 276-280.

Kingshott P, St John H A, Griesser H J. Direct detection of proteins adsorbed on synthetic materials by matrix-assisted laser desorption ionization-mass spectrometry. Anal Biochem 1999; (273): 156-162.

Kinumi T, Saisu T, Takayama M, Niwa H. Matrix-assisted laser desorption/ionization time-of-flight mass spectrometry using an inorganic particle matrix for small molecule analysis. J Mass Spectrom 2000; (35): 417-422.

Kirby B J, Wheeler A R, Zare R N, Fruetel J A, Shepodd T J. Programmable modification of cell adhesion and zeta potential in silica microchips. Lab Chip 2003; (3): 5-10.

Knorr S D, Combe E C, Wolff L F, Hodges J S. The surface free energy of dental gold-based materials. Dent Mater 2005; (21): 272-277.

Ko I K, Iwata H. An approach to constructing three-dimensional tissue. Ann N Y Acad Sci 2001; (944): 443-455.

Ko T M, Lin J C, Cooper S L. Surface characterization and platelet adhesion studies

of plasma-sulphonated polyethylene. Biomaterials 1993; (14): 657-664.

Kociba KJ. Temperature calibration of TMAs using modulated temperature and Curie temperature reference standards. J Thermal Anal Calorim 2000; (60): 779-784.

Kohler T R, Stratton J R, Kirkman T R, Johansen K H, Zierler B K, Clowes A W. Conventional versus high-porosity polytetrafluoroethylene grafts: clinical evaluation. Surgery 1992; (112): 901-907.

Koller A, Dawant B, Liu A, Popel AS, Johnson PC. Quantitative analysis of arteriolar network architecture in cat sartorius muscle. Am J Physiol 1987; (253): H154-H164.

Kopesky ET, Haddad TS, McKinley GH, Cohen RE. Miscibility and viscoelastic properties of acrylic polyhedral oligomeric silsesquioxane-poly(methyl methacrylate) blends. Polymer 2005; (46): 4743-4752.

Korff T, Augustin H G. Tensional forces in fibrillar extracellular matrices control directional capillary sprouting. J Cell Sci 1999; (112 (Pt 19)): 3249-3258.

Kostakoglu N, Manek S, Green C J. The development of neovascularisation in flap perfabrication with vascular implantation: an experimental study. Br J Plast Surg 1997; (50): 428-434.

Kowligi R R, von Maltzahn W W, Eberhart R C. Fabrication and characterization of small-diameter vascular prostheses. J Biomed Mater Res 1988; (22): 245-256.

Krijgsman B, Seifalian A M, Salacinski H J, Tai N R, Punshon G, Fuller B J, Hamilton G. An assessment of covalent grafting of RGD peptides to the surface of a compliant poly(carbonate-urea)urethane vascular conduit versus conventional biological coatings: its role in enhancing cellular retention. Tissue Eng 2002; (8): 673-680.

Kroll S S, Rosenfield L. Perforator-based flaps for low posterior midline defects. Plast Reconstr Surg 1988; (81): 561-566.

Kroon M E, Van Schie M L, Van D V, Van Hinsbergh V W, Koolwijk P. Collagen type 1 retards tube formation by human microvascular endothelial cells in a fibrin matrix. Angiogenesis 2002; (5): 257-265.

Ku DN, Allen RC. Vascular Grafts. In: The Biomedical Engineering Handbook. (Ed.JD Bronzino). Boca Raton, Florida: CRC Press Inc., 1995; 1st Ed: 1871-1878.

Kuberka M, von Heimburg D, Schoof H, Heschel I, Rau G. Magnification of the pore size in biodegradable collagen sponges. Int J Artif Organs 2002; (25): 67-73.

Kubota Y, Kleinman H K, Martin G R, Lawley T J. Role of laminin and basement membrane in the morphological differentiation of human endothelial cells into capillary-like structures. J Cell Biol 1988; (107): 1589-1598.

Kuo L, Davis M J, Chilian W M. Longitudinal gradients for endothelium-dependent and -independent vascular responses in the coronary microcirculation. Circulation 1995; (92): 518-525.

Kwan AT, Efremov MY, Olson EA. Nanoscale calorimetry of isolated polyethylene single crystals. Polym Sci B Polym Phys 2001; (39): 1237-1245.

L'Heureux N, Paquet S, Labbe R, Germain L, Auger F A. A completely biological tissue-engineered human blood vessel. FASEB J 1998; (12): 47-56.

Labow R S, Santerre J P, Waghray G. The effect of phospholipids on the biodegradation of polyurethanes by lysosomal enzymes. J Biomater Sci Polym Ed 1997; (8): 779-795.

Labow R S, Meek E, Santerre J P. Synthesis of cholesterol esterase by monocyte-

derived macrophages: a potential role in the biodegradation of poly(urethane)s. J Biomater Appl 1999; (13): 187-205.

Lambda NMK, Woodhouse KA, Cooper SL. Polyurethanes in biomedical applications. CRC Publishers, New York 1998.

Lambert A W, Fox A D, Williams D J, Horrocks M, Budd J S. Experience with heparin-bonded collagen-coated grafts for infrainguinal bypass. Cardiovasc Surg 1999; (7): 491-494.

Lateef S S, Boateng S, Hartman T J, Crot C A, Russell B, Hanley L. GRGDSP peptide-bound silicone membranes withstand mechanical flexing in vitro and display enhanced fibroblast adhesion. Biomaterials 2002; (23): 3159-3168.

Lau H, Cheng S W. Is the preferential use of ePTFE grafts in femorofemoral bypass justified? Ann Vasc Surg 2001; (15): 383-387.

Laube H R, Duwe J, Rutsch W, Konertz W. Clinical experience with autologous endothelial cell-seeded polytetrafluoroethylene coronary artery bypass grafts. J Thorac Cardiovasc Surg 2000; (120): 134-141.

Laurencin C T, Pierre-Jacques H M, Langer R. Toxicology and biocompatibility considerations in the evaluation of polymeric materials for biomedical applications. Clin Lab Med 1990; (10): 549-570.

Lee A, Xiao J, Feher FJ. New approach in the synthesis of hybrid polymers grafted with polyhedral oligomeric silsesquioxane and their physical and viscoelastic properties. Macromolecules 2005; (38): 438-444.

Lee HB, Kim SS, Khang G. Polymers used as biomaterials. In: The Biomedical Engineering Handbook. (Ed.JD Bronzino). Boca Raton CRC, 1995; 1st: 580-591.

Lee JS, Skalak TC. Microvascular Mechanics. Springer-Verlag, New York 1989.

Lee LT, Jha BK, Malmsten M, Holmberg K. Lipase-surfactant interactions studied by neutron reflectivity and ellipsometry. J Phy Chem 1999; (103): 7489.

Lee S, Sutton D, Fenster M, Schmid-Schonbein GW. Biomechanical model for skeletal muscle microcirculation with reference to red and white blood cell perfusion and autoregulation. In: Cell Mechanics and Cellular Engineering. (Eds.Mow VC, Guilak F, Transon-Tay, Hochmuth RM). New York: Springer-Verlag, 1994; 534-564.

Lee YJ, Kuo SW, Huang WJ, Lee HY, Chang FC. Miscibility, Specific Interactions and Self-Assembly Behavior of Phenolic/Polyhedral Oligomeric Silsesquioxane Hybrids. Journal of Polymer Science: Part B: Polymer Physics 2004; (42): 1127-1136.

Lee YJ, Huang JM, Kuo SW, Lu JS, Chang FC. Polyimide and polyhedral oligomeric silsesquioxane nanocomposites for low-dielectric applications. Polymer 2005; (46): 173-181.

Lee A, Lichtenhan J D. Viscoelastic Responses of Polyhedral Oligosilsesquioxane Reinforced Epoxy Systems. Macromolecules 1998; (31): 4970-4974.

Lee G, Arscott P G, Bloomfield V A, Evans D F. Scanning tunneling microscopy of nucleic acids. Science 1989; (244): 475-477.

Lee J H, Jung H W, Kang I K, Lee H B. Cell behaviour on polymer surfaces with different functional groups. Biomaterials 1994; (15): 705-711.

Lee J H, Lee J W, Khang G, Lee H B. Interaction of cells on chargeable functional group gradient surfaces. Biomaterials 1997; (18): 351-358.

Lee J W, Gardella J A, Jr. Quantitative TOF-SIMS analysis of oligomeric degradation products at the surface of biodegradable poly(alpha-hydroxy acid)s. J Am Soc Mass Spectrom 2002; (13): 1108-1119.

Lee S H, Pumprueg S, Moudgil B, Sigmund W. Inactivation of bacterial endospores by photocatalytic nanocomposites. Colloids Surf B Biointerfaces 2005; (40): 93-98.

Lehle K, Buttstaedt J, Birnbaum D E. Expression of adhesion molecules and cytokines in vitro by endothelial cells seeded on various polymer surfaces coated with titaniumcarboxonitride. J Biomed Mater Res 2003; (65A): 393-401.

Lehmann K, Muller-Glauser W, Bittmann P, Bay U, Dittes P, von Segesser L, Turina M. [Development of a small-lumen vascular prosthesis coated with autologous endothelial cells]. Helv Chir Acta 1989; (56): 39-43.

Lelah MD, Cooper SL. Polyurethanes in medicine. CRC Press, Boca Raton, FL 1986.

Lenza R F, Jones J R, Vasconcelos W L, Hench L L. In vitro release kinetics of proteins from bioactive foams. J Biomed Mater Res 2003; (67A): 121-129.

Lesesne C B. Textured surface silicone breast implants: histology in the human. Aesthetic Plast Surg 1997; (21): 93-96.

Leu CM, Chang YT, Wei KH. Polyimide-side-chain tethered polyhedral oligomeric silsesquioxane nanocomposites for low-dielectric film applications. Chem Mater 2005; (15): 3721-3727.

Levick J R, ed. An introduction to cardiovascular physiology. 3rd edition Arnold, (London) 2003.

Levick J R. Flow through interstitium and other fibrous matrices. Q J Exp Physiol 1987; (72): 409-437.

Levine D W, Simmons B P, Koris M J, Daltroy L H, Hohl G G, Fossel A H, Katz J N. A self-administered questionnaire for the assessment of severity of symptoms and functional status in carpal tunnel syndrome. J Bone Joint Surg Am 1993; (75): 1585-1592.

Lewis A L, Hughes P D, Kirkwood L C, Leppard S W, Redman R P, Tolhurst L A, Stratford P W. Synthesis and characterisation of phosphorylcholine-based polymers useful for coating blood filtration devices. Biomaterials 2000; (21): 1847-1859.

Lewis G, Daniels A U. Use of isothermal heat-conduction microcalorimetry (IHCMC) for the evaluation of synthetic biomaterials. J Biomed Mater Res 2003; (66B): 487-501.

Lhoest J B, Wagner M S, Tidwell C D, Castner D G. Characterization of adsorbed protein films by time of flight secondary ion mass spectrometry. J Biomed Mater Res 2001; (57): 432-440.

Li GZ, Wang LC, Toghiani H, Daulton TL, Koyama K, Pittman CU. Viscoelastic and mechanical properties of epoxy/multifunctional polyhedral oligomeric silsesquioxane nanocomposites and epoxy/ladderlike polyphenylsilsesquioxane blends. Macromolecules 2001; (34): 8686-8693.

Li GZ, Cho H, Wang LC, Toghiani H, Pittman CU. Synthesis and properties of poly(isobutyl methacrylateco-butanediol dimethacrylate-co-methacryl polyhedral oligomeric silsesquioxane) nanocomposites. J Polym Sci Pt A - Polym Chem 2005; (43): 355-372.

Li J, Ng H T, Chen H. Carbon nanotubes and nanowires for biological sensing. Methods Mol Biol 2005; (300): 191-224.

Li Y, Ma T, Yang S T, Kniss D A. Thermal compression and characterization of

three-dimensional nonwoven PET matrices as tissue engineering scaffolds. Biomaterials 2001; (22): 609-618.

Li Y, Neoh K G, Cen L, Kang E T. Physicochemical and blood compatibility characterization of polypyrrole surface functionalized with heparin. Biotechnol Bioeng 2003; (84): 305-313.

Lichtenhan JD. Polyhedral oligomeric silsesquioxanes - building blocks for silsesquioxane-based polymers and hybrid materials. Comments on Inorganic chemistry 1995; (17): 115-130.

Lim F, Yang C Z, Cooper S L. Synthesis, characterization and ex vivo evaluation of polydimethylsiloxane polyurea-urethanes. Biomaterials 1994; (15): 408-416.

Lin P H, Bush R L, Yao Q, Lumsden A B, Chen C. Evaluation of platelet deposition and neointimal hyperplasia of heparin-coated small-caliber ePTFE grafts in a canine femoral artery bypass model. J Surg Res 2004; (118): 45-52.

Lindner V, Maciag T. The putative convergent and divergent natures of angiogenesis and arteriogenesis. Circ Res 2001; (89): 747-749.

Lindon J N, McManama G, Kushner L, Merrill E W, Salzman E W. Does the conformation of adsorbed fibrinogen dictate platelet interactions with artificial surfaces? Blood 1986; (68): 355-362.

Linn T, Erb D, Schneider D, Kidszun A, Elcin A E, Bretzel R G, Elcin Y M. Polymers for induction of revascularization in the rat fascial flap: application of vascular endothelial growth factor and pancreatic islet cells. Cell Transplant 2003; (12): 769-778.

Lipowsky HH, Kovalcheck S, ZweifachBW. The distribution of blood rheological parameters in the microvasculature of cat mesentery. Circ Res 1978; (43): 738-749.

Liu HZ, Zheng SX. Polyurethane networks nanoreinforced by polyhedral oligorneric silsesquioxane. Macromol Rapid Comm 2005; (26): 196-200.

Liu Y, Shigley JE. Iridescence color of a shell of the mollusk Pinctada Margaritifera caused by diffraction. Optics Express 1999; (4): 177-182.

Liu J C, Heilshorn S C, Tirrell D A. Comparative cell response to artificial extracellular matrix proteins containing the RGD and CS5 cell-binding domains. Biomacromolecules 2004; (5): 497-504.

Liu L G. [A preliminary study of the fibrous capsules around silicone mammary implants in Chinese women]. *Zhonghua Zheng Xing Shao Shang Wai Ke Za Zhi* 1992; (8): 174-6, 246.

Liu Y L, Hsu C Y, Su Y H, Lai J Y. Chitosan-silica complex membranes from sulfonic acid functionalized silica nanoparticles for pervaporation dehydration of ethanol-water solutions. Biomacromolecules 2005; (6): 368-373.

Lo H, Kadiyala S, Guggino S E, Leong K W. Poly(L-lactic acid) foams with cell seeding and controlled-release capacity. J Biomed Mater Res 1996; (30): 475-484.

Lou S, Gu P, Chen F, He C, Wang M, Lu C. The effect of bone marrow stromal cells on neuronal differentiation of mesencephalic neural stem cells in Sprague-Dawley rats. Brain Res 2003; (968): 114-121.

Lu JR, Li ZX, Smallwood J, Thomas RK, Penfold J. Detailed structure of the hydrocarbon chain in a surfactant monolayer at the air-water interface from complex mixtures, measured by specular neutron reflection. J Phys Chem 1995; (99): 8233.

Lu L, Peter S J, Lyman M D, Lai H L, Leite S M, Tamada J A, Vacanti J P, Langer R, Mikos A G. In vitro degradation of porous poly(L-lactic acid) foams. Biomaterials 2000; (21): 1595-1605.

Lu L, Peter S J, Lyman M D, Lai H L, Leite S M, Tamada J A, Uyama S, Vacanti J P, Langer R, Mikos A G. In vitro and in vivo degradation of porous poly(DL-lactic-co-glycolic acid) foams. Biomaterials 2000; (21): 1837-1845.

Lucke A, Tessmar J, Schnell E, Schmeer G, Gopferich A. Biodegradable poly(D,L-lactic acid)-poly(ethylene glycol)-monomethyl ether diblock copolymers: structures and surface properties relevant to their use as biomaterials. Biomaterials 2000; (21): 2361-2370.

Luke J L, Kalasinsky V F, Turnicky R P, Centeno J A, Johnson F B, Mullick F G. Pathological and biophysical findings associated with silicone breast implants: a study of capsular tissues from 86 cases. Plast Reconstr Surg 1997; (100): 1558-1565.

Lumsden A B, Chen C, Coyle K A, Ofenloch J C, Wang J H, Yasuda H K, Hanson S R. Nonporous silicone polymer coating of expanded polytetrafluoroethylene grafts reduces graft neointimal hyperplasia in dog and baboon models. J Vasc Surg 1996; (24): 825-833.

Lutolf M P, Lauer-Fields J L, Schmoekel H G, Metters A T, Weber F E, Fields G B, Hubbell J A. Synthetic matrix metalloproteinase-sensitive hydrogels for the conduction of tissue regeneration: engineering cell-invasion characteristics. Proc Natl Acad Sci U S A 2003; (100): 5413-5418.

Lyman D J, Murray-Wijelath J, Ambrad-Chalela E, Wijelath E S. Vascular graft healing. II. FTIR analysis of polyester graft samples from implanted bi-grafts. J Biomed Mater Res 2001; (58): 221-237.

Lyn D, Liu X, Bennett N A, Emmett N L. Gene expression profile in mouse myocardium after ischemia. Physiol Genomics 2000; (2): 93-100.

Ma P X, Zhang R. Synthetic nano-scale fibrous extracellular matrix. J Biomed Mater

Res 1999; (46): 60-72.

Ma P X, Choi J W. Biodegradable polymer scaffolds with well-defined interconnected spherical pore network. Tissue Eng 2001; (7): 23-33.

Ma T, Li Y, Yang S T, Kniss D A. Tissue engineering human placenta trophoblast cells in 3-D fibrous matrix: spatial effects on cell proliferation and function. Biotechnol Prog 1999; (15): 715-724.

Macey A C, Burke F D, Abbott K, Barton N J, Bradbury E, Bradley A, Bradley M J, Brady O, Burt A, Brown P. Outcomes of hand surgery. British Society for Surgery of the Hand. J Hand Surg [Br] 1995; (20): 841-855.

Maciejewski M. Computational aspects of kinetic analysis Part B: The ICTAC kinetics project - the decomposition kinetics of calcium carbonate revisited, or some tips on survival in the kinetic minefield. Thermochim Acta 2000; (355): 145-154.

Magoshi T, Matsuda T. Formation of polymerized mixed heparin/albumin surface layer and cellular adhesional responses. Biomacromolecules 2002; (3): 976-983.

Malmsten M, Burns N, Veide A. Electrostatic and Hydrophobic Effects of Oligopeptide Insertions on Protein Adsorption. J Colloid Interface Sci 1998; (204): 104-111.

Maquet V, Boccaccini A R, Pravata L, Notingher I, Jerome R. Preparation, characterization, and in vitro degradation of bioresorbable and bioactive composites based on Bioglass-filled polylactide foams. J Biomed Mater Res 2003; (66A): 335-346.

Marcolli C, Calzaferri G. Monosubstituted octasilasesquioxanes. Appl Organomet Chem 1999; (13): 213.

Mark JE, Erman B. Rubber-like elasticity. A molecular primer. Wiley-Interscience, New York 1998.

Mark JE. Some Unusual Elastomers and Experiments on Rubber-like Elasticity. Prog Polym Sci 2003; (28): 1205-1221.

Mark JE. Some Recent Theory, Experiments and Simulations on Rubberlike Elasticity. J Phys Chem B 2003; (107): 903-913.

Mark J E. Some interesting things about polysiloxanes. Acc Chem Res 2004; (37): 946-953.

Marler J J, Guha A, Rowley J, Koka R, Mooney D, Upton J, Vacanti J P. Soft-tissue augmentation with injectable alginate and syngeneic fibroblasts. Plast Reconstr Surg 2000; (105): 2049-2058.

Martin D J, Warren L A, Gunatillake P A, McCarthy S J, Meijs G F, Schindhelm K. Polydimethylsiloxane/polyether-mixed macrodiol-based polyurethane elastomers: biostability. Biomaterials 2000; (21): 1021-1029.

Massia S P, Stark J. Immobilized RGD peptides on surface-grafted dextran promote biospecific cell attachment. J Biomed Mater Res 2001; (56): 390-399.

Masuda H, Asahara T. Post-natal endothelial progenitor cells for neovascularization in tissue regeneration. Cardiovasc Res 2003; (58): 390-398.

Mata A, Fleischman AJ, Roy S. Characterization of polydimethylsiloxane (PDMS) properties for biomedical micro/nanosystems. Biomed Microdevices 2005; (7): 281-293.

Mathot VBF. New routes for thermal analysis and calorimetry as applied to polymeric systems. J Thermal Anal Calorim 2001; (64): 15-35.

Mathur A B, Collier T O, Kao W J, Wiggins M, Schubert M A, Hiltner A, Anderson J M. In vivo biocompatibility and biostability of modified polyurethanes. J Biomed Mater Res 1997; (36): 246-257.

Matsuda T, Akutsu T, Kira K, Matsumoto H. Development of hybrid compliant graft: rapid preparative method for reconstruction of a vascular wall. ASAIO Trans 1989; (35): 553-555.

Matsuda T, Nakayama Y. Surface microarchitectural design in biomedical applications: in vitro transmural endothelialization on microporous segmented polyurethane films fabricated using an excimer laser. J Biomed Mater Res 1996; (31): 235-242.

Maxim N, Magusin PCMM, Kooyman PJ, van Wolput JHMC, van Santen RA, Abbenhuis HCL. Microporous Mg-Si-O and Al-Si-O materials derived from metal silsesquioxanes. Mater Chem 2001; (13): 2958-2964.

McAnally G D, Everall N J, Chalmers J M, Smith W E. Analysis of thin film coatings on poly(ethylene terephthalate) by confocal Raman microscopy and surface-enhanced Raman scattering. Appl Spectrosc 2003; (57): 44-50.

McCarthy D J, Chapman H L. Ultrastructure of collapsed metatarsophalangeal silicone elastomer implant. J Foot Surg 1988; (27): 418-427.

McDowell F. Plastic surgery in the twentieth century. Ann Plast Surg 1978; (1): 217-224.

McGregor IA, McGregor AD. Fundamental techniques of plastic surgery. Churchill Livingstone, Edinburgh 1995.

Meijs G F, McCarthy S J, Rizzardo E, Chen Y C, Chatelier R C, Brandwood A,

Schindhelm K. Degradation of medical-grade polyurethane elastomers: the effect of hydrogen peroxide in vitro. J Biomed Mater Res 1993; (27): 345-356.

Meinhart J, Deutsch M, Zilla P. Eight years of clinical endothelial cell transplantation. Closing the gap between prosthetic grafts and vein grafts. ASAIO J 1997; (43): M515-M521.

Meinhart J G, Deutsch M, Fischlein T, Howanietz N, Froschl A, Zilla P. Clinical autologous in vitro endothelialization of 153 infrainguinal ePTFE grafts. Ann Thorac Surg 2001; (71): S327-S331.

Mena E A, Kossovsky N, Chu C, Hu C. Inflammatory intermediates produced by tissues encasing silicone breast prostheses. J Invest Surg 1995; (8): 31-42.

Meneghetti P, Qutubuddin S. Synthesis of poly(methyl methaerylate) nanocomposites via emulsion polymerization using a zwitterionic surfactant. Langmuir 2004; (20): 3424-3430.

Meng G, Cao A, Cheng J Y, Ajayan P M. Carbon nanotubes grafted on silicon oxide nanowires. J Nanosci Nanotechnol 2004; (4): 712-715.

Merkel T C, Freeman B D, Spontak R J, He Z, Pinnau I, Meakin P, Hill A J. Ultrapermeable, reverse-selective nanocomposite membranes. Science 2002; (296): 519-522.

Merrett K, Cornelius R M, McClung W G, Unsworth L D, Sheardown H. Surface analysis methods for characterizing polymeric biomaterials. J Biomater Sci Polym Ed 2002; (13): 593-621.

Merzkirch C, Davies N, Zilla P. Engineering of vascular ingrowth matrices: are protein domains an alternative to peptides? Anat Rec 2001; (263): 379-387.

Merzlyakov MJ, Schick C. Optimization of experimental parameters in TMDSC - The influence of non-linear and non-stationery thermal response. J Thermal Anal Calorim 2000; (61): 649-659.

Middleton J C, Tipton A J. Synthetic biodegradable polymers as orthopedic devices. Biomaterials 2000; (21): 2335-2346.

Migita H, Satozawa N, Lin J H, Morser J, Kawai K. RORalpha1 and RORalpha4 suppress TNF-alpha-induced VCAM-1 and ICAM-1 expression in human endothelial cells. FEBS Lett 2004; (557): 269-274.

Mikos A G, Sarakinos G, Leite S M, Vacanti J P, Langer R. Laminated three-dimensional biodegradable foams for use in tissue engineering. Biomaterials 1993; (14): 323-330.

Mikos A G, Lyman M D, Freed L E, Langer R. Wetting of poly(L-lactic acid) and poly(DL-lactic-co-glycolic acid) foams for tissue culture. Biomaterials 1994; (15): 55-58.

Min S X, Jin A M, Tong B H, Zhu L X, Tian J. Three-dimensional porous poly-DL-lactide/basic fibroblast growth factor composites for bone defect repair: an experimental study. *Di Yi Jun Yi Da Xue Xue Bao* 2003; (23): 318-322.

Mironov V, Boland T, Trusk T, Forgacs G, Markwald R R. Organ printing: computer-aided jet-based 3D tissue engineering. Trends Biotechnol 2003; (21): 157-161.

Mirzadeh H, Katbab A A, Khorasani M T, Burford R P, Gorgin E, Golestani A. Cell attachment to laser-induced AAm- and HEMA-grafted ethylene-propylene rubber as biomaterial: in vivo study. Biomaterials 1995; (16): 641-648.

Mitchell S L, Niklason L E. Requirements for growing tissue-engineered vascular grafts. Cardiovasc Pathol 2003; (12): 59-64.

Miwa H, Matsuda T, Tani N, Kondo K, Iida F. An in vitro endothelialized compliant vascular graft minimizes anastomotic hyperplasia. ASAIO J 1993; (39): M501-M505.

Miyamoto K, Sugimoto T, Okada M, Maeda S. Experimental studies on application of small-caliber vascular prosthesis produced by polyurethane. Ann Thorac Cardiovasc Surg 1999; (5): 174-181.

Moerman R, Frank J, Marijnissen J C, Schalkhammer T G, Van Dedem G W. Miniaturized electrospraying as a technique for the production of microarrays of reproducible micrometer-sized protein spots. Anal Chem 2001; (73): 2183-2189.

Moiemen N S, Staiano J J, Ojeh N O, Thway Y, Frame J D. Reconstructive surgery with a dermal regeneration template: clinical and histologic study. Plast Reconstr Surg 2001; (108): 93-103.

Moldovan N I, Goldschmidt-Clermont P J, Parker-Thornburg J, Shapiro S D, Kolattukudy P E. Contribution of monocytes/macrophages to compensatory neovascularization: the drilling of metalloelastase-positive tunnels in ischemic myocardium. Circ Res 2000; (87): 378-384.

Moldovan N I, Ferrari M. Prospects for microtechnology and nanotechnology in bioengineering of replacement microvessels. Arch Pathol Lab Med 2002; (126): 320-324.

Montanez E, Casaroli-Marano R P, Vilaro S, Pagan R. Comparative study of tube assembly in three-dimensional collagen matrix and on Matrigel coats. Angiogenesis 2002; (5): 167-172.

Montesano R, Orci L, Vassalli P. In vitro rapid organization of endothelial cells into capillary-like networks is promoted by collagen matrices. J Cell Biol 1983; (97): 1648-1652.

Montesano R, Vassalli J D, Baird A, Guillemin R, Orci L. Basic fibroblast growth factor induces angiogenesis in vitro. Proc Natl Acad Sci U S A 1986; (83): 7297-7301.

Montesano R, Orci L. Phorbol esters induce angiogenesis in vitro from large-vessel endothelial cells. J Cell Physiol 1987; (130): 284-291.

Montesano R, Pepper M S, Vassalli J D, Orci L. Phorbol ester induces cultured endothelial cells to invade a fibrin matrix in the presence of fibrinolytic inhibitors. J Cell Physiol 1987; (132): 509-516.

Mooney D J, Baldwin D F, Suh N P, Vacanti J P, Langer R. Novel approach to fabricate porous sponges of poly(D,L-lactic-co-glycolic acid) without the use of organic solvents. Biomaterials 1996; (17): 1417-1422.

Moreau J J, Vellutini L, Wong Chi M M, Bied C. Shape-controlled bridged silsesquioxanes: hollow tubes and spheres. Chemistry 2003; (9): 1594-1599.

Moreau J J, Vellutini L, Wong Chi M M, Bied C, Dieudonne P, Bantignies J L, Sauvajol J L. Lamellar Bridged Silsesquioxanes: Self-Assembly through a Combination of Hydrogen Bonding and Hydrophobic Interactions. Chemistry 2005; (11): 1527-1537.

Morozov V N, Seeman N C, Kallenbach N R. New methods for depositing and imaging molecules in scanning tunneling microscopy. Scanning Microsc 1993; (7): 757-776.

Motwani J G, Topol E J. Aortocoronary saphenous vein graft disease: pathogenesis, predisposition, and prevention. Circulation 1998; (97): 916-931.

Moussatov A, Ayrault C, Castagnede B. Porous material characterization--ultrasonic method for estimation of tortuosity and characteristic length using a barometric chamber. Ultrasonics 2001; (39): 195-202.

Mrksich M, Sigal B. Surface plasmon resonance permits in sit measurement of protein adsorption on self-assembled monolayers of alkanethiolates on gold. Langmuir 1995; 11: 4383-4385.

Muggli D S, Burkoth A K, Anseth K S. Crosslinked polyanhydrides for use in orthopedic applications: degradation behavior and mechanics. J Biomed Mater Res 1999; (46): 271-278.

Muller B, Riedel M, Michel R, De Paul SM, Hofer R, Heger D, Grutzmacher D. Impact of nanometer-scale roughness on contact-angle hysteresis and globulin adsorption. J Vac Sci Technol B 2001; (19.5): 1715-1720.

Muller M, Werner C, Grudke K, Eichhorn KJ, Jacobasch HJ. Spectroscopic and thermodynamic characterisation of the adsorption of plasma proteins onto cellulosic substrates. Macromol Symp 103, 55-72. 1996. (Abstract)

Muller G H. [Breast implants and their history]. Ann Chir Plast Esthet 1996; (41): 666-675.

Munk O L, Keiding S, Bass L. Capillaries within compartments: microvascular interpretation of dynamic positron emission tomography data. J Theor Biol 2003; (225): 127-141.

Murohara T, Ikeda H, Duan J, Shintani S, Sasaki K, Eguchi H, Onitsuka I, Matsui K, Imaizumi T. Transplanted cord blood-derived endothelial precursor cells augment postnatal neovascularization. J Clin Invest 2000; (105): 1527-1536.

Murohara T. Therapeutic vasculogenesis using human cord blood-derived endothelial progenitors. Trends Cardiovasc Med 2001; (11): 303-307.

Murray-Wijelath J, Lyman D J, Wijelath E S. Vascular graft healing. III. FTIR analysis of ePTFE graft samples from implanted bigrafts. J Biomed Mater Res

2004; (70B): 223-232.

Muschler G F, Midura R J. Connective tissue progenitors: practical concepts for clinical applications. Clin Orthop 2002;66-80.

Nagasawa A, Kitano T, Watanabe T, Fujisawa K. Control of surface free energy for surface modification by using photo-curable resin and surface modifier. Sen-I-Gakkaishi 2004; (60): 183-187.

Naka K, Itoh H, Park SY, Chujo Y. Synthesis of nanocomposites of metal nanoparticles utilizing miscible polymers. Polym Bulletin 2004; (52): 171-176.

Nakamura K, KInoshita E, Hatakeyama T. Thermal measurement of swelling behaviour of polysaccharide hydrogels. K Thermochim Acta 2000;352-353.

Nakao H, Hyon S H, Tsutsumi S, Matsumoto T, Takahashi J. Control of pore size in L-lactide/epsilon-caprolactone copolymer foams for tissue regeneration by the freeze-drying method. Dent Mater J 2003; (22): 262-271.

Nam Y S, Park T G. Biodegradable polymeric microcellular foams by modified thermally induced phase separation method. Biomaterials 1999; (20): 1783-1790.

Neal C R, Bates D O. Measurement of hydraulic conductivity of single perfused Rana mesenteric microvessels between periods of controlled shear stress. J Physiol 2002; (543): 947-957.

Nehls V, Herrmann R. The configuration of fibrin clots determines capillary morphogenesis and endothelial cell migration. Microvasc Res 1996; (51): 347-364.

Neumann T, Nicholson B S, Sanders J E. Tissue engineering of perfused microvessels. Microvasc Res 2003; (66): 59-67.

Ng S Y, Vandamme T, Taylor M S, Heller J. Controlled drug release from self-catalyzed poly(ortho esters). Ann N Y Acad Sci 1997; (831): 168-178.

Nguyen K T, West J L. Photopolymerizable hydrogels for tissue engineering applications. Biomaterials 2002; (23): 4307-4314.

Nichter L S, Morgan R F, Nichter M A. The impact of Indian methods for total nasal reconstruction. Clin Plast Surg 1983; (10): 635-647.

Nicosia R F, Ottinetti A. Modulation of microvascular growth and morphogenesis by reconstituted basement membrane gel in three-dimensional cultures of rat aorta: a comparative study of angiogenesis in matrigel, collagen, fibrin, and plasma clot. In Vitro Cell Dev Biol 1990; (26): 119-128.

Nishino T, Meguro M, Nakamae K. Poly(vinyl alcohol) with low surface free energy by fluorination. International Journal of Adhesion and Adhesives 1999; (19): 399-403.

Nishino T, Urushihara Y, Meguro M, Nakamae K. Surface properties and structures of diblock and random copolymers with perfluoroalkyl side chains. J Colloid Interface Sci 2004; (279): 364-369.

Nitschke M, Schmack G, Janke A, Simon F, Pleul D, Werner C. Low pressure plasma treatment of poly(3-hydroxybutyrate): toward tailored polymer surfaces for tissue engineering scaffolds. J Biomed Mater Res 2002; (59): 632-638.

Nor J E, Peters M C, Christensen J B, Sutorik M M, Linn S, Khan M K, Addison C L, Mooney D J, Polverini P J. Engineering and characterization of functional human microvessels in immunodeficient mice. Lab Invest 2001; (81): 453-463.

Norquist J M, Fitzpatrick R, Dawson J, Jenkinson C. Comparing Alternative Rasch-Based Methods vs Raw Scores in Measuring Change in Health. Med Care 2004; (42): I-I2536.

Notingher I, Imhof R E, Xiao P, Pascut F C. Spectral depth profiling of arbitrary surfaces by thermal emission decay-Fourier transform infrared spectroscopy. Appl Spectrosc 2003; (57): 1494-1501.

Novak B. Hybrid Nanocomposite Materials - Between Inorganic Glasses and Organic Polymers. Advanced Materials 1993; (5): 422.

Nyilas E, Ward R S, Jr. Development of blood-compatible elastomers. V. Surface structure and blood compatibility of avcothane elastomers. J Biomed Mater Res 1977; (11): 69-84.

O'Brien WJ. Dental materials and their selection. Quintessence Publishing Co., Chicago 1997.

Oaten M, Choudhury NR. Silsesquioxane-urethane hybrid for thin film applications. Macromolecules 2005; (38): 6392-6401.

Ochoa E R, Vacanti J P. An overview of the pathology and approaches to tissue engineering. Ann N Y Acad Sci 2002; (979): 10-26.

Ogawa R, Iwasaki Y, Ishihara K. Thermal property and processability of elastomeric polymer alloy composed of segmented polyurethane and phospholipid polymer. J Biomed Mater Res 2002; (62): 214-221.

Okoshi T, Soldani G, Goddard M, Galletti P M. Very small-diameter polyurethane vascular prostheses with rapid endothelialization for coronary artery bypass grafting. J Thorac Cardiovasc Surg 1993; (105): 791-795.

Olander J V, Bremer M E, Marasa J C, Feder J. Fibrin-enhanced endothelial cell organization. J Cell Physiol 1985; (125): 1-9.

Oleinikov V A, Feofanov A V, Shiian S D, Tuzikov A B, Kriukov E I, Ianul' A I, Bovin N B, Nabiev I R. [Surface enhanced Raman spectroscopy for characterization of structural characteristics of carbon chains in alpha1-acid glycoprotein and pseudoglycoproteins]. Bioorg Khim 1998; (24): 412-421.

Olivieri M P, Tweden K S. Human serum albumin and fibrinogen interactions with an adsorbed RGD-containing peptide. J Biomed Mater Res 1999; (46): 355-359.

Olson EA, Efremov MY, Kwan AT. Scanning calorimeter for nanoliter-scale liquid samples. Appl Phys Lett 2000; (77): 2671-2673.

Oulevey F, Burnham NA, Gremaud G. Dynamic mechanical analysis at the submicron scale. Polymer 2000; (41): 3087-3092.

Ouyang T, Guo E, Zhang M. [Experimental study on vascularized area of the prefabricated axial skin flap after implantation of vascular bundles]. *Zhonghua Zheng Xing Shao Shang Wai Ke Za Zhi* 1996; (12): 326-329.

Ozawa T. Thermal analysis-review and prospect. Thermochim Acta 2000; (355): 35-42.

Pacheco F, Gonzalez M, Medina A, Velumani S, Ascencio JA. Structural analysis of cobalt titanate nanoparticles obtained by sol-gel process. Appl Phys A-Mat Sci Proc 2004; (78): 531-536.

Painter PC, Pehlert GJ, Hu YH, Coleman MM. Infrared band broadening and interactions in polar systems. Macromolecules 1999; (32): 2055-2057.

Pal M, Bid S, Pradhan SK, Nath BK, Das D, Chakravorty D. Synthesis of nanocomposites comprising iron and barium hexaferrites. J Magnetism Magnetic Mat 2004; (269): 42-47.

Pan G, Mark JE, Schaefer DW. Synthesis and Characterization of Fillers of Controlled Structure Based on POSS cages and Their Use in Reinforcing Silicone Elastomers. J Polym Sci Polym Phys Ed 2003; (41): 3314-3323.

Park H D, Lee W K, Ooya T, Park K D, Kim Y H, Yui N. In vitro biocompatibility assessment of sulfonated polyrotaxane-immobilized polyurethane surfaces. J Biomed Mater Res 2003; (66A): 596-604.

Park J C, Park B J, Lee D H, Suh H, Kim D G, Kwon O H. Evaluation of the cytotoxicity of polyetherurethane (PU) film containing zinc diethyldithiocarbamate (ZDEC) on various cell lines. Yonsei Med J 2002; (43): 518-526.

Park J H, Park K D, Bae Y H. PDMS-based polyurethanes with MPEG grafts: synthesis, characterization and platelet adhesion study. Biomaterials 1999; (20): 943-953.

Park J H, Bae Y H. Hydrogels based on poly(ethylene oxide) and poly(tetramethylene oxide) or poly(dimethyl siloxane): synthesis, characterization, in vitro protein adsorption and platelet adhesion. Biomaterials 2002; (23): 1797-1808.

Park Y D, Tirelli N, Hubbell J A. Photopolymerized hyaluronic acid-based hydrogels and interpenetrating networks. Biomaterials 2003; (24): 893-900.

Pasic M, Muller-Glauser W, von Segesser L K, Lachat M, Mihaljevic T, Turina M I. Superior late patency of small-diameter Dacron grafts seeded with omental microvascular cells: an experimental study. Ann Thorac Surg 1994; (58): 677-683.

Patrick C W, Jr., Chauvin P B, Hobley J, Reece G P. Preadipocyte seeded PLGA scaffolds for adipose tissue engineering. Tissue Eng 1999; (5): 139-151.

Payne M P, Kenny L C. Comparison of models for the estimation of biological partition coefficients. J Toxicol Environ Health A 2002; (65): 897-931.

Pego A P, Van Luyn M J, Brouwer L A, Van Wachem P B, Poot A A, Grijpma D W, Feijen J. In vivo behavior of poly(1,3-trimethylene carbonate) and copolymers of 1,3-trimethylene carbonate with D,L-lactide or epsilon-caprolactone: Degradation and tissue response. J Biomed Mater Res 2003; (67A): 1044-1054.

Pego A P, Siebum B, Van Luyn M J, Van Seijen X J, Poot A A, Grijpma D W, Feijen J. Preparation of degradable porous structures based on 1,3-trimethylene carbonate and D,L-lactide (co)polymers for heart tissue engineering. Tissue Eng 2003; (9): 981-994.

Peirce S M, Skalak T C. Microvascular remodeling: a complex continuum spanning angiogenesis to arteriogenesis. Microcirculation 2003; (10): 99-111.

Pelletier L, Angonin R, Regnard J, Fellmann D, Charbord P. Human bone marrow angiogenesis: in vitro modulation by substance P and neurokinin A. Br J Haematol 2002; (119): 1083-1089.

Pennisi V R. Long-term use of polyurethane breast prostheses: a 14-year experience. Plast Reconstr Surg 1990; (86): 368-371.

Perez-Luna V H, Horbett T A, Ratner B D. Developing correlations between fibrinogen adsorption and surface properties using multivariate statistics. Student Research Award in the Doctoral Degree Candidate Category, 20th annual meeting of the Society for Biomaterials, Boston, MA, April 5-9, 1994. J Biomed Mater Res 1994; (28): 1111-1126.

Perktold K, Leuprecht A, Prosi M, Berk T, Czerny M, Trubel W, Schima H. Fluid dynamics, wall mechanics, and oxygen transfer in peripheral bypass anastomoses. Ann Biomed Eng 2002; (30): 447-460.

Peter S J, Yaszemski M J, Suggs L J, Payne R G, Langer R, Hayes W C, Unroe M R, Alemany L B, Engel P S, Mikos A G. Characterization of partially saturated poly(propylene fumarate) for orthopaedic application. J Biomater Sci Polym Ed 1997; (8): 893-904.

Peter S J, Miller S T, Zhu G, Yasko A W, Mikos A G. In vivo degradation of a poly(propylene fumarate)/beta-tricalcium phosphate injectable composite scaffold. J Biomed Mater Res 1998; (41): 1-7.

Peters W, Smith D, Lugowski S, McHugh A, MacDonald P, Baines C. Silicon and silicone levels in patients with silicone implants. Curr Top Microbiol Immunol 1996; (210): 39-48.

Peters W, Smith D, Lugowski S, Pritzker K, Holmyard D. Calcification properties of saline-filled breast implants. Plast Reconstr Surg 2001; (107): 356-363.

Pignataro B, Conte E, Scandurra A, Marletta G. Improved cell adhesion to ion beam-irradiated polymer surfaces. Biomaterials 1997; (18): 1461-1470.

Piiper J, Scheid P. Cross-sectional PO2 distributions in Krogh cylinder and solid cylinder models. Respir Physiol 1986; (64): 241-251.

Pinchuk L. A review of the biostability and carcinogenicity of polyurethanes in medicine and the new generation of 'biostable' polyurethanes. J Biomater Sci Polym Ed 1994; (6): 225-267.

Pocock T M, Bates D O. In vivo mechanisms of vascular endothelial growth factor-mediated increased hydraulic conductivity of Rana capillaries. J Physiol 2001; (534): 479-488.

Polarz S, Smarsly B. Nanoporous materials. J Nanosci Nanotechnol 2002; (2): 581-612.

Polson A, Ruiz-Bravo C. Fractionation of plasma with polyethylene glycol. Vox Sang 1972; (23): 107-118.

Polzonetti G, Iucci G, Frontini A, Infante G, Furlani C, Avigliano L, Del Principe D, Palumbo G, Rosato N. Surface reactions of a plasma-sprayed CaO-P2O5-SiO2-based glass with albumin, fibroblasts and granulocytes studied by XPS, fluorescence and chemiluminescence. Biomaterials 2000; (21): 1531-1539.

Pope EJA, Mackenzie J D. Sol-gel processing of silica. 2. The role of the catalyst. Journal of Non-Crystalline Solids 1986; (87): 185.

Porjazoska A, Kayaman-Apohan N, Karal-Yilmaz O, Cvetkovska M, Baysal K, Baysal B M. Synthesis and characterization of glycolide, L-lactide, and PDMS-based terpolymers as a support for cell cultures. J Biomater Sci Polym Ed 2002; (13): 1119-1134.

Prager M, Polterauer P, Bohmig H J, Wagner O, Fugl A, Kretschmer G, Plohner M, Nanobashvili J, Huk I. Collagen versus gelatin-coated Dacron versus stretch polytetrafluoroethylene in abdominal aortic bifurcation graft surgery: results of a seven-year prospective, randomized multicenter trial. Surgery 2001; (130): 408-414.

Prasad Chennazhy K, Krishnan L K. Effect of passage number and matrix characteristics on differentiation of endothelial cells cultured for tissue engineering. Biomaterials 2005; (26): 5658-5667.

Price RJ, Skalak TC. A circumferential stress-growth rule predicts arcade arteriole formation in a network model. Microcirculation 1995; (2): 41-51.

Pries AR, Secomb TW, Gaehtgens P. Structural adaptation and stability of microvascular networks: theory and simulations. Am J Physiol 1998; (275): H349-H360.

Pyun J, Matyjaszewski K, Kowalewski T, Savin D, Patterson G, Kickelbick G, Huesing N. Synthesis of well-defined block copolymers tethered to polysilsesquioxane nanoparticles and their nanoscale morphology on surfaces. J

Am Chem Soc 2001; (123): 9445-9446.

Quirynein M, Bollen CML. The influence of surface-roughness and surface-free energy on supragingival and subgingival plaque-formation in man - A review of the literature. Journal of Clinical Periodontology 1995; (22): 1-14.

Raiche A T, Puleo D A. In vitro effects of combined and sequential delivery of two bone growth factors. Biomaterials 2004; (25): 677-685.

Raki L, Beaudoin JJ, Mitchell L. Layered double hydroxide-like materials: nanocomposites for use in concrete. Cem Concr Res 2004; (34): 1717-1724.

Rakvin B, Zilic D, Dalal N S, North J M, Cevc P, Arcon D, Zadro K. An EPR method for probing surface magnetic fields, dipolar distances, and magnetization fluctuations in single molecule magnets. Spectrochim Acta A Mol Biomol Spectrosc 2004; (60): 1241-1245.

Ramires P A, Mirenghi L, Romano A R, Palumbo F, Nicolardi G. Plasma-treated PET surfaces improve the biocompatibility of human endothelial cells. J Biomed Mater Res 2000; (51): 535-539.

Rashid S T, Salacinski H J, Hamilton G, Seifalian A M. The use of animal models in developing the discipline of cardiovascular tissue engineering: a review. Biomaterials 2004; (25): 1627-1637.

Ratner B D, Tyler B J, Chilkoti A. Analysis of biomedical polymer surfaces: polyurethanes and plasma-deposited thin films. Clin Mater 1993; (13): 71-84.

Rebouillat S, Steffenino B, Letellier B. Hydrodynamics of high speed fibre impregnation. Chemical Engineering Science 2000; (55): 15-24.

Redmond E M, Cahill P A, Sitzmann J V. Perfused transcapillary smooth muscle and

endothelial cell co-culture--a novel in vitro model. In Vitro Cell Dev Biol Anim 1995; (31): 601-609.

Reed R K, Laurent U B. Turnover of hyaluronan in the microcirculation. Am Rev Respir Dis 1992; (146): S37-S39.

Reichert WM. Evasnescent detection of adsorbed films. CRC Rev Biocomp 1989; 5: 173-195.

Renke-Gluszko M, El Fray M. The effect of simulated body fluid on the mechanical properties of multiblock poly(aliphatic/aromatic-ester) copolymers. Biomaterials 2004; (25): 5191-5198.

Renkin E M. Capillary transport of macromolecules: pores and other endothelial pathways. J Appl Physiol 1985; (58): 315-325.

Renkin E M. Cellular and intercellular transport pathways in exchange vessels. Am Rev Respir Dis 1992; (146): S28-S31.

Ribatti D, Nico B, Vacca A, Roncali L, Burri P H, Djonov V. Chorioallantoic membrane capillary bed: a useful target for studying angiogenesis and anti-angiogenesis in vivo. Anat Rec 2001; (264): 317-324.

Ribot F, Sanchez C. Organically functionalized metallic oxo-clusters: Structurally well-defined nanobuilding blocks for the design of hybrid organic-inorganic materials. Comments on Inorganic chemistry 1999; (20): 327-371.

Riddle D R, Sonntag W E, Lichtenwalner R J. Microvascular plasticity in aging. Ageing Res Rev 2003; (2): 149-168.

Riedel M, Muller B, Wintermantel E. Protein adsorption and monocyte activation on germanium nanopyramids. Biomaterials 2001; (22): 2307-2316.

Riepe G, Loos J, Imig H, Schroder A, Schneider E, Petermann J, Rogge A, Ludwig M, Schenke A, Nassutt R, Chakfe N, Morlock M. Long-term in vivo alterations of polyester vascular grafts in humans. Eur J Vasc Endovasc Surg 1997; (13): 540-548.

Riesen R, Vogel K, Schubnell M. DSC by TGA/SDTA851(e) considering mass changes. J Thermal Anal Calorim 2001; (64): 243-252.

Rivard C H, Chaput C J, DesRosiers E A, Yahia L H, Selmani A. Fibroblast seeding and culture in biodegradable porous substrates. J Appl Biomater 1995; (6): 65-68.

Rivard C H, Chaput C, Rhalmi S, Selmani A. [Bio-absorbable synthetic polyesters and tissue regeneration. A study of three-dimensional proliferation of ovine chondrocytes and osteoblasts]. Ann Chir 1996; (50): 651-658.

Riviere JC. Surface analytical techniques (Monographs on the Physics and Chemistry of Materials). Oxford Science Publications, 1990.

Roach MR, Burton AC. The reason for the shape of the distensibility curves of arteries. Can J Biochem Physiol 1957; (35): 681-690.

Robert A.Freitas Jr. Nanomedicine. Landes Bioscience, Georgetown, Texas. 2003.

Roduit B. Computational aspects of kinetic analysis Part E: The ICTAC kinetics project - numerical techniques and kinetics of solid state processes. Thermochim Acta 2000; (355): 171-180.

Roether J A, Boccaccini A R, Hench L L, Maquet V, Gautier S, Jerjme R. Development and in vitro characterisation of novel bioresorbable and bioactive composite materials based on polylactide foams and Bioglass for tissue engineering applications. Biomaterials 2002; (23): 3871-3878.

Roggendorf E. [Biostability of plastic endotheses]. Polim Med 1976; (6): 13-26.

Rubanyi G M. The role of endothelium in cardiovascular homeostasis and diseases. J Cardiovasc Pharmacol 1993; (22 Suppl 4): S1-14.

Rubino C, Mazzarello V, Farace F, D'Andrea F, Montella A, Fenu G, Campus G V. Ultrastructural anatomy of contracted capsules around textured implants in augmented breasts. Ann Plast Surg 2001; (46): 95-102.

Ryu G H, Han D K, Park S, Kim M, Kim Y H, Min B. Surface characteristics and properties of lumbrokinase-immobilized polyurethane. J Biomed Mater Res 1995; (29): 403-409.

Sachlos E, Czernuszka J T. Making tissue engineering scaffolds work. Review: the application of solid freeform fabrication technology to the production of tissue engineering scaffolds. Eur Cell Mater 2003; (5): 29-39.

Sahota P S, Burn J L, Heaton M, Freedlander E, Suvarna S K, Brown N J, MacNeil S. Development of a reconstructed human skin model for angiogenesis. Wound Repair Regen 2003; (11): 275-284.

Saito N, Nojiri C, Kuroda S, Sakai K. Photochemical grafting of alpha-propylsulphate-poly(ethylene oxide) on polyurethane surfaces and enhanced antithrombogenic potential. Biomaterials 1997; (18): 1195-1197.

Salacinski H, Tiwari A, Hamilton G, Seifalian A M. Performance of a polyurethane vascular prosthesis carrying a dipyridamole (Persantin) coating on its lumenal surface. J Biomed Mater Res 2002; (61): 337-338 (*Salacinski, 2002a)

Salacinski H J, Tai N R, Punshon G, Giudiceandrea A, Hamilton G, Seifalian A M. Optimal endothelialisation of a new compliant poly(carbonate-urea)urethane

vascular graft with effect of physiological shear stress. Eur J Vasc Endovasc Surg 2000; (20): 342-352.

Salacinski H J, Tiwari A, Hamilton G, Seifalian A M. Cellular engineering of vascular bypass grafts: role of chemical coatings for enhancing endothelial cell attachment. Med Biol Eng Comput 2001; (39): 609-618. (*Salacinski, 2001a)

Salacinski H J, Punshon G, Krijgsman B, Hamilton G, Seifalian A M. A hybrid compliant vascular graft seeded with microvascular endothelial cells extracted from human omentum. Artif Organs 2001; (25): 974-982. (*Salacinski, 2001b)

Salacinski H J, Goldner S, Giudiceandrea A, Hamilton G, Seifalian A M, Edwards A, Carson R J. The mechanical behavior of vascular grafts: a review. J Biomater Appl 2001; (15): 241-278. (*Salacinski, 2001c)

Salacinski H J, Tai N R, Carson R J, Edwards A, Hamilton G, Seifalian A M. In vitro stability of a novel compliant poly(carbonate-urea)urethane to oxidative and hydrolytic stress. J Biomed Mater Res 2002; (59): 207-218. (*Salacinski, 2002b)

Salacinski H J, Odlyha M, Hamilton G, Seifalian A M. Thermo-mechanical analysis of a compliant poly(carbonate-urea)urethane after exposure to hydrolytic, oxidative, peroxidative and biological solutions. Biomaterials 2002; (23): 2231-2240. (*Salacinski, 2002c)

Salacinski H J, Hamilton G, Seifalian A M. Surface functionalization and grafting of heparin and/or RGD by an aqueous-based process to a poly(carbonate-urea)urethane cardiovascular graft for cellular engineering applications. J Biomed Mater Res 2003; (66A): 688-697.

Salzman EW. Measurement of platelet adhesiveness: a simple in vitro technique demonstrating an abnormality in von Willebrand disease. J Lab Clin Med 1963; (62): 274.

Sanchez-Cortes S, Berenguel R M, Madejon A, Perez-Mendez M. Adsorption of polyethyleneimine on silver nanoparticles and its interaction with a plasmid DNA: a surface-enhanced Raman scattering study. Biomacromolecules 2002; (3): 655-660.

Sanchez C, Soler-Illia G J D A, Ribot F, Lalot T, Mayer C R, Cabuil V. Designed hybrid organic-inorganic nanocomposites from functional nanobuilding blocks. Chemistry of Materials 2001; (13): 3061-3083.

Sanchez Munoz O L, Hernandez E P, Lammerhofer M, Lindner W, Kenndler E. Estimation and comparison of zeta-potentials of silica-based anion-exchange type porous particles for capillary electrochromatography from electrophoretic and electroosmotic mobility. Electrophoresis 2003; (24): 390-398.

Sangster J. Octane-water partition coefficients: fundamentals and physical chemistry. Wiley, 1997.

Santerre J P, Labow R S, Adams G A. Enzyme-biomaterial interactions: effect of biosystems on degradation of polyurethanes. J Biomed Mater Res 1993; (27): 97-109.

Santerre J P, Labow R S. The effect of hard segment size on the hydrolytic stability of polyether-urea-urethanes when exposed to cholesterol esterase. J Biomed Mater Res 1997; (36): 223-232.

Santos J M, Fagelman K, Guthrie J T. Characterisation of the surface Lewis acid-base properties of poly(butylene terephthalate) by inverse gas chromatography. J Chromatogr A 2002; (969): 111-118.

Sarge SM, Hohne GWH, Cammenga HK. Temperature, heat and heat flow rate calibration of scanning calorimeters in the cooling mode. KThermochim Acta 2000; (361): 1-20.

Sato T, Yamamoto Y, Fujishiro Y, Uchida S. Intercalation of iron oxide in layered H2Ti4O9 and H4Nb6O17: Visible-light induced photocatalytic properties. Journal of the Chemical Society-Faraday Transactions 1996; (92): 5089-5092.

Sawyer P N. The effect of various metal interfaces on blood and other living cells. Ann N Y Acad Sci 1968; (146): 49-65.

Schick C, Jonsson U, Vassiliev T. Applicability of 80CB for temperature calibration of temperature-modulated calorimeters. Thermochim Acta 2000; (347): 53-61.

Schidmt H, Kasemann R, Burkhart T, Wagner G, Arpac E, Geiter E. Inorganic-organic hybrid coatings for metal and glass surfaces. ACS Symposium Series 1995; (585): 331-347.

Schmedlen R H, Masters K S, West J L. Photocrosslinkable polyvinyl alcohol hydrogels that can be modified with cell adhesion peptides for use in tissue engineering. Biomaterials 2002; (23): 4325-4332.

Schmedlen R H, Elbjeirami W M, Gobin A S, West J L. Tissue engineered small-diameter vascular grafts. Clin Plast Surg 2003; (30): 507-517.

Schmid-Scho¨nbein GW. Mechanism of granulocyte-capillary-plugging. Prog Appl Microcirc 1987; (12): 223-230.

Schmid-Scho¨nbein GW. Biomechanics of microcirculatory blood perfusion. Annu Rev Biomed Eng 1999;73-102.

Schmidt H. Nanoparticles by chemical synthesis, processing to materials and innovative application. Applied Organometallic Chemistry 2001; (15): 331-343.

Scholtzová E, Mach P, Hricovíni M. Structure of sulfated monosaccharides studied by quantum chemical methods. Molecules 2003; (8): 770-779.

Scholz D, Ziegelhoeffer T, Helisch A, Wagner S, Friedrich C, Podzuweit T, Schaper W. Contribution of arteriogenesis and angiogenesis to postocclusive hindlimb perfusion in mice. J Mol Cell Cardiol 2002; (34): 775-787.

Schubell MJ. J Thermal Anal Calorim 2000; 61: 1005-1011.

Schubert M A, Wiggins M J, Anderson J M, Hiltner A. Role of oxygen in biodegradation of poly(etherurethane urea) elastomers. J Biomed Mater Res 1997; (34): 519-530.

Schugens C, Maquet V, Grandfils C, Jerome R, Teyssie P. Polylactide macroporous biodegradable implants for cell transplantation. II. Preparation of polylactide foams by liquid-liquid phase separation. J Biomed Mater Res 1996; (30): 449-461.

Secomb TW, Hsu R, Pries AR. A model for red blood cell motion in glycocalyx-lined capillaries. Am J Physiol 1998; (274): H1106-H1022.

Secomb T W, Hsu R, Pries A R. A model for red blood cell motion in glycocalyx-lined capillaries. Am J Physiol 1998; (274): H1016-H1022.

Seeger J M, Ingegno M D, Bigatan E, Klingman N, Amery D, Widenhouse C, Goldberg E P. Hydrophilic surface modification of metallic endoluminal stents. J Vasc Surg 1995; (22): 327-335.

Seifalian A M, Salacinski H J, Punshon G, Krijgsman B, Hamilton G. A new technique for measuring the cell growth and metabolism of endothelial cells seeded on vascular prostheses. J Biomed Mater Res 2001; (55): 637-644.

Seifalian A M, Tiwari A, Hamilton G, Salacinski H J. Improving the clinical patency of prosthetic vascular and coronary bypass grafts: the role of seeding and tissue engineering. Artif Organs 2002; (26): 307-320.

Seifalian A M, Salacinski H J, Tiwari A, Edwards A, Bowald S, Hamilton G. In vivo biostability of a poly(carbonate-urea)urethane graft. Biomaterials 2003; (24): 2549-2557.

Sepulveda P, Jones J R, Hench L L. Bioactive sol-gel foams for tissue repair. J Biomed Mater Res 2002; (59): 340-348.

Shanklin D R, Smalley D L. Dynamics of wound healing after silicone device implantation. Exp Mol Pathol 1999; (67): 26-39.

Sharma DR, Mathur R, Vadera SR, Kumar N, Kutty TRN. Synthesis of nanocomposites of Ni-Zn ferrite in aniline formaldehyde copolymer and studies on their pyrolysis products. J Alloys Compounds 2003; (358): 193-204.

Shastri V P, Martin I, Langer R. Macroporous polymer foams by hydrocarbon templating. Proc Natl Acad Sci USA 2000; (97): 1970-1975.

Sheng YJ, Lin WJ, Chen WC. The network structures of polyhedral oligomeric silsesquioxane-based nanocomposites studied by continuous-space Monte Carlo simulations. J Chem Phys 2004; (121): 9693-9701.

Sheridan R L, Morgan J R, Cusick J L, Petras L M, Lydon M M, Tompkins R G. Initial experience with a composite autologous skin substitute. Burns 2001; (27): 421-424.

Shibayama M, Suetsugu M, Sakurai S. Structure characterisation of polyurethanes containing poly(dimethylsiloxane). Macromolecules 1991; (24): 6254-6262.

Shin H., Seongbong J., Mikos A.G. Biomimetic materials for tissue engineering. Biomaterials 2003; (24): 4353-4364.

Shin M, Matsuda K, Ishii O, Terai H, Kazeempur-Mofrad M, Borenstein J, Detmar M, Vacanti JP. Endothelialized networks with a vascular geometry in microfabricated poly(dimethyl siloxane). Biomed Microdevices 2004; (6): 269-278.

Shin H, Quinten R P, Mikos A G, Jansen J A. In vivo bone and soft tissue response to injectable, biodegradable oligo(poly(ethylene glycol) fumarate) hydrogels. Biomaterials 2003; (24): 3201-3211.

Shin Y C, Han D K, Kim Y H, Kim S C. Antithrombogenicity of hydrophilic polyurethane-hydrophobic polystyrene IPNs. II. In vitro and ex vivo studies. J Biomater Sci Polym Ed 1994; (6): 281-295.

Shinoka T, Shum-Tim D, Ma P X, Tanel R E, Isogai N, Langer R, Vacanti J P, Mayer J E, Jr. Creation of viable pulmonary artery autografts through tissue engineering. J Thorac Cardiovasc Surg 1998; (115): 536-545.

Shireman P K, Greisler H P. Mitogenicity and release of vascular endothelial growth factor with and without heparin from fibrin glue. J Vasc Surg 2000; (31): 936-943.

Shore A C. Capillaroscopy and the measurement of capillary pressure. Br J Clin Pharmacol 2000; (50): 501-513.

Shu X Z, Ghosh K, Liu Y, Palumbo F S, Luo Y, Clark R A, Prestwich G D. Attachment and spreading of fibroblasts on an RGD peptide-modified injectable hyaluronan hydrogel. J Biomed Mater Res 2004; (68A): 365-375.

Shum-Tim D, Stock U, Hrkach J, Shinoka T, Lien J, Moses M A, Stamp A, Taylor G, Moran A M, Landis W, Langer R, Vacanti J P, Mayer J E, Jr. Tissue engineering of autologous aorta using a new biodegradable polymer. Ann Thorac Surg 1999; (68): 2298-2304.

Siggelkow W, Faridi A, Spiritus K, Klinge U, Rath W, Klosterhalfen B. Histological analysis of silicone breast implant capsules and correlation with capsular

contracture. Biomaterials 2003; (24): 1101-1109.

Sikavitsas V I, Bancroft G N, Mikos A G. Formation of three-dimensional cell/polymer constructs for bone tissue engineering in a spinner flask and a rotating wall vessel bioreactor. J Biomed Mater Res 2002; (62): 136-148.

Silver J H, Myers C W, Lim F, Cooper S L. Effect of polyol molecular weight on the physical properties and haemocompatibility of polyurethanes containing polyethylene oxide macroglycols. Biomaterials 1994; (15): 695-704.

Silver J H, Hergenrother R W, Lin J C, Lim F, Lin H B, Okada T, Chaudhury M K, Cooper S L. Surface and blood-contacting properties of alkylsiloxane monolayers supported on silicone rubber. J Biomed Mater Res 1995; (29): 535-548.

Silver J H, Lin J C, Lim F, Tegoulia V A, Chaudhury M K, Cooper S L. Surface properties and hemocompatibility of alkyl-siloxane monolayers supported on silicone rubber: effect of alkyl chain length and ionic functionality. Biomaterials 1999; (20): 1533-1543.

Simon F, Hermel G, Lunkwitz D, Werner C, Eichhorn KJ, Jacobasch HJ. Surface modification of expanded poly(tetrafluoroethylene) by means of pressure microwave plasma for improvement of adhesion and growth of human endothelial cells. Macromolecular Symposia 1996; 103: 243-252.

Simon P, Kolman L. DSC study of oxidation induction periods. J Thermal Anal Calorim 2001; (64): 813-820.

Simon SL, McKenna GB. Quantitative analysis of errors in TMDSC in the glass transition region. Thermochim Acta 2000; (348): 77-89.

Sims C D, Butler P E, Cao Y L, Casanova R, Randolph M A, Black A, Vacanti C A, Yaremchuk M J. Tissue engineered neocartilage using plasma derived polymer substrates and chondrocytes. Plast Reconstr Surg 1998; (101): 1580-1585.

Sinclair T M, Kerrigan C L, Buntic R. Biodegradation of the polyurethane foam covering of breast implants. Plast Reconstr Surg 1993; (92): 1003-1013.

Singer V L, Jones L J, Yue S T, Haugland R P. Characterization of PicoGreen reagent and development of a fluorescence-based solution assay for double-stranded DNA quantitation. Anal Biochem 1997; (249): 228-238.

Sinha R, Cresswell T R, Mason R, Chakrabarti I. Functional benefit of Dupuytren's surgery. J Hand Surg [Br] 2002; (27): 378-381.

Sipehia R. X-ray photoelectron spectroscopy studies, surface tension measurements, immobilization of human serum albumin, human fibrinogen and human fibronectin onto ammonia plasma treated surfaces of biomaterials useful for cardiovascular implants and artificial cornea implants. Biomater Artif Cells Immobilization Biotechnol 1993; (21): 647-658.

Sixma J J, Hindriks G, Van Breugel H, Hantgan R, de Groot P G. Vessel wall proteins adhesive for platelets. J Biomater Sci Polym Ed 1991; (3): 17-26.

Slevin M, Kumar S, Gaffney J. Angiogenic oligosaccharides of hyaluronan induce multiple signaling pathways affecting vascular endothelial cell mitogenic and wound healing responses. J Biol Chem 2002; (277): 41046-41059.

Soker S, Machado M, Atala A. Systems for therapeutic angiogenesis in tissue engineering. World J Urol 2000; (18): 10-18.

Soldani G, Losi P, Milioni C, Raffi A. Light microscopy evaluation of polyurethane vascular grafts porosity by Sudan Black B staining. J Microsc 2002; (206): 139-145.

Song J X, Xing X, Chen J P. [Reconstruction of digital avulsion with pre-fabricated

subdermal vascular network skin flap by ultrasonic liposuction]. *Zhongguo Xiu Fu Chong Jian Wai Ke Za Zhi* 2001; (15): 196-198.

Song S P, Crimp M A, Ayres V M, Collard C J, Holloway J P, Brake M L. New hetero silicon-carbon nanostructure formation mechanism. J Nanosci Nanotechnol 2004; (4): 817-823.

Sonoda H, Takamizawa K, Nakayama Y, Yasui H, Matsuda T. Small-diameter compliant arterial graft prosthesis: Design concept of coaxial double tubular graft and its fabrication. J Biomed Mater Res 2001; (55): 266-276.

Springer M L, Ozawa C R, Banfi A, Kraft P E, Ip T K, Brazelton T R, Blau H M. Localized arteriole formation directly adjacent to the site of VEGF-induced angiogenesis in muscle. Mol Ther 2003; (7): 441-449.

Stokes K. Polyurethane pacemaker leads (chapter). In: Clinical evaluation of medical devices: principles and case studies. (Ed, Witkin KB). Totawa, NJ: Humana Press Inc, 1998.

Stokes K, McVenes R, Anderson J M. Polyurethane elastomer biostability. J Biomater Appl 1995; (9): 321-354.

Strahler AN. Hyposometric (area latitude) analysis of erosional topology. Bull Gel Soc Am 1952; (63): 1117-1142.

Stuart B. Polymer analysis. Wiley, London 2002.

Sugihara-Seki M, Skalak R. Asymmetric flows of spherical particles in a cylindrical tube. Biorheology 1997; (34): 155-169.

Suhr J, Koratkar N, Keblinski P, Ajayan P. Viscoelasticity in carbon nanotube composites. Nat Mater 2005; (4): 134-137.

Suma H. Arterial grafts in coronary bypass surgery. Ann Thorac Cardiovasc Surg 1999; (5): 141-145.

Sunner J, Dratz E, Chen Y C. Graphite surface-assisted laser desorption/ionization time-of-flight mass spectrometry of peptides and proteins from liquid solutions. Anal Chem 1995; (67): 4335-4342.

Suresh S, Zhou W, Spraul B, Laine R M, Ballato J, Smith D W, Jr. Novel fluoropolymer functionalized silsesquioxanes for nanoscale architecture of hybrid composites. J Nanosci Nanotechnol 2004; (4): 250-253.

Sutton DW, Schmid-Scho¨nbein GW. The pressure-flow relation for plasma in whole organ skeletal muscle and its verification. J Biomech Eng 1991; (113): 452-457.

Swedenborg J, Bengtsson L, Clyne N, Dryjski M, Gillis C, Rosfors S, Haegerstrand A. In vitro endothelialisation of arteriovenous loop grafts for haemodialysis. Eur J Vasc Endovasc Surg 1997; (13): 272-277.

Sykes P, Openshaw M, Sutherland D. Surgical dressing after nail surgery. Nurs Times 1987; (83): 45.

Szycher M. Biostability of polyurethane elastomers: a critical review. J Biomater Appl 1988; (3): 297-402.

Tabata Y. Tissue regeneration based on growth factor release. Tissue Eng 2003; (9 Suppl 1): S5-15.

Tai N R, Salacinski H J, Edwards A, Hamilton G, Seifalian A M. Compliance properties of conduits used in vascular reconstruction. Br J Surg 2000; (87): 1516-1524.

Tampieri A, Celotti G, Landi E, Sandri M, Roveri N, Falini G. Biologically inspired synthesis of nanocomposites for bone tissue regeneration. Euro Ceramics VIII, Pts 1-3 Key Engineering Materials 2004; (264-268): 1937-1940.

Tanaka K, Tamura J, Kawanabe K, Nawa M, Oka M, Uchida M, Kokubo T, Nakamura T. Ce-TZP/Al2O3 nanocomposite as a bearing material in total joint replacement. J Biomed Mater Res 2002; (63): 262-270.

Tanaka Y, Sung K C, Tsutsumi A, Ohba S, Ueda K, Morrison W A. Tissue engineering skin flaps: which vascular carrier, arteriovenous shunt loop or arteriovenous bundle, has more potential for angiogenesis and tissue generation? Plast Reconstr Surg 2003; (112): 1636-1644.

Tang Y W, Labow R S, Santerre J P. Enzyme-induced biodegradation of polycarbonate polyurethanes: dependence on hard-segment concentration. J Biomed Mater Res 2001; (56): 516-528.

Tang Y W, Labow R S, Revenko I, Santerre J P. Influence of surface morphology and chemistry on the enzyme catalyzed biodegradation of polycarbonate-urethanes. J Biomater Sci Polym Ed 2002; (13): 463-483.

Tang Y W, Labow R S, Santerre J P. Isolation of methylene dianiline and aqueous-soluble biodegradation products from polycarbonate-polyurethanes. Biomaterials 2003; (24): 2805-2819.

Tang Y W, Labow R S, Santerre J P. Enzyme induced biodegradation of polycarbonate-polyurethanes: dose dependence effect of cholesterol esterase. Biomaterials 2003; (24): 2003-2011.

Tanihara M, Suzuki Y, Yamamoto E, Noguchi A, Mizushima Y. Sustained release of basic fibroblast growth factor and angiogenesis in a novel covalently crosslinked gel of heparin and alginate. J Biomed Mater Res 2001; (56): 216-221.

Tanyanyiwa J, Leuthardt S, Hauser P C. Conductimetric and potentiometric detection in conventional and microchip capillary electrophoresis. Electrophoresis 2002; (23): 3659-3666.

Taylor D G, Bert J L, Bowen B D. A mathematical model of interstitial transport. II. Microvascular exchange in mesentery. Microvasc Res 1990; (39): 279-306.

Taylor G I, Palmer J H. The vascular territories (angiosomes) of the body: experimental study and clinical applications. Br J Plast Surg 1987; (40): 113-141.

Taylor L M, Jr., Edwards J M, Porter J M. Present status of reversed vein bypass grafting: five-year results of a modern series. J Vasc Surg 1990; (11): 193-205.

Teebken O E, Bader A, Steinhoff G, Haverich A. A new concept for substitutes in vascular surgery. Langenbecks Arch Chir Suppl Kongressbd 1998; (115): 1256-1259.

Teebken O E, Pichlmaier A M, Haverich A. Cell seeded decellularised allogeneic matrix grafts and biodegradable polydioxanone-prostheses compared with arterial autografts in a porcine model. Eur J Vasc Endovasc Surg 2001; (22): 139-145.

Teebken O E, Haverich A. Tissue engineering of small diameter vascular grafts. Eur J Vasc Endovasc Surg 2002; (23): 475-485.

Tegou E, Bellas V, Gogolides E, Argitis D. Polyhedral oligomeric silsesquioxane (POSS) acrylate co-polymers for microfabrication: properties and formulation of resist materials. Microelectronic Engineering 2004; (73-74): 238-243.

Tengvall P, Askendal A, Lundstrom I. Studies on protein adsorption and activation of complement on hydrated aluminium surfaces in vitro. Biomaterials 1998; (19): 935-940.

Tepper O M, Galiano R D, Kalka C, Gurtner G C. Endothelial progenitor cells: the promise of vascular stem cells for plastic surgery. Plast Reconstr Surg 2003; (111): 846-854.

Thomas A C, Campbell G R, Campbell J H. Advances in vascular tissue engineering. Cardiovasc Pathol 2003; (12): 271-276.

Thomson R C, Mikos A G, Beahm E, Lemon J C, Satterfield W C, Aufdemorte T B, Miller M J. Guided tissue fabrication from periosteum using preformed biodegradable polymer scaffolds. Biomaterials 1999; (20): 2007-2018.

Tiwari A, Salacinski H J, Hamilton G, Seifalian A M. Tissue engineering of vascular bypass grafts: role of endothelial cell extraction. Eur J Vasc Endovasc Surg 2001; (21): 193-201.

Tiwari A, Salacinski H J, Punshon G, Hamilton G, Seifalian A M. Development of a hybrid cardiovascular graft using a tissue engineering approach. FASEB J 2002; (16): 791-796.

Tiwari A, Salacinski H, Seifalian A M, Hamilton G. New prostheses for use in bypass grafts with special emphasis on polyurethanes. Cardiovasc Surg 2002; (10): 191-197.

Tiwari A, Kidane A, Salacinski H, Punshon G, Hamilton G, Seifalian A M. Improving endothelial cell retention for single stage seeding of prosthetic grafts: use of polymer sequences of arginine-glycine-aspartate. Eur J Vasc Endovasc Surg 2003; (25): 325-329.

Tran HV, Hung RJ, Loy DA, Wheeler DR, Byer J, Conley W, Willson CG. Fluoropolymer Resist Materials for 157 nm Microlithography. J. Photopolym. Sci. Technol. 2001;(14): 669-674.

Tubiana R. Dupuytren's disease of the radial side of the hand. Hand Clin 1999; (15):

149-159.

Turi EA. Thermal characterization of polymeric materials. Academic Press, New Jersey 1981.

Turri S, Levi M. Structure, dynamic properties, and surface behavior of nanostructured ionomeric polyurethanes from reactive polyhedral oligomeric silsesquioxanes. Macromolecules 2005; (38): 5569-5574.

Tyler B J, Ratner B D, Castner D G, Briggs D. Variations between Biomer lots. I. Significant differences in the surface chemistry of two lots of a commercial poly(ether urethane). J Biomed Mater Res 1992; (26): 273-289.

Uchida N, Emoto H, Kambic H, Harasaki H, Chen J F, Hsu S H, Murabayashi S, Nose Y. Compliance effect on patency of small diameter vascular grafts. ASAIO Trans 1989; (35): 556-558.

Uchida N, Kambic H, Emoto H, Chen J F, Hsu S, Murabayshi S, Harasaki H, Nose Y. Compliance effects on small diameter polyurethane graft patency. J Biomed Mater Res 1993; (27): 1269-1279.

Ueda H, Tabata Y. Polyhydroxyalkanonate derivatives in current clinical applications and trials. Adv Drug Deliv Rev 2003; (55): 501-518.

Uldall R, DeBruyne M, Besley M, McMillan J, Simons M, Francoeur R. A new vascular access catheter for hemodialysis. Am J Kidney Dis 1993; (21): 270-277.

Urry D W, Pattanaik A. Elastic protein-based materials in tissue reconstruction. Ann N Y Acad Sci 1997; (831): 32-46.

Urry D W. Elastic molecular machines in metabolism and soft-tissue restoration. Trends Biotechnol 1999; (17): 249-257.

Vacanti J P, Langer R. Tissue engineering: the design and fabrication of living replacement devices for surgical reconstruction and transplantation. Lancet 1999; (354 Suppl 1): SI32-SI34.

Vailhe B, Vittet D, Feige J J. In vitro models of vasculogenesis and angiogenesis. Lab Invest 2001; (81): 439-452.

Vaissiere G, Chevallay B, Herbage D, Damour O. Comparative analysis of different collagen-based biomaterials as scaffolds for long-term culture of human fibroblasts. Med Biol Eng Comput 2000; (38): 205-210.

Van den Driesche S, Mummery C L, Westermann C J. Hereditary hemorrhagic telangiectasia: an update on transforming growth factor beta signaling in vasculogenesis and angiogenesis. Cardiovasc Res 2003; (58): 20-31.

Van der Lei B, Wildevuur C R. From a synthetic, microporous, compliant, biodegradable small-caliber vascular graft to a new artery. Thorac Cardiovasc Surg 1989; (37): 337-347.

Van Tienen T G, Heijkants R G, Buma P, de Groot J H, Pennings A J, Veth R P. Tissue ingrowth and degradation of two biodegradable porous polymers with different porosities and pore sizes. Biomaterials 2002; (23): 1731-1738.

Van Zeghbroeck B. Lattice scattering (chapter). In: Principles of semiconductor devices. 2004; 1st Ed. (University of Colorado). online edition http://ecewww.colorado.edu/~bart/book/

Vasilets V N, Hermel G, Konig U, Werner C, Muller M, Simon F, Grundke K, Ikada Y, Jacobasch H J. Microwave CO2 plasma-initiated vapour phase graft polymerization of acrylic acid onto polytetrafluoroethylene for immobilization of human thrombomodulin. Biomaterials 1997; (18): 1139-1145.

Vernon R B, Lara S L, Drake C J, Iruela-Arispe M L, Angello J C, Little C D, Wight T N, Sage E H. Organized type I collagen influences endothelial patterns during "spontaneous angiogenesis in vitro": planar cultures as models of vascular development. In Vitro Cell Dev Biol Anim 1995; (31): 120-131.

Vert M, Mauduit J, Li S. Biodegradation of PLA/GA polymers: increasing complexity. Biomaterials 1994; (15): 1209-1213.

Vestweber D. Molecular mechanisms that control endothelial cell contacts. J Pathol 2000; (190): 281-291.

Vittet D, Prandini M H, Berthier R, Schweitzer A, Martin-Sisteron H, Uzan G, Dejana E. Embryonic stem cells differentiate in vitro to endothelial cells through successive maturation steps. Blood 1996; (88): 3424-3431.

Von Degenfeld G, Banfi A, Springer M L, Blau H M. Myoblast-mediated gene transfer for therapeutic angiogenesis and arteriogenesis. Br J Pharmacol 2003; (140): 620-626.

Von Von R A. Design and characterization of a metal-ion beam and nitrogen-radical beam source PVD system with in-situ AES constitution and HEED structure analysis. Application to the growth of Cu-N film. Anal Bioanal Chem 1996; (355): 543-548.

Voronkov MG, Lavrentyev VL. Polyhedral OligoSilsesquixanes and their homoderivatives. Top Curr Chem 1982; 102: 199-236.

Vozzi G, Flaim C, Ahluwalia A, Bhatia S. Fabrication of PLGA scaffolds using soft lithography and microsyringe deposition. Biomaterials 2003; (24): 2533-2540.

Vyalov S, Langille B L, Gotlieb A I. Decreased blood flow rate disrupts endothelial repair in vivo. Am J Pathol 1996; (149): 2107-2118.

Vyazovkin S. Thermal analysis. Anal Chem 2002; (74): 2749-2762.

Vyorykka J, Paaso J, Tenhunen M, Tenhunen J, Iitti H, Vuorinen T, Stenius P. Analysis of depth profiling data obtained by confocal Raman microspectroscopy. Appl Spectrosc 2003; (57): 1123-1128.

Wada K, Watanabe N, Yamada K, Kondo T, Mitsudo T A. Synthesis of novel starburst and dendritic polyhedral oligosilsesquioxanes. Chem Commun (Camb) 2005;95-97.

Wagner H, Beller F K, Pfautsch M. Electron and light microscopy examination of capsules around breast implants. Plast Reconstr Surg 1977; (60): 49-55.

Wahlberg E. Angiogenesis and arteriogenesis in limb ischemia. J Vasc Surg 2003; (38): 198-203.

Wan ACA. Fabrication of poly(phosphoester) nerve guides by immersion precipitation and the control of porosity. Biomaterials 2001; (22): 1147-1153.

Wang RZ, Suo Z, Evans AG, Yao N, Aksay IA. Deformation mechanisms in nacre. J Mater Res 2001; (16): 2485-2493.

Wang C, Wang Q, Mao T, Wang H, Zhu X. [The construction and physical-mechanical characterization of polymer foams of D. L-PLA]. Sheng Wu Yi Xue Gong Cheng Xue Za Zhi 2000; (17): 396-399.

Wang Y, Kim Y M, Langer R. In vivo degradation characteristics of poly(glycerol sebacate). J Biomed Mater Res 2003; (66A): 192-197.

Ward RS. Surface modification prior to surface formation. Med Plastics Biomater 1995; (2): 34-41.

Ward RS. The effect of phase separation and end group chemistry on in vivo biostability of polyurethanes. Am Soc Art Int Org Journal 1996; (42): 17.

Watanabe E, Smith D M, Jr., Delcarpio J B, Sun J, Smart F W, Van M C, Jr., Claycomb W C. Cardiomyocyte transplantation in a porcine myocardial infarction model. Cell Transplant 1998; (7): 239-246.

Weibel D, Wong S, Lockyer N, Blenkinsopp P, Hill R, Vickerman J C. A C60 primary ion beam system for time of flight secondary ion mass spectrometry: its development and secondary ion yield characteristics. Anal Chem 2003; (75): 1754-1764.

Weinberg C B, Bell E. A blood vessel model constructed from collagen and cultured vascular cells. Science 1986; (231): 397-400.

Weiser L, Bhargava M, Attia E, Torzilli P A. Effect of serum and platelet-derived growth factor on chondrocytes grown in collagen gels. Tissue Eng 1999; (5): 533-544.

Weiwei Du. Electrostatic Self-Assembly of Biocompatible Thin Films. 2000. Virginia Polytechnic Institute and State University. (Thesis/Dissertation)

Welm B, Mott J, Werb Z. Developmental biology: vasculogenesis is a wreck without RECK. Curr Biol 2002; (12): R209-R211.

Wendt D, Marsano A, Jakob M, Heberer M, Martin I. Oscillating perfusion of cell suspensions through three-dimensional scaffolds enhances cell seeding efficiency and uniformity. Biotechnol Bioeng 2003; (84): 205-214.

Werner C, Jacobasch H J. Surface characterization of polymers for medical devices. Int J Artif Organs 1999; (22): 160-176.

Wetzels G M, Koole L H. Photoimmobilisation of poly(N-vinylpyrrolidinone) as a means to improve haemocompatibility of polyurethane biomaterials. Biomaterials 1999; (20): 1879-1887.

White R A, Klein S R, Shors E C. Preservation of compliance in a small diameter microporous, silicone rubber vascular prosthesis. J Cardiovasc Surg (Torino) 1987; (28): 485-490.

Wiggins M J, Wilkoff B, Anderson J M, Hiltner A. Biodegradation of polyether polyurethane inner insulation in bipolar pacemaker leads. J Biomed Mater Res 2001; (58): 302-307.

Wijmans JG, Baaij JPB, Smolders CA. The mechanism of formation of microporous or skinned membranes produced by immersion precipitation. J Membran Sci 1983; (14): 263-274.

Williams D A. Network assessment of capillary hydraulic conductivity after abrupt changes in fluid shear stress. Microvasc Res 1999; (57): 107-117.

Williams R L, Wilson D J, Rhodes N P. Stability of plasma-treated silicone rubber and its influence on the interfacial aspects of blood compatibility. Biomaterials 2004; (25): 4659-4673.

Wilsnack R E. Quantitative cell culture biocompatibility testing of medical devices and correlation to animal tests. Biomater Med Devices Artif Organs 1976; (4): 235-261.

Wilson G J, MacGregor D C, Klement P, Dereume J P, Weber B A, Binnington A G, Pinchuk L. The composite Corethane/Dacron vascular prosthesis. Canine in vivo evaluation of 4 mm diameter grafts with 1 year follow-up. ASAIO Trans 1991; (37): M475-M476.

Wilson G J, Courtman D W, Klement P, Lee J M, Yeger H. Acellular matrix: a

biomaterials approach for coronary artery bypass and heart valve replacement. Ann Thorac Surg 1995; (60): S353-S358.

Wintermantel E, Mayer J, Blum J, Eckert K L, Luscher P, Mathey M. Tissue engineering scaffolds using superstructures. Biomaterials 1996; (17): 83-91.

Wisser D, Steffes J. Skin replacement with a collagen based dermal substitute, autologous keratinocytes and fibroblasts in burn trauma. Burns 2003; (29): 375-380.

Wissink M J, Beernink R, Poot A A, Engbers G H, Beugeling T, van Aken W G, Feijen J. Improved endothelialization of vascular grafts by local release of growth factor from heparinized collagen matrices. J Control Release 2000; (64): 103-114.

Wolfe M S, Dean D, Chen J E, Fisher J P, Han S, Rimnac C M, Mikos A G. In vitro degradation and fracture toughness of multilayered porous poly(propylene fumarate)/beta-tricalcium phosphate scaffolds. J Biomed Mater Res 2002; (61): 159-164.

Woo G L, Mittelman M W, Santerre J P. Synthesis and characterization of a novel biodegradable antimicrobial polymer. Biomaterials 2000; (21): 1235-1246.

Wu J, Lin J, Yin S, Sato T. Synthesis and photocatalytic properties of layered HNbWO6/(Pt, Cd0.8Zn0.2S) nanocomposites. Journal of Materials Chemistry 2001; (11): 3343-3347.

Wu Y K, Lodoen G A, Anderson J M, Baer E, Hiltner A. Creep of a poly(etherurethane urea) in an oxidative environment. J Biomed Mater Res 1994; (28): 515-522.

Wu Z, Xanthopoulos N, Reymond F, Rossier J S, Girault H H. Polymer microchips bonded by O2-plasma activation. Electrophoresis 2002; (23): 782-790.

Wulf M, Michel S, Grundke K, del Rio O I, Kwok D Y, Neumann A W. Simultaneous Determination of Surface Tension and Density of Polymer Melts Using Axisymmetric Drop Shape Analysis. J Colloid Interface Sci 1999; (210): 172-181.

Xiang K, Pandey R, Pernisz UC, Freeman C. Theoretical study of structural and electronic properties of H-Silsesquioxanes. J Phys Chem B 1998; (102): 8704.

Xu H, Kuo SW, Huang CF, Chang FC. Poly(acetoxystyrene-co-isobutylstyryl POSS) Nanocomposites: Characterization and Molecular Interaction. J Polym Res 2002; (9): 239-244.

Xu H, Kuo SW, Huang CF, Chang FC. Characterization of Poly(vinyl pyrrolidone-*co*isobutylstyryl polyhedral oligomeric silsesquioxane) nanocomposites. Journal of Applied Polymer Science 2004; (9): 2208-2215.

Xu HY, Kuo SW, Huang CF, Chang FC. Characterization of poly(vinyl pyrrolidone-co-isobutylstyryl polyhedral oligomeric silsesquioxane) nanocomposites. J Appl Polym Sci 2004; (91): 2208-2215.

Xu G, Chance M R. Radiolytic modification of acidic amino acid residues in peptides: probes for examining protein-protein interactions. Anal Chem 2004; (76): 1213-1221.

Xu Y, Watson J T, Bruening M L. Patterned monolayer/polymer films for analysis of dilute or salt-contaminated protein samples by MALDI-MS. Anal Chem 2003; (75): 185-190.

Xue L, Greisler H P. Biomaterials in the development and future of vascular grafts. J Vasc Surg 2003; (37): 472-480.

Yang H G, Zeng H C. Synthetic architectures of TiO2/H2Ti5O11.H2O, ZnO/H2Ti5O11.H2O, ZnO/TiO2/H2Ti5O11.H2O, and ZnO/TiO2 nanocomposites.

J Am Chem Soc 2005; (127): 270-278.

Yen RT, Fung YC. Effect of velocity of distribution on red cell distribution in capillary blood vessels. J R Coll Gen Pract Occas Pap 1978; (235): H251-H257.

Yeoh G, Russell P, Jenkins E. Spectrum of histological changes reactive to prosthetic breast implants: a clinopathological study of 84 patients. Pathology 1996; (28): 232-235.

Yoon KH, Polk MB, Park JH, Min BG, Schiraldi DA. Properties of poly(ethylene terephtalate) containing epoxy-functionalized polyhedral oligomeric silsesquioxane. Polym Int 2005; (54): 47-53.

Yu J, Liu RYF, oon B, azarenko S, oloski T, argo T, iltner A, aer E. Polymers with palladium nanoparticles as active membrane materials. Journal of Applied Polymer Science 2004; (92): 749-756.

Zaremba CM, Belcher AM, Fritz M, Hansma PK, Li Y, Morse DE, Speck S, Stucky D. Critical transitions in the biofabrication of abalone shells and flat pearls . Chem Mater 1996; (8): 679-690.

Zrahala RJ. Small calibre vascular grafts. J Biomat Appl 1996; 10(4): 309-329.

Zhang Y, Sun H, Chen C. Superhard cubic BC2N compared to diamond. Phys Rev Lett 2004; (93): 195504.

Zhang Z, Marois Y, Guidoin R G, Bull P, Marois M, How T, Laroche G, King M W. Vascugraft polyurethane arterial prosthesis as femoro-popliteal and femoro-peroneal bypasses in humans: pathological, structural and chemical analyses of four excised grafts. Biomaterials 1997; (18): 113-124.

Zhao Q, Casas-Bejar J, Urbanski P, Stokes K. Glass wool-H2O2/CoCl2 test system

for in vitro evaluation of biodegradative stress cracking in polyurethane elastomers. J Biomed Mater Res 1995; (29): 467-475.

Zheng J, Manuel W S, Hornsby P J. Transfection of cells mediated by biodegradable polymer materials with surface-bound polyethyleneimine. Biotechnol Prog 2000; (16): 254-257.

Zheng J, Li X, Zhou Y, Gu R. [Self-assembly of nano-structured silver particle and its surface-enhanced Raman spectroscopic application]. *Guangpuxue Yu Guangpu Fenxi 2000*; (20): 814-816.

Zilla P, Fasol R, Deutsch M, Fischlein T, Minar E, Hammerle A, Krupicka O, Kadletz M. Endothelial cell seeding of polytetrafluoroethylene vascular grafts in humans: a preliminary report. J Vasc Surg 1987; (6): 535-541.

Zilla P, Fasol R, Grimm M, Fischlein T, Eberl T, Preiss P, Krupicka O, von Oppell U, Deutsch M. Growth properties of cultured human endothelial cells on differently coated artificial heart materials. J Thorac Cardiovasc Surg 1991; (101): 671-680.

Zisch A H, Lutolf M P, Hubbell J A. Biopolymeric delivery matrices for angiogenic growth factors. Cardiovasc Pathol 2003; (12): 295-310.

PUBLICATIONS

R.Y.Kannan, H.J.Salacinski, A.Narula, A.Ghairavi, M.Odlyha, P.E.Butler, A.M.Seifalian. Silsesquioxane nanocomposites as tissue implants. Plast Reconst Surg (in print)

R.Y.Kannan, H.J.Salacinski, M.J.Edirisinghe, G.Hamilton, A.M.Seifalian. Polyhedral oligomeric silsesquioxane nanocomposite microvessels : the building blocks of an artificial capillary bed. *Biomaterials* 2006 Sep;27(26):4618-26.

R.Y.Kannan, P.E.Butler, A.M.Seifalian. **Vascular networks (chapter)**. *Wiley's Encyclopedia of Biomedical Engineering* 2006 ed.

G.Conn, A.G.Kidane, G.Punshon, **R.Y.Kannan**, G.Hamilton, A.M.Seifalian. Is there an alternative to systemic anticoagulation, as related to interventional biomedical devices? Expert Rev Med Devices. 2006 Mar;3(2):245-61.

R.Y.Kannan, H.J.Salacinski, P.E.Butler, A.M.Seifalian, M.Odylha. Review paper: principles and applications of surface analytical techniques at the vascular interface. J Biomater Appl. 2006 Jul;21(1):5-32.

R.Y.Kannan, H.J.Salacinski, M.Odlyha, P.E.Butler, A.M.Seifalian. The degradative resistance of polyhedral oligomeric silsesquioxane nanocore integrated polyurethanes: an in vitro study. Biomaterials. 2006 Mar;27(9):1971-9.

N.Alobaid, H.J.Salacinski, K.M.Sales, B.Ramesh, **R.Y.Kannan**, G.Hamilton, A.M.Seifalian. Nanocomposite containing bioactive peptides promote endothelialisation by circulating progenitor cells: an in vitro evaluation. Eur J Vasc Endovasc Surg. 2006 Jul;32(1):76-83.

R.Y.Kannan, K.M.Sales, H.J.Salacinski, P.E.Butler, A.M.Seifalian. The cytocompatibility of polyhedral oligomeric silsesquioxane nanocomposites for cardiovascular tissue engineering. *Cell Biochem & Biophysics* 2006;45(2):129-36.

R.Y.Kannan, H.J.Salacinski, J.De Groot, I.Clatworthy, L.Bozec, M.Horton, P.E.Butler, A.M.Seifalian. The anti-thrombogenic potential of polyhedral oligomeric silsesquioxane nanocomposites. *Biomacromolecules* 2006 Jan 9;7(1):215-223.

R.Y.Kannan, H.J.Salacinski, P.E.Butler, A.M.Seifalian. Polyhedral Oligomeric Silsesquioxanes Nanocomposites: The Next Generation Of Materials For Biomedical Applications. *Accounts in Chemical Research* 2005 Nov; 38(11):879-84.

R.Y.Kannan, H.J.Salacinski, K.M.Sales, P.E.M.Butler, A.M.Seifalian. The roles of tissue engineering and vascularisation in the development of microvascular networks. *Biomaterials* 2005 May; 26(14):1857-75.

R.Y.Kannan, H.J.Salacinski, P.E.M.Butler, G.Hamilton, A.M.Seifalian. 'Current status of prosthetic bypass grafts'. *J Biomed Mater Res B Appl Biomat* 2005 Jul; 74(1): 570-581.

R.Y.Kannan, H.Salacinski, K.M.Sales, P.E.M.Butler, A.Seifalian. 'Artificial nerve conduits in peripheral nerve repair'. *Biotechnol Appl Biochem.* 2005 Jun; 41(Pt 3):193-200.

D.S.Vara, H.J.Salacinski, **R.Y.Kannan**, L.Bordenave,G.Hamilton, A.M.Seifalian. Cardiovascular tissue engineering: state of the art. *Pathologie* Biologie 2005 Dec;53(10):599-612.

R.Y.Kannan, K.M.Sales, H.J.Salacinski, P.E.M. Butler, A.M. Seifalian. Cytotoxicity analysis of poly(carbonate-siloxane-urea)urethane. *Medical Journal of Malaysia* 2004; 59(B): 99-100.

R.Y.Kannan, K.M.Sales, H.J.Salacinski, P.E.M. Butler, A.M.Seifalian Endothelialisation of poly(carbonate-siloxane-urea)urethane. *Malaysian Medical Journal* 2004; 59(B): 107-108.

PRESENTATIONS

R.Y.Kannan, H.J.Salacinski, J. DeGroot, A.M.Seifalian, P.E.Butler. Silsesquioxane nanocomposites at the vascular interface. **Plastic Surgery Research Council** 2006, Dana Point, California, USA.

R.Y.Kannan, H.J.Salacinski, P.E. Butler, A.M.Seifalian. Nanomaterials at the vascular interface. **UCL Cardiovascular Science & Medicine Day** 2005, Institute of Child Health, UCL, London.

R.Y.Kannan, H.J.Salacinski, P.E. Butler, A.M.Seifalian. The anti-thrombogenic potential of POSS nanocomposites. **Trends in Nanotechnology** 2005, Oviedo, Spain.

R.Y.Kannan, H.J.Salacinski, A.M.Seifalian, P.E.Butler. Silsesquioxane nanocomposites: A new material for breast implant shells. Winter meeting of the **British Association of Plastic Surgeons** 2005, London, UK.

R.Y.Kannan, H.J.Salacinski, A.M.Seifalian, P.E.Butler. 'Smart' microvascular prostheses: Developing artificial free flaps. Winter meeting of the **British Association of Plastic Surgeons** 2005, London, UK.

R.Y.Kannan, H.J.Salacinski, A.M.Seifalian, P.E.Butler. 'Smart' microvascular prostheses: Developing artificial capillary beds. **Douglas Murray Prize** 2005 Meeting, Birmingham, UK.

A.M.Seifalian, **R.Y.Kannan**, H.J.Salacinski, P.E.Butler. Nanomaterials at the vascular interface. **British Vascular Society Meeting** 2005, Bournemouth, UK.

H.J.Salacinski, **R.Y.Kannan**, P.E.Butler, A.M.Seifalian. A New Approach To Improved Stent Graft Design: Development Of A Nano-Cage Containing Polymer That Is Both Anti-Platelet And Protein Inhibitory But Not Drug Releasing. 2005 **Summer Bioengineering Conference**, Vail, Colorado, USA.

R.Y.Kannan, H.J.Salacinski, P.E. Butler, A.M.Seifalian. 'Smart' Biomimetic Nanocomposite Microvessels. **UCL poster awards competition** 2005**,** UCL, London.

R.Y.Kannan, H.J.Salacinski, P.E. Butler, A.M.Seifalian. Improved stent graft design: development of a polymer that is both anti-platelet and coagulation cascade inhibitory. **Michael Faraday NPL** 2005 meeting, Nottingham, UK.

R.Y.Kannan, H.J.Salacinski, P.E. Butler, A.M.Seifalian. 'Artificial capillary beds: the Birth of Organ Cultivation.' **Younger Engineer of the Year Contest 2004**, House of Commons Science, Engineering & Technology meeting, London.

R.Y.Kannan, K.M.Sales, H.J.Salacinski, P.E.Butler, A.M.Seifalian. Cytotoxicity analysis of poly(carbonate-siloxane-urea)urethane. **International conference on biomaterials and tissue engineering** 2004, Kuala Lumpur, Malaysia.

R.Y.Kannan, K.Sales, H.J.Salacinski, P.E. Butler, A.M.Seifalian Endothelialisation of poly(carbonate-siloxane-urea)urethane. **International conference on biomaterials and tissue engineering** 2004, Kuala Lumpur, Malaysia.

R.Y.Kannan, H.J.Salacinski, P.E. Butler, A.M.Seifalian 'Microvascular networks'. UK focus for biomedical engineering. **Royal Academy of Engineering**. Liverpool 2004, UK.

R.Y.Kannan, H.J.Salacinski, P.E. Butler, A.M.Seifalian. 'Artificial capillary beds: The birth of organ cultivation'. 3rd place **Royal Free Univ. College Medical School Poster Competition 2004**, London.